Patient-Specific Modelling of the Cardiovascular System for Diagnosis and Therapy Assistance in Critical Care

Christina Starfinger

A thesis submitted for the degree of

Doctor of Philosophy

in

Mechanical Engineering,
University of Canterbury,
Christchurch, New Zealand.

11 April 2008

Acknowledgements

There are a several people I would like to thank for various reasons,

Geoff Chase, my main supervisor, for giving me the opportunity to come back to New Zealand for 3 years and doing my PhD here. I really appreciated his support and guidance, his contributions and farsightedness throughout the project.

Chris Hann and Geoff Shaw, my co-supervisors, for their support and enthusiasm throughout the project. Special thanks to Chris Hann for providing the basis for this research, the integral-based identification method and the efficient way of implementing.

Bram Smith and Thomas Desaive, representatives of the research groups in Aalborg, Denmark and Liège, Belgium, for providing me with data of porcine experiments of PEEP titrations, pulmonary embolism and septic shock. Without their data this PhD thesis would not exist.

My mum, sister, family and friends in Germany, Austria, New Zealand and around the world, for your friendship and support.

Abstract

Critical care is provided to patients who require intensive monitoring and often the support of failing organs. Cardiovascular and circulatory diseases and dysfunctions are extremely common in this group of patients. However, cardiac disease states are highly patient-specific and every patient has a unique expression of the disease or underlying dysfunction. Clinical staff must consider many combinations of different disease scenarios based on frequently conflicting or confusing measured data on a patient's condition. Successful diagnosis and treatment therefore often rely on the experience and intuition of clinical staff, increasing the likelihood for clinical errors.

A cardiovascular (CVS) computerized model that uniquely represents the patient and underlying dysfunction or disease is developed. The CVS model is extended to account for the known physiologic mechanisms during spontaneous breathing and mechanical ventilation, thus increasing the model's accuracy of representing a critically ill patient in the intensive care unit (ICU). The extended CVS model is validated by correctly simulating several well known circulatory mechanisms and interactions.

An integral-based system parameter identification method is refined and extended to account for much smaller subsets of available input data, as usually seen in critical care units. For example, instead of requiring the continuous ventricle pressure and volume waveforms, only the end-systolic (ESV) and end-diastolic (EDV) volume values are needed, which can be even further reduced to only using the global end-diastolic volume (GEDV) and estimating the ventricle volumes. These changes make the CVS model and its application to monitoring more applicable to a clinical environment.

The CVS model and integral-based parameter identification approach are validated on data from porcine experiments of pulmonary embolism (PE), positive end-expiratory pressure (PEEP) titrations at different volemic levels, and 2 different studies of induced endotoxic (septic) shock. They are also validated on 3 adrenaline dosing data sets obtained from published studies in humans. Overall, these studies are used to show how the model and realistic clinical measurements may be used to provide a clear clinical picture in real-time.

A wide range of clinically measured hemodynamics were successfully captured over time. The integral-based method identified all model parameters, typically with less than 10% error versus clinically measured pressure and volume signals. Moreover, patient-specific parameter relationships were formulated allowing the forward prediction of the patient's response towards clinical interventions, such as administering a fluid bolus or changing the dose of an inotrope. Hence, the model and methods are able to provide diagnostic information and therapeutic decision support.

In particular, tracking the model parameter changes over time can assist clinical staff in finding the right diagnosis, for example an increase in pulmonary vascular resistance indicates a developing constriction in the pulmonary artery caused by an embolus. Furthermore, using the predictive ability of the model and developed methods, different treatment choices and their effect on the patient can be simulated. Thus, the best individual treatment for each patient can be developed and chosen, and unnecessary or even harmful interventions avoided.

This research thus increases confidence in the clinical applicability and validity of this overall diagnostic monitoring and therapy guidance approach. It accomplishes this goal using a novel physiological model of the heart and circulation. The integral-based parameter identification methods take dense, numerical data from diverse measurements and aggregate them into a clearer physiological picture of CVS status. Hence, the broader accomplishment of this thesis is the transformation, using computation and models, of diverse and often confusing measured data into a patient-specific physiological picture - a new model-based therapeutic.

Contents

List of Figures

List of Tables

Nomenclature

Roman Symbols

C	Compliance
E	Elastance
I	Current
L	Inertance
P	Pressure
Q	Electrical charge
Q	Flow
R	Resistance
S	Saturation
S	Septum
t	Time
U	Potential
V	Volume

Greek Symbols

κ	Parameter used for calculating initial V_{vc}, usually 1.25
λ	Parameter in EDPVR
σ	Reflection coefficient, representing membrane permeability

σ_{mws}	Myocardial wall stress
θ	Zero matrix

Subscripts

ao	Aorta
av	Aortic valve
C	Capillary
cap	Capillary
d	Unstressed
dia	Diastolic
eb	Beginning of ejection period for LV
$eb2$	Beginning of ejection period for RV
ef	End of ejection period for LV
$ef2$	End of ejection period for RV
eff	Effective
fb	Beginning of filling period for LV
$fb2$	Beginning of filling period for RV
ff	End of filling period for LV
$ff2$	End of filling period for RV
la	Left atrium
lvf	Left ventricle free wall
max	Maximum
min	Minimum
mt	Mitral valve
N	Normalized

o	value at zero pressure
p	pulse (oximetry)
pa	Pulmonary artery
pcd	Pericardium
pl	Pleural
pu	Pulmonary vein
pul	Pulmonary
pv	Pulmonary valve
ra	Right atrium
rvf	Right ventricle free wall
spt	Septum
sys	Systemic
sys	Systolic
T	Tissue
tc	Tricuspid valve
th	Intrathoracic
tot	Total
vc	Vena cava
vr	Venous return
$\bar{v}$	mixed venous

Other Symbols

Δ	Parameter used for vasoconstriction/ -dilation
$C(a-v)O_2$	Arterial-venous O_2 content difference
CO_2	Carbon Dioxide

O_2	Oxygen

Acronyms

AV	Atrioventricular
BAN	British Approved Name
BGA	Blood gas analysis
BSA	Body Surface Area
BV	Change in blood volume (in ml) as caused by an infusion or blood loss (external bleeding)
CABG	Coronary artery bypass grafting
CAD	Coronary artery disease
CI	Cardiac Index
CO	Cardiac output
CPR	Cardiopulmonary resuscitation
CPS	Cardiopulmonary system
CVS	Cardiovascular system
CVVH	Continuous veno-venous hemofiltration
ECG	Electrocardiogram
EDP	End-diastolic pressure
EDPVR	End-diastolic pressure volume relationship
EDV	End-diastolic volume
ESP	End-systolic pressure
ESPVR	End-systolic pressure volume relationship
ESV	End-systolic volume
GEDV	Global end-diastolic volume

HF	Hemofiltration
HR	Heart Rate
ICU	Intensive Care Unit
INN	International Nonproprietary Name
ITBV	Intrathoracic blood volume
KG	Patient weight in kg
LBB	Left bundle branch block
LV	Left ventricle
LVAD	Left ventricular assist device
MCFP	Mean circulatory filling pressure
NDF	Net driving force
PBV	Pulmonary blood volume
PE	Pulmonary Embolism
PEEP	Positive end-expiratory pressure
PP	Pulse pressure
PPV	Positive pressure ventilation
RV	Right ventricle
SA	Sinoatrial
SV	Stroke volume
TPR	Total peripheral resistance
VR	Venous Return

Chapter 1

Introduction and Motivation

Critical care is provided to patients who are amongst the sickest in the hospital. They have potentially severe physiologic instability and require intensive monitoring as well as frequently requiring the support of failing organs. Therapeutic and diagnostic support is fundamental for the optimal management of critically ill patients. However, excess information can exceed human decision making limits. In contrast, insufficient and limited data can confuse the clinical picture. Therefore, critical care patient management requires balancing information levels and clarity to optimize decision making.

Cardiovascular diseases are extremely common and claimed nearly 1 million lives in the United States in 2004, which equals 36.6% of all deaths or 1 of every 2.8 deaths (American Heart Association, Cardiovascular Disease Statistics). It has been estimated that more than 50% of postoperative deaths are caused by cardiac events (Mangano, 1994; Ramsey, 1999). Many admissions to the intensive care unit (ICU) are for cardiac or circulatory monitoring or dysfunction, and many unplanned ICU admissions are for treatment of acute cardiovascular and circulatory dysfunctions that occur intraoperatively (Ramsey, 1999).

Even in non-cardiac surgery patients, about one third have coronary artery disease (CAD) or two or more major risk factors for CAD or are older then 65 years (Mangano, 1994). Therefore, it can almost be expected that in this large group of patients, when subjected to stress during the perioperative period, cardiovascular complications develop. Overall it is estimated that approximately 1 million patients will suffer severe perioperative cardiac morbidity following non-cardiac surgery in the United States. Thirty three billion USD in costs are attributable to these cardiovascular complications following an operation each year (Mangano, 1994).

Thus, circulatory dysfunctions and associated diseases, such as various kinds of circulatory or cardiac shock account for a significant amount of ICU admissions. In particular, severe sepsis and septic shock have long been a challenge for intensive care clinicians because of their frequent occurrence, significant mortality rates of 30-50%, and high associated costs (Karlsson *et al.*, 2007). Another recent study found the following disease conditions leading to ICU admission and their occurrence rates for patients aged 65-74 years in Olmsted County, Minnesota: Cardiovascular (58.2%), Respiratory diseases (17.4%), Gastrointestinal (8.5%), Neurologic (6.5%), Toxin/trauma (2%), Other (7.5%) (Seferian & Afessa, 2006). Again, cardiovascular dysfunction accounts for a dramatic majority of admissions.

However, managing these patients is challenging. In particular, both diagnosis and therapy can be very difficult, as cardiac disease state is highly patient-specific. Every patient has an unique expression of a given disease or dysfunction. Hence, it is difficult to accurately diagnose due to the often limited measurements available. In addition, the body's natural reflex responses to restore circulatory equilibrium can often mask the underlying symptoms.

Hence, clinical staff must consider many combinations of different disease scenarios based on frequently conflicting data on a patient's condition, including clinical history and non-invasive and/or invasive studies (Grenvik *et al.*, 1989). Thus, successful diagnosis and treatment often rely on the experience and intuition of clinical staff, increasing the likelihood for clinical errors. Unfortunately, clinical error rates are common (1-50%) and occur frequently (Abramson *et al.*, 1980; Donchin *et al.*, 1995; Morris, 2001; Suresh *et al.*, 2004).

As difficult as diagnosing cardiac disease states is, it is also not trivial to treat them properly. In particular, all patients are different and may have different responses towards the same treatment and therapy. Moreover, the multitude of interacting mechanisms in the cardiovascular system makes successful reasoning about therapy effects very difficult. These difficulties are further aggravated by the various disease states that change the physiological relationships.

Thus, the primary issue is integrating the diverse clinical data available into a complete and accurate assessment of patient state. This integration is based on the mental models and understanding of clinical staff. A physiological, identifiable and validated computer model offers several potential advantages in diagnosis and therapy selection. In particular, the ability to aggregate diverse patient data into

a compact, patient-specific, clinically relevant assessment of circulatory status, can offer significant potential advantages in creating a clear physiological picture.

1.1 Hemodynamic Monitoring in ICUs

Critically ill patients in the ICU are hemodynamically monitored to identify cardiovascular insufficiency as well as the probable cause and potential response to therapy. The following list summarizes 3 arguments that can be made for using specific monitoring devices (Pinsky, 2007):

- Prior experience has shown that monitoring can identify diseases and/or complications, even though the link between monitored variable and disease may not be known.
- Monitoring is used to define the cardiovascular status of the patient and it is assumed that a restoration to normal physiologic values will prevent further organ injury and reduce mortality.
- Monitoring-treatment protocols can influence and determine the therapy in otherwise unexpected ways.

However, when monitoring devices do not drive treatment protocols, they cannot improve outcome. In particular, only treatment can improve outcome for patients, but not monitoring alone. Clearly, as several studies (Connors *et al.*, 1996; Pinsky, 2007; Sandham *et al.*, 2003; Yu *et al.*, 2003) have shown, just inserting a catheter to make measurements without a defined and effective treatment protocol requiring such information, is unlikely to result in improved patient outcomes. Thus, over the years, treatment protocols have been developed and established that link monitored variables, such as mixed venous oxygen saturation ($S\bar{v}O_2$), to special treatment options.

The goal in this research is to integrate the CVS model into this process chain, starting from ICU admission and transferring to diagnosis and therapy. The CVS model and methods developed not only assist clinical staff in finding the right diagnosis, but can also provide information about therapy responses. The result can enable more consistent care and reduce variation. Importantly, variation in clinical management is linked to suboptimal outcomes for patients, as well as increased costs and lengths of stay in the hospital. Tools for assisting

with diagnosis and therapy guidance can help in reducing variation in clinical practice, resulting in more consistent care, which in turn has a positive impact on patient outcomes.

1.1.1 Application of Computerized Models and Protocols

Over the last few years, evidence-based and (early) goal-directed therapeutic protocols have become much more popular and commonly used, as they can be applied for complex clinical problems to create patient-specific therapy. Clinical trials in the emergency department by Rivers *et al.* (2001) have clearly documented improved outcome, especially if the goal-directed therapy is initiated as early as possible. Importantly, in the study by Rivers *et al.* (2001), the total amount of administered fluids was similar in the treatment and control groups, but the treatment group received the fluids early when the control group did not require them based on traditional hemodynamic measures such as mean arterial pressure (MAP) and right atrial pressure (P_{ra}). This result shows that the earlier the treatment is begun, the better the likely outcome for the patient.

The cardiovascular (CVS) model in this research could favorably be integrated into this process of decision making by offering clinicians the possibility of collecting the diverse data into a clearer physiological picture. As such, it can help in diagnosis as well as allowing testing of different therapeutic procedures and their likely effect on the patient. Early in the treatment process, the CVS model could be used to give valuable insight into the patient-specific condition and underlying dysfunction, where typically measured variables may still be at normal target levels. The best individual treatment for each patient could thus be chosen, and unnecessary or even harmful interventions avoided.

1.2 Motivation and Goals for this Research

This PhD research employs a physiologically validated minimal CVS model based on (Smith, 2004; Smith *et al.*, 2004), capable of capturing patient dynamics commonly seen in an ICU. In an ICU, catheters are often already in place and special monitoring devices are used. As a result, a larger, more useful range of measurements is available. However, it has to be mentioned that the more invasive measurements that are performed, the greater the potential risk for the patient

(Metnitz *et al.*, 2004). Thus, one goal of this research is to investigate how using only a relatively small number of physiological variables can still result in accurate model identifications, resulting diagnosis, and therapy predictions. The use of minimized clinical data is especially important, as most ICUs still only measure blood pressure (BP), heart rate (HR) and oxygen saturation by pulse oximetry (SpO_2), as they have done for the last 20 years (Pinsky, 2007).

A highly efficient model implementation method (Hann *et al.*, 2005) provides the necessary simplicity, flexibility and rapid forward simulation required in a clinical environment. Finally, a linear, convex and integral-based identification method based on Hann *et al.* (2006) allows virtually all the model parameters to be identified, and is employed to create patient-specific models from clinical data. These patient-specific models are tuned to the individual patient and uniquely represent their condition. The combination of rapid patient-specific parameter identification and fast accurate forward simulation enables the potential for real-time diagnosis and therapy selection decision support in the ICU.

The main goals of this PhD research are to clinically validate the CVS model and make improvements where needed based on these results. The identification process is revisited and transferred from a theoretical framework into clinically applicable methods that allow real-time identification of the model parameters and ensure the accuracy of the identified parameters. The final results presented in this thesis are the first clinical validations of these models and methods using porcine animal experiments and data from human trials in an intensive care setting.

1.2.1 Example for a Potential Use of the CVS Model

For hemodynamically unstable patients admitted to the ICU, there are usually 3 important functional questions that have to be asked by the clinical staff. The answers determine the type of treatment that will be initiated (Pinsky, 2007):

- Will cardiac output (CO) increase with fluid resuscitation and if so, by how much?
- In the hypotensive patient, is the vasomotor tone increased, decreased or normal?
- Is the heart capable of sustaining an effective cardiac output (CO) once arterial pressure is restored or will it go into failure?

To answer the first question and assess the preload responsiveness of the patient, intravascular fluid challenges are commonly administered. In this case, a bolus of fluid is rapidly infused and the subsequent changes in specific flow-dependent variables (CO, MAP, $S\bar{v}O_2$ and P_{ra}) are measured. However, the problems with performing a fluid challenge for clinical decision making are multiple (Pinsky, 2007):

- Only half of the hemodynamically unstable patients administered a volume challenge will respond with an increase in CO (Michard & Teboul, 2002). Thus, the correct treatment may have been delayed in the other half of the patients.
- In the half not responding and who are thus not preload responsive, volume loading may be directly injurious, as for example in left ventricle (LV) failure.
- Dynamic measures, such as stroke volume variation (SVV), pulse pressure variation (PPV) and systolic pressure variation (SPV) are usually used to predict fluid responsiveness. However:
  - They assume a constant R-R interval and are thus unreliable for varying R-R intervals as in atrial fibrillation.
  - They may lose accuracy if tidal volume varies from breath to breath as may occur with assisted and spontaneous ventilation (Backer *et al.*, 2005; Reuter *et al.*, 2003). Thus, these approaches are limited to only a small amount of ICU patients.
  - Preload responsiveness does not mean that a patient requires volume resuscitation, as healthy subjects are also preload responsive (Pinsky, 2004).

Hence, there is a scenario where the outcome or situation is unknown. Typical clinical response cannot distinguish between significantly contrasting treatment options from the data and methods available.

The CVS model could potentially be used in this difficult scenario to answer the first question by forward simulating and predicting the patient's response towards a fluid challenge. Even different types and amounts of fluids could be simulated and the most appropriate chosen for the patient. Moreover, the CVS

model could still be used where normal hemodynamic variables (for example SVV in atrial fibrillation or for assisted ventilation) are unreliable or cannot be used at all.

Finally, although specific patterns of hemodynamic variables exist that describe specific types of diseases, they do not predict individual patient response to therapy. However, the goal of this research is, to develop a CVS model and parameter identification process that can be used as a basis for a diagnostic assistance system and in guiding therapy. This system could then potentially help overcome such problems by allowing realistic and physiologically correct predictions of patient-specific responses to different treatment choices.

Chapter 2

Cardiovascular Physiology

This chapter gives a brief introduction in cardiovascular and respiratory anatomy and physiology. It is designed to provide the reader with the essential background information needed to understand the discussions and explanations in the following chapters.

2.1 Circulation

The circulatory system is responsible for transporting blood through the body to its cells. This flow provides an adequate amount of nutrients and oxygen, also assuring the removal of metabolic end products. The heart connects the two major parts of the circulation, the systemic circulation and the pulmonary circulation. In the pulmonary circulation, blood is pumped through the right atrium and ventricle of the heart to the lungs, where carbon dioxide is exchanged for oxygen. The oxygenated blood returns to the heart via the pulmonary vein. It then circulates through the left atrium and ventricle and exits the heart through the aorta. The blood vessels in the systemic circulation transport the blood throughout the rest of the body. Systemic circulation provides nourishment for all of the body's tissues, except for the heart and lungs. Figure 2.1 shows an overview of the circulation, including the systemic and pulmonary circulation.

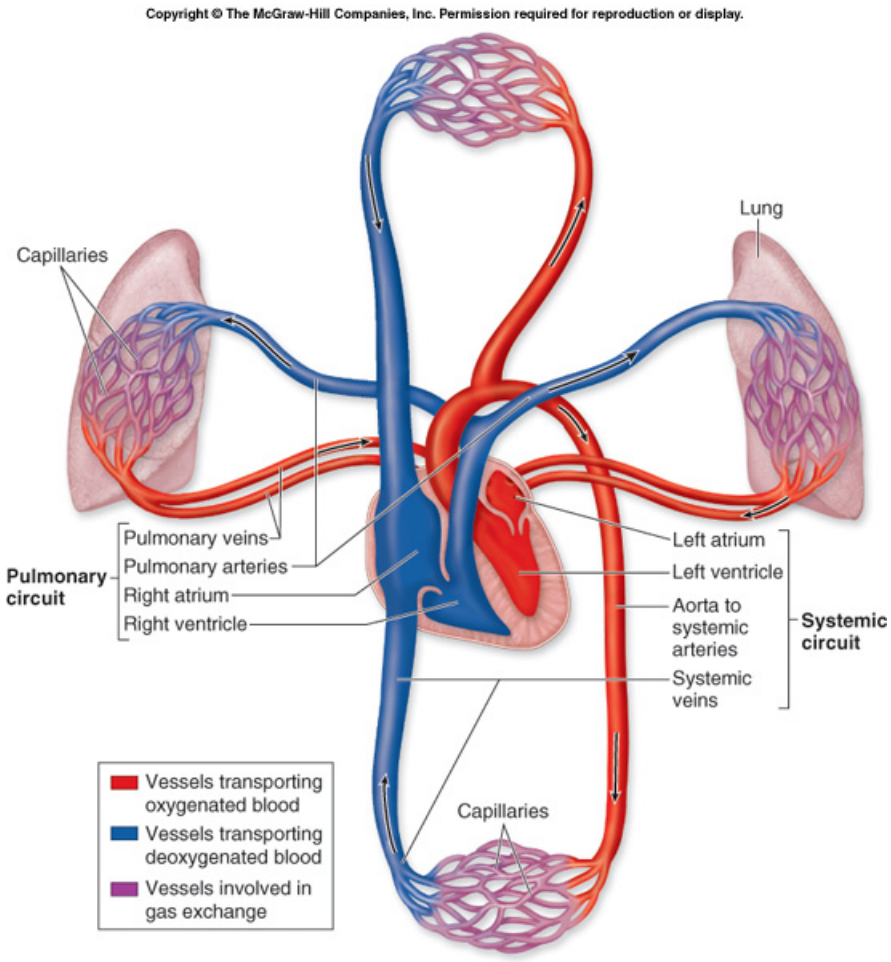

Figure 2.1: Overview of pulmonary and systemic circulation (McKinley & O'Loughlin, 2007)

2.1.1 Arterial and Venous System

The arteries are the blood vessels that initially transport the oxygenated blood from the heart under high pressure to the tissues. The arterioles are the last small branch of the arterial system through which blood is released into the capillaries. The capillaries are very small, thin-walled blood vessels where the exchange of gases, nutrients, and waste products takes place between the cells and the blood.

Blood flows with almost no resistance in the larger blood vessels, but in the arterioles and capillaries, considerable resistance to flow occurs because these vessels are so small in diameter that the blood must squeeze all its contents through them. The venules collect blood from the capillaries and gradually feed into progressively larger veins. The venous system thus transports the blood from the tissues back to the heart. The walls of the veins are thin and very elastic and can fold or expand to act as a reservoir for extra blood, if required.

2.1.2 Capillary System

The capillary system delivers what is needed to the cells and removes what is not needed. They are made up of a single layer of endothelial cells with a wall thickness of $0.5 - 1.0 \mu m$ and an average diameter of about the size of a red blood cell, thus around $7 - 8 \mu m$. There are about 40 billion capillary cells in the body and they are distributed such that no cell is further away than $0.1 mm$ from a capillary. This prevalence and proximity is the basis for the diffusion of nutrients and waste products into and out of the tissue cells (Mehler & Sompayrac, 2001). Capillaries form a network of parallel connections between the arterioles and venules, as shown in Figure 2.2.

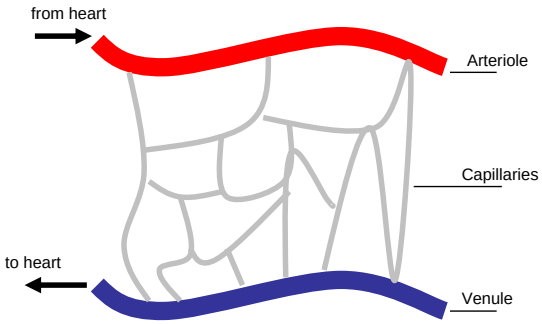

Figure 2.2: Capillary system: connecting arterial and venous sides of the circulation.

2.2 Anatomy of the Heart

The heart is the muscular pump that connects the systemic and pulmonary vascular systems. It has two separate sides. One is designed to pump deoxygenated blood into the pulmonary circulation where the blood becomes oxygenated. The second, is designed to pump the oxygenated blood into the systemic circulation where the blood is transported through the body to the tissue cells. Each of these sides consists of one ventricle and one atrium.

The left ventricle (LA) and atrium form the so-called left heart and pump oxygenated blood from the pulmonary system into the systemic circulation. The right heart is formed by the right ventricle (RV) and atrium and pumps deoxygenated blood from the vena cava into the pulmonary circulation. The right and left ventricle share a common wall, the interventricular septum.

The heart also consists of four heart valves which ensure a unidirectional flow and prevent backwards flow (regurgitation). The right atrium is separated from the right ventricle by the tricuspid valve ($_{tc}$), the left atrium and left ventricle by the mitral valve ($_{mt}$). The pulmonary valve ($_{pv}$) lies between the right ventricle and the pulmonary artery and the aortic valve ($_{av}$) between the left ventricle and aorta. Figure 2.3 shows the internal architecture of the heart.

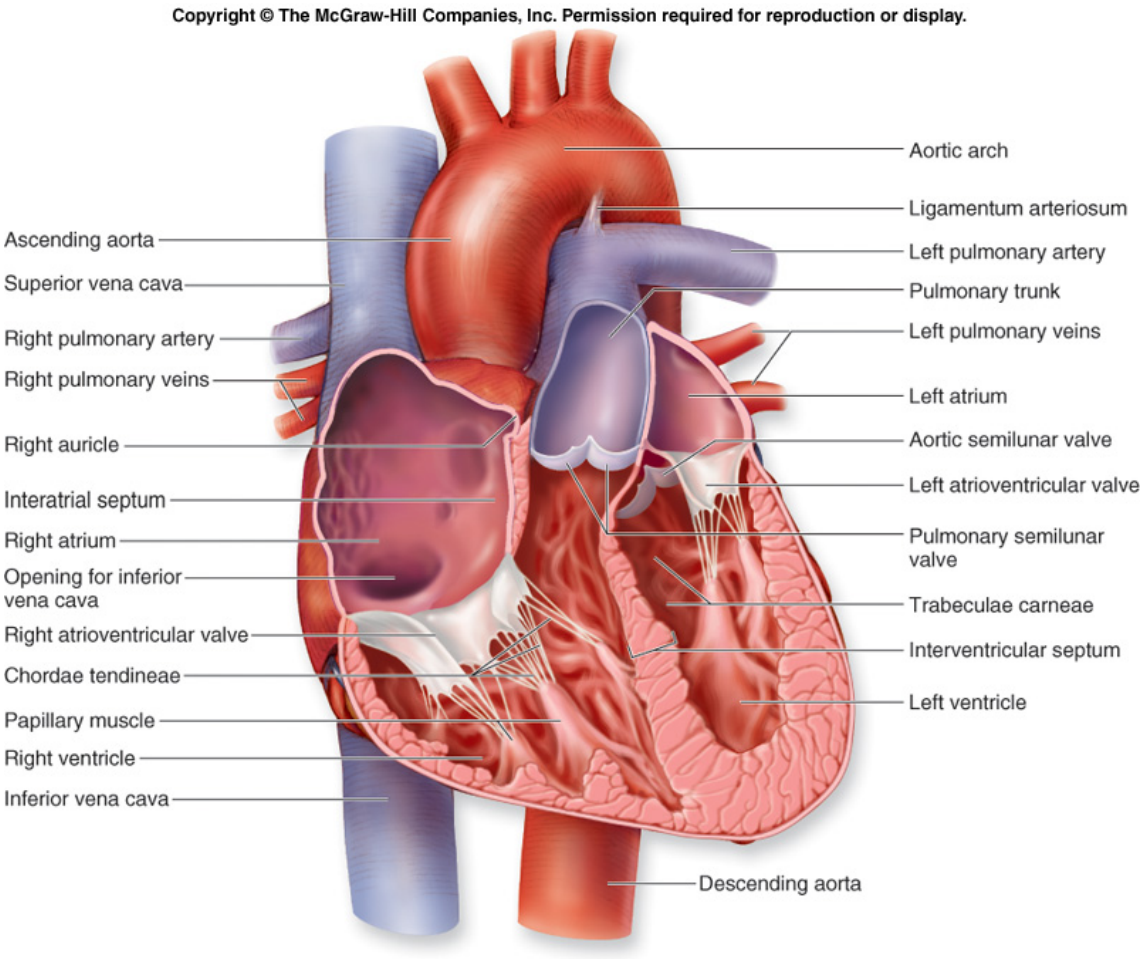

Figure 2.3: Internal view of the heart (McKinley & O'Loughlin, 2007)

2.3 Normal Cardiac Electrical Activation

The action potentials generated by the sinoatrial (SA) node spread through the atria. The conduction velocity of action potentials in the atrial muscle is about $0.5m/s$. As the wave of action potentials depolarizes the atrial muscle, the cardiomyocytes contract by a process termed excitation-contraction coupling (Klabunde, 2004).

In a healthy heart, the only pathway available for action potentials to enter the ventricles is through a specialized region of cells, the so-called atrioventricular (AV) node, which is located in the interatrial septum. The AV node is a distinct conducting tissue that slows the impulse conduction substantially to about $0.05m/s$. It thus allows time for complete atrial depolarization and contraction (systole) prior to ventricular depolarization and contraction.

Subsequently, the impulses enter the ventricle at the Bundle of His and follow the left and right bundle branches along the interventricular septum. These specialized fibers conduct the impulses at a high velocity of about $2m/s$. The bundle branches divide into the so-called Purkinje fibers that conduct the impulses at a velocity of about $4m/s$ through the ventricles. This action results in depolarization of ventricular myocytes and ventricular contraction (Klabunde, 2004). This conduction system is thus very important for an organized depolarization and repolarization of the ventricle myocytes to generate an adequate pressure during the different phases of the cardiac cycle. The conduction times are different in the left and right ventricle whereby the right ventricle is activated after around $0.21s$ and the left ventricle after $0.23s$. This sequence and timing of activation is depicted in Figure 2.4.

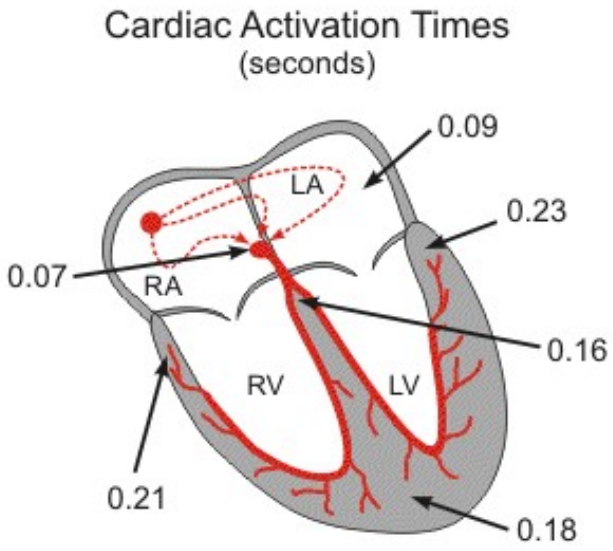

Figure 2.4: Sequence of cardiac electrical activation and times to reach specific locations (Klabunde, 2004).

2.4 Mechanical Properties of the Heart

Assessment of left and right ventricular systolic and diastolic pump properties is vital for understanding cardiovascular physiology. Since 1895, when Otto Frank (Frank, 1895) published the first cardiovascular investigations, numerous articles have been published on this topic. As a result, greater insight has been gained into the fundamental concepts of cardiovascular physiology and pathophysiology, as well as the fundamental mechanics of the heart muscle in different states.

Important information about the functioning of the left ventricle can be obtained by examining the commonly measured Pressure-Volume (PV) loop. This loop is obtained when plotting the left ventricle volume (V_{lv}) versus the left ventricle pressure (P_{lv}). Figure 2.5 shows a PV loop labelling the critical points and actions in the cardiac cycle. Point A marks the opening of the mitral/tricuspid valves and thus the beginning of the filling process, which ends at point B with the closing of the two heart valves. The ejection period starts at point C with the opening of the aortic/pulmonary valves and finishes at point D where the valves close again. V_d is the unstressed chamber volume and V_o the volume at zero pressure.

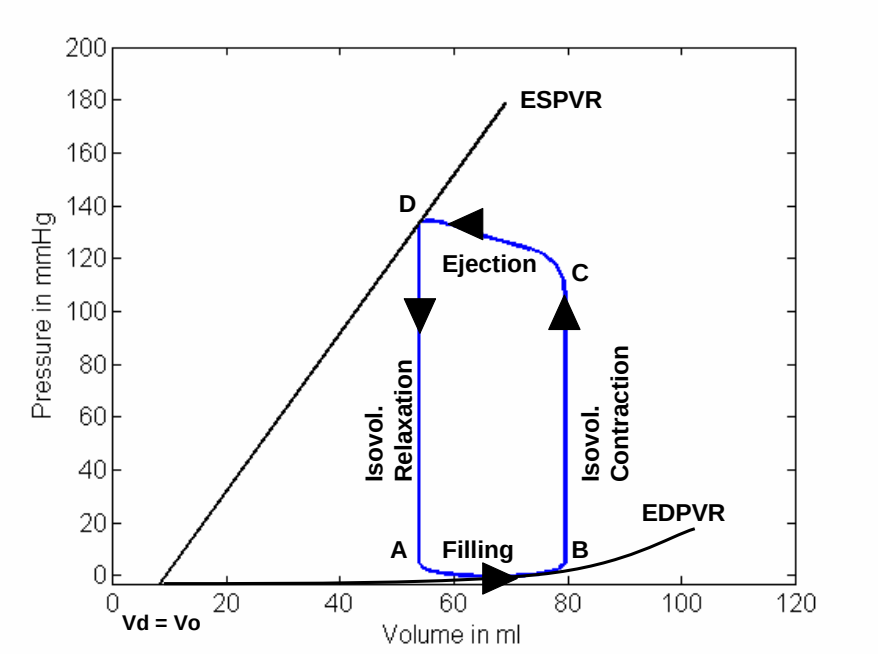

Figure 2.5: PV loop for the cardiac cycle and the variations in end-diastolic (EDPVR) and end-systolic (ESPVR) pressure-volume relationships.

The PV loops change whenever significant dysfunction occurs. For example, when the preload, which is the hemodynamic stretch or load that is exerted on the heart during diastole, is rapidly changed, such as through a vena cava occlusion, the PV loops will change in a characteristic way. This behaviour or change can be seen in Figure 2.6. In particular, the end-diastolic volume (EDV) decreases, but nothing else is modified about the heart or arterial system properties. From this figure it can be seen how the PV loop is confined by the end-diastolic pressure volume relationship (EDPVR) and the end-systolic pressure volume relationship (ESPVR).

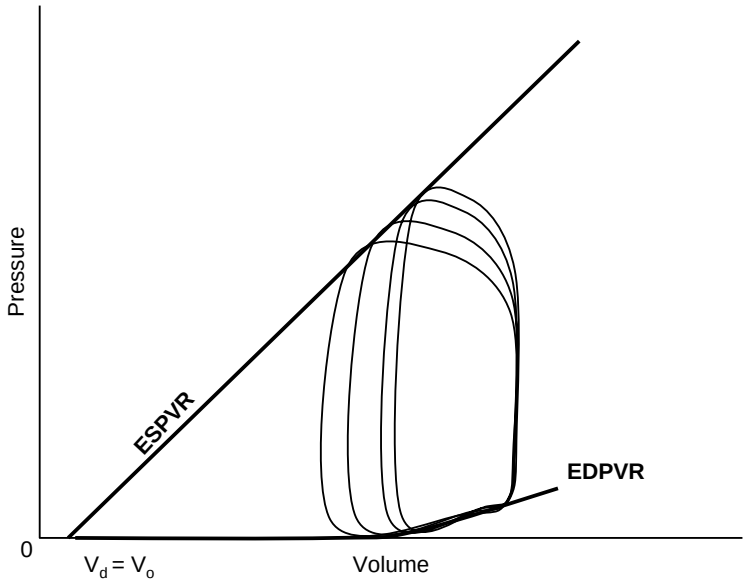

Figure 2.6: Pressure- Volume (PV) loop for several heart beats during simulated vena cava occlusion showing the ESPVR and EDPVR. The end-diastolic volume decreases (moves left) as the occlusion and its effect become larger.

2.4.1 EDPVR

The end-diastolic pressure-volume relationship (EDPVR) represents the elastance of the ventricle in the frozen state of end-diastole, at maximum filling and relaxation. The EDPVR is a non-linear relationship, which intercepts the x-axis at V_o, which is defined as the volume at zero pressure.

$$EDPVR = P_0(e^{\lambda(V-V_o)} - 1) \tag{2.1}$$

where λ, P_0 and V_o define curvature, gradient and volume at zero pressure.

2.4.2 ESPVR

The end-systolic pressure volume relationship (ESPVR) represents the elastance of the ventricle in the state of end-systole, thus in an activated state of contraction. The ESPVR intercepts the x-axis at a positive volume value V_d, which indicates that some amount of volume must be in the ventricle before a pressure is

generated. It can be assumed that $V_d = V_o$, which will introduce a comparatively small error, but simplify further discussions (Burkhoff, 2002).

$$ESPVR = E_{es}(V - V_d) \tag{2.2}$$

where V_d is the unstressed chamber volume and E_{es} the end-systolic elastance.

2.4.3 Time-Varying Elastance Function $E(t)$

Only the elastances of the ventricle in the two states of end-systole and end-diastole have been so far examined. In between these two states (B-C and D-A in Figure 2.5) the elastance changes in a characteristic way from EDPVR to ESPVR during systole and back during diastole. These changes in elastance are the largely vertical portions of the PV loop during isovolumetric contraction (B-C) and relaxation (D-A). This change is illustrated in Figure 2.7.

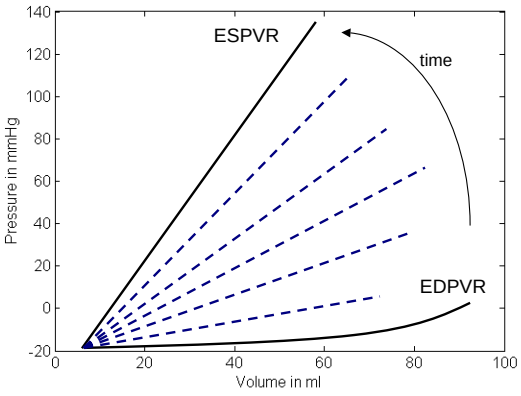

Figure 2.7: Time-Varying Elastance $E(t)$ from diastole to systole

All these pressure- volume relationships are approximately linear and share a common x-axis intercept V_d. It is thus possible to describe the time course of change in ventricle elastance, and therefore in the ventricle properties, by plotting the slope of the pressure- volume relations versus time (Burkhoff, 2002). Figure 2.8 illustrates the time-varying elastance function $E(t)$ throughout the cardiac cycle for a heart beat period of $0.8s$ obtained using this approach.

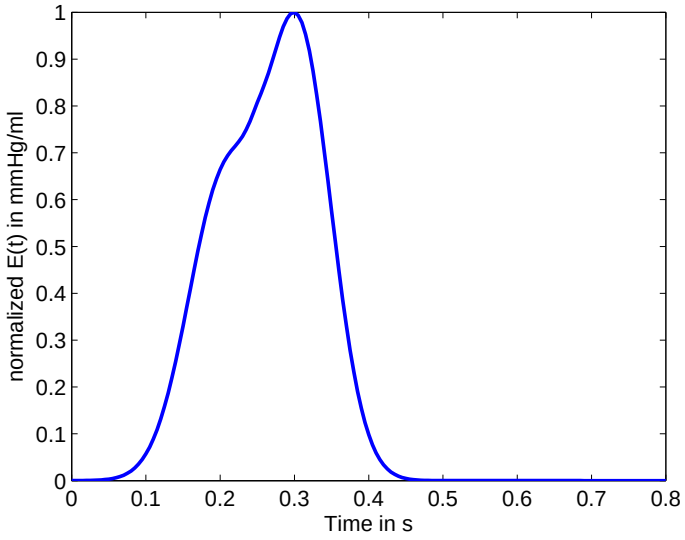

Figure 2.8: Normalized time-varying elastance $E(t)$ for one cardiac cycle

2.5 Basic Concepts: Preload, Afterload and Contractility

This section explains some of the basic concepts and metrics with regard to cardiovascular physiology. These concepts are of vital importance for all further discussions as they are commonly used to describe cardiovascular and circulatory states. It is important to appreciate that stroke volume (SV) and blood pressure (BP) are determined by the interaction between the heart, the arterial system (afterload) and the venous system (preload). This fundamental concept is often used clinically to simply characterize the cardiovascular state by the relationship between these major "players".

2.5.1 Preload

Preload can be defined as the initial stretching of the myocardium prior to ejection (Klabunde, 2004). Preload in the right ventricle is determined by the systemic venous return (VR) that flows back to the heart, more specifically to the right atrium. Left ventricle preload is correlated to the left ventricle end-diastolic volume (LVEDV) and thus influenced by the pulmonary flow into the left atrium.

Changes in ventricular preload have a crucial effect on stroke volume and thus on cardiac output. The mechanism by which increased preload or ventricular

filling increases stroke volume is called the Frank-Starling mechanism. In the 19th century, Otto Frank discovered that the ventricles contract with more strength when they are stretched prior to contraction, that is when preload increases. By doing so the ventricle contracts more forcefully and more volume is ejected. Ernest Starling continued these observations in the 20th century.

A change in preload can easily be seen in a PV loop diagram as shown in Figure 2.9. Subfigure 'A' represents the baseline PV loop and subfigure 'B' the new PV loop with increased preload. Figure 2.9 shows how an increased preload increases the end-diastolic volume (EDV) and thus the stroke volume (SV). However both afterload and contractility remain unchanged, as will be explained in subsequent sections and Figures 2.10 and 2.11.

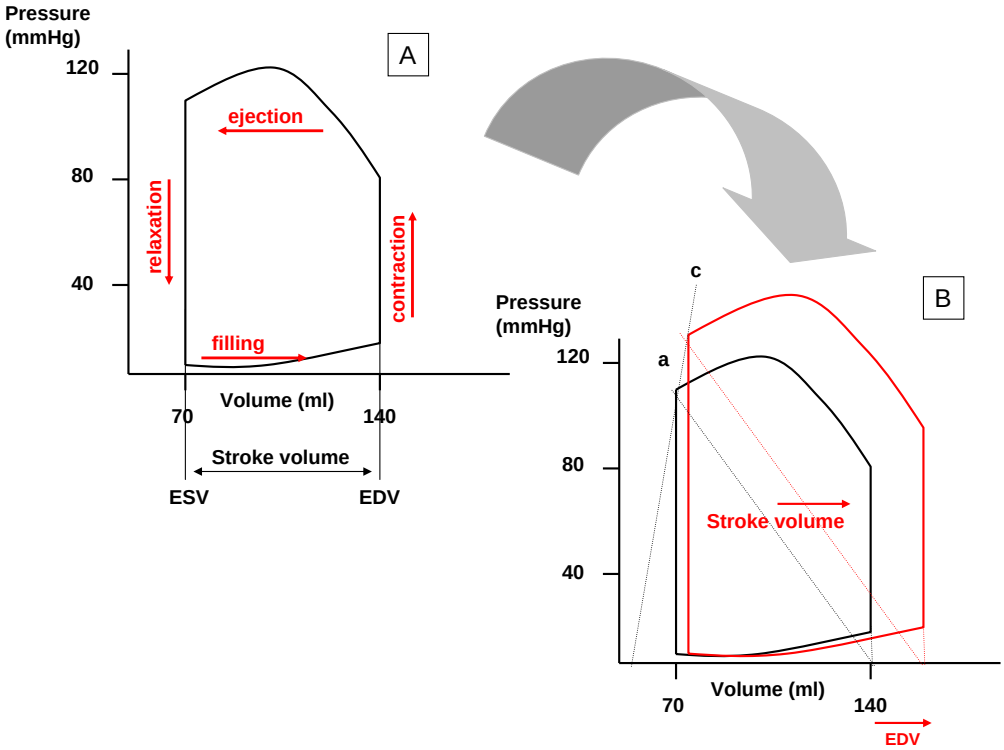

Figure 2.9: Effect of increased preload on pressure-volume loop.

2.5.2 Afterload

Afterload is the hydraulic load imposed on the ventricle during ejection (Burkhoff, 2002) or the force against which the heart must pump. Under normal, healthy conditions afterload is imposed on the heart by the arterial system. Under pathologic conditions, for example when the mitral valve is insufficient or the aortic valve stenotic, afterload is determined by factors other than the properties of the arterial system. There are various measurements or surrogates that determine and characterize afterload, including (Burkhoff, 2002):

- Aortic or arterial pressure (P_{ao})
- Systemic resistance (R_{sys})
- Arterial impedance
- Myocardial peak wall stress (σ_{mws})

Aortic (or arterial) pressure (P_{ao}) provides a measure of the pressure that the ventricle must overcome to eject blood. However, it has the disadvantage that it is not constant during ejection. In addition, it does not provide a measure of only the arterial properties, but of the combined arterial system and ventricle.

Systemic arterial resistance (R_{sys}), also called total peripheral resistance (TPR), is the ratio between the mean pressure drop across the arterial system and mean flow in and out of the arterial system. It is thus the ratio of the pressure gradient ($P_{ao} - P_{sys}$) and stroke volume (SV). In the CVS model, the parameter R_{sys} represents or characterizes this definition of afterload.

Two other surrogates for afterload are arterial impedance and myocardial peak wall stress. Arterial impedance is an analysis of the relationship between pulsatile flow and pressure waves in the arterial system. It is based on the theories of Fourier analysis in which flow and pressure waves are decomposed into their harmonic components and the ratio between the magnitudes of pressure and flow waves are determined on a harmonic-by-harmonic basis. Thus, in simplified terms, impedance provides a measure of resistance at different driving frequencies. Unlike TPR, impedance allows one to relate instantaneous pressure and flow (Burkhoff, 2002).

Wall stress (σ_{mws}) is the force per unit cross sectional area of muscle and is simplistically interrelated to intraventricular pressure (P_{lv}) using Laplace's law:

$$\sigma_{mws} = P_{lv} \cdot \frac{r}{h} \tag{2.3}$$

where r is the internal radius of curvature of the chamber and h is the wall thickness. In terms of the muscle performance, the peak wall stress relates to the amount of force and work the muscle does during a contraction. Therefore, peak wall stress is sometimes used as an index of afterload (Burkhoff, 2002).

A measure of afterload can be obtained from the PV loop, where the left or right ventricular pressure is plotted against the ventricular volume. Specifically, an index of afterload can be represented on the PV diagram, called E_a, which stands for effective arterial elastance and is closely related to R_{sys}. This value is shown schematically in Figure 2.10.

The hemodynamic consequences of an increase in left ventricular afterload are shown in the PV loop in Figure 2.10. Afterload E_a is represented by the slope of the dotted line connecting end-diastolic volume (EDV) on the x-axis and end-systolic pressure (P_{es}) on the y-axis. The first plot to the left (denoted by 'A') represents the baseline PV loop, plot 'B' to the right shows both the baseline PV loop and the PV loop with increased afterload. Point "a" represents P_{es} for loop 1 and "c" P_{es} for loop 2, respectively. As preload and thus EDV remain the same for both PV loops, it can clearly be seen in subfigure 'B' that loop 2 has an increased afterload represented by the increased slope of the E_a- line. It can also be noted, that the stroke volume (SV) is decreased for PV loop 2 as a result of having to pump against increased resistance or afterload.

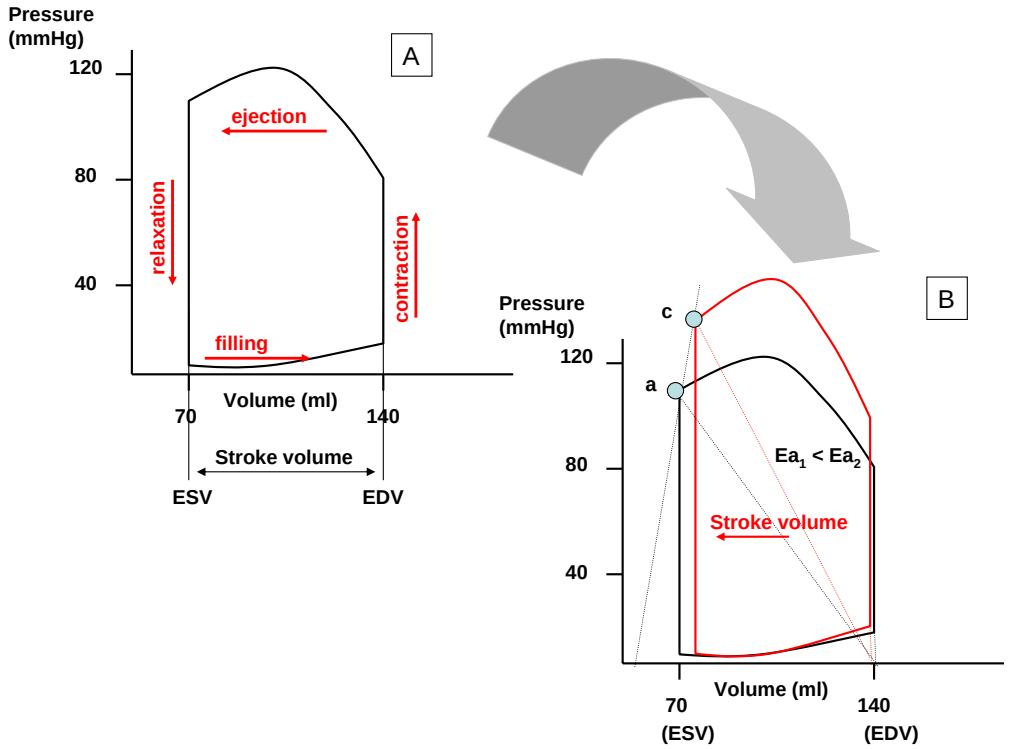

Figure 2.10: Effect of increased afterload on pressure-volume (PV) loop. The slope of the E_a- line increases for PV loop 2 and the SV decreases. Points "a" and "c" represent the end-systolic pressures (P_{es}).

2.5.3 Contractility

Myocardial contractility can be defined as the intrinsic ability of the myocardial muscle fibre to contract at a given fibre length. Physiologically, this intrinsic ability depends on the degree of binding between myosin and actin filaments within the fibre. The degree of binding in turn depends on the calcium concentration in the cell.

Effects of an increase in left ventricular contractility are shown in the PV loop in Figure 2.11. Subfigure 'A' represents the baseline PV loop and subfigure 'B' the PV loop with increased contractility. Contractility is represented by the slope of the end-systolic pressure volume relationship (ESPVR), which connects end-systolic pressure (P_{es}) with the x-axis volume intercept (V_0). Afterload (line E_a) and preload (EDV) remain unchanged. However, the contractility line, as denoted by "a" for the baseline loop and "c" for the increased contractility loop, respectively, is increased. In Figure 2.11 it can also be seen how the stroke

volume (SV) increases with increased contractility, illustrating how more blood is pumped per cycle as contractility of the heart muscle is increased.

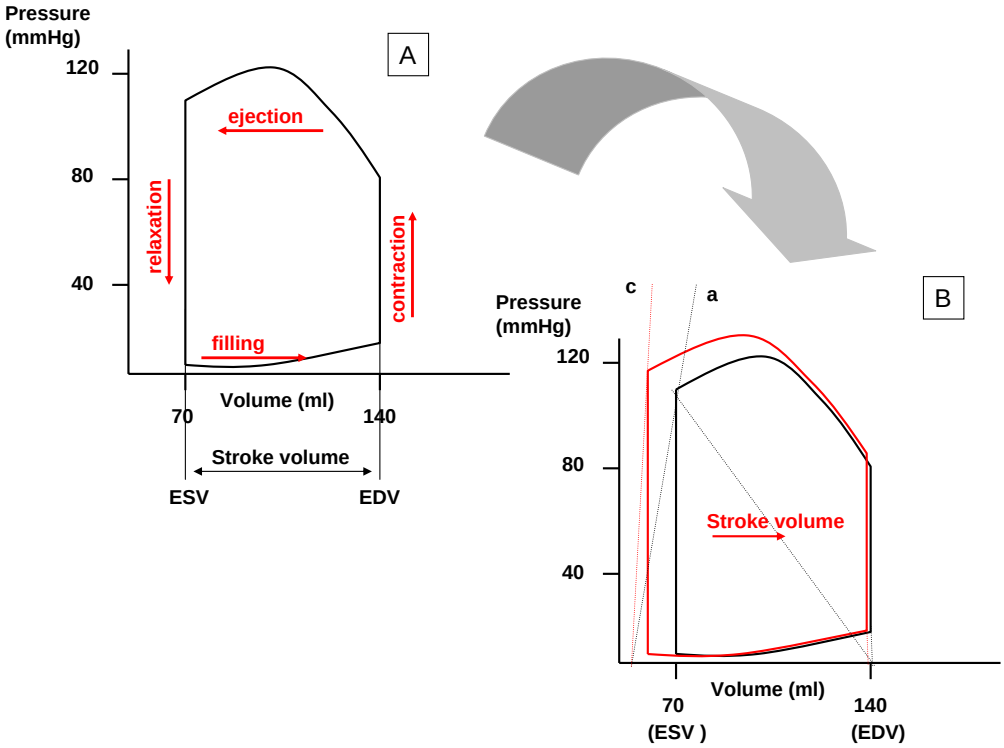

Figure 2.11: Effect of increased contractility on pressure-volume loop.

2.6 Ventricular Interaction

The right and left ventricle are connected via the interventricular septum. Ventricular interaction describes the interaction between the two ventricles. Thus, a change in the characteristics in one of the ventricles influences the other ventricle. Ventricular interaction across the interventricular septum is also called a direct interaction, whereas the delayed interaction via the pulmonary or systemic circulation is named a series interaction. The interventricular septum is shown in Figure 2.3 and a schematic given in Figure 2.12.

Septal motion can be obtained from echocardiographic observations (Hess *et al.*, 1979; Laurenceau & Dumesnil, 1976; Vieillard-Baron *et al.*, 2002) and normal motion is characterized by a leftward motion towards the left ventricle during systole. This motion occurs because in the healthy heart, the septum is bulged

convexly in a right anterior direction due to the comparatively high pressure in the left ventricle and the different anatomic shapes of the two ventricles. During systole and septal activation, the septum shortens and thus moves towards the left ventricle (Laurenceau & Dumesnil, 1976).

Despite the increasing transmural pressure gradient (P_{spt}) , which favours a rightward movement, the active septum continues to move leftwards until the end of systole (Chung *et al.*, 1997; Olansen *et al.*, 2000). During diastole, the septum becomes more compliant and thus more receptive towards changes in P_{spt}. The septum moves back towards the right ventricle. Figure 2.12 shows a schematic of the normal septal shape at the end of diastole.

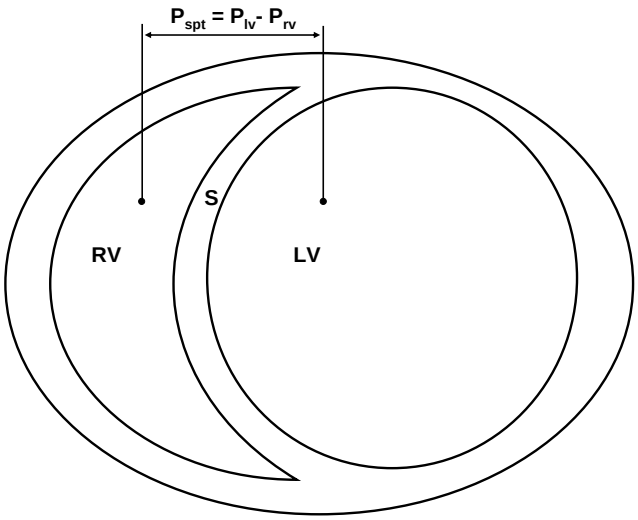

Figure 2.12: Schematic representation of the septum at end-diastole. During systole, the septum shortens, and posterior motion is observed (Laurenceau & Dumesnil, 1976). LV = left ventricle, RV = right ventricle and S = Septum.

In contrast to this normal septal shape, Figure 2.13 shows a schematic of the septal shape at end-diastole for an overloaded right ventricle. In this scenario, an anterior septal motion occurs as result of the septal shortening during systole (Laurenceau & Dumesnil, 1976).

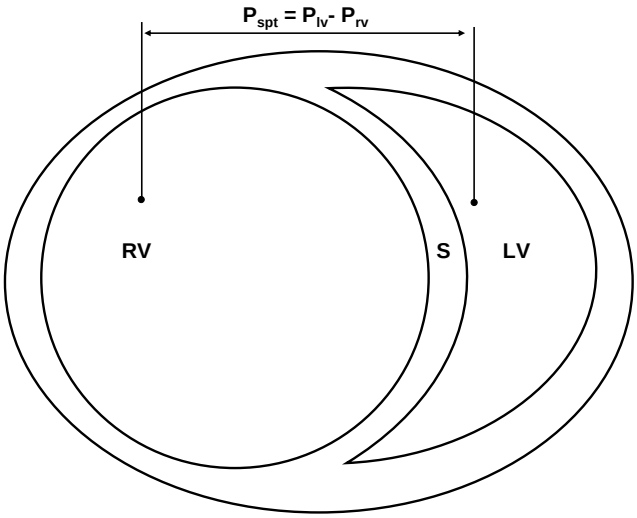

Figure 2.13: Septal shape at end-diastole for a significantly overloaded right ventricle (Laurenceau & Dumesnil, 1976). LV = left ventricle, RV = right ventricle and S = Septum.

2.6.1 Pericardium

The pericardium is a thin fibrous sac that surrounds the heart and consists of two layers, the visceral and parietal pericardium. An illustration of the pericardium is given in Figure 2.14. As the pericardium is relatively rigid, it prevents the ventricles from extensive dilation and thus plays an important role in ventricular interaction (Elzinga *et al.*, 1974; Little & Freeman, 2006). Furthermore, the pericardium appears essential for immediate bi-ventricular compensatory mechanisms in response to sudden changes in ventricular volumes (Kroeker *et al.*, 2003).

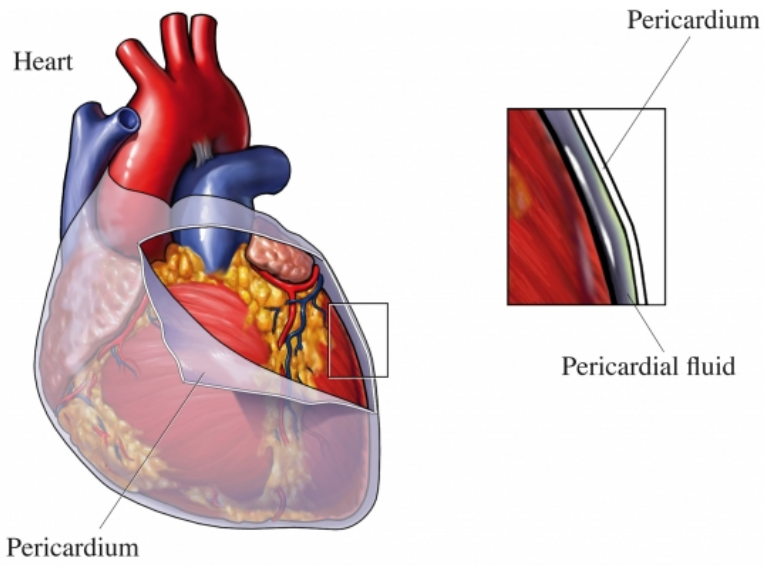

Figure 2.14: Illustration of the pericardium, obtained from The Ohio Heart and Vascular Center (Per, 2008).

2.7 Anatomy of the Lung

The lung consists of two parts, which are on either side of the heart. The left lung consists of two lobes, whereas the right lung has three lobes. Two main bronchi resulting from the bifurcation of the trachea enter the root of the lung where they continue to further divide. The lung's principal function is to transport oxygen into the bloodstream during inspiration, and to exchange it with carbon dioxide from the bloodstream during expiration. This gas exchange is accomplished by specialized cells that form millions of tiny, thin-walled air sacs. These alveolar sacs are made up of clusters of alveoli, like individual grapes within a bunch. The individual alveoli are tightly wrapped in blood vessels, and gas exchange occurs by diffusion. Figure 2.15 shows the anatomical overview of the lung and Figure 2.16 shows the more detailed view of the alveolar sacs within the lung.

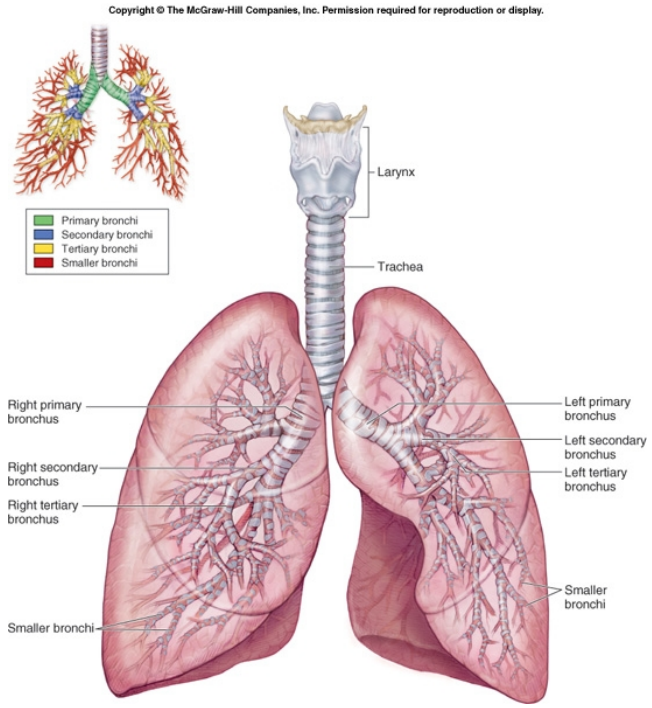

Figure 2.15: Overview of the lung (McKinley & O'Loughlin, 2007)

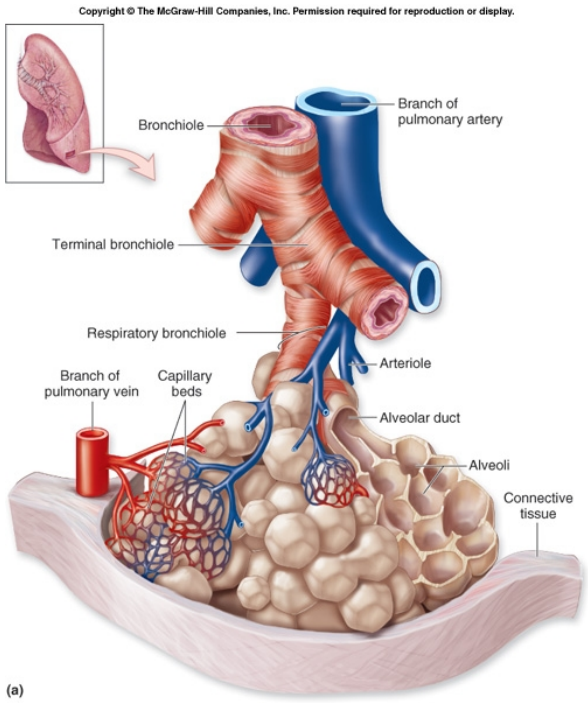

Figure 2.16: Overview of lung alveoli (McKinley & O'Loughlin, 2007)

2.8 Respiratory Physiology and Cardiopulmonary Interactions

Spontaneous breathing and ventilation can have extensive effects on thoracic cavity pressure and thus on cardiovascular function. These effects are usually well tolerated in healthy subjects, but may cause detrimental hemodynamic effects in critically ill patients, where pulmonary and/or cardiovascular diseases and dysfunction are present. It is thus important to understand the cardiopulmonary interactions and account for them when modelling the cardiovascular system.

2.8.1 Spontaneous Breathing

Spontaneous inspiration is characterized by a decrease in intrathoracic pressure (P_{th}), whereas expiration causes an increase in P_{th}. Intrathoracic pressure (P_{th}) is the pressure within the thoracic cavity. The following subsections briefly explain the different effects of P_{th} and pulmonary function on both ventricles. It has to be mentioned that in healthy patients the effects on the right heart usually predominate.

2.8.1.1 Cardiovascular Effects on the Right Ventricle

Preload Because the right atrium is an intrathoracic structure, changes in intrathoracic pressure directly affect right atrial pressure (P_{ra}). When intrathoracic pressure decreases, such as during inspiration, P_{ra} decreases. As a result, the backward pressure for venous return (VR) decreases, increasing VR. Reflex mechanisms will restore the pressure gradient by increasing the upstream pressure and thus regulate venous return to a steady value. Conversely, increases in P_{th} will increase P_{ra} and thus decrease RV preload and VR as happens during expiration.

Afterload Spontaneous inspiration will increase RV afterload. As inspiration decreases P_{th} and as both the heart and the pulmonary vessels are surrounded by P_{th}, the pressure load against which the RV must eject is given as pulmonary artery pressure (P_{pa}) relative to P_{th}. Conversely, expiration will have the opposite effect on RV afterload (Fessler, 1997).

2.8.1.2 Cardiovascular Effects on the Left Ventricle

Preload The left ventricle is affected by a change in venous return by direct and series ventricular interaction. Series interaction is effective through the pulmonary circulation and as the right ventricle output decreases so will eventually the left ventricle input from the pulmonary veins. The second mechanism is direct ventricular interaction. When venous return increases and the RV distends, the septum is shifted leftwards and the LV compliance during diastole is reduced. Thus, less blood will enter the LV during diastole and LV preload is reduced (Miro & Pinsky, 2005).

Afterload LV afterload is defined as systolic transmural LV pressure, which is given as intraluminal LV pressure minus P_{th}. (Fessler, 1997; Miro & Pinsky, 2005). From this fact it follows that at constant aortic pressure, when P_{th} decreases, LV afterload increases and vice versa. Usually, the preload effect of the RV dominates the afterload effect of the LV.

2.8.2 Positive Pressure Ventilation (PPV)

Positive pressure ventilation in critical care is common and increases P_{th}. When a positive end-expiratory pressure (PEEP) is added, P_{th} will be increased during the whole respiratory cycle. The hemodynamic consequences are similar to those already described, but with the salient difference that here P_{th} is always increased, even during inspiration.

The positive effects of positive pressure ventilation are, amongst others, that as P_{th} increases, LV afterload decreases. This outcome is desirable in patients with impaired myocardial function where a lowered afterload can help in restoring normal hemodynamic function (Shekerdemian & Bohn, 1990). Another benefit is that mechanical ventilation can reduce the cost or work of breathing and thus help to restore an adequate oxygen supply-demand relationship (Miro & Pinsky, 2005).

Figure 2.17 illustrates the different components of the airway pressure during mechanical ventilation, shown for an inspiratory-hold maneuver (Beers, 2006). Peak airway pressure is measured at the opening of the airway and is routinely displayed by ventilators. The peak airway pressure represents the pressure that is needed to overcome the inspiratory inflow resistance, the elastic recoil of the

lung and chest wall, and the alveolar pressure at the beginning of the breath. PEEP in the alveoli is normally the same as atmospheric pressure.

However, a distinction has to be made between intrinsic PEEP (autoPEEP) and therapeutically applied PEEP. Intrinsic PEEP is due to the aveoli failing to empty completely because of airway obstruction, airflow limitation or shortened expiratory time (Beers, 2006). Whereas, whenever PEEP is mentioned in this research, it refers to the externally applied PEEP, which is applied throughout the respiratory cycle. This therapeutic PEEP increases end-expiratory lung volume and reduces airway closure at the end of expiration, thus improving oxygenation and lung unit recruitment.

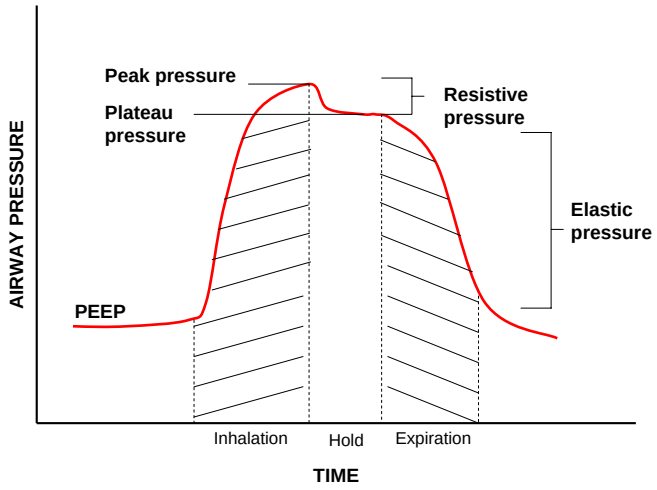

Figure 2.17: Components of airway pressure during mechanical ventilation, illustrated by an inspiratory-hold maneuver (Beers, 2006). The shaded areas indicate inhalation and expiration, respectively.

2.9 Summary

This chapter provided an overview of the cardiovascular anatomy and the basic cardiovascular and circulatory physiology concepts, such as preload, afterload and contractility were explained. Furthermore, the basic principles of ventricular interaction and heart-lung interactions during spontaneous and mechanically aided ventilation were presented. These fundamental ideas and concepts are used to

develop the cardiovascular system (CVS) model, which is presented in the next two chapters.

Chapter 3

Cardiovascular System (CVS) Model

This chapter describes the extended CVS model developed and utilized in this research. It thus explains how and why it was developed as it is for this diagnostic and decision support application. The first section provides a short overview of the physical and electrical background on how to calculate pressures, volumes and flows, and relates them to their corresponding equivalents in an electrical circuit. The remaining sections develop the model from these well-accepted fundamentals.

3.1 Overview of Cardiovascular System (CVS) Models

Mathematical representations can usually be divided into two categories: distributed and lumped. Distributed models are commonly described by using partial differential equations. Applications include modelling the velocity patterns in the heart and describing flows and pressures in arteries. Examples of such models are given in e.g. (Pedley, 1980; Peskin & McQueen, 1992; Smith *et al.*, 2003). Lumped models are obtained by discretizing the partial differential equations, yielding a system of ordinary differential equations and each discretized variable represents a compartment within the CVS model, e.g. (Chung *et al.*, 1997; Noordergraaf, 1978; Ottesen *et al.*, 2004; Smith *et al.*, 2004).

There are many CVS models in the literature ranging from very complex finite element models (Hunter & Smaill, 1991; Legrice *et al.*, 1997; McQueen *et al.*, 1982;

Pedley, 1980; Peskin & McQueen, 1992) to relatively simpler pressure volume approaches (Chung *et al.*, 1997; Stergiopulos *et al.*, 1999; Ursino, 1999). However, the focus is often on only specific areas of CVS dysfunction, such as modelling the arterial tree (Lanzarone *et al.*, 2007), simulating cardiovascular dynamics for healthy and diseased heart valves (Korakianitis & Shi, 2006), simulating baroreflex control (Schulz *et al.*, 1998) or simulating the effect of a left ventricular assist device (LVAD) on energetic relationships inside the left ventricle (Lazzari *et al.*, 1994). This list contains a selective few examples of many in the full literature.

There are full CVS models available (Kappel *et al.*, 2007; Liang & Liu, 2005; Olansen *et al.*, 2000; Ottesen *et al.*, 2004). However, patient-specific parameter optimization is either not considered or restricted to small subsets of the overall, much larger parameter set to describe specific aspects of the CVS, e.g. (Mukkamala & Cohen, 2001; Ottesen *et al.*, 2004). This approach dramatically limits the range of CVS disturbances that can be detected, thus prohibiting use as a broader diagnostic or monitoring tool. It equally limits the patient-specificity obtained with equal outcome. For relatively larger, more complex system models computational cost and feasibility can also be a major issue limiting or negating patient-specific modelling.

3.1.1 Windkessel Models

The simplest, fundamental model compartments are usually described using a Windkessel model, which was first described by the German physiologist Otto Frank in 1899 (Frank, 1899). 'Windkessel' is the German word for 'air chamber' and in the Windkessel model, a closed hydraulic circuit with a water pump is connected to a chamber. This circuit is filled with water except for a pocket of air in the chamber. As water is pumped into the chamber, the water compresses the air in it and water is pushed out of the chamber, back to the pump. The compressibility of the air in the chamber simulates the distensibility of the arteries, as blood is pumped into them (representing the compliance C). The resistance that the outflowing water encounters while flowing back to the pump, represents the resistance of the arterial tree and capillaries (resistance R). Finally, the inertia of the blood flow is represented by the inertance L.

3.1.2 Electrical Circuit Analogy

The cardiovascular system (CVS) can be modelled in terms of electrical circuits and many CVS models use an electrical analogy (Olansen *et al.*, 2000; Ottesen *et al.*, 2004; Smith, 2004). The CVS model in this research is also developed based on electrical circuits. Thus, a short overview about the cardiovascular-electrical correspondences is given in the following paragraphs.

In the electrical analogy used, electrical charge (Q) represents blood volume (V), while potential (U) represents pressure (P) and current (I) corresponds to flow rate (Q). An overview of these variables is given in Table 3.1.

Electrical and cardiovascular correspondences	
Electrical	Cardiovascular
Electrical charge (Q)	Blood volume (V)
Potential (U)	Pressure (P)
Current (I)	Flow (Q)
Resistance (R)	Resistance (R)

Table 3.1: Electrical and cardiovascular correspondences used to model the cardiovascular system.

In the CVS model, a vessel or group of vessels is described by the appropriate combination of resistors, capacitors and inductors, as shown in Figure 3.1 for the left ventricle. Blood vessel resistances, such as determined by the vessel diameter and blood viscosity, are modelled by resistors. The ability to accumulate ('store') and release blood due to elastic recoil is modelled by capacitors (compliance). Blood inertia is modelled using inductors. Finally, the heart valves are modelled as diodes to capture the one way nature of flow.

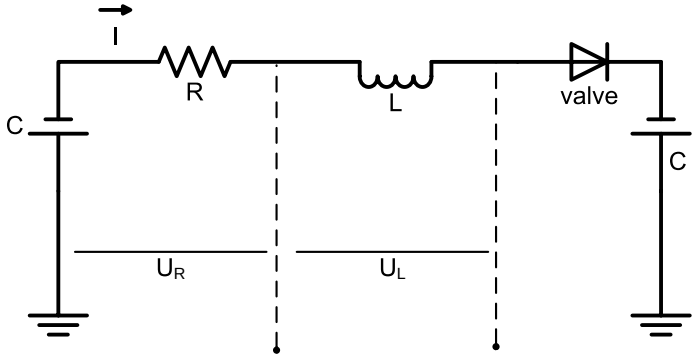

Figure 3.1: Electrical circuit analogy for CVS model (left ventricle).

Figure 3.1 shows the electrial components and Figure 3.2 the corresponding cardiovascular elements, as simulated for the left ventricle (LV) and aorta ($_{ao}$).

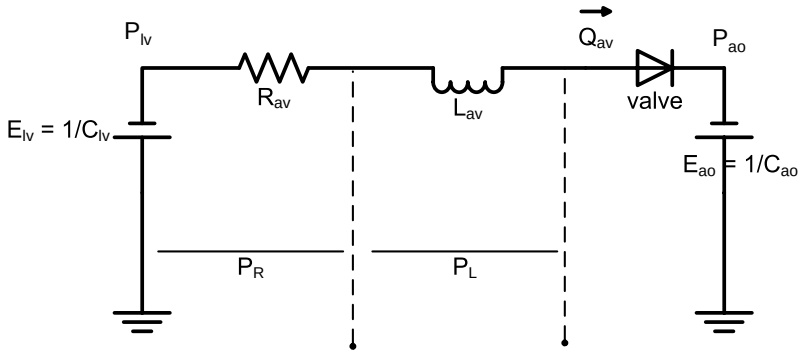

Figure 3.2: Cardiovascular elements for CVS model (left ventricle).

Equivalent systems of equations can be derived that govern the electrical and cardiovascular circuits:

Electrical resistance $\rightarrowtail$ vessel resistance

$$U = R \cdot I \tag{3.1}$$

as given by Ohm's law. From Equation 3.1 it follows that:

$$R = \frac{U}{I} \tag{3.2}$$

$$R = \frac{P}{Q} \tag{3.3}$$

Capacitance $\rightarrowtail$ vessel compliance

$$I = C \cdot \frac{dU}{dt} \tag{3.4}$$

From Equation 3.4 it follows that:

$$Q = C \cdot \frac{dP}{dt} \tag{3.5}$$

$$Q = \frac{1}{E} \cdot \frac{dP}{dt} \tag{3.6}$$

$$\frac{dP}{dt} = E \cdot Q \tag{3.7}$$

$$P = E \cdot \int Q dt \tag{3.8}$$

$$P = E \cdot V \tag{3.9}$$

Inductance $\rightarrowtail$ blood inertia

$$U = L \cdot \frac{dI}{dt} \tag{3.10}$$

From Equation 3.10 it follows that:

$$P = L \cdot \frac{dQ}{dt} \tag{3.11}$$

Diode $\rightarrowtail$ heart valve

$$I = \begin{cases} 0 & \text{if } U \leq 0 \\ \frac{U}{R} & \text{if } U > 0 \end{cases} \tag{3.12}$$

From Equation 3.12 follows:

$$Q = \begin{cases} 0 & \text{if } P \leq 0 \\ \frac{P}{R} & \text{if } P > 0 \end{cases} \tag{3.13}$$

Table 3.2 summarizes the analogies used in Equations 3.1-3.13.

Electrical and cardiovascular correspondences	
Electrical	Cardiovascular
Electrical resistance (R) $U = I \cdot R$	Vessel resistance (R) $P = Q \cdot R$
Electrical capacitance (C) $I = C \cdot \frac{dU}{dt}$	Vessel compliance (C) $Q = C \cdot \frac{dP}{dt}$
Inductance (L) $U = L \cdot \frac{dI}{dt}$	Blood inertia (L) $P = L \cdot \frac{dQ}{dt}$
Diode $I = \begin{cases} 0 & \text{if } U \leq 0 \\ \frac{U}{R} & \text{if } U > 0 \end{cases}$	Heart valve $Q = \begin{cases} 0 & \text{if } P \leq 0 \\ \frac{P}{R} & \text{if } P > 0 \end{cases}$

Table 3.2: Further Electrical and cardiovascular correspondences used to model the cardiovascular system.

Finally, from Equations 3.1-3.13 it follows that the overall system equations can be defined.

$$\Delta P = P_L + P_R \tag{3.14}$$

$$\Delta P = L \cdot \frac{dQ}{dt} + Q \cdot R \tag{3.15}$$

$$(P_1 - P_2) = L \cdot \frac{dQ}{dt} + Q \cdot R \tag{3.16}$$

$$\frac{dQ}{dt} = \frac{(P_1 - P_2) - Q \cdot R}{L} \tag{3.17}$$

From Equation 3.17 for example, the flow out of the left ventricle and across the aortic valve Q_{av} can be determined.

$$\dot{Q_{av}} = \frac{(P_{lv} - P_{ao}) - Q_{av} \cdot R_{av}}{L_{av}} \tag{3.18}$$

Similarly, equations for the right ventricle and pulmonary and systemic circulations are formulated, as detailed in the next section.

3.2 Definition of the CVS Model

The CVS model is a lumped parameter model that was previously developed by (Smith, 2004; Smith *et al.*, 2004) and is based in part on earlier similar work (Chung *et al.*, 1997; Lu *et al.*, 2001; Olansen *et al.*, 2000; Ottesen *et al.*, 2004). The original model consisted of six elastic chambers, with two active chambers for the left and right ventricle, respectively (Smith, 2004; Smith *et al.*, 2004). These pressure-volume chambers are each characterized by the flow in and out of the chamber, the pressure up- and downstream, the resistances of the heart valves, and inertia of the blood.

Figure 3.3 gives an overview of the volumes and pressures included in this CVS model for capturing clinically observed cardiovascular and circulatory dynamics. The original model has been extended in this research. An overview schematic of this new, extended model is given in Figure 3.4.

The following overall pressure and volume equations are derived:

$$V_{lv} = V_{lvf} + V_{spt} \tag{3.19}$$

$$V_{rv} = V_{rvf} - V_{spt} \tag{3.20}$$

$$V_{pcd} = V_{lv} + V_{rv} \tag{3.21}$$

$$P_{pcd} = P_{0pcd} \cdot (e^{\lambda_{pcd}(V_{pcd} - V_{0pcd})} - 1) \tag{3.22}$$

$$P_{peri} = P_{pcd} + P_{th} \tag{3.23}$$

where V_{pcd} represents the volume in the pericardium and P_{pcd} is the corresponding pressure across the pericardium and given by a time-varying P-V relationship. P_{peri} is the fluid pressure in the pericardial space. Volumes V_{lvf} and V_{rvf} are the left and right ventricle free wall volumes and V_{spt} is the septum volume. The flows in and out of the ventricles are defined:

$$\dot{Q_{av}} = \frac{(P_{lv} - P_{ao} - Q_{av} \cdot R_{av})}{L_{av}} \tag{3.24}$$

$$\dot{Q_{mt}} = \frac{(P_{pu} - P_{lv} - Q_{mt} \cdot R_{mt})}{L_{mt}} \tag{3.25}$$

$$\dot{Q_{pv}} = \frac{(P_{rv} - P_{pa} - Q_{pv} \cdot R_{pv})}{L_{pv}} \tag{3.26}$$

$$\dot{Q_{tc}} = \frac{(P_{vc} - P_{rv} - Q_{tc} \cdot R_{tc})}{L_{tc}} \tag{3.27}$$

where Q is the flow across the corresponding heart valve, L is the inertance and R the resistance. The subscripts $_{av}$, $_{pv}$, $_{mt}$ and $_{tc}$ stand for the aortic, pulmonary, mitral and tricuspid valves, respectively.

The pressures, volumes and flows in the pulmonary vein and artery, vena cava, aorta, and systemic and pulmonary capillaries are defined:

$Pressures:$

$$P_{pu} = E_{pu} \cdot (V_{pu} - V_{dpu}) + P_{th} \tag{3.28}$$

$$P_{pa} = E_{pa} \cdot (V_{pa} - V_{dpa}) + P_{th} \tag{3.29}$$

$$P_{vc} = E_{vc} \cdot (V_{vc} - V_{dvc}) + P_{th} \tag{3.30}$$

$$P_{ao} = E_{ao} \cdot (V_{ao} - V_{dao}) \tag{3.31}$$

$$P_{sys} = E_{sys} \cdot (V_{sys} - V_{dsys}) \tag{3.32}$$

$$P_{cap} = E_{cap} \cdot (V_{cap} - V_{dcap}) \tag{3.33}$$

$Volumes:$

$$\dot{V}_{pv} = Q_{pulout} - Q_{mt} \tag{3.34}$$

$$\dot{V}_{pa} = Q_{pv} - Q_{pulin} \tag{3.35}$$

$$\dot{V}_{vc} = Q_{vr} - Q_{tc} \tag{3.36}$$

$$\dot{V}_{ao} = Q_{av} - Q_{sys} \tag{3.37}$$

$$\dot{V}_{sys} = Q_{sys} - Q_{vr} \tag{3.38}$$

$$\dot{V}_{cap} = Q_{pulin} - Q_{pulout} \tag{3.39}$$

$$Flows:$$

$$Q_{sys} = \frac{(P_{ao} - P_{sys})}{R_{sys}} \tag{3.40}$$

$$Q_{vr} = \frac{(P_{sys} - P_{vc})}{R_{vr}} \tag{3.41}$$

$$Q_{pulin} = \frac{(P_{pa} - P_{cap})}{R_{pulin}} \tag{3.42}$$

$$Q_{pulout} = \frac{(P_{cap} - P_{pu})}{R_{pulout}} \tag{3.43}$$

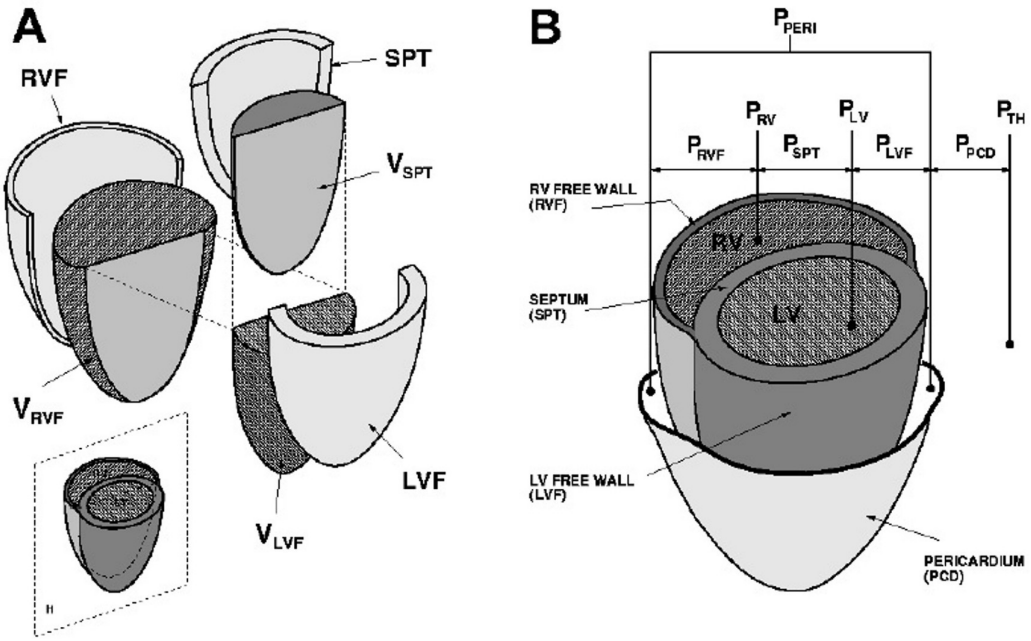

Figure 3.3: Volumes and pressure definitions used for modelling the heart and septal interaction (Chung *et al.*, 1997)

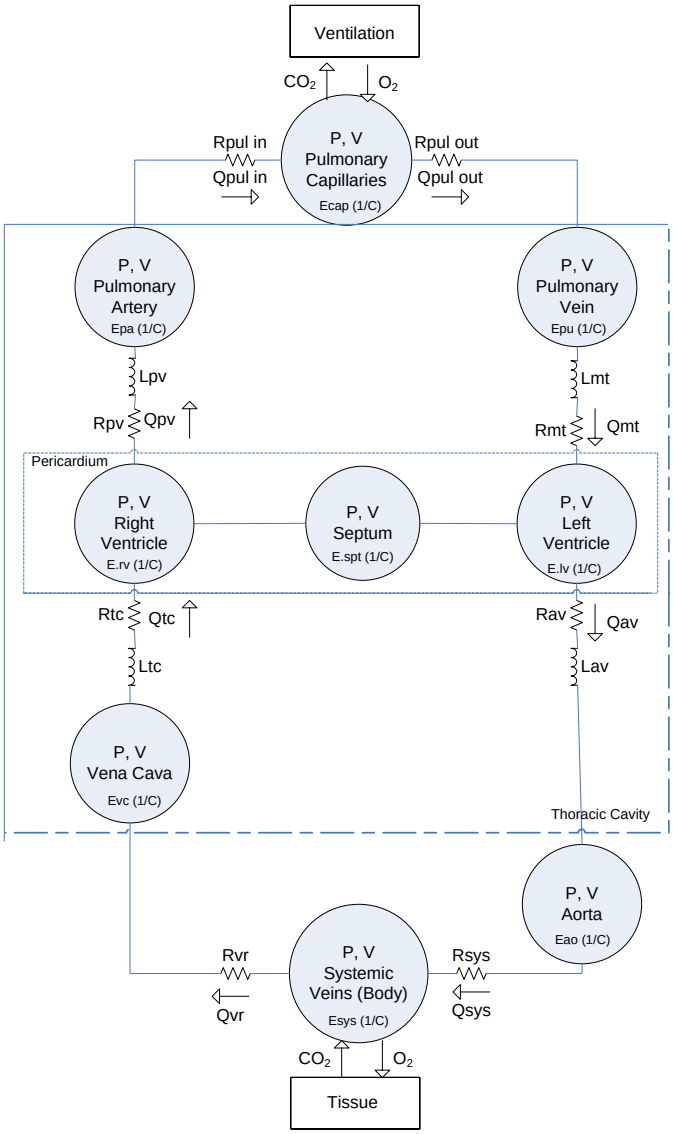

Figure 3.4: Overview of the extended CVS model used in this research with all major variables labelled.

3.2.1 Activation (Driver) Function

As discussed in Section 2.4, the time-varying elastance relates the ventricular pressure to its volume. In the CVS model we also need such a mechanism to relate the ventricle volume to its pressure. There are different ways of representing this time-varying elastance. In Section 2.4 the simplest possible relationship, a linear relationship, was used to show the basic concepts. To be more realistic and physiologically correct, a better mathematical representation is needed and introduced in this section as the activation (driver) function.

The linear ESPVR and non-linear EDPVR lines are defined (Chung *et al.*, 1997):

$$ESPVR = E_{eslvf} \cdot (V_{lvf} - V_{dlvf}) \tag{3.44}$$

$$EDPVR = P_{0lvf} \cdot (e^{\lambda_{lvf}(V_{lvf} - V_{0lvf})} - 1) \tag{3.45}$$

The driver function is then implemented as a sum of Gaussian terms (Chung *et al.*, 1997):

$$e(t) = \sum_{i=1}^{3} A_i \cdot e^{-B_i(t-C_i)^2} \tag{3.46}$$

where A, B and C are parameters corresponding to the magnitude, width and delay of the Gaussian curves, and are given in Table 3.3.

Driver Function $e(t)$			
Parameter [Unit]	i = 1	i = 2	i = 3
$A_i[unitless]$	0.9556	0.6249	0.018
$B_i[s^{-2}]$	255.4	225.3	4225.0
$C_i[s]$	0.3060	0.2026	0.2491

Table 3.3: Driver Function e(t) parameters.

Thus, the ventricle pressure is related to the ventricle volume by the relationship:

$$P_{lvf} = driL \cdot ESPVR_{LV} + (1 - driL) \cdot EDPVR_{LV} \tag{3.47}$$

$$P_{rvf} = driR \cdot ESPVR_{RV} + (1 - driR) \cdot EDPVR_{RV} \tag{3.48}$$

Substituting Equations 3.44 and 3.45 into Equations 3.47 and 3.48 yields the equations for the pressures in the left and right ventricles:

$$P_{lvf} = driL \cdot E_{eslvf} \cdot (V_{lvf} - V_{dlvf}) + (1 - driL) \cdot P_{0lvf} \cdot (e^{\lambda_{lvf}(V_{lvf} - V_{0lvf})} - 1) \tag{3.49}$$

$$P_{rvf} = driR \cdot E_{esrvf} \cdot (V_{rvf} - V_{drvf}) + (1 - driR) \cdot P_{0rvf} \cdot (e^{\lambda_{rvf}(V_{rvf} - V_{0rvf})} - 1) \tag{3.50}$$

$$P_{lv} = P_{lvf} + P_{peri} \tag{3.51}$$

$$P_{rv} = P_{rvf} + P_{peri} \tag{3.52}$$

with $driL$ and $driR$ being the driver functions for the left and right ventricle, respectively. Elastances E_{eslvf} and E_{esrvf} are the end-systolic elastances, and P_{0lvf} and P_{0rvf} are the end-diastolic elastances. Note that E_{eslvf} and E_{esrvf} are a measure of the ventricles' contractilities, whereas P_{0lvf} and P_{0rvf} are a measure of ventricle stiffness during diastole.

It can be seen from Equations 3.49 and 3.50 that the pressure is not completely linearly related to the volume throughout the cardiac cycle, but is represented as a sum of the "systolic" and "diastolic" terms. During systole, the right term of Equations 3.49 and 3.50 decreases and becomes zero at end-systole. At that point the pressure is only given by the ESPVR line using a linear relationship. During diastole the left term decreases, as the driver decreases, and the pressure is solely defined by the EDPVR line via the non-linear exponential term. Figure 3.5 shows the pressure that results from using this driver function in Equations 3.49-3.50 for a ventricle volume from $74ml$ to $127ml$, with $E_{eslvf} = 2.38$, $P_{olvf} = 0.56$, $\lambda_{lvf} = 0.033$, $V_o = V_d = 0$ and a heart beat period of $0.8s$.

3.2.1.1 Driver Functions for the Left and Right Ventricle

Figure 2.8 shows the time-varying elastance derived from the mechanical properties for the left ventricle. The time t_{max}, which defines the time when the maximum elastance E_{max} and therefore full depolarization is achieved, is approximately $0.3s$. It has been previously shown in human subjects that when the time-varying elastance $E(t)$ is normalized by its amplitude E_{max}, as well as the time t_{max}, the normalized $E_N(t_N)$ has a remarkably consistent shape, even in presence of a wide variety of cardiac dysfunctions (Senzaki *et al.*, 1996).

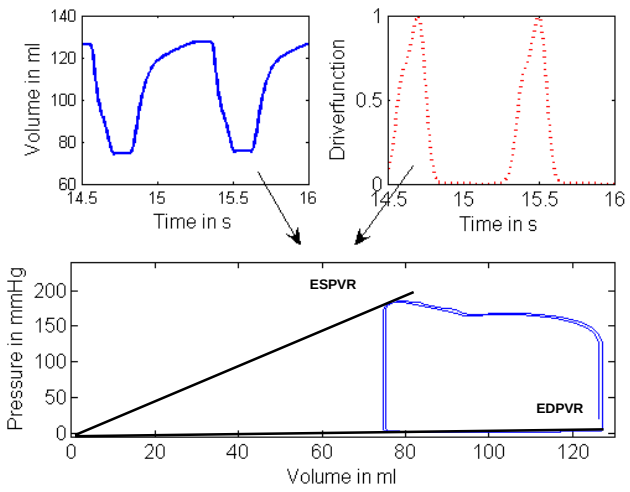

Figure 3.5: Relationship between ventricle volume and pressure via the driver function using Equations 3.49-3.50.

Hence, it can be assumed that this basic shape can be used as a general driver function for the CVS model. The shape of the driver function will thus remain constant. However, depending on the heart beat period, the function will need to either be compressed or stretched to account for the different electrical activation times.

For a healthy heart and assuming a normal electrical activation, it can be seen in Figure 2.4 that the impulse conduction through the left and right ventricle differs slightly. The right ventricle finishes depolarization a few milliseconds before the left ventricle. However, in a healthy heart these differences can be neglected and only one driver function proves to be sufficient (Chung *et al.*, 1997; Olansen *et al.*, 2000).

Given that assumption, it may be useful to simulate different electrical activation patterns. For example, in cases where electrical dysfunctions are present, such as bundle branch blocks. Hence, it might prove useful to allow different timing effects for the left and right ventricle.

To accomplish this possibility, the basic shape of the driver function remains constant, but the timing for the left and right ventricle will be different. For example, for a left bundle branch block (LBB) , the left ventricle and septum

will have a delayed activation. To account for such a difference, the normalized $E_N(t_N)$ is transformed using two different activation durations, one for the left and one for the right ventricle. Figure 3.6 demonstrates the two resulting driver functions for three heart beats and zoomed into one heart beat for better comparison of the two functions.

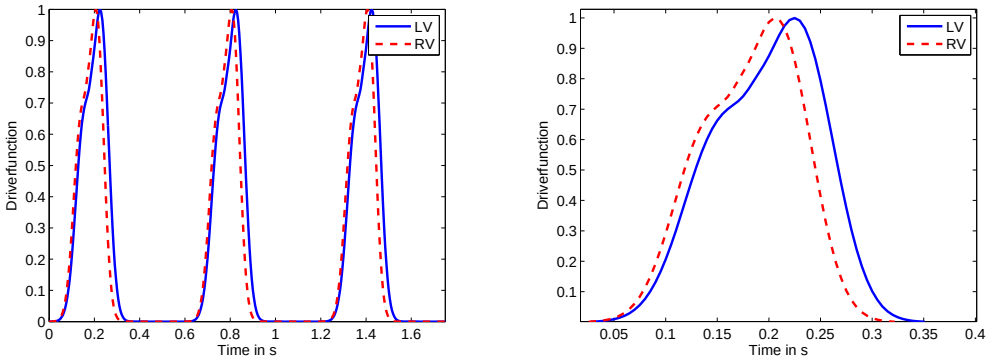

(a) for 3 heart beats and durations of activation of $0.55s$ and $0.6s$, respectively

(b) zoomed into one heart beat

Figure 3.6: Left ventricle (LV) and right ventricle (RV) driver functions

During this research, it has turned out that using one driver function and keeping this driver function constant throughout the identification process, has several advantages for the consistent identification of the model parameters during developing disease states. This choice is physiologically justifiable as long as it can be assumed that there is no developing abnormality in impulse conduction. Second, keeping the driver function fixed, guarantees that all effects attributable to an enhanced ventricle pressure generation are because of a change in contractility and thus because of a change in the ESPVR. In contrast, if the driver function were to be changed, the effect of a change in ESPVR and the two ventricle contractilities (E_{eslvf}, E_{esrvf}) would be lost, which would potentially impact diagnostic capability. Consequently it would be much more difficult to correctly identify all the parameters of the CVS model as a change in the driver function may have unforeseen or masking effects on the other CVS model parameters identified. Therefore, in this research the driver function, as given by Table 3.3, is kept constant.

3.2.2 Ventricular Interaction

Ventricular interaction is an important dynamic because it directly relates the hemodynamic functioning of one ventricle to the other, as described in Section 2.6. It thus needs to be taken into account when modelling the heart, as it can be a factor for significant differences between left and right ventricle output signals such as volumes and pressures that otherwise cannot be explained. This requirement is especially valid in cases of abnormal pathological conditions, such as overloaded right ventricles during pulmonary hypertension where direct ventricular interaction contributes significantly to LV filling impairment (Gan *et al.*, 2006).

3.2.2.1 Septum Volume Calculation

Ventricular interaction is included in the CVS model by modelling the septum as given in Equations 3.19 and 3.20. These equations are repeated here for clarity:

$$V_{lv} = V_{lvf} + V_{spt} \tag{3.53}$$

$$V_{rv} = V_{rvf} - V_{spt} \tag{3.54}$$

where V_{lvf} and V_{rvf} are the right and left ventricle free wall volumes, V_{lv} and V_{rv} are the volumes in the left and right ventricle, and V_{spt} is the volume of the interventricular septum. From Equation 3.53 follows that an increase in V_{lv} results in an outward displacement of the left ventricular free wall and thus in a displacement of the septum towards the right ventricle. Thus, a rightward shift of the septum from the left towards the right ventricle is represented by an increase in V_{spt}, whereas a leftward shift is represented by a decrease in V_{spt}. The septum volume is described by a time-varying P-V relationship defined (Chung *et al.*, 1997):

$$P_{spt} = driS \cdot E_{esspt}(V_{spt} - V_{dspt}) + (1 - driS) \cdot P_{0spt}(e^{\lambda_{spt}(V_{spt} - V_{ospt})} - 1) \tag{3.55}$$

where the driver function $driS$ describes the activation of the septum. The septum volume V_{spt} can be determined analytically using the methods given in Hann *et al.* (2006):

$$V_{spt} = a/b \tag{3.56}$$

with a and b defined:

$$\begin{aligned} a = \Bigg(& driS \cdot E_{esspt} \cdot V_{dspt} \\ & + driL \cdot E_{eslvf} \cdot (V_{lv} - V_{dlvf}) \\ & - driR \cdot E_{esrvf} \cdot (V_{rv} - V_{drfv}) \\ & - (1 - driS) \cdot P_{0spt} \cdot (b_{spt} e^{-\lambda_{spt} V_{ospt}} - 1) \\ & + (1 - driL) \cdot P_{0lvf} \cdot (b_{lvf} e^{\lambda_{lvf}(V_{lv} - V_{olvf})} - 1) \\ & - (1 - driR) \cdot P_{0rvf} \cdot (b_{rvf} e^{\lambda_{rvf}(V_{rv} - V_{orvf})} - 1) \Bigg) \end{aligned} \tag{3.57}$$

$$\begin{aligned} b = \Bigg(& driS \cdot E_{esspt} \\ & - driL \cdot E_{eslvf} - driR \cdot E_{esrvf} \\ & + (1 - driS) \cdot P_{0spt} \cdot a_{spt} e^{-\lambda_{spt} V_{ospt}} \\ & - (1 - driL) \cdot P_{0lvf} \cdot a_{lvf} e^{\lambda_{lvf}(V_{lv} - V_{olvf})} \\ & + (1 - driR) \cdot P_{0rvf} \cdot a_{rvf} e^{\lambda_{rvf}(V_{rv} - V_{orvf})} \Bigg) \end{aligned} \tag{3.58}$$

where a_{spt}, a_{lvf}, a_{rvf}, b_{spt}, b_{lvf} and b_{rvf} are defined:

$$x_1 = V_{spt,old} + \triangle V_{spt} \tag{3.59}$$

$$x_2 = V_{spt,old} - \triangle V_{spt} \tag{3.60}$$

$$a_{spt} = \frac{e^{\lambda_{spt} x_2} - e^{\lambda_{spt} x_1}}{x_2 - x_1} \tag{3.61}$$

$$a_{lvf} = \frac{e^{\lambda_{lvf} x_2} - e^{\lambda_{lvf} x_1}}{x_2 - x_1} \tag{3.62}$$

$$a_{rvf} = \frac{e^{\lambda_{rvf} x_2} - e^{\lambda_{rvf} x_1}}{x_2 - x_1} \tag{3.63}$$

$$b_{spt} = e^{\lambda_{spt} x_1} - (e^{\lambda_{spt} x_2} - \frac{e^{\lambda_{spt} x_1}}{x_2 - x_1} x_1) \tag{3.64}$$

$$b_{lvf} = e^{\lambda_{lvf} x_1} - (e^{\lambda_{lvf} x_2} - \frac{e^{\lambda_{lvf} x_1}}{x_2 - x_1} x_1) \tag{3.65}$$

$$b_{rvf} = e^{\lambda_{rvf} x_1} - (e^{\lambda_{rvf} x_2} - \frac{e^{\lambda_{rvf} x_1}}{x_2 - x_1} x_1) \tag{3.66}$$

$$\tag{3.67}$$

where $V_{spt,old}$ is the V_{spt} in the previous time step and $\triangle V_{spt} = 0.1ml$.

Figure 3.7 shows in the upper panels the right and left ventricle free wall volumes (V_{lvf}, V_{rvf}) and in the bottom panel the septum volume (V_{spt}). The solid lines represent a healthy heart, where the septum moves towards the left ventricle during systole. The dotted lines represent a left bundle branch block (LBB) with a delayed left ventricle and septum activation, as explained earlier in Section 3.2.1.1. In the lower panel it can be seen that V_{spt} shows an abnormal (paradoxical) septal motion towards the right ventricle during systole, as clinically observed during LBB conditions (Olansen *et al.*, 2000). The LBB condition was simulated choosing a time delay of $60ms$ for the left ventricle and $20ms$ for the septum.

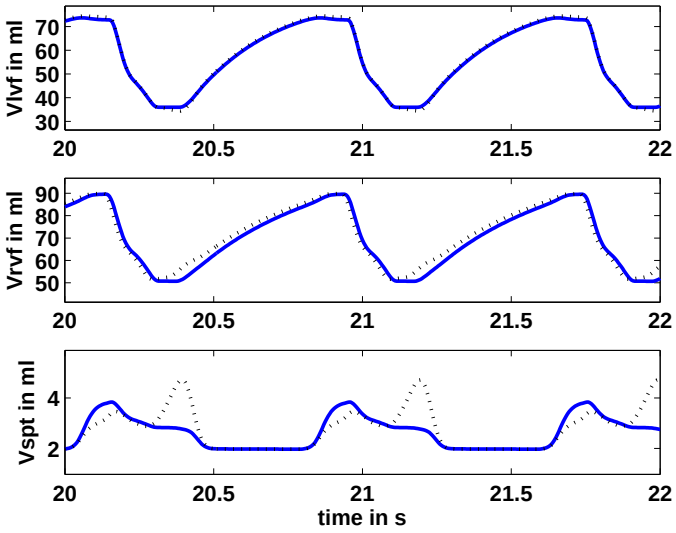

Figure 3.7: Left ventricle free wall (V_{lvf}), right ventricle free wall (V_{rvf}) and septum volume (V_{spt}) during normal electrical activation (solid lines) and LBB (dotted lines).

3.3 Summary

This chapter gave an overview of the different approaches to model the cardiovascular system and explained how the extended CVS model used in this research was derived using well-accepted electrical circuit analogies. Additionally, all CVS model pressures, volumes and flows were defined and the direct ventricular interaction was described in terms of systolic and diastolic interdependencies. The activation (driver) function was revisited and an example of an abnormal electrical impulse conduction provided.

Appendix A summarizes the CVS model equations for the ventricle volumes and flows in Equations A.1-A.9. The remaining CVS model pressures, volumes and flows are given in Equations A.10-A.25. Additionally, the driver (activation) function is summarized in Equation A.26 and Table A.1. The definition of ventricular interaction and the septum volume calculation are available in Equations A.34-A.44.

Chapter 4

Integration with Cardiopulmonary System and Circulation

This chapter outlines the interactions between the cardiovascular, cardiopulmonary systems and circulation. As mentioned in Section 2.8, the respiratory system and cardiovascular system are coupled and heart-lung interactions occur with every breath. These heart-lung interactions are usually not very profound in healthy subjects, but are often exaggerated in critically ill patients (Fessler, 1997; Miro & Pinsky, 2005; Pinsky, 2005; Smith *et al.*, 1982).

4.1 Hemodynamic Effects of Ventilation

Section 2.8 gave a brief overview of the different effects spontaneous and mechanical ventilation have on the left and right ventricle pump performance. The CVS model was developed and formulated in Section 3.2 to account for these occurrences. This section gives a more detailed description of how the CVS model works and how respiration-specific phenomena are captured by the model.

Note that in Section 3.2, the intrathoracic pressure, P_{th}, in Equations 3.28-3.43 is added only to the pulmonary artery, vein and vena cava. However, it is not added to the aorta and pulmonary capillaries. This modelling choice has been made to correctly represent the specific anatomy where the pulmonary arteries and veins, and the vena cava are within the thoracic cavity. However, neither the aorta, as modelled as part of the systemic circulation, nor the lung

capillaries, surrounded by alveolar pressure, are surrounded by P_{th}. As a result, the cardiopulmonary interactions during spontaneous or mechanical ventilation can be correctly simulated, based on an accurate physiological representation of pulmonary pressures. A brief summary of these interactions and the expected hemodynamic changes as caused by changes in P_{th} are given in Table 4.1.

Cardiopulmonary Interactions				
Pth	RV - afterload	RV - preload	LV - afterload	LV - preload
increase ↑	*decrease* ↓	*decrease* ↓	*decrease* ↓	*decrease* ↓
decrease ↓	*increase* ↑	*increase* ↑	*increase* ↑	*increase* ↑

Table 4.1: Cardiopulmonary interactions as caused by changes in intrathoracic pressure P_{th}.

Usually the preload effect of the RV is predominant over the afterload effect of the LV. By substituting an increased or decreased value for P_{th} into Equations 3.28 - 3.43, it can be seen that an increase in P_{th} causes the RV preload to decrease, as the pressure gradient for VR is reduced by this change. RV afterload is also decreased not by increasing the pressure gradient for flow out of the RV, but by increasing the pressure gradient for flow into the lung (Q_{pulin}). Thus, the resistance R_{pulin} is a direct measure for RV afterload in this CVS model. Furthermore, it can be seen that LV preload decreases as the pressure gradient for flow out of the lung (Q_{pulout}) decreases and LV afterload decreases as the pressure gradient for ejection from the LV increases. Opposite effects can be observed when P_{th} decreases.

4.1.1 Transient Effects

As respiratory-induced changes in P_{th} are transmitted directly to all vessels in the thoracic cavity, fluctuations obtained when measuring pressure signals, such as the pressures in the pulmonary artery (P_{pa}) or vena cava (P_{vc}), implicitly give information about the magnitude of changes in P_{th} (Miro & Pinsky, 2005). These variations are known as transient effects because they occur during any given respiratory cycle. Figure 4.1 summarizes the different transient effects on RV and LV venous return caused by changes in P_{th}. During spontaneous

inspiration, P_{th} decreases and VR increases. The opposite effect occurs during positive pressure inspiration, where P_{th} increases and VR drops.

Figure 4.2(a) shows these transient effects for P_{pa} (upper panel) and P_{vc} (middle panel) during spontaneous inspiration where P_{th} decreases during the respiratory cycle. However, the fluctuations in the pressure in the aorta (P_{ao}, lower panel) are much lower. This is an expected result because the aorta in the CVS model is modelled outside the thoracic cavity. Thus, strictly speaking, it does not represent the aorta specifically, but instead covers the aorta and the arterial system of the systemic circulation. Hence, the fluctuations are lower because they do not extend to the entire arterial system, captured by this model compartment.

Figure 4.2(b) shows the venous return flow for the RV (Q_{vr}) in the upper panel and the venous return to the LV (Q_{pulout}) in the lower panel. It can clearly be seen that when P_{th} decreases during inspiration, Q_{vr} and Q_{pulout} increase. Clinically and physiologically, this result is also as expected.

Figures 4.2 and 4.1 were obtained by running the CVS model with changing values for P_{th}. During spontaneous inspiration, intrathoracic pressure (P_{th}) decreases, but on positive-pressure ventilation (PPV), inspiration occurs by an increase in intrathoracic pressure. Therefore, for spontaneous breathing P_{th} varied from $0mmHg$ to $-6mmHg$ during inspiration and back to $0mmHg$ during expiration. For positive pressure ventilation (PPV) P_{th} decreased from $2mmHg$ to $6mmHg$ during inspiration and dropped back to $2mmHg$ during expiration, representing a PEEP of $2.72cmH_2O$.

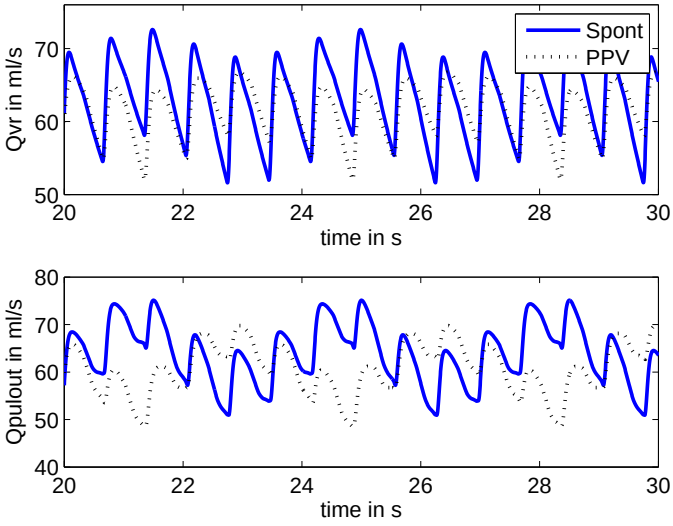

Figure 4.1: Transient effects during spontaneous breathing (solid line) and PPV (dotted line)

4.1.2 Steady-State Effects

Steady-state effects are prolonged effects in the cardiovascular system. They are characterized by changes in cardiac output and/or changes in blood volume distribution caused by mechanical and compensatory reflex mechanisms. Mechanical ventilation, for example PPV with additional PEEP, can cause profound steady-state effects in critically ill patients.

More specifically, it is known that PEEP often reduces VR and thus cardiac output (CO) (Cassidy *et al.*, 1948; Fessler, 1997; Miro & Pinsky, 2005; Shekerdemian & Bohn, 1990). Over the years there has been some controversy about how, exactly, PEEP alters VR. Some investigators have concluded that PEEP decreases VR by reducing the pressure gradient ($P_{sys} - P_{ra}$) (Johnston *et al.*, 1989; Wise *et al.*, 1981). Note that clinically P_{sys} is the mean systemic pressure, which is also known as mean circulatory filling pressure (MCFP). Furthermore, because the CVS model does not explicitly model the right atrium, but lumps it together with the vena cava, P_{ra} is represented in the model by P_{vc}. In contrast, other researchers have demonstrated that P_{sys} and P_{ra} change equally during positive airway pressure, and thus a change in the driving pressure gradient cannot be the reason for decreases in VR during PEEP (Fessler, 1997; Jellinek *et al.*, 2000; Peters *et al.*, 2001). Recent publications suggest that the main effect by which

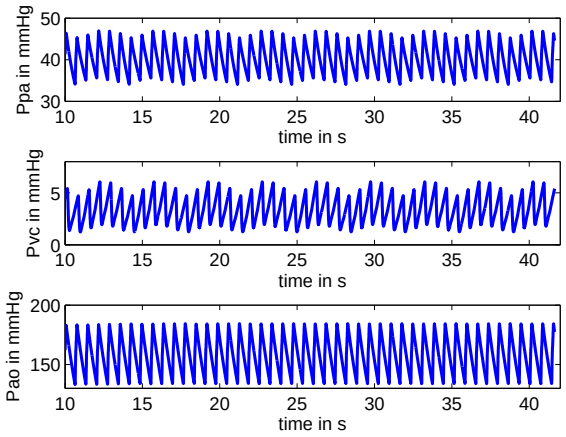

(a) Pressure in pulmonary artery (P_{pa}, top), vena cava (P_{vc}, middle) and aorta (P_{ao}, bottom)

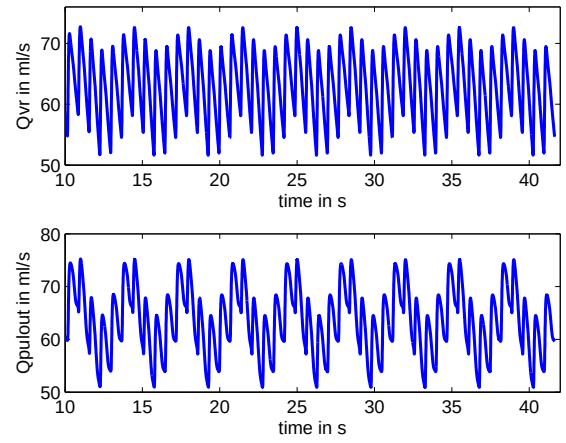

(b) Venous return flow for RV (Q_{vr}, top) and LV (Q_{pulout}, bottom)

Figure 4.2: Heart-lung interactions, as simulated during spontaneous breathing

PEEP decreases venous return is by increasing the resistance to venous return (Fessler, 1997; Miro & Pinsky, 2005; Shekerdemian & Bohn, 1990), as modelled by R_{vr} in the model.

4.1.2.1 Simulating PEEP in the CVS Model

To accurately simulate different values of PEEP in the CVS model, certain model parameters need to be adjusted whenever PEEP is applied. These parameters are the resistance to VR, R_{vr}, and to a lesser extent R_{pulout}. Another parameter that needs adjusting is the venous capacitance or the venous vascular tone, which together with the amount of stressed and unstressed blood volume determines how much blood is contained in the venous vascular system. Figure 4.3 illustrates the relationship between unstressed (V_{dsys}) and stressed (V_{sys}) vascular volume, systemic elastance (E_{sys}), and the mean systemic pressure (P_{sys}).

It can be seen from Figure 4.3 that several factors affect venous volume, which in turn plays an important part in determining venous return to the right heart. When the compliance of the venous system decreases, or the elastance E_{sys} increases, P_{sys} is increased and so is the pressure gradient for VR. This pressure gradient is also elevated when volume is increased either by an infusion, as part of fluid resuscitation or therapy, or a shift from the unstressed to the stressed volume.

During PEEP, VR is decreased not by altering the pressure gradient ($P_{sys} - P_{ra}$) but by increasing R_{vr}. Thus, different PEEP levels are simulated in the CVS model by adjusting the values for R_{vr}. However, reflex response mechanisms of the body then act to counter this effect by decreasing unstressed volume and thus increasing stressed volume. This action, in turn, leads to a rise in the effective systemic volume (V_{syseff}) and thus in P_{sys}. This overall net action helps to sustain the pressure gradient for VR (Jacobsohn *et al.*, 1997; Peters *et al.*, 2001).

These reflex response mechanisms have to be taken into account when modelling the hemodynamic effects of PEEP. However, during hypovolemia, PPV and PEEP may inhibit the additional fluid absorption from the tissues to increase stressed plasma volume. This occurs because the elevated venous pressures may cause fluid losses into the interstitium from the capillaries (Peters *et al.*, 2001).

To summarize, the effect of PEEP is therefore simulated in the CVS model by a/an:

- Increase in P_{th} (Fessler, 1997; Miro & Pinsky, 2005; Pinsky, 2005)
- Volume shift from ITBV to systemic volume ⇒ decrease in PBV and decrease in V_{dsys} ⇒ increase in V_{syseff} (Jacobsohn *et al.*, 1997; Nanas & Madger, 1992; Peters *et al.*, 2001)

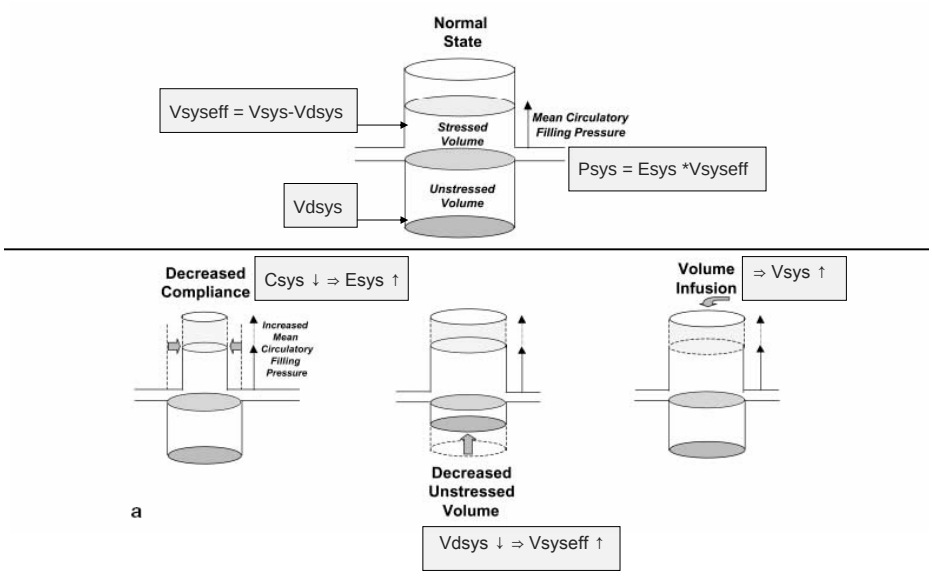

(a) Relationship between V_{dsys}, V_{sys}, E_{sys} and P_{sys}

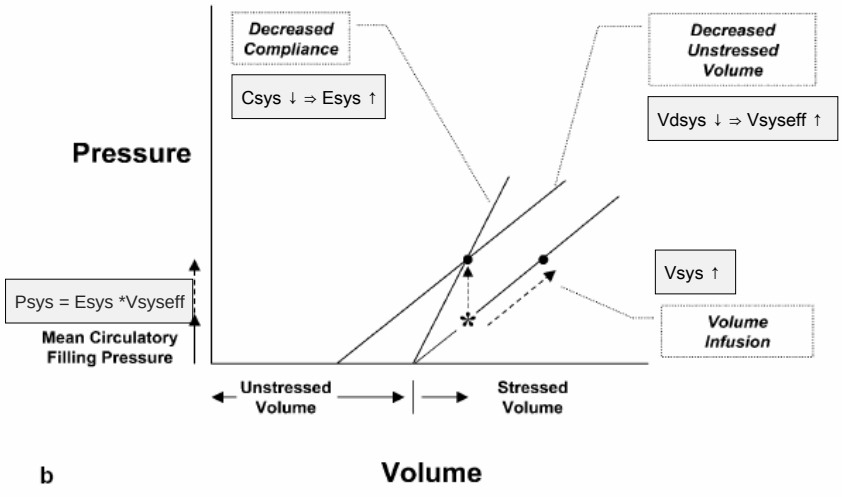

(b) Systemic Pressure Volume Relationships

Figure 4.3: Factors influencing venous return by increasing P_{sys} (Peters *et al.*, 2001)

- Decrease in RV preload ⇒ increase in R_{vr} (Fessler, 1997; Miro & Pinsky, 2005; Pinsky, 2005)
- Increase in pulmonary vascular resistance as caused by lung inflation at high lung volumes ⇒ increase in R_{pulin} (Fessler, 1997; Miro & Pinsky, 2005; Pinsky, 2005)
- Decrease in LV afterload ⇒ decrease in R_{sys} (Fessler, 1997; Miro & Pinsky, 2005; Pinsky, 2005)

4.2 Volume Effects in the CVS Model

Following from these considerations, it is obvious that the systemic volume V_{sys} is not only modelled using Equation 3.38, but that the effects of reduced or increased stressed and/or unstressed volume have to be taken into account as well. The same logic applies for the volume associated with the pulmonary capillaries compartment, V_{cap}.

Note, that for reasons of simplicity, the unstressed volumes in all other volume compartments are omitted. This omission is justifiable, as basically only one compartment on either side of the pulmonary and systemic circulation is necessary for simulating the clinical and physiological actions where changes in stressed and/or unstressed volume occur. These compartments should logically be the compartments where the most volume is contained and where any changes occur in stressed and unstressed volume. Thus, choosing V_{sys} and V_{cap} makes sense as they are the largest volumes and the compartments where exchanges in volume occur. The other volume compartments in the CVS model, such as V_{vc}, V_{ao}, V_{pa} and V_{pv} mainly serve as blood 'transferring' compartments moving stressed volume around the circulation.

Note that one significant limitation of this simplification process is introduced by setting the unstressed volume zero ($V_d = 0$) for the left and right ventricle volumes. Figure 4.4 shows the different ESPVR curves that are obtained for the same P-V loop with $V_{d1} = 0ml$ compared to $V_{d2} = 10ml$. Thus, the identification process would obtain somewhat inaccurate contractility values when $V_d = 0$ is incorrectly assumed.

However, as for most of the experiments, the ventricle volumes V_{lv}, V_{rv} are not measured, but only estimated. Thus, there is no way to prevent this issue as

it is not possible to identify both E_{es} and V_d due to the limited amount of data that is readily available. Therefore, for reasons of comparability and consistency V_d is set to 0 for all identifications. However, as a result, when interpreting the value of the identified E_{es} value one has to take the effects of V_d into account.

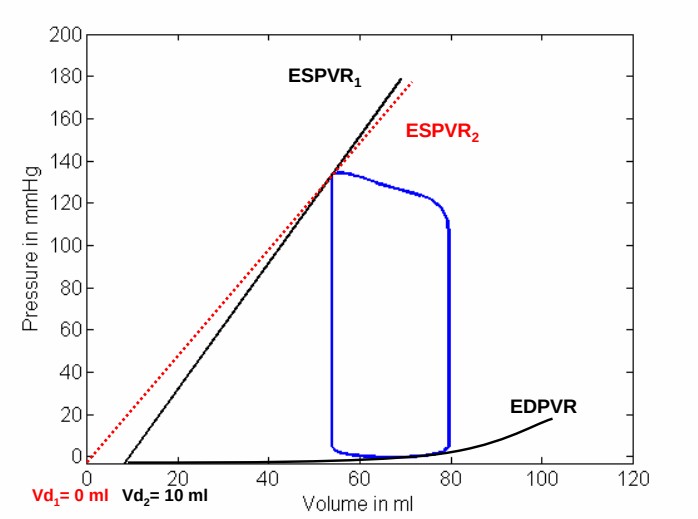

Figure 4.4: Different ESPVR curves are obtained for different V_d values, but the same P-V loop in all other respects.

There are no such similar problems for the other volume compartments. It does not matter how much volume these compartments contain as only the compartment pressures are important. In other words, as the pressure is the product of volume and elastance, the more volume these compartments contain, the smaller the elastance will be (the bigger the compliance) and vice versa. However, these peripheral compartment elastances are not measurable to specific values and not clinically important aside from trends as condition changes. Thus, not accounting for $V_d \neq 0$ has little outcome effect.

More specifically, it can be shown in the CVS model that different volumes in these compartments do not significantly affect the other model parameters. Importantly, similar parameters are identified in these parametric studies, independent of how the initial volume estimates are chosen. The only difference that can be expected are changes in the elastances to compensate for changes in the volumes as discussed previously. Of course, it must be ensured that all volume estimations are within a reasonable physiological range to avoid elastance and other parameter values that are completely unphysiological.

As mentioned before, $V_{syseff} = V_{sys} - V_{dsys}$, the stressed (or effective) volume, should be independent from changes in Q_{vr} and Q_{sys} to find the new steady-state baseline value. Once this new baseline for V_{syseff} is found by either adding or subtracting volume, the change in V_{sys} can be modelled as in Equation 3.38 as the difference between the in- and outflow into/from the V_{sys} compartment.

The mechanisms by which the effective systemic volume is regulated are manifold. Here, V_{syseff} is modelled as $(V_{sys} - V_{dsys})$, where the unstressed volume V_{dsys} includes not only the intravascular, unstressed volume, but also the extravascular volume that is lost from the capillaries into the tissues. Hence, V_{dsys} is defined:

$$V_{dsys} = V_{unstressed} + V_{extravascular} \tag{4.1}$$

where the unstressed volume changes with, for example, different PEEP values as has been reported by Nanas & Madger (1992), who showed that increasing PEEP values decrease V_{dsys}. The simplest approach to modelling the extravascular volume and thus capillary-tissue fluid balance is to set the inflow and outflow to be equal in steady state. Thus, the extravascular volume will remain constant for a given hemodynamic state and so will the effective systemic volume V_{syseff} as long as no additional fluids are given or lost from the body. A more advanced

approach to modelling capillary fluid exchange would include modelling the fluid transfer in the form of a net driving force (NDF) (Klabunde, 2004):

$$NDF = (P_C - P_T) - \sigma(\pi_C - \pi_T) \tag{4.2}$$

with σ = reflection coefficient (represents permeability of the membrane), P_C = capillary hydrostatic pressure, P_T = tissue hydrostatic pressure, π_C = capillary plasma oncotic pressure and π_T = tissue fluid oncotic pressure. If NDF is positive, filtration into the tissues occurs, and if negative, reabsorption into the capillaries.

4.2.1 Volume Calculations Based on TBV and GEDV

The parameter identification process needs the two ventricle volumes V_{lv}, V_{rv} as input signals to accurately determine some of the parameters. More specifically, the end-diastolic and end-systolic volumes (EDV, ESV) are needed. However, these volumes are usually not available in a clinical environment and thus need to be estimated. Currently, the LVEDV and RVEDV are estimated based on an estimated total blood volume (TBV) and the measured global end-diastolic volume (GEDV). As the stroke volume (SV) is a measured variable, ESV can be calculated by subtracting SV from EDV. The total blood volume is estimated as 85 ml/kg, with 25 ml/kg being stressed volume and 60 ml/kg unstressed volume (Rothe, 1979). GEDV is the end-diastolic volume of the left and right ventricle and the two atria. Furthermore, from data of several studies e.g. (Luecke *et al.*, 2004; Neumann, 1999; Nirmalan *et al.*, 2004; Preisman *et al.*, 2002), it can be reasoned that the right ventricle usually contains more blood than the left ventricle and that within the heart, blood is distributed with 60% in the ventricle and 40% in the atrium. Hence the LVEDV and RVEDV are given by following equations:

$$LVEDV = GEDV \cdot \frac{2}{3} \cdot 0.4 \tag{4.3}$$

$$RVEDV = GEDV \cdot \frac{2}{3} \cdot 0.6 \tag{4.4}$$

Note, that GEDV is corrected here by a factor of $\frac{2}{3}$ as the CVS model only models the ventricles and not the two atria. The volume in the pulmonary capillary and vein compartments (V_{cap}, V_{pv}) are given by the pulmonary blood volume (PBV) which is calculated as:

$$PBV = \frac{GEDV}{4} \tag{4.5}$$

Equation 4.5 can be derived from the following two Equations (Pulsion Medical Systems, 2005):

$$ITBV = GEDV + PBV \tag{4.6}$$

$$ITBV = 1.25 \cdot GEDV \tag{4.7}$$

where ITBV is the intrathoracic blood volume. It is assumed, that the pulmonary blood volume is distributed with 60% in the pulmonary vein and 40% in the pulmonary capillaries resulting in:

$$V_{capeff} = PBV \cdot 0.4 \tag{4.8}$$

$$V_{pv} = PBV \cdot 0.6 \tag{4.9}$$

The volumes in aorta and pulmonary artery are also directly given, as the pressures P_{ao} and P_{pa} are given or readily measured clinically and the elastances E_{ao} and E_{pa} may be calculated, as presented in detail in Section 5.2.1. The two volumes V_{ao} and V_{pa} are thus given by following equation:

$$V = \frac{P}{E} \tag{4.10}$$

As mentioned previously, the unstressed volumes are omitted for all volume compartments except the systemic and pulmonary volume compartments (V_{sys}, V_{cap}). The latter two are both modelled using stressed and unstressed volumes. Further, as a result of these estimations, some specific detailed clinical questions may not be answerable because information is lost on how one ventricle expands relative to the other (e.g. RVEDV/LVEDV expansion index). However, whenever the ventricle volumes are not measured directly, it is not as important to identify specific ventricular volumes as it is to identify the change in SV, which is always directly given as a measured signal.

4.2.2 Volume Calculations Based on Blood Distribution

More critically, it is important to keep volume calculations consistent. Otherwise, different or mixed methods of calculating volumes can have a profound effect on the model simulation output. The clinical outcome, when using the model for diagnosis, is that it would become very difficult to observe accurate and true clinically relevant trends in the identified parameters.

As already mentioned, the volumes in the ventricles are either directly measured or estimated based on GEDV and SV measurements. The volumes in the pulmonary capillary and vein compartments are always estimated based on PBV. The volumes in aorta and pulmonary artery are directly given via Equation 4.10. The remaining model volumes V_{vc} and V_{sys} are then estimated based on known blood distributions (Guyton & Hall, 2000; Klabunde, 2004).

The volume in the vena cava compartment (V_{vc}) does not have a significant effect on the parameter identification process as noted previously. This lack of effect occurs because only the pressure (P_{vc}) is used for the identification integrals discussed in detail in Chapter 5. Thus, a slightly overestimated V_{vc} will lead to a decrease in identified E_{vc} and vice versa, effectively cancelling any moderate error in a clinical efficacy sense. However, keeping the estimation of V_{vc} consistent and physiologically realistic ensures that no unphysiological changes in E_{vc} occur. Hence, any subsequent changes in E_{vc} are more likely to be attributable to real physiological events. For example, an increase in E_{vc} is expected during a vena cava compression.

The volume V_{vc} is estimated as being proportional to the volume leaving the right ventricle, which is the stroke volume (SV). This assumption makes sense because there should be a correlation between the volumes entering and leaving the right ventricle, just as there is a correlation between the venous return and systemic flow entering and leaving the heart. More specifically, venous return and cardiac output are interrelated by the Frank-Starling Mechanism. Hence, V_{vc} can be estimated as:

$$V_{vc} = \kappa \cdot SV \tag{4.11}$$

with a typical value of $\kappa = 1.25$. This value is approximated from the relationship between the known blood distribution in the vena cava and a normal and healthy

SV (Klabunde, 2004). Finally, V_{syseff} can be estimated as the residual stressed volume, defined:

$$V_{syseff} = TBV_{eff} - V_{ao} - LVEDV - RVEDV - V_{pa} - V_{capeff} - V_{pv} - V_{vc} \tag{4.12}$$

with TBV_{eff}, the stressed total blood volume, given as 25 ml/kg for a healthy state (Rothe, 1979). Note that TBV_{eff} changes during volume losses or fluid therapy.

The unstressed volumes V_{dsys} and V_{dcap} are calculated as:

$$V_{dsys} = TBV_{ineff} \cdot 0.8 \tag{4.13}$$

$$V_{dcap} = TBV_{ineff} \cdot 0.2 \tag{4.14}$$

where TBV_{ineff} is the unstressed TBV, which baseline value is given as 60 ml/kg (Rothe, 1979).

4.2.3 Volume Calculations for Stressed and Unstressed Volume

The unstressed total blood volume (TBV_{ineff}) is given as 60 ml/kg and the stressed volume as 25 ml/kg (TBV_{eff}) for a healthy state (Rothe, 1979). However, adjustments to these two values have to be made during changes in hemodynamic and volemic conditions, such as hypo- and hypervolemia and venous or arterial constriction and/or dilation. Hence, they must adapt for use in a real-time diagnostic model.

The terms 'vasoconstriction' and 'vasodilation' can relate to either arterial or venous constriction or dilation. The term 'vaso' is derived from the Latin 'vas', which simply means 'vessel'. Arterial vasoconstriction and/or -dilation is represented in the CVS model by a change in R_{sys}. Venous constriction and/or -dilation are also termed 'venoconstriction' and 'venodilation', respectively. The majority of the circulating blood is held in the venous system. The modelling of venodilation and -constriction is described in this section, as they determine the stressed and unstressed circulating blood volume.

Figure 4.5 shows the effect of a blood infusion (hypervolemia) or loss (hypovolemia) on the stressed and unstressed systemic volume. It can be seen that

during a volume infusion or volume loss, the unstressed volume remains constant and is not significantly affected. However, the stressed volume decreases or increases, which in turn changes MCFP or P_{sys}, the effects of which thus alter the circulation and cardiovascular performance, as expected.

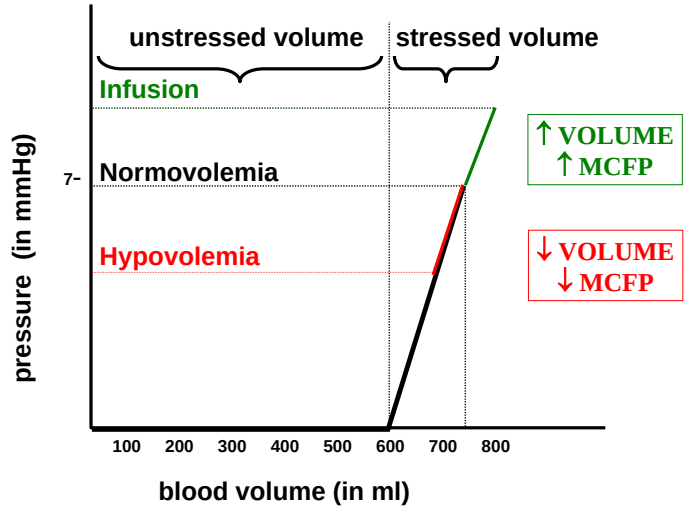

Figure 4.5: Effect of volume infusions and blood loss (hypovolemia) on MCFP (P_{sys}) and the distribution of stressed and unstressed blood volume.

Figures 4.6 and 4.7 illustrate the effects of venous constriction and dilation on the stressed (V_{eff}) and unstressed (V_d) volumes. Venoconstriction is a constriction of the smooth muscle surrounding the veins, usually caused by sympathetic reflex mechanisms or vasoconstrictor substances such as catecholamines and angiotensin II (Klabunde, 2004). Figure 4.6 displays how venoconstriction causes a shift from the unstressed to the stressed volume, thereby decreasing V_d and increasing V_{eff}. Additionally, venous compliance is decreased (elastance is increased), which increases MCFP.

Figure 4.7 displays how venodilation affects V_{sys} and MCFP (P_{sys}). Venous dilators are often used in treating cardiovascular disorders to reduce MCFP and thus RV preload, which in turn reduces the oxygen demand (Klabunde, 2004). Another main purpose of reducing MCFP is to reduce capillary fluid filtration and thus the formation of edema (Klabunde, 2004). In Figure 4.7 it can be seen how MCFP decreases (venous compliance increases) and how the unstressed volume V_d increases.

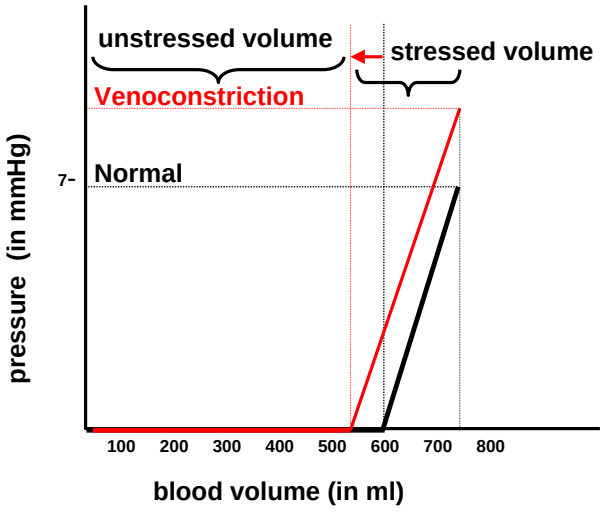

Figure 4.6: Effect of venoconstriction on MCFP (P_{sys}) and the distribution of stressed and unstressed blood volume.

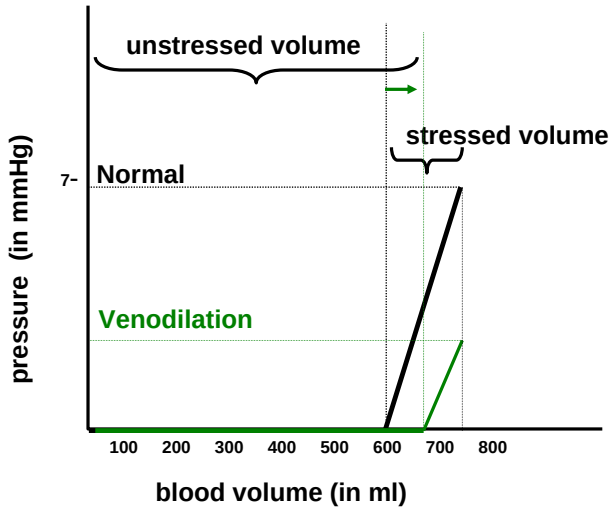

Figure 4.7: Effect of venodilation on MCFP (P_{sys}) and the distribution of stressed and unstressed blood volume.

4.2.3.1 Volume Infusion and Blood Loss

Changes in total effective and ineffective blood volume (TBV_{eff}, TBV_{ineff}), as caused by volume infusions and blood losses, are accounted for by:

$$TBV_{eff} = 25ml/kg \cdot KG + BV \tag{4.15}$$

$$TBV_{ineff} = 60ml/kg \cdot KG \tag{4.16}$$

with KG = patient weight in kilograms and BV = value of lost or added blood in ml. Note that it would also be possible to change both, TBV_{eff} and TBV_{ineff} with regard to a blood infusion or loss (BV). However, as can also be seen in Figure 4.5, only the effective (stressed) volume, and not the ineffective (unstressed) volume, is affected by a volume loss or infusion (Guyton & Hall, 2000; Peters *et al.*, 2001).

4.2.3.2 Venoconstriction and Venodilation

Venoconstriction is modelled as a shift from the unstressed volume to stressed volume, thus increasing the effective volume TBV_{eff} and reducing TBV_{ineff}. Venodilation is modelled by the opposite shift, increasing TBV_{ineff} and reducing TBV_{eff}. Equations 4.15 and 4.17 are therefore extended:

$$TBV_{eff,norm} = (25 + \triangle)[ml/kg] \tag{4.17}$$

$$TBV_{ineff,norm} = (60 - \triangle)[ml/kg] \tag{4.18}$$

$$TBV_{eff} = TBV_{eff,norm} \cdot KG + BV \tag{4.19}$$

$$TBV_{ineff} = TBV_{ineff,norm} \cdot KG \tag{4.20}$$

where $\triangle$ represents the severity of venoconstriction and -dilation. Note, that a negative $\triangle < 0$ represents venodilation and a positive $\triangle > 0$ venoconstriction.

The combined effect of volume infusion/loss together with the compensatory reflex mechanism of either venoconstriction (for blood loss) or venodilation (for volume infusion) is shown in Figure 4.8. The normalized TBV_{eff} ($TBV_{eff,norm}$) decreases during volume infusion (BV = positive values), reflecting the venodilation mechanisms at work. However, during hypovolemic states (negative BV values) $TBV_{eff,norm}$ increases, reflecting the action of reflex mechanisms associated with venoconstriction.

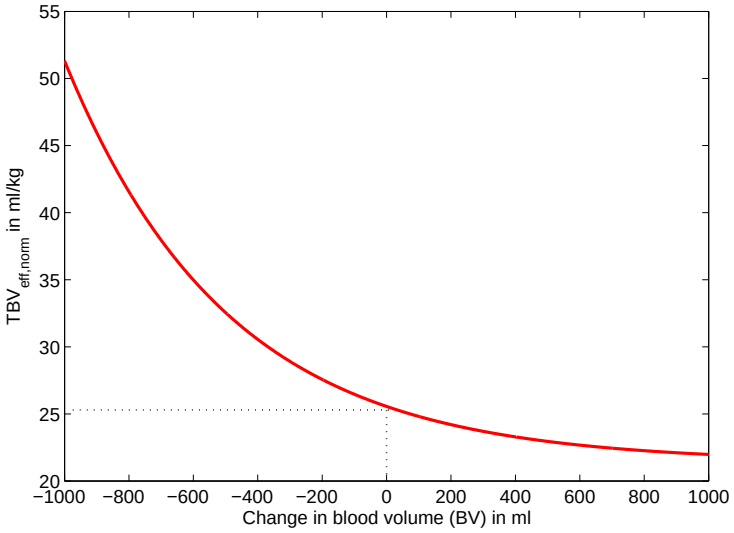

Figure 4.8: Effect of volume loss and infusion on the normalized effective (stressed) TBV, as given in ml/kg, BV = change in blood volume.

This relationship between $TBV_{eff,norm}$ and BV is implemented in the CVS model as:

$$TBV_{eff,norm} = 4.2 \cdot e^{(-0.002 \cdot BV)} + 21.5 \tag{4.21}$$

The constant values $(4.2; -0.002; 21.5)$ were found by fitting an exponential to experimental data obtained from porcine experiments during levels of hypo-, normo- and hypervolemia (Lambert *et al.*, 2007). Note that Equation 4.21 only reflects healthy subjects, which are able to adjust to different volemic levels using adequate reflex responses. Equation 4.21 might also need to be adjusted during different disease or drug induced circulatory states, where, for example, higher levels of venoconstriction have to be accounted for.

4.3 Simulating the Circulation

When creating a physiological simulation model it is important that the derived equations are a physiologically correct representation of the real world, at least to the degree of abstraction wanted for the intended use of the model. Therefore, some basic principles observed in the human circulatory system are simulated with the CVS model as a means of validating the model structure and its components.

Central venous pressure (CVP) or mean capillary filling pressure (MCFP) are key measurements for a functioning circulatory system. Both an increase in systemic volume (V_{syseff}) and venous vasoconstriction, which in the latter case reduces the compliance of the veins and thus increases their elastance, increase CVP. Similarly, arterial dilatation will increase CVP (represented by P_{sys} in the model), as additional amounts of blood on the arterial side are allowed through to enter the veins. Arterial dilatation can be simulated by a decrease in systemic vascular resistance (R_{sys}), which in turn leads to a higher systemic flow Q_{sys} entering the venous side. This increase in Q_{sys} in turn increases V_{syseff} resulting in an expected increase in P_{sys}. The end result is that an increase in P_{sys} increases the venous return (VR) back to the right heart, concomitantly increasing the ventricular filling and consequently SV and CO. Therefore, the following relationship can be observed (Mehler & Sompayrac, 2001):

$$CVP \uparrow \rightarrow CO \uparrow \tag{4.22}$$

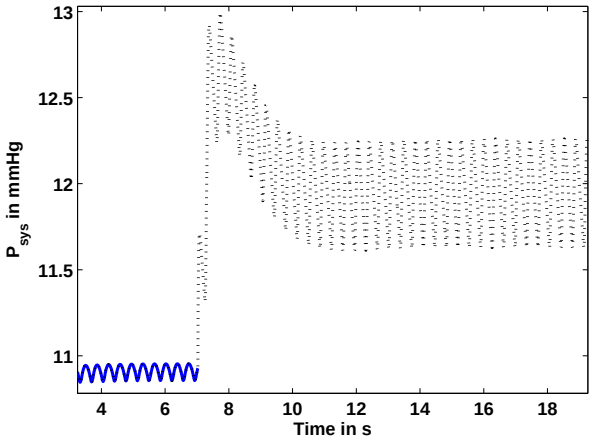

Figure 4.9: Simulated increase in P_{sys}, as caused by a simulated decrease in R_{sys}. The solid line represents the baseline simulation signal and the dotted line represents the simulation output signal resulting from a decrease in R_{sys}.

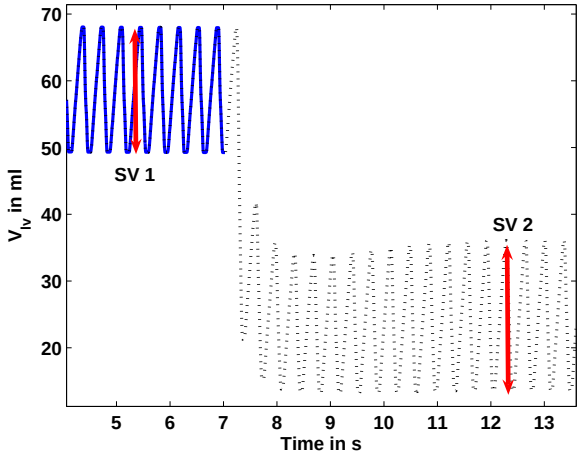

Figure 4.10: Resulting increase in left ventricular stroke volume and thus in cardiac output. The solid line represents the baseline simulation signal and the dotted line represents the resulting increase in SV and hence CO.

Figures 4.9 and 4.10 show the simulation results obtained for simulating an increase in P_{sys}, which leads to a subsequent increase in CO, as expected.
Similarly, the following relationship holds true (Mehler & Sompayrac, 2001):

$$CVP \downarrow \rightarrow CO \downarrow \tag{4.23}$$

Figures 4.11 and 4.12 show the simulation results obtained for simulating a decrease in P_{sys}, which leads to a subsequent expected decrease in CO.

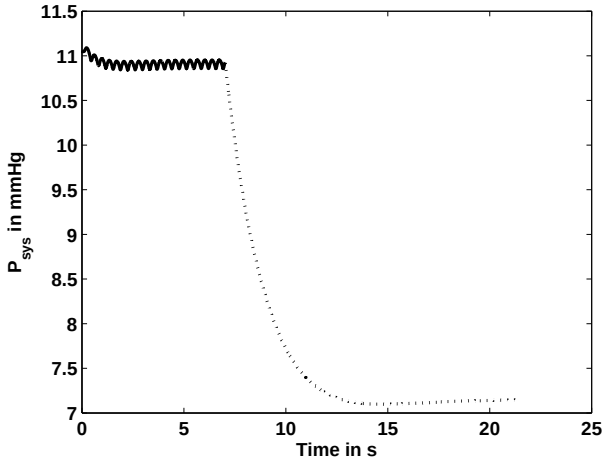

Figure 4.11: Simulated decrease in P_{sys}, as caused by a simulated increase in R_{sys}. The solid line represents the baseline simulation signal and the dotted line represents the resulting decrease in P_{sys} as simulated by an increase in R_{sys}.

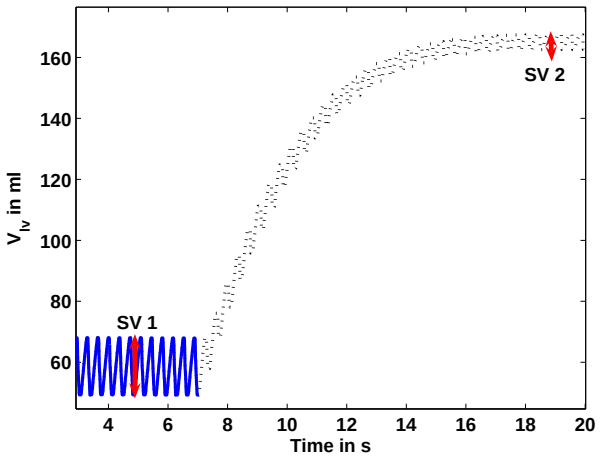

Figure 4.12: Resulting decrease in left ventricular stroke volume and thus in cardiac output. The solid line represents the baseline simulation signal and the dotted line represents the resulting decrease in SV and hence CO.

Furthermore, it can be observed that a rise in CO lowers CVP, and that a reduction in CO raises CVP. Hence, CO and CVP are inversely related. This inverse

relationship can be explained by looking at the venous return. If VR is raised and subsequently increases SV and thus CO, more blood is taken out from the venous side and put into the arterial side, thus lowering P_{sys}. Consequently, the following equation can be derived (Mehler & Sompayrac, 2001):

$$CO \uparrow \rightarrow CVP \downarrow \tag{4.24}$$

Figures 4.13 and 4.14 show the simulation results obtained for simulating an increase in VR and thus CO, which leads to the subsequent expected decrease in P_{sys}.

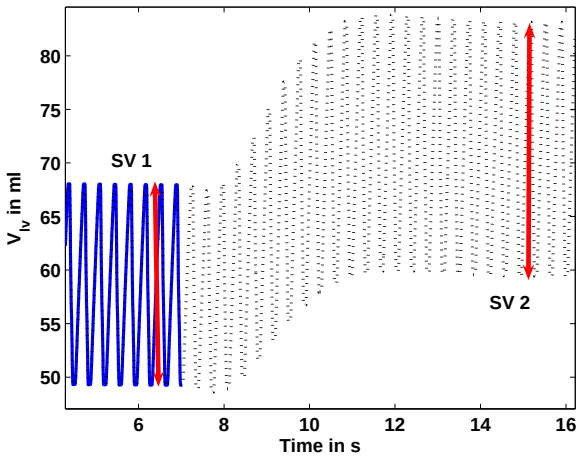

Figure 4.13: Simulated increase in VR and CO, as caused by a simulated decrease in R_{vr}. The solid line represents the baseline simulation signal and the dotted line represents the resulting increase in CO as simulated by a decrease in R_{vr}.

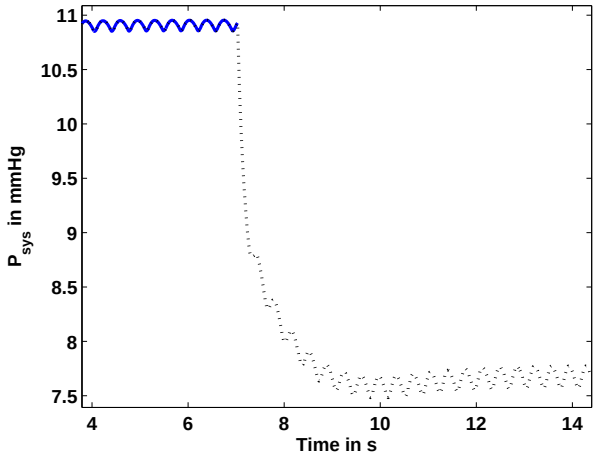

Figure 4.14: Resulting decrease in P_{sys} as blood is transferred from the venous side into the arterial side. The solid line represents the baseline simulation signal and the dotted line represents the resulting decrease in P_{sys}.

Combining these relationships in Equations 4.22-4.24 yields (Mehler & Sompayrac, 2001):

$$CVP \uparrow \rightarrow CO \uparrow \rightarrow CVP \downarrow \rightarrow CO \downarrow \tag{4.25}$$

From Equation 4.25 it can be seen how CVP and CO modulate each other and thus stabilize the circulatory system. It is important to ensure that these fundamental relationships are correctly captured and simulated with the CVS model to guarantee results that are physiologically expected, relevant and consistent, as shown in Figures 4.9-4.14.

4.4 Limitations

All of the volume calculations serve the primary purpose of keeping the volume distributions within the model as physiologically correct as possible during a variety of scenarios, including different levels of normo-, hypo- and hypervolemia, other disease states, and/or variable hemodynamic conditions. Because this CVS model is a relatively minimal model, not all relevant physiological aspects can be strictly accounted for in this research. More specifically, internal blood volume

shifts, which are for example caused by reflex mechanisms, are only minimally accounted and not necessarily specifically or accurately captured.

4.5 Summary

This chapter illustrated the interactions between the heart (cardiovascular) and lung (cardiopulmonary) systems for spontaneous and mechanically aided ventilation, commonly observed in critically ill patients. Transient and steady-state effects were investigated and the observed physiological behaviours modelled in the CVS system.

Additionally, all volume-based calculations were presented and details given for the modelling of the stressed and unstressed blood volumes, taking the effects of hyper- and hypovolemia, as well as vasodilation and -constriction into account. Finally, basic circulatory simulations were performed to validate the CVS model and its structure and components. This chapter thus finalizes the description of the CVS model.

Appendix B summarizes the equations for the cardiopulmonary and circulatory parts of the CVS model. The volume calculations are given in Equations B.1-B.16.

Chapter 5

Parameter Identification

This chapter explains the methods used to identify the patient-specific parameters from the CVS model. A previously described integral-based method (Hann *et al.*, 2006) forms the basis for the identification process. The integral method has been extended to allow identification for the new model parameters and adjustments have been made to improve the identification process. For details about this method and its advantages compared to traditional identification methods, the interested reader is referred to (Hann *et al.*, 2006; Starfinger *et al.*, 2007b).

5.1 Overview of Identification Approaches and Methods

In contrast to the many CVS models available in literature, which mainly concentrate on simulating the entire cardiovascular/circulatory system or parts thereof, there are only very few approaches and methods published that are concerned with the system identification of such models. There are even less methods available for predicting therapy effects as based on a CVS model and parameter identification.

An example for a CVS model identification and therapy prediction is available in (Heldt *et al.*, 2006; Samar *et al.*, 2005), where subset selection-based optimization algorithms are used to overcome the ill-conditioned parameter estimation problem as caused by a model built at a resolution too high to allow for accurate estimation of all model parameters from the available input signals.

A second example can be found in (Sun *et al.*, 2000), where a CVS model consisting of 28 differential equations with over 100 circulatory parameters is tried to be identified. However, as a nonlinear optimization algorithm is used, this algorithm may fail to find the global minimum if it attempts to adjust too many model parameters at the same time.

Another example is available in (Long *et al.*, 1994). This research is based on known physiological relationships between parameters such as MAP, CO and LVEDP. Disease states such as mitral and aortic stenosis are represented by an altered relationship between the physiologic parameters. For example, mitral stenosis is characterized as causing a pressure gradient in diastole between left atrium and ventricle. Other diseases and/or treatments are modelled in a similar way. However, this approach has several weaknesses, as it is neither patient-specific nor does it describe the whole circulatory system of a particular patient with all the possible underlying dysfunctions. Therefore, if a pathological state, such as heart failure, has not yet been adequately covered by the model, unreliable predictions are made and the model is difficult to adjust to a particular patient and condition as it needs constant alterations in the relationships between the parameters.

The identification process as presented in the following chapter, however uses the optimized patient-specific parameters, which are obtained during the course of the ICU stay and thus characterize the evolution of any underlying dysfunctions and diseases the patient may have. Hence, these parameter trends can be used to diagnose the hemodynamic condition of each individual patient and point the clinical staff in the right direction, for example showing if the volume status or ventricle contractility are improving or worsening.

5.2 Integral Identification Problem Formulation

Consider the CVS model as defined in Equations 3.28 to 3.43. Assume that all flows, pressures and volumes are measured or estimated and note, that the following equations apply during ejection (systole) and filling (diastole):

$$V_{lv}(eb:ef) - V_{lv}(eb) = -\int_{eb}^{ef} Q_{av}\,\mathrm{d}t \tag{5.1}$$

$$V_{lv}(fb:ff) - V_{lv}(fb) = \int_{fb}^{ff} Q_{mt}\,\mathrm{d}t \tag{5.2}$$

$$V_{rv}(eb2:ef2) - V_{rv}(eb2) = -\int_{eb2}^{ef2} Q_{pv}\,\mathrm{d}t \tag{5.3}$$

$$V_{rv}(fb2:ff2) - V_{rv}(fb2) = \int_{fb2}^{ff2} Q_{tc}\,\mathrm{d}t \tag{5.4}$$

where eb,$eb2$=ejection begin for the LV,RV; ef,$ef2$=ejection finish for the LV,RV; fb,$fb2$= filling begin for the LV,RV and ff,$ff2$=filling finish for the LV,RV. These volumes are for example measured by using a conductance catheter. Similar substitutions can be made for the other volumes and flows, for example V_{ao} is given by:

$$V_{ao}(t) - V_{ao0} = \int_0^t (Q_{av} - Q_{sys})\,\mathrm{d}t \tag{5.5}$$

Using Equation 5.5, the Equation defining the pressure in the aorta, P_{ao}, can be rewritten as:

$$P_{ao}(t) = P_{ao0} + E_{ao} \cdot \int_0^t (Q_{av} - Q_{sys})\,\mathrm{d}t \tag{5.6}$$

which after substituting Equation 3.40 into Equation 5.6 and reordering yields the following matrix for determining the parameter E_{ao}:

$$\begin{pmatrix} \int Q_{av} & \int P_{ao} & \int P_{sys} \end{pmatrix} \cdot \begin{pmatrix} E_{ao} \\ A_1 \\ A_2 \end{pmatrix} = \begin{pmatrix} P_{ao} - P_{ao0} \end{pmatrix} \tag{5.7}$$

with $A_1 = \frac{-Eao}{Rsys}$ and $A_2 = \frac{Eao}{Rsys}$. Similarly, the following matrices are obtained for E_{pa}, E_{vc}, E_{pu}, E_{cap}, E_{sys}, R_{sys}, R_{pulin}, R_{vr} and R_{pulout}. Note, that for reasons

of simplicity and clarity, the differential dt and the upper and lower limits of the integration symbol $\int$ are omitted. Usually and if not stated otherwise, the integration is done over one heart beat. In cases where matrices are constructed separately for ejection and filling periods, the integrals are only calculated during these periods.

$$\begin{pmatrix} \int Q_{pv} & \int P_{pa} & \int P_{cap} \end{pmatrix} \cdot \begin{pmatrix} E_{pa} \\ A_3 \\ A_4 \end{pmatrix} = \begin{pmatrix} P_{pa} - P_{pa0} \end{pmatrix} \tag{5.8}$$

with $A_3 = \frac{-Epa}{Rpulin}$ and $A_4 = \frac{Epa}{Rpulin}$.

$$\begin{pmatrix} \int Q_{av} & \int V_{sys,eff} & P_{ao} - P_{ao0} \end{pmatrix} \cdot \begin{pmatrix} R_{sys} \\ E_{sys} \\ A_5 \end{pmatrix} = \begin{pmatrix} \int P_{ao} \end{pmatrix} \tag{5.9}$$

with $A_5 = \frac{-Rsys}{Eao}$.

$$\begin{pmatrix} \int Q_{pv} & \int V_{cap,eff} & P_{pa} - P_{pa0} \end{pmatrix} \cdot \begin{pmatrix} R_{pulin} \\ E_{cap} \\ A_6 \end{pmatrix} = \begin{pmatrix} \int P_{pa} \end{pmatrix} \tag{5.10}$$

with $A_6 = \frac{-Rpulin}{Epa}$.

$$\begin{pmatrix} \int Q_{tc} & \int V_{vc} & P_{vc} - P_{vc0} \end{pmatrix} \cdot \begin{pmatrix} R_{vr} \\ E_{vc} \\ A_7 \end{pmatrix} = \begin{pmatrix} \int P_{sys} - \int P_{th} \end{pmatrix} \tag{5.11}$$

with $A_7 = \frac{Rvr}{Evc}$.

$$\begin{pmatrix} \int Q_{mt} & \int V_{pv} & P_{pu} - P_{pu0} \end{pmatrix} \cdot \begin{pmatrix} R_{pulout} \\ E_{pu} \\ A_8 \end{pmatrix} = \begin{pmatrix} \int P_{cap} - \int P_{th} \end{pmatrix} \tag{5.12}$$

with $A_8 = \frac{Rpulout}{Epu}$. Note that the flow integrals $\int Q_{mt}$, $\int Q_{av}$, $\int Q_{tc}$ and $\int Q_{pv}$ in Equations 5.7 - 5.12 are substituted by their corresponding volumes as given by Equations 5.1 - 5.4. This has the advantage that the volumes in the ventricles are measured or at least estimated signals whereas the flows are usually not measured or estimated.

For the remaining model parameters the following calculations, using Equations 5.1 to 5.4 during filling and ejection periods, are performed:

$$\mathbf{A} \cdot \begin{pmatrix} L_{av} \\ L_{mt} \\ L_{tc} \\ L_{pv} \\ E_{eslvf} \\ P_{0lvf} \\ E_{esrvf} \\ P_{0rvf} \\ R_{av} \\ R_{mt} \\ R_{tc} \\ R_{pv} \\ P_{0pcd} \end{pmatrix} = \vec{b} \tag{5.13}$$

where matrix $\mathbf{A}$ and vector $\vec{b}$ are given by:

$$\mathbf{A} = \begin{pmatrix} \mathbf{A_{lv,eject}} \\ \mathbf{A_{lv,fill}} \\ \mathbf{A_{rv,eject}} \\ \mathbf{A_{rv,fill}} \end{pmatrix} \tag{5.14}$$

$$\vec{b} = \begin{pmatrix} \vec{b}_{lv,eject} \\ \vec{b}_{lv,fill} \\ \vec{b}_{rv,eject} \\ \vec{b}_{rv,fill} \end{pmatrix} \tag{5.15}$$

and the matrix for the left ventricle during ejection, $\mathbf{A_{lv,eject}}$, is given by:

$$\mathbf{A_{lv,eject}} = \begin{pmatrix} Q_{av}(eb:ef) & \vec{0} & \vec{0} & \vec{0} & -Ie_1 & -Ie_2 & \vec{0} & \vec{0} & V_{lv}(eb:ef) - V_{lv}(eb) & \vec{0} & \vec{0} & \vec{0} & -Ie_5 \end{pmatrix} \tag{5.16}$$

with Ie_1, Ie_2 and Ie_5 defined as:

$$Ie_1 = \int_{eb}^{ef} ((V_{lvf} - V_{dlvf}) \cdot driL) \tag{5.17}$$

$$Ie_2 = \int_{eb}^{ef} ((1 - driL) \cdot (e^{(\lambda_{lvf} \cdot (V_{lvf} - V_{olvf}))} - 1)) \tag{5.18}$$

$$Ie_5 = \int_{eb}^{ef} (e^{(\lambda_{pcd} \cdot (V_{lv} + V_{rv} - V_{opcd})} - 1) \tag{5.19}$$

The matrix for the left ventricle during filling, $\mathbf{A_{lv,fill}}$, is given by:

$$\mathbf{A_{lv,fill}} =$$
$$\begin{pmatrix} \vec{0} & Q_{mt}(fb:ff) & \vec{0} & \vec{0} & If_1 & If_2 & \vec{0} & \vec{0} & \vec{0} & V_{lv}(fb:ff) - V_{lv}(fb) & \vec{0} & \vec{0} & If_5 \end{pmatrix} \tag{5.20}$$

with If_1, If_2 and If_5 defined as:

$$If_1 = \int_{fb}^{ff} ((V_{lvf} - V_{dlvf}) \cdot driL) \tag{5.21}$$

$$If_2 = \int_{fb}^{ff} ((1 - driL) \cdot (e^{(\lambda_{lvf} \cdot (V_{lvf} - V_{olvf}))} - 1)) \tag{5.22}$$

$$If_5 = \int_{fb}^{ff} (-e^{(\lambda_{pcd} \cdot (V_{lv} + V_{rv} - V_{opcd})} - 1) \tag{5.23}$$

Vector $\vec{b}_{lv,eject}$ for the left ventricle during ejection is given by:

$$\vec{b}_{lv,eject} = P_{th} \cdot (t_{new}(eb:ef) - t_{new}(eb)) - \int P_{ao} \tag{5.24}$$

Vector $\vec{b}_{lv,fill}$ for the left ventricle during filling is given by:

$$\vec{b}_{lv,fill} = \int P_{pu} - P_{th} \cdot (t_{new}(fb:ff) - t_{new}(fb)) \tag{5.25}$$

where t_{new} is defined as:

$$t_{new} = t - t(1) \tag{5.26}$$

and t is the time period over which the identification takes place. Similar equations are obtained for the right ventricle during filling and ejection.

5.2.1 New Formulation for Arterial Elastances E_{ao} and E_{pa}

Arterial compliance is defined as the change in volume following a change in pressure. Arterial elastance is given as the reciprocal of the compliance and thus by a pressure change ($\triangle P$) following a volume change ($\triangle V$). Many researchers have concluded, that arterial elastance can consequently be calculated by substituting the pulse pressure (PP) for $\triangle P$ and stroke volume SV for $\triangle V$ as given by following equations (Chemla *et al.*, 1998; Zhu *et al.*, 1995):

$$E_{ao} = \frac{PP_{ao}}{SV} \tag{5.27}$$

$$E_{pa} = \frac{PP_{pa}}{SV} \tag{5.28}$$

Hence, E_{ao} and E_{pa} are not identified anymore, but are directly given by the measured arterial and pulmonary artery pulse pressure (PP_{ao}, PP_{pa}) and the stroke volume. Note, that if P_{pa} is not measured, than at least E_{ao} is given as it can be assumed that P_{ao} and SV are measured signals.

In this research, Equations 5.27 and 5.28 are adjusted by a multiplying factor of 1.25 as it was found that adding this factor improves the estimate for E_{ao} and E_{pa}. Otherwise, both elastances would have been slightly underestimated compared to what was clinically observed; resulting in poor matches for the arterial pulse pressures PP_{ao} and PP_{pa} when the identified model was re-simulated. This multiplying factor was found by observing the relationship between stroke volume and change in volume in V_{ao} and V_{pa}. The arterial elastances in the CVS model are defined (assuming zero unstressed volumes V_{dao} and V_{dpa}):

$$E_{ao} = \frac{P_{ao}}{V_{ao}} \tag{5.29}$$

$$E_{pa} = \frac{P_{pa} - P_{th}}{V_{pa}} \tag{5.30}$$

which can be rewritten as:

$$E_{ao,max} = \frac{\Delta P_{ao}}{\Delta V_{ao}} \tag{5.31}$$

$$= \frac{PP_{ao}}{\Delta V_{ao}} \tag{5.32}$$

$$E_{pa,max} = \frac{\Delta (P_{pa} - P_{th})}{\Delta V_{pa}} \tag{5.33}$$

$$= \frac{PP_{pa}}{\Delta V_{pa}} \tag{5.34}$$

As the maximum changes in V_{ao} and V_{pa} (ΔV_{ao}, ΔV_{pa}) are usually hard to measure or estimate, the maximum changes in V_{lv} (LVSV) and V_{rv} (RVSV) are used, respectively. These maximum changes are the stroke volumes from the left and right ventricles. However, the stroke volumes are not identical to the maximum changes in V_{ao} and V_{pa}, but are highly correlated as shown in Figures 5.1 and 5.2. The following Equations are derived linking ΔV_{ao} and ΔV_{pa} to the stroke volumes LVSV and RVSV:

$$LVSV = 1.25 \cdot \Delta V_{ao} \tag{5.35}$$

$$RVSV = 1.25 \cdot \Delta V_{pa} \tag{5.36}$$

Hence, Equations 5.27 and 5.28 are multiplied by the factor 1.25. Importantly, the effect of a slightly inaccurate value for E_{ao} and E_{pa} will cancel as the trends over time of these arterial elastances are what is clinically important, rather than their absolute values.

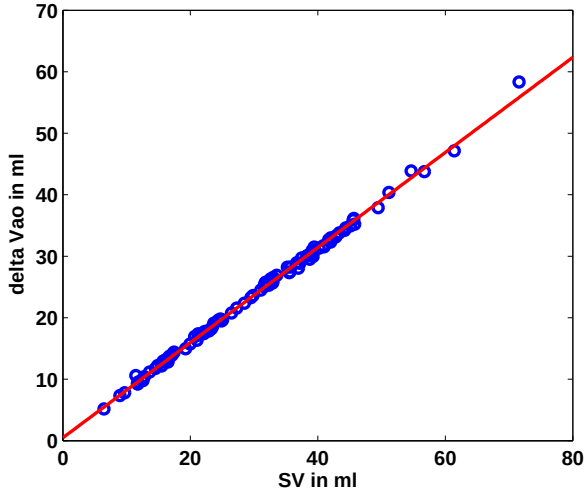

Figure 5.1: Relationship between ΔV_{ao} and SV.

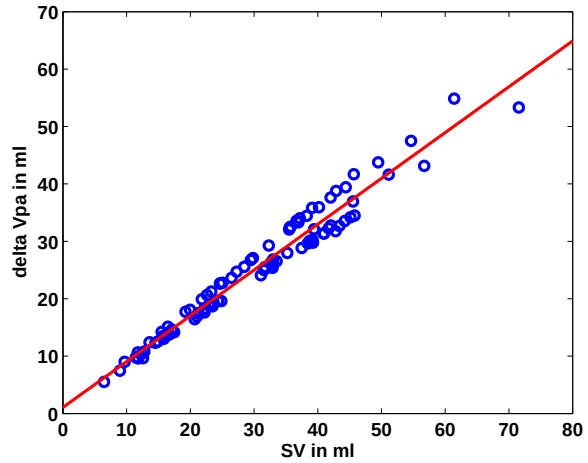

Figure 5.2: Relationship between ΔV_{pa} and SV.

Furthermore, as E_{ao} is given, Equation 5.9 can now directly be solved for R_{sys} and E_{sys}:

$$R_{sys} = \frac{E_{ao} \cdot (\int P_{sys} - \int P_{ao})}{(P_{ao} - P_{ao0} - \int Q_{av} \cdot E_{ao})} \tag{5.37}$$

$$E_{sys} = \frac{\int P_{ao} - R_{sys} \cdot (\int Q_{av} - 1/E_{ao} \cdot (P_{ao} - P_{ao0}))}{\int V_{syseff}} \tag{5.38}$$

Similarly, Equation 5.10 can be solved for R_{pulin} and E_{cap}:

$$R_{pulin} = \frac{E_{pa} \cdot (\int P_{cap} - \int P_{pa})}{(P_{pa} - P_{pa0} - \int Q_{pv} \cdot E_{pa})} \tag{5.39}$$

$$E_{cap} = \frac{\int P_{pa} - R_{pulin} \cdot (\int Q_{pv} - 1/E_{pa} \cdot (P_{pa} - P_{pa0}))}{\int V_{capeff}} \tag{5.40}$$

5.2.2 New Matrix Formulation

Given the new formulation for E_{ao} and E_{pa} (Equations 5.27 and 5.28) and the resulting simplified calculation of R_{sys}, E_{sys}, R_{pulin} and E_{cap} as given by Equations 5.37-5.40, the new matrix system can be defined as:

$$\mathbf{A_{all}} = \begin{pmatrix} \mathbf{A_{app}} & \theta \\ \theta & \mathbf{A} \end{pmatrix} \tag{5.41}$$

$$\vec{b}_{all} = \begin{pmatrix} \vec{b}_{app} \\ \vec{b} \end{pmatrix} \tag{5.42}$$

where matrix $\mathbf{A}$ and vector $\vec{b}$ have already been defined in Equation 5.14, θ is a zero matrix with the corresponding number of rows and columns and matrix $\mathbf{A_{app}}$ is given by:

$$\mathbf{A_{app}} = \begin{pmatrix} \mathbf{A_{vr}} & \theta \\ \theta & \mathbf{A_{pulout}} \end{pmatrix} \tag{5.43}$$

$$\vec{b}_{app} = \begin{pmatrix} \vec{b}_{vr} \\ \vec{b}_{pulout} \end{pmatrix} \tag{5.44}$$

with $\mathbf{A_{vr}}$ and $\mathbf{A_{pulout}}$ defined:

$$\mathbf{A_{vr}} \cdot \vec{x}_{vr} = \vec{b}_{vr} \tag{5.45}$$

$$\begin{pmatrix} \int Q_{tc} & P_{vc} - P_{vc0} \end{pmatrix} \cdot \begin{pmatrix} R_{vr} \\ A_7 \end{pmatrix} = \begin{pmatrix} \int P_{sys} - \int P_{vc} \end{pmatrix} \tag{5.46}$$

$$\mathbf{A_{pulout}} \cdot \vec{x}_{pulout} = \vec{b}_{pulout} \tag{5.47}$$

$$\begin{pmatrix} \int Q_{mt} & P_{pu} - P_{pu0} \end{pmatrix} \cdot \begin{pmatrix} R_{pulout} \\ A_8 \end{pmatrix} = \begin{pmatrix} \int P_{cap} - \int P_{pu} \end{pmatrix} \tag{5.48}$$

where A_7 and A_8 are already given in Equations 5.11 and 5.12, respectively.

5.3 Identification Process

The previous section gave an overview of the integral formulation and the equations involved in identifying the patient-specific parameters. This section describes the process of identifying the parameters.

5.3.1 Identification Inputs

In order to work reliably, the more measured input signals are available the better. The more input signals have to be estimated, the less reliable the identification will be, as more uncertainty is included. Table 5.1 gives the input signals, which are either continuously measured or available in discrete time steps or only estimated.

Input signals for Identification Process	
Signal [Unit]	Comments
Arterial Pressure P_{ao} [mmHg]	Obtained from PiCCO monitor or directly measured from catheter (discrete or continuous waveform)
Pulmonary Artery Pressure P_{pa} [mmHg]	Directly measured from catheter or estimated (continuous waveform if measured)
Central venous pressure CVP [mmHg]	Obtained from PiCCO monitor (discrete waveform)
Ventricle volumes V_{lv}, V_{rv} [ml]	Directly measured from conductance catheter or estimated (continuous waveform if measured)
Stroke volume SV [ml]	Directly measured from conductance catheter or obtained from PiCCO monitor (continuous or discrete waveform)
Heart Rate HR [s^{-1}]	Measured from ECG or obtained from PiCCO monitor (discrete waveform)
Global end-diastolic volume $GEDV$ [ml]	Obtained from PiCCO monitor discrete waveform, only needed when V_{lv}, V_{rv} are not measured directly

Table 5.1: Input signals for parameter identification

5.3.2 Scaling Model Outputs - Discrete Data

For discrete data, the waveforms are not known, therefore the integral method of (Hann *et al.*, 2006) cannot be directly applied. However, waveforms can be artificially generated by scaling a set of previously calculated model outputs to best fit the maximum and minimum measured data values for the pressures and volumes. The assumption is that these validated model waveforms are reasonably conformable with the actual clinical case. In return, significantly less measurement and potentially fewer invasive catheters are required.

The scaled signal, Sig_{new}, is obtained from a previously calculated signal, Sig_{old}, as follows:

$$Sig_{new} = a \cdot Sig_{old} + b \tag{5.49}$$

$$a = \frac{(Sig_{m,max} - Sig_{m,min})}{(Sig_{s,max} - Sig_{s,min})} \tag{5.50}$$

$$b = \frac{(Sig_{s,max} \cdot Sig_{m,min} - Sig_{m,max} \cdot Sig_{s,min})}{(Sig_{s,max} - Sig_{s,min})} \tag{5.51}$$

where the subscript s refers to simulated output and the subscript m refers to measured data.

5.3.3 Scaling Model Outputs - Continuous Data

For some of the porcine experiments, continuous waveforms are measured in V_{lv}, V_{rv}, P_{ao} and P_{pa}. However, the same scaling approach can be used to simplify the parameter identification. In particular, scaling effectively filters noise and unmodelled dynamics from the data. The identification problem is thus restricted to dynamics in the model. Note that the final comparison is still made to the original data and this approach is only done to minimize computational effort and complexity in the identification process. An example of scaling in this clinical porcine case is shown in Figure 5.3, for the pressure in the aorta (P_{ao}) before and after scaling, with $a = 0.5871$ and $b = 6.7166$. However, matching only the maximum and minimum values has the limitation that the waveform shape may not be precisely captured.

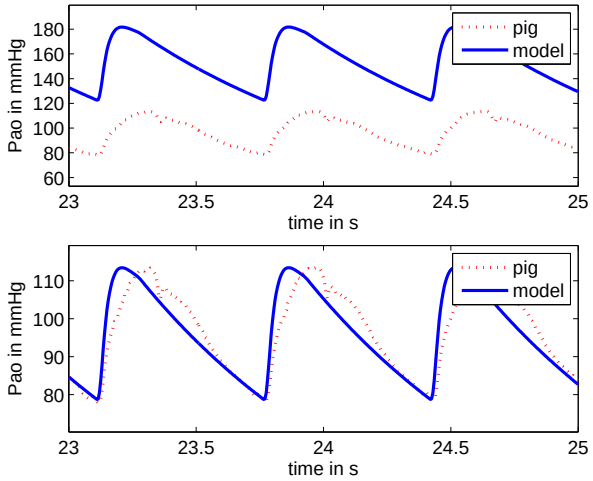

Figure 5.3: Porcine Pulmonary Embolism: Pressure in aorta (P_{ao}) before and after scaling with a = 0.5871 and b = 6.7166. The dotted line represents the measured, clinical porcine data. The solid line represents the model data before (upper panel) and after (lower panel) scaling.

5.3.4 Substitution of Flow Integrals During the Scaling Process

Another adjustment has been made to better calculate the parameters that are determined by the flows in and out of the ventricles. Previously, these flows have been used in the identification process and thus significant error was introduced during the scaling process, where only the pressure and volume signals are scaled, however not the flows as they are unknown. The flow integrals $\int Q_{mt}$, $\int Q_{av}$, $\int Q_{tc}$ and $\int Q_{pv}$ are now substituted by their corresponding volumes as given in Equations 5.1 - 5.4 and shown in Figure 5.4. This change has the advantage that the volumes in the ventricles are measured, or at least estimated signals whereas the flows themselves are not usually directly measured or estimated. Hence, significantly less error is introduced during the scaling part of the parameter identification process.

Figure 5.5 shows in the upper panel the flow integral and corresponding volume signal for the flow across the aortic valve (Q_{av}) from simulated data. The lower panel shows the difference between both signals, which is negligible ($< 1\%$) relative to the signal.

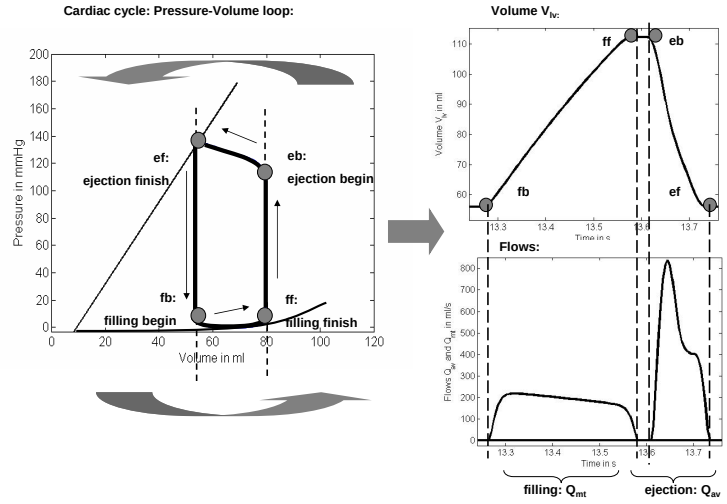

Figure 5.4: Overview of cardiac cycle with filling (fb:ff) and ejection (eb:ef) periods, which produces the volume in the left ventricle (V_{lv}) and the two flows in (across mitral valve: Q_{mt}) and out (across aortic valve: Q_{av}) of the ventricle.

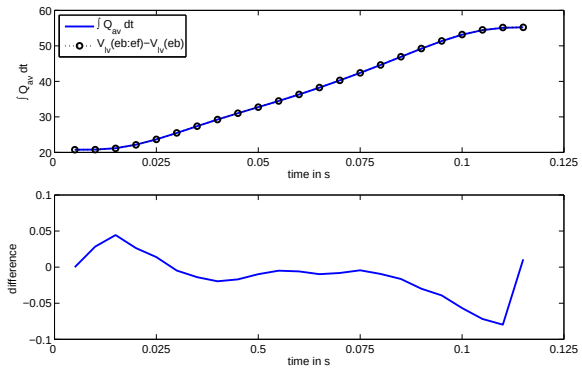

Figure 5.5: Substitution of flow signal with volume signal during identification process (upper panel) and difference between these two signals (lower panel).

5.3.5 Simulation Using Optimized Parameters

Figure 5.6 shows the overall process of the simulation and parameter identification algorithm. After the patient-specific parameters have been identified for a respective point in time, these parameters are then used to rerun the model simulation. The simulated output is then compared to the clinical data. However, due to errors in the initial parameter approximations and the process of scal-

ing output signals, parameter identification should be iterated to ensure optimal convergence. Fast convergence consistently occurred within 5-10 iterations and is stopped when the relative error between model output and clinical data reaches a set tolerance.

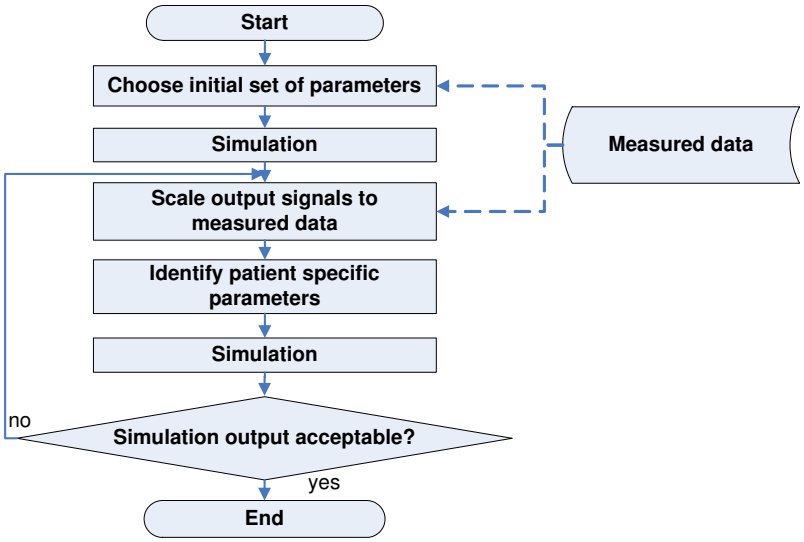

Figure 5.6: Parameter identification algorithm: 1.) a set of parameters is used for an initial simulation, 2.) data is then scaled to match the measured data and 3.) identified. This process is iterated until the simulation output is acceptable.

5.3.5.1 Summary of the Identification Process

Figure 5.6 gives an overview of the identification process, which is based on previous work (Hann *et al.*, 2006; Starfinger *et al.*, 2007b). The following steps are performed:

1. Obtain clinical measurements and signals as shown in Table 5.1
2. Use volume calculations to estimate the initial volume conditions for the CVS model
3. Use initial set of parameters to obtain first simulation output (Starfinger *et al.*, 2007b)
4. Scale simulation output signals (P_{pa}, P_{ao}, V_{lv}, V_{rv}) to match the clinical, porcine data (Starfinger *et al.*, 2007b)
5. Identify the animal-specific parameters for the scaled signals using the integral-based methods based on (Hann *et al.*, 2006)
6. Re-scale the simulation output signals to better match the porcine data
7. Repeat steps 4 to 6
8. Stop the iterative process when a set error tolerance is reached

5.3.5.2 Example

The following Figures show how the left and right ventricle signals improve with each iteration starting with the initial first simulation in Figures 5.7 and 5.8 and ending with Figures 5.13 and 5.14. Each Figure shows the pressure in left/right ventricle (P_{lv}/P_{rv}), pressure in aorta/pulmonary artery (P_{ao}/P_{pa}) and volume in left/right ventricle (V_{lv}/V_{rv}). The solid lines represent the clinical data (simulated) which are tried to identify the model parameters for. After re-simulation the model output signals are matched to the true clinical signals. The dotted lines are the model simulation output signals. Figures 5.7 and 5.8 show the true signals and CVS model output signals before the first iteration, as obtained for the initially chosen parameter set. Figures 5.9 and 5.10 show the true signals and CVS model output signals after the first parameter identification and re-simulation with the identified parameters has taken place.

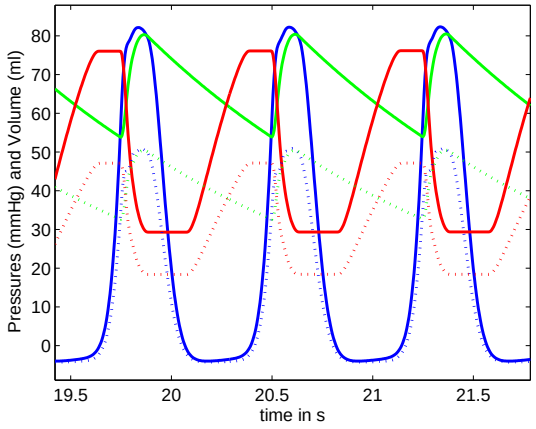

Figure 5.7: Left ventricle (LV): True (solid) pressure and volume signals vs. simulated CVS model output signals (dotted) before first parameter identification.

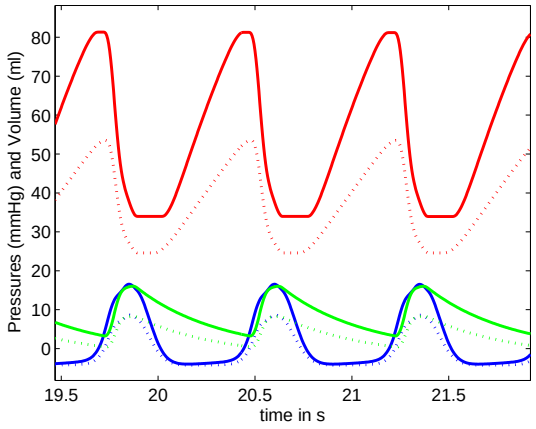

Figure 5.8: Right ventricle (RV): True (solid) pressure and volume signals vs. simulated CVS model output signals (dotted) before first parameter identification.

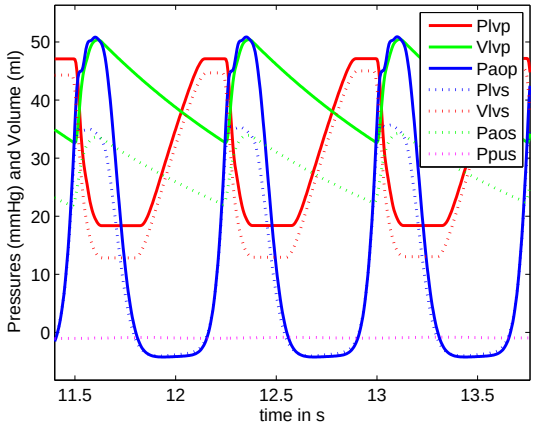

Figure 5.9: Left ventricle (LV): True (solid) pressure and volume signals vs. simulated CVS model output signals (dotted) after first parameter identification.

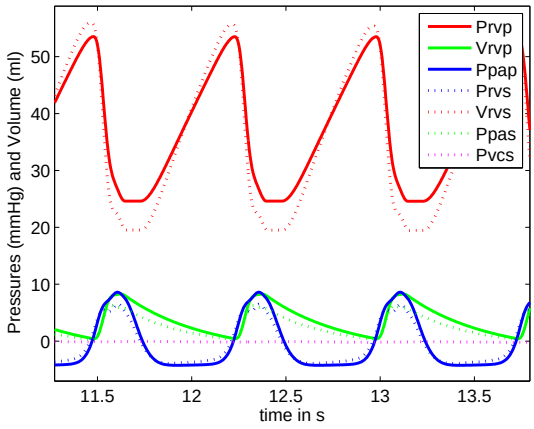

Figure 5.10: Right ventricle (RV): True (solid) pressure and volume signals vs. simulated CVS model output signals (dotted) after first parameter identification.

Figures 5.11, 5.12 and Figures 5.13, 5.14 show the true signals and CVS model output signals after subsequent iterations of the parameter identification process and following re-simulation with the identified parameters. In Figures 5.7 to 5.14, it can clearly be seen how the model output signals slowly converge with the true signals and the minimum and maximum values move closer to the true signal values. Note that the scaling used for creating these Figures is a simple minimum/maximum scaling, explaining why the waveforms slightly differ between the model output and true signal.

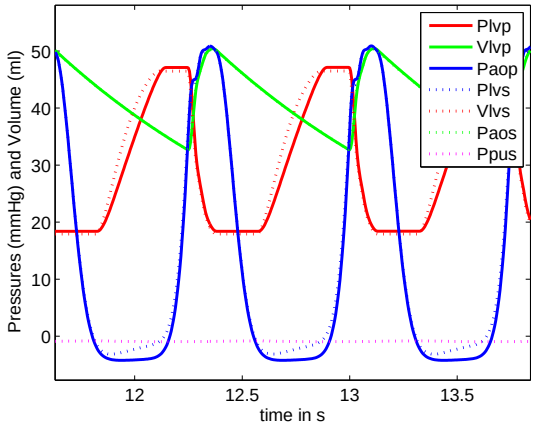

Figure 5.11: Left ventricle (LV): True (solid) pressure and volume signals vs. simulated CVS model output signals (dotted) after second parameter identification.

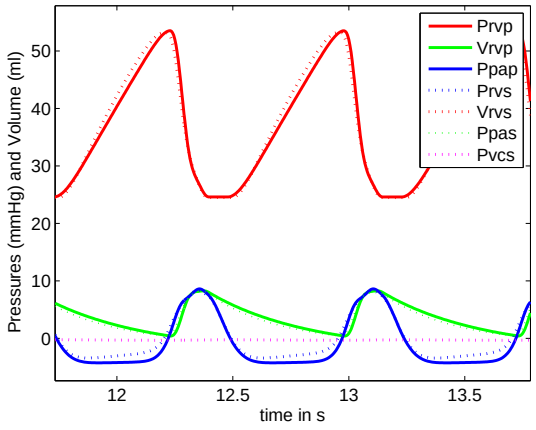

Figure 5.12: Right ventricle (RV): True (solid) pressure and volume signals vs. simulated CVS model output signals (dotted) after second parameter identification.

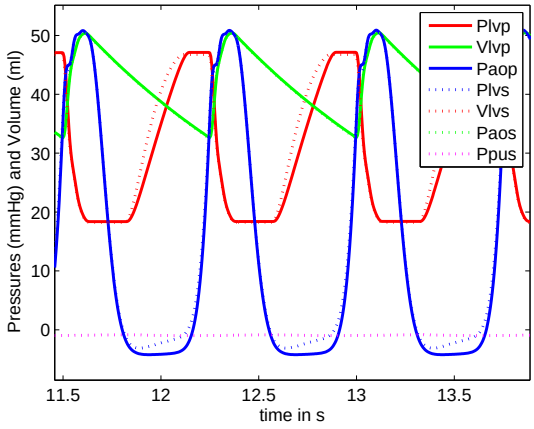

Figure 5.13: Left ventricle (LV): True (solid) pressure and volume signals vs. simulated CVS model output signals (dotted) after third parameter identification.

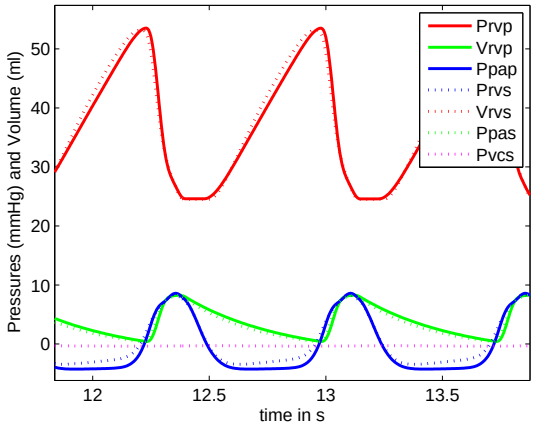

Figure 5.14: Right ventricle (RV): True (solid) pressure and volume signals vs. simulated CVS model output signals (dotted) after third parameter identification.

5.4 Structural Identifiability

The conventional identifiability theory only holds for either linear differential equations or polynomial differential equations e.g. with saturation. This theory cannot be easily applied in this full non-linear model including ventricular interaction. However, by making P_{pu} and P_{vc} constant in the full model, setting $V_{spt} = 0ml$ and $P_{peri} = 0mmHg$, the left ventricle systemic system is separated from the right ventricle pulmonary system. The theory can now be applied, but only on the separate stages of filling and ejection, as across a complete heart beat there are nonlinear Heaviside functions due to the open on pressure, close on flow valve law. From these equations it can be shown that the model is structurally identifiable. A more useful theory would be to take into account modelling error and noise, but no identifiability theory currently exists to handle this case.

5.5 Summary

This chapter presented the integral-based methods for the CVS model parameter identification process. More details and the derivation of Equations 5.7-5.12 can be found in (Hann *et al.*, 2006). The parameter identification process was further explained as illustrated in Figure 5.6 and Section 5.3.5.1, summarizing the iterative steps of the process.

The scaling method was presented in Section 5.3.2 and an example given in Figures 5.7-5.14. Table 5.1 summarized the input signals for the identification process. These signals are commonly monitored and measured in a clinical environment. Finally, the structural identifiability was mentioned, ensuring the identification of unique parameter values.

Chapter 6

Application to Clinical Data: Model and Identification Process Validation

This chapter clarifies and details the primary physiological and computational reasons for modifying and extending the original CVS model, as well as the associated adjustments to the parameter identification process. The extended CVS model and all newly developed methods are justified with regard to their intended purpose of patient-specific model-based parameter identification using a physiological cardiovascular and circulatory model. The application to a real-time clinical environment with critical care patients also adds focus to some of the modelling decisions made.

6.1 Introduction

Model validation is the most important part of developing a model for clinical use. A model will only be accepted and used when it has passed rigorous validation tests that convince clinicians of its safety and efficacy. However, every simulation model can only be an approximation of the actual system and will never fully represent the true system. A model is thus only accurate for the special purpose for which it was developed.

More specifically, the CVS model presented in Chapters 3 and 4, is an accurate representation of the macro-dynamics of the cardiovascular and circulatory system as typically seen in ICU patients. It is not intended to use the CVS model,

or any extensions to it, for micro-analysis, such as analyzing flow rates or shear stresses at the arterial wall. These analyses would require for more localized or detailed models, or some form of multi-scale modelling approach.

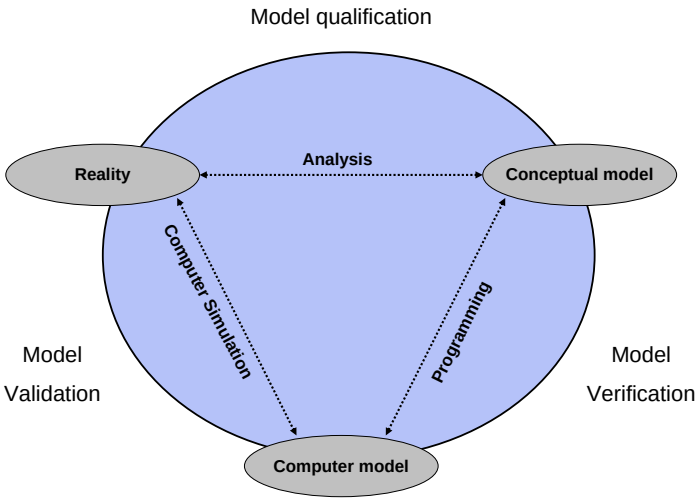

Figure 6.1: Validation process for simulation models, source: (Schlesinger, 1980).

Figure 6.1 shows a general framework of validating simulation models (Schlesinger, 1980). As can be seen in Figure 6.1, a conceptual model is generated by analysis of the real world. Subsequently, the model is programmed and the correctness of the programming needs to be verified. Once this task has been achieved, the model needs to be validated for its purpose.

6.2 Model Qualification

This part of the model validation process is concerned with whether the model is an accurate representation of the real system with regard to its intended purpose. More specifically, it has to be clarified if the CVS model is a correct representation of the true circulatory system and an appropriate balance between model complexity and accuracy has to be found. Thus, the model has to be a reasonable representation for the intended purpose of its use, in this case as a diagnostic and therapy decision support tool.

The CVS model has been validated in several simulation studies (Smith *et al.*, 2004, 2006, 2007) and in porcine experiments of Pulmonary Embolism, Septic shock and PEEP titrations at different volemic levels (Desaive *et al.*, 2007, 2008; Starfinger *et al.*, 2007b, 2008d,e). In all studies, the model and developed methods were able to identify the main hemodynamic trends during healthy and diseased states. In addition, it was able to identify specific parameter changes and trends at the onset of diseases and/or treatments that were clinically and physiologically expected. These validation studies thus increase the confidence in the CVS model and parameter identification process and the model seems to be a legitimate description of the real circulatory system.

6.3 Model Verification

Model verification is used to determine if the computer model (programmed in Matlab) properly represents the conceptual description of the model, as illustrated in the overview given in Figure 3.4. After extensively testing the Matlab program and provided that there are no internal coding or source program errors, it can be assumed that the computer program works within the tested range. It should be noted that no computer program can ever realistically be fully verified to guarantee a 100% error-free implementation.

6.4 Model Validation

Model validation is defined as determining that the model output signals have sufficient accuracy for the model's intended purpose and over the domain of the model's intended applicability (Martis, 2006; Sargent, 1998). In this case, the goal of the CVS model validation is to increase the model's credibility. Increased credibility would make it a useful tool that, clinically, addresses the right problems and provides accurate information about the circulatory system being modelled to attending clinical staff.

The following paragraphs highlight the problems encountered during the model and parameter identification validation process. As a result, the original CVS model (Smith, 2004) and identification method (Hann *et al.*, 2006) have been extended in this research. The new and modified form is presented in Chapters 3, 4 and 5, respectively.

This chapter therefore summarizes the modifications that were developed to solve problems encountered during the validation process using the original model of Smith (2004); Smith *et al.* (2004). The problems are briefly discussed here and solutions are provided that resolved the problems. Note that all problems mentioned in this chapter are problems of the original CVS model and identification process and have been resolved for the extended model and methods. The overall goal is to use these issues to further highlight the extended model presented in a clinically relevant and physiological fashion.

6.4.1 Problems of the Original Identification Process

If the CVS model is uniquely identifiable then there is always only one set of parameters that satisfies the integrals in the identification equations. Naturally, this state can only be achieved when the simulated model output matches all true clinical signals, such as all flows, volumes and pressures. However, this scenario is very unlikely in a real world application with noise and sensor error. Thus, estimations have to be performed, which will introduce error.

Introducing error by not providing all possible signals during the identification process will result in a non-unique parameter set. In other words, there will be different sets of parameters, which may all produce a subset of similar output signals from the model to those that were measured. When subsequently used as model parameters for forward simulations erroneous predictions and trends may result. These different output signals may only vary slightly with negligible small differences in the signals that are used to identify the data. However, there will most likely be differences in certain volumes, such as the volume in the aorta (V_{ao}). Hence, there have to be some restrictions and pre-assumptions about these not readily available signals to guarantee that the best parameter set is found, which also satisfies these additional physiological or clinical constraints.

Furthermore, there are parameters that compensate for each other. Thus, if one parameter is low the other one is typically high, but taken together produce the same output yielded if the first parameter is high and the second low. There are some obvious compensation mechanisms. For example, R_{sys} usually trades off with E_{vc}, as both parameters share integral equations and thus one integral matrix in the identification process.

However, there seems to be no simple way of characterizing all the possible compensation mechanisms, as all main parameters compensate each other in a

more or less obvious way. These trade-offs are the reason for obtaining non-unique parameter sets. Hence, restrictions on certain parameters have to be introduced to not allow all parameters to freely change. This need for added constraints is especially true for the valve resistances (R_{av}, R_{mt}, R_{tc} and R_{pv}), which should remain largely fixed during the identification process, especially when no stenosis or regurgitation are expected to develop.

Note, that these constraints should not hinder the identification of the best or true parameter set. An initial parameter set is chosen to start, and all subsequent identifications are based on these parameters and change relative to them. Thus for example, if a stenosis is present, the first identified resistance value serves as the baseline value and it can be assumed that the stenotic condition will not change significantly during the course of time (assumed to relatively short) where identifications are performed. It can further be assumed that the respective resistance remains largely constant during the identification process, justifying the process of keeping the valve resistance parameters fixed.

However, to use the identification process for real clinical data, one has to guarantee that all estimations and initial parameter guesses are valid. Furthermore, it has to be determined, which parameters have to be identified and which can be kept at fixed values.

The questions that are raised are obvious: How does one know which set of parameters is the correct one? How can false parameter changes be prevented? What parameters should remain constant? The overall question is one of adding constraints or bounds to the identification process to enhance and ensure identifiability of the model in the presence of limited, noisy clinical data.

The following paragraphs explain how these problems were resolved and provide explanations for adjustments made to the CVS model and identification process presented in Chapters 3, 4 and 5. This description is thus provided to further highlight the capability and structure of the model and as an added source or form of model validation.

6.4.2 Solution 1: Improving the Identification Process

6.4.2.1 Predetermining Model Parameters

To overcome identification trade off problems, it is vital to carefully examine the CVS model to get an idea of how and why the parameters change, and how

they interact with each other. After running several simulations and identifying different output signals with different volumes, certain mechanisms that link parameters to model output signal changes become obvious. These parameter - output signal mechanisms can be described by equations. For example, from the CVS model structure it can be directly derived that R_{sys} has to correlate with $(P_{ao} - P_{sys})/SV$, which is also clinically and physiologically expected.

Further correlations can be found within the CVS model and good correlations are found between left ventricle elastance E_{eslvf} and the ratio of $SAP/LVESV$. This relationship is expected because E_{eslvf} is derived from the end-systolic pressure and volume relationship (ESPVR), and characterizes the ventricle contractility. The same applies for E_{esrvf} and $SPAP/RVESV$. The overall idea is to use these clinically and physiologically expected model correlations to constrain some of the parameter values.

Parameter values can be fixed at pre-determined values, which can either be well known population values found in the literature or, as in this case, pre-calculated values. This approach has the advantage of making the model more identifiable as less parameters need to be optimized. Keeping model parameters at constant values will introduce some error, but this error is consistent over all identifications. Hence, this scenario is likely to be preferred over an identification where the parameters are less likely to be uniquely identifiable or consistently identified over time. Note that in the latter case, inconsistent identification due to poor identifiability would likely result in missing trends in parameter values as CVS dysfunction occurs - i.e. missed or poor diagnosis.

6.4.2.2 Example: Pre-determining E_{esrvf} and E_{eslvf}

Approach 1, E_{es} = SAP/ESV: The left and right ventricular end-systolic elastances are defined as the slope of the ESPVR and can be obtained from the PV-loop. Theoretically, one needs at least two PV-loops to measure the slope of the ESPVR. However, the first and simplest assumption might be that the x-axis intercept V_d is zero, which gives the approximate E_{es} value defined:

$$E_{es} = \frac{systolic\ arterial\ pressure}{ESV - Vd} \tag{6.1}$$

$$= \frac{systolic\ arterial\ pressure}{ESV} \tag{6.2}$$

Because V_d is only used in the ESPVR equation (see Equation 3.44) in the entire CVS model, one can see that V_d directly trades off with E_{es}. Thus, a higher V_d value will cause a higher E_{es} value and vice versa. It therefore follows that there will be no effect on the other model signals using this approach and that a $V_d = 0$ value will only change the absolute value of E_{es}, but will have no effect on its trends or on the other parameters.

Further, each E_{es} value obtained can later be adjusted to the true absolute value by correcting the V_d value to a more realistic value, such as for example $V_d = 20ml$. Several simulations were performed to confirm this assumption and no difference in the signals and subsequently identified parameters was found.

Approach 2, Single-beat ESPVR estimation: To improve the initial E_{es} parameter value estimate used, a second approach has been studied. This approach calculates E_{es} based on a previously published single-beat estimation method (Brimioulle *et al.*, 2003). Briefly, this method uses an isovolumetric ventricular pressure (P_{rv}, P_{lv}) for a single heart beat to determine the end-systolic pressure-volume relationship (ESPVR). Figure 6.2 shows this method schematically, where $A \rightarrow B$ is the isovolumetric contraction, $B \rightarrow C$ the ejection period, $C \rightarrow D$ represents the isovolumetric relaxation phase and $D \rightarrow A$ the filling. The end-systolic pressure volume relationship is given by the $V_d - C$ line and ESPVR is assumed to be linear and afterload independent.

In particular, trace $ABCD$ is the P-V loop for a normal beat, where A is the end-diastolic point at the end of the filling period, B is the point after isovolumetric contraction just before ejection, C is the point after ejection (end-systolic) and D is the point after isovolumetric relaxation, shortly before filling starts again. Traditionally, the ESPVR is determined by progressively increasing the afterload at the same preload (for example by using a pulmonary artery constriction) and recording several P-V loops as shown in Figure 6.2. The end-systolic points of the recorded P-V loops will then all lie on one line, forming the ESPVR.

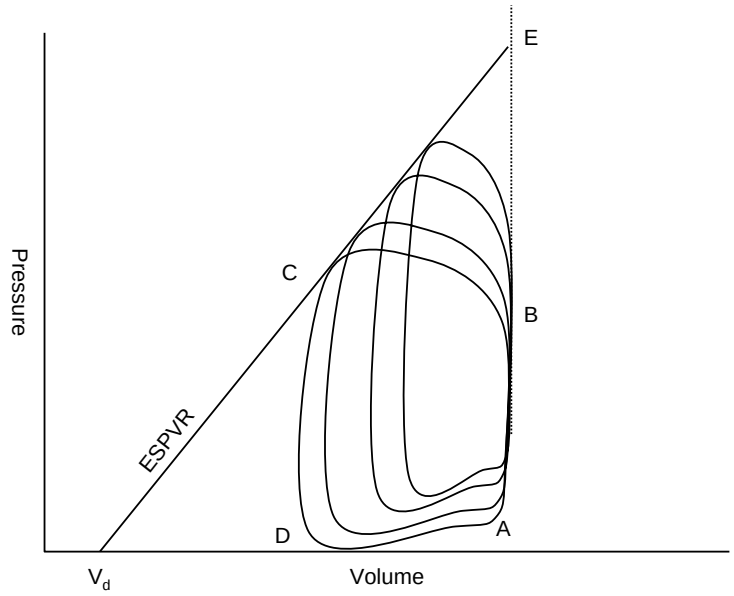

Figure 6.2: Principle of single-beat ESPVR estimation, adapted from (Brimioulle *et al.*, 2003). The line through C for a single beat that intersects V_d and the AB isovolumetric line at point E is used to estimate ESPVR and E_{es}.

In contrast, in the single-beat approach, only one P-V loop is needed and the point E is the calculated maximal pressure of an isovolumetric beat ($P_{max,iso}$). The line E-C will then define the ESPVR. The value of V_d is given as the x-axis intercept. To determine $P_{max,iso}$, a pressure reading (P_{lv}, P_{rv}) of one heart beat is used and the isovolumetric pressures are defined as the pressure values before the maximum first derivative $\frac{dP}{dt}$ and after minimal $\frac{dP}{dt}$. The maximum pressure ($P_{max,iso}$) is obtained by fitting the following equation to the isovolumetric pressure values (Brimioulle *et al.*, 2003):

$$P = a + b \cdot \sin(c \cdot t + d) \tag{6.3}$$

where t equals time. $P_{max,iso}$ is obtained as the maximum of the fitted pressure curve as can be seen in the left panel of Figure 6.3. The right panel of Figure 6.3 shows how this $P_{max,iso}$ is then used to obtain the ESPVR in the P-V loop. The end-systolic point C is calculated as the intercepting point of the ventricular and arterial pressure. Note that due to noise in the pressure signals, one additional

P-V value before and after the end-systolic P-V value is calculated and finally, E_{es} and V_d are determined as the mean over these 3 values.

However, when this new approach of calculating ESPVR with the corresponding E_{es} and V_d values was validated using simulated model output data with various V_d and E_{es} values, problems in the identification of V_d and thus ESPVR became obvious, as can be seen in the examples shown in Figures 6.4 and 6.5.

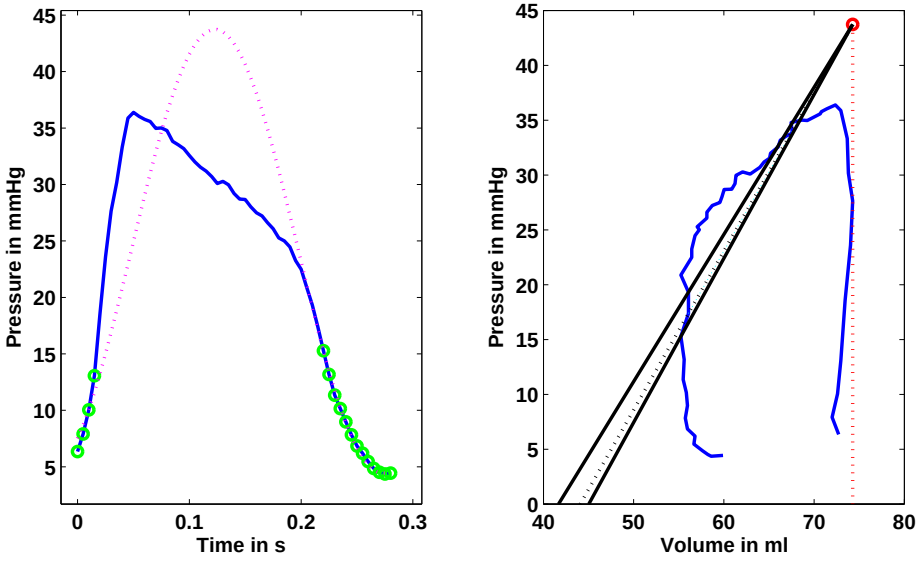

Figure 6.3: Determination of E_{esrvf} and V_d from the maximum isovolumetric pressure $P_{rvmax,iso}$, adapted from (Brimioulle *et al.*, 2003).

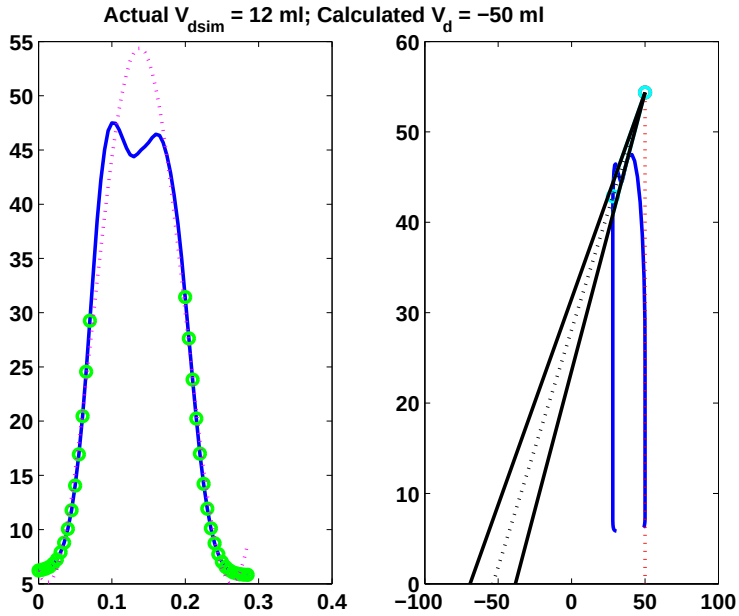

Figure 6.4: Determination of E_{esrvf} and V_d from simulated data with $V_{dsim} = 12ml$ and $V_{dcalc} = -50ml$.

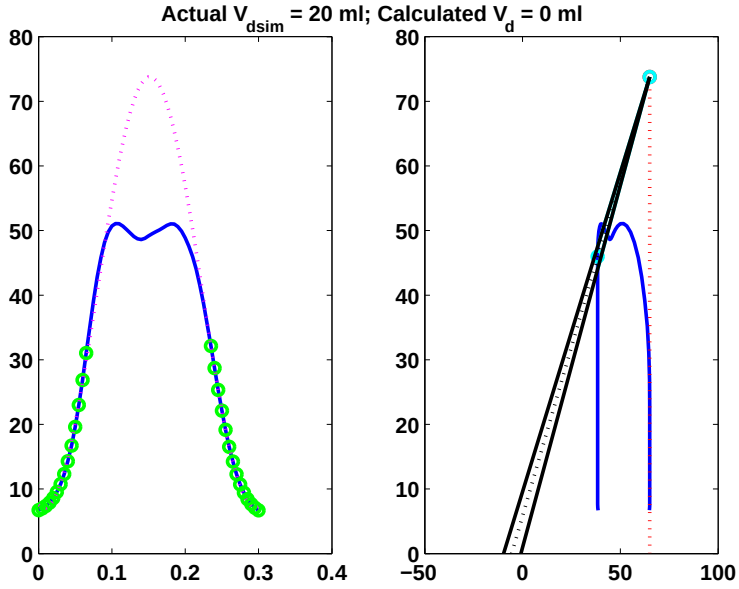

Figure 6.5: Determination of E_{esrvf} and V_d from simulated data with $V_{dsim} = 20ml$ and $V_{dcalc} = 0ml$.

Figures 6.4 and 6.5 show the results obtained using the single-beat ESPVR estimation method for simulated model outputs with no added noise. Figure 6.4 shows the results for a simulated $V_d = 12ml$ and Figure 6.5 for a simulated $V_d = 20ml$. It can clearly be seen how the single-beat method obtains an incorrect ESPVR and thus a very different V_d value compared with the true (simulated) value. The correct determination of the end-systolic point (V_{es}, P_{es}) is especially sensitive, which is crucial in determining the correct slope of ESPVR. In this case, only simulated data was used, thus providing a very clear, defined end-systolic point. However, the results obtained are poor and will likely become even worse using real clinical data where measurement noise will complicate the correct determination of the (V_{es}, P_{es}) values used.

Nevertheless, it should be mentioned that this single-beat method might well be suitable for determining the correct ESPVR slope directly from clinical data. However, it is not suitable for use with our model data. This difference occurs because the model output signals yield different waveform shapes compared to clinical data because only a minimal model that does not perfectly capture all the dynamics seen in clinical measurements is used in this study.

Therefore, in the CVS model simulations presented, E_{eslvf} and E_{esrvf} are calculated as described in Approach 1 (Section 6.4.2.2) and V_{dlvf} and V_{drvf} are set to be zero.

6.4.2.3 Example: Pre-determining E_{ao} and E_{pa}

This approach of pre-calculating model parameters can similarly be applied to other parameters in the CVS model. Thus, suitable approximations for the arterial elastances E_{ao} and E_{pa} are described in Section 5.2.1, in Equations 5.27 and 5.28.

6.4.2.4 Example: Pre-determining E_{sys}, E_{cap}, E_{vc} and E_{pu}

Similarly to the arterial elastances E_{ao} and E_{pa}, the remaining CVS model elastances can be estimated using known or estimated pressures and volumes. For example, the initial E_{sys} value can be estimated:

$$E_{sys} = \frac{P_{sys}}{V_{syseff}} \tag{6.4}$$

where P_{sys} is either measured or estimated and V_{syseff} results from the volume calculations described in Section 4.2. The other elastances are estimated in a similar way.

Importantly, these estimations are only used for the initial parameter set. The estimated elastance parameters are then used to obtain the first simulation output signals to start the identification process. During this process these elastances are more specifically identified.

6.4.2.5 Improving the Scaling Process

Scaling naturally introduces error. In particular, it is important to remember that the true signals are not used for identification. Instead model output signals are used and then scaled to match the true signal peak values. This approach assumes that the waveforms are not too different between the true and simulated signals. However, this assumption only holds true when sufficient effort has been spent to pre-match the signals and thus guarantee a good initial parameter set before the real identification process takes place.

To improve the results and decrease the likelihood for errors introduced in the scaling process, the scaling has been improved. The typically unknown flow signals (Q_{mt}, Q_{av}, Q_{tc}, Q_{pv}) are replaced by the measured or estimated volume signals, as first illustrated in Section 5.3.4. This approach has the advantage that a scaled, and thus new and changed volume signal, does not only affect the parameter identifications for parameters that are directly obtained from the volumes (such as E_{eslvf}, E_{esrvf} and the four valve resistances), but also parameters that are calculated using the flow signals (such as R_{sys} and R_{pulin}). Hence, with this approach it is guaranteed that a new and updated volume signal affects all possible parameters.

6.4.2.6 Volume Restrictions

As has been mentioned before in Section 6.4.1, the more input signals that are measured or estimated, the better the model parameter identification should be and the more likely it is that unique model parameters are found. For example, it might well be that two different sets of CVS model parameters can be used to simulate the same (or very similar) V_{lv} and P_{ao} model output signals. However, the V_{pv} and V_{cap} signals could be quite different, thus distinguishing the 2 parameter sets. However, if these signals are not known and/or ignored during the

identification process, the correct parameters may not be found. It is thus much better if as many signals as possible are included in the identification process, and using physiologically or clinically validated estimates aids this process.

Therefore, the identification process also includes the CVS model compartment volumes V_{vc}, V_{pv}, V_{cap} and V_{sys}. This inclusion means that the identification process uses additional input information and tries to match the CVS model output signals to these 4 additional volume signals. As these volume signals are estimated (see Section 4.2 in Chapter 4), it has to be kept in mind that these signals could also hinder the correct parameter set being found.

In particular, the CVS model may no be able to simulate these exact signals correctly. However, slight differences in the target and simulated model output signals can be incorporated into the identification process to prevent this issue from arising. Hence, it is always ensured that the identified parameters, when re-run in the CVS model simulation, not only produce good matches to the main input signals, such as V_{lv}, V_{rv}, P_{ao} and P_{pa}, but also good matches to the other estimated CVS model volumes and pressures P_{sys}, P_{cap}, V_{sys}, V_{cap}, V_{vc}, V_{pv}, V_{ao} and V_{pa}.

6.4.3 Solution 2: Improving the CVS Model

It is obvious, that a more realistic and physiologically correct CVS model will allow simulations that produce realistic results. It also means that parameters can be identified, whose values can be directly explained by physiology, and, generally speaking, all observed parameter changes are expected or clinically explainable. However, a less correct model or a model missing important dynamics will make it more difficult to obtain parameter values that can be similarly explained, or that can be used to make useful predictions about future parameter values or changes. An insufficient model structure where essential parameters are missing will also lead to other model parameters being misused to produce the expected output. The ID process will therefore identify parameter values that cannot be explained clinically or physiologically and behave different than expected.

As the CVS model does not have its own compartment for the atrium, the atrial properties are lumped together with the adjacent pressure-volume compartment, which is for the left ventricle the pulmonary vein (P, V_{pu}). For the right ventricle it is the vena cava (P, V_{vc}) compartment. In cases where the atrial pressure becomes negative, it would be advisable to also allow a negative P_{vc} and P_{pu}

pressure to capture this behavior. However, in the original CVS model (Smith, 2004) a negative P_{vc} pressure is not possible unless the volume V_{vc} becomes negative, as well. The modified and extended CVS model solves this problem by adding the intrathoracic pressure, as can be seen in Figure 3.4 and Equations 3.28 - 3.30, allowing these effects to be captured.

Other modifications included adding two additional P,V- compartments, one for the systemic capillaries (body) and one for the lung capillaries. P, V_{sys} and P, V_{cap} are added, as depicted in Figure 3.4, to enable more realistic model behavior in situations where arterial and venous resistances behave in opposite directions. For example, during the application of PPV and PEEP, LV afterload and RV preload decrease, resulting in an drop in R_{sys}, but an increase in R_{vr}, as explained in more detail in Section 4.1.2.1.

Another advantage of adding R_{vr} (resistance to venous return) into the CVS model is that a change in RV preload can now easily be simulated by adjusting R_{vr}. For example, in the original CVS model, vena cava constriction (VCC) is simulated by increasing the resistance R_{tc} (Smith *et al.*, 2006). However, this resistance is really the tricuspid valve resistance and not the resistance for controlling all of or the majority of venous return. The new modified CVS model allows R_{tc} and R_{vr} to change separately from each other, one resistance controlling venous return while the other characterizes the valve mechanics, such as stenosis or regurgitation.

6.5 Summary

This chapter investigated the model qualification, verification and validation. Necessary adjustments to the model structure and components, and to the identification process were included to allow the optimal model parameters to be identified in a consistent way. These adjustments included the pre-calculation of model parameters, such as E_{eslvf}, E_{esrvf}, E_{ao} and E_{pa}. By pre-calculating these parameters, less model parameters have to be identified and the identifiability of the remaining model parameters increases. Thus, a more optimal and consistent set of parameters can be found.

Further adjustments include the estimation of the initial model compartment volumes (V_{sys}, V_{cap}, V_{vc}, V_{pv}, V_{ao} and V_{pa}). Using these volumes in the identification process guarantees consistency over all identifications and subjects as the

CVS model output signals are not only matched to the main pressure and volume signals, but also to these compartment volumes. Note, that by using these estimated volumes, the initial estimation of the CVS model elastances E_{sys}, E_{cap}, E_{vc} and E_{pu} is possible. These elastances are then used to produce the first simulation output signals to start the identification process, and are then subsequently identified and optimized.

Chapter 7

Application to Porcine Experiments of Pulmonary Embolism (PE)

This chapter[1] gives initial results obtained when combining the CVS model with the extended integral based parameter identification method to track drug induced pulmonary embolism in porcine data from an initial healthy state to the fully developed disease state.

7.1 Introduction

7.1.1 Epidemiology and Pathophysiology of PE

Pulmonary Embolism usually develops from thrombi that form in the deep veins of the legs, pelvis or arms and dislodge and embolize to the pulmonary arteries. Pulmonary embolism is a serious condition that can cause permanent damage to the affected lung, low oxygen levels and damage to other organs as caused by the decrease in oxygen supply. If a clot is large, or if there are many clots, pulmonary embolism can cause death.

Pulmonary arterial obstruction and the release of vasoactive agents such as serotonin by platelets elevate pulmonary vascular resistance. Alveolar dead space increases which impedes gas exchange and reflex bronchoconstriction increases airway resistance and lung edema decrease pulmonary compliance resulting in an

[1]This chapter is based on (Starfinger *et al.*, 2007b).

increased right ventricular afterload and subsequently dilatation, ischemia and dysfunction of the right heart (Goldhaber, 1998).

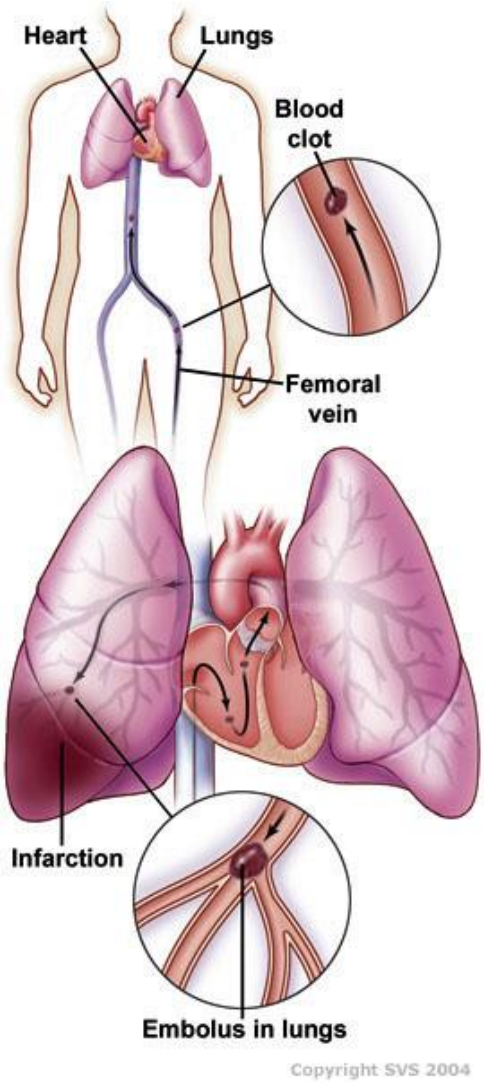

Figure 7.1: Schematic illustration of Pulmonary Embolism with an embolus formed in the femoral vein and travelling to the infarction site in the lung, obtained from the website of the Society of Vascular Surgery (SVS).

7.1.2 Incidence of PE and Diagnostic Methods

Diagnosing Pulmonary Embolism accurately and in a timely manner is challenging as the clinical signs and symptoms are heterogenous and non-specific and thus a wide range of symptoms is possible. The mortality rate of acute PE patients is higher than in patients with acute myocardial infarction, exceeding 10% at 30 days and 16% at 3 months (Goldhaber *et al.*, 1999). Thus, as PE is potentially lethal, a fast and accurate diagnosis is essential.

Clinical suspicion of PE exist, when the patient complains about acute dyspnea without an apparent cause (Nijkeuter & Huisman, 2005). Other symptoms include acute chest pain, cough, hemoptysis (coughing up of blood or blood-stained sputum), cyanosis and fainting. Clinical signs present are acute right ventricular dysfunction, including tachycardia, low arterial blood pressure, neck vein distention and an accentuated pulmonary component of the second heart sound or a tricuspid regurgitation murmur. However, these signs are non-specific and inconsistently found in PE patients. Hence, further diagnostic tests are necessary, which usually include clinical prediction rules (for example Well's score and Geneva score), $_D$-dimer testing ($_D$-dimers are degradation products of fibrin which are released when a thrombus is degraded by fibrinolysis) and/or imaging techniques (such as lung scintigraphy and helical CT). However, these diagnostic tests are often very costly and consume a considerable amount of resources.

Thus, having a diagnostic tool which can accurately identify pulmonary embolism would be beneficial and help provide a better and more consistent patient care. The goal of this research is to demonstrate the applicability of the CVS model for identifying the varying PE disease states from the healthy state to the onset of the disease and fully diseased state.

In this research, the full range of hemodynamic responses was captured with mean identification errors of 4.1% in the pressures and 3.1% in the volumes for 6 sets of clinical data. Pulmonary resistance increased significantly with the onset of embolism in all cases, as expected, with the percentage increase ranging from 89.98% to 261.44% of the initial state. The model also predicted an increase in the right ventricle expansion index and a decrease in septum volume consistent with known physiological response to pulmonary embolism. These results are a first clinical validation of this model-based cardiac diagnostic approach.

7.2 Methods

Under the control of the Ethics committee of the Medical Faculty of the University of Liège, pulmonary embolization was induced in pigs with autologous blood clots (Desaive *et al.*, 2005; Ghuysen *et al.*, 2008). The clots were injected every two hours with decreasing concentrations. Aortic pressure and pulmonary artery pressure are measured using micromanometer-tipped catheters (Sentron pressure-measuring catheter; Cordis, Miami, FL) while right and left ventricle pressures are measured using 7F, 12 electrodes (8-mm interelectrode distance) conductance micromanometer tipped catheters (CD Leycom, Zoetermeer, The Netherlands).

The conductance catheter technique is based on measuring time varying conductance of the blood in the ventricle. This conductance is approximately linearly proportional to the blood volume in the ventricle. To improve the accuracy, the ventricle is divided in several segments and the conductance of each segment is obtained by measuring the voltage between two adjacent electrodes of the conductance catheter. The ventricular volume is obtained as the sum of the segmental volumes (Baan *et al.*, 1984).

The pigs were bled during the experiment. However, the exact blood loss was not measured. In order to account for the blood loss, the volume available in the circulation is approximately linearly reduced. The initial start volume is estimated using a total blood volume of $65 - 70ml/kg$ (Morton *et al.*, 1993) and the distribution of blood volume in heart, pulmonary system, aorta and vena cava (Klabunde, 2004). The blood loss is then approximated using the reduction in left ventricular end-diastolic volume (LVEDV) as obtained from (Preisman *et al.*, 2002). It is worth noting that the total volume is, despite not being part of the parameter set, also identifiable as the volume which allows the best fit to the given clinical data. Additionally it should be mentioned, that to maintain simplicity the minimal CVS model ignores the unstressed volume, thus the volumes at zero pressure (V_d and V_o) are set to zero for all chambers, except for the septum volume.

7.3 Results

The parameter identification method is applied to the pig data. The identified parameters are used to rerun the CVS model and produce pressure and volume curves, which are then compared to the clinical data. This process is repeated in

all the measured periods during the pulmonary embolism experiment using the pig's steady state response data. The results are shown for two of the pigs in detail followed by a summary of the results in all pigs.

7.3.1 Pig 1

7.3.1.1 Beginning of Experiment - "Healthy" Status at 30 mins

Figure 7.2 shows the simulated model output for the pressure in the left and right ventricles (P_{lvs}, P_{rvs}), the volume in the left and right ventricles (V_{lvs}, V_{rvs}) and the pressure in the aorta, pulmonary artery (P_{aos}, P_{pas}) overlaid with the corresponding clinical data ($P_{lvp}/P_{rvp}, V_{lvp}/V_{rvp}, P_{aop}/P_{pap}$) at 30 mins into the pulmonary embolism experiment. The simulation data matches the measured porcine data very well with errors within 4.2 mmHg and 4.4 ml for maximum and minimum pressures and volumes respectively.

Figure 7.3 shows the Volume-Pressure waveforms for the left and right ventricles in more detail. The upper panel in Figure 7.3 is the simulated ventricle volume and the dotted line is the measured porcine volume for 2 heartbeats. The lower panel shows the same results obtained for the ventricle pressure. Finally, Figure 7.4 shows the resulting Pressure-Volume relationships (P-V loops) for the left and right ventricles. Errors in all cases are in the range of 0.15% to 4.76%.

7. APPLICATION TO PORCINE EXPERIMENTS OF PULMONARY EMBOLISM (PE)

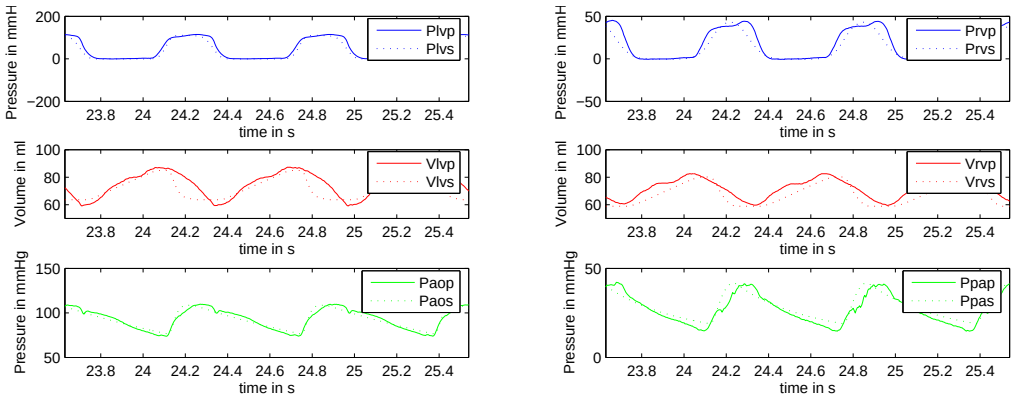

(a) 30 mins, left ventricle

(b) 30 mins, right ventricle

Figure 7.2: Pig 1, Model output vs clinical data

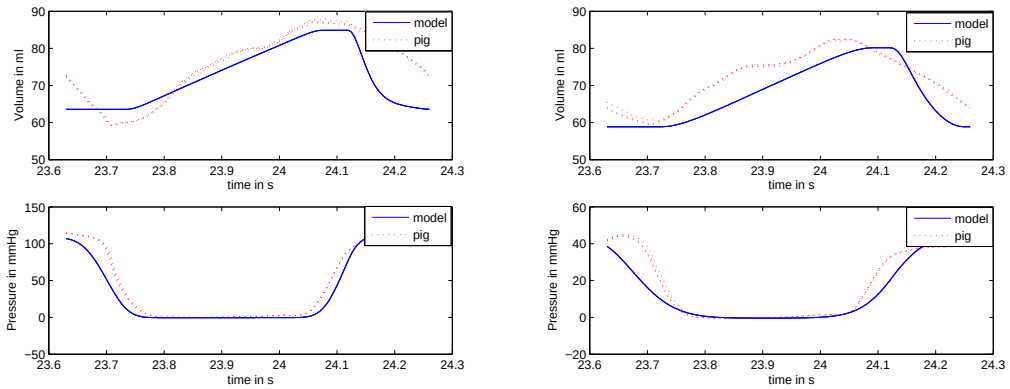

(a) 30 mins, left ventricle

(b) 30 mins, right ventricle

Figure 7.3: Pig 1, Model output vs clinical data for Pressure and Volume

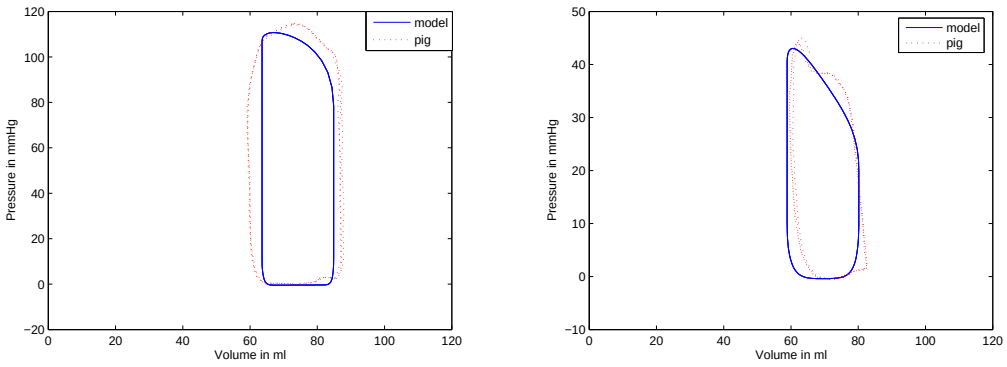

(a) 30 mins, left ventricle

(b) 30 mins, right ventricle

Figure 7.4: Pig 1, Pressure-Volume Relationship

7.3.1.2 During the Experiment - at 120 mins

Figure 7.5 shows the P-V loops for the left and right ventricle 120 minutes into the pulmonary embolism experiment. Although the model didn't exactly capture all the volume shapes in the left and right ventricles, the pressure waveform shapes were accurately captured, as well as the maximum and minimum pressures and volumes. Overall, the errors in the maximum pressures and volumes that are typically used to define trends in different disease states are within 0.17% to 4.95%, respectively.

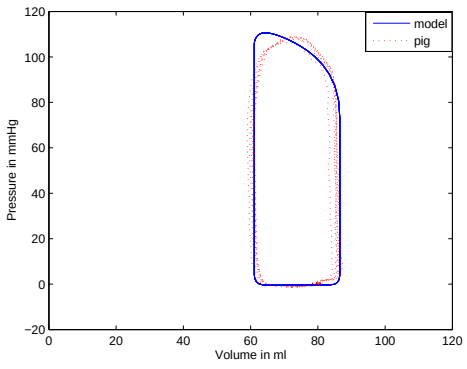

(a) 120 mins, left ventricle

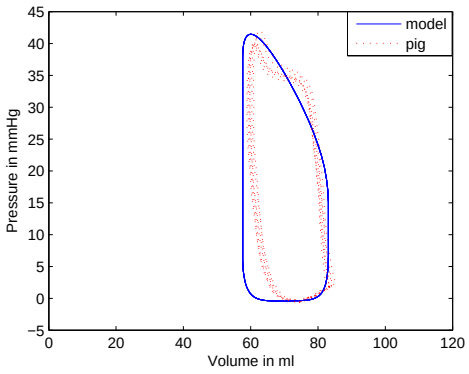

(b) 120 mins, right ventricle

Figure 7.5: Pig 1, Pressure-Volume Relationship

7.3.1.3 End of Experiment - at 180 mins

Figure 7.6 displays the P-V loops at 180 minutes, which was the end of the experiment. Again the results show a very close match. Errors in the maximum pressures and volumes are all within 0.20% and 6.59% respectively.

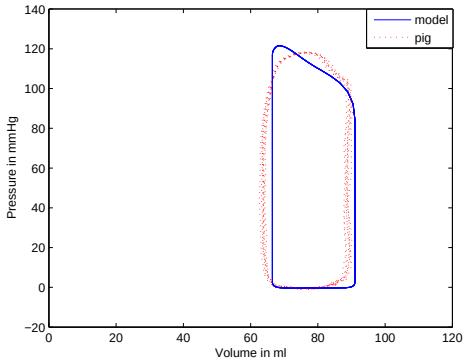

(a) 180 mins, left ventricle

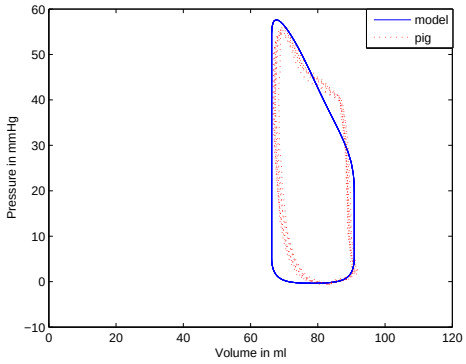

(b) 180 mins, right ventricle

Figure 7.6: Pig 1, Pressure-Volume Relationship

7.3.1.4 Summary of Identified Parameters

The identified subject (pig) specific parameters systemic and pulmonary vascular resistance, R_{sys} and R_{pul}, differ significantly between healthy and disease state as Figure 7.7 shows with R_{pul} increasing by 261.44%.

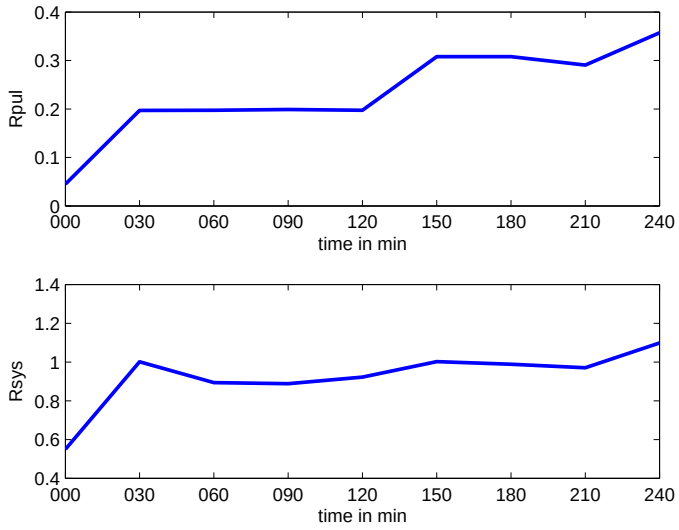

Figure 7.7: Pig 1: Pulmonary and vascular systemic resistance during pulmonary embolism experiment

7.3.2 Pig 2

Figure 7.8 thumbnails the P-V loops for pig 2 at 0, 120 and 180 mins. Similar accuracy in capturing the clinically observed dynamics is evidenced. The errors in the maximum pressures and volumes are all within 0.01% and 9.86% respectively. Figure 7.9 shows that the identified pulmonary and systemic vascular resistance (R_{pul}, R_{sys}) differ significantly between healthy and diseased state, as expected, with R_{pul} increasing by 89.98%.

The model also captures the specific hemodynamic changes resulting from pulmonary embolism. The volume in the right ventricle (V_{rv}) increases during pulmonary embolism due to the increased afterload, which causes right ventricle dilation. Figure 7.10 shows the time evolution of the left and right end-diastolic volume ratio (RVEDV/LVEDV) as an index for the expansion of the right ventricle during the experiment. As expected, this index increases.

Ventricular interaction changes are also captured, where Figure 7.11 shows the time evolution of the mean value of the septum volume (V_{spt}) over a cardiac cycle, decreasing from the beginning to the end of the experiment. This result agrees with the physiological fact that the overfilled right ventricle compresses the underfilled left ventricle during the embolization. Hence, V_{spt} decreases because it is defined as being part of the right ventricle volume (Chung *et al.*, 1997; Smith, 2004). Finally, it's worth nothing that as the embolism grows and left ventricle volume decreases the systemic resistance, R_{sys}, increases in Figure 7.9, in the reflexive attempt to divert more blood to the heart. However, R_{sys} drops at the end likely due to the near death of the pig and very low blood volume.

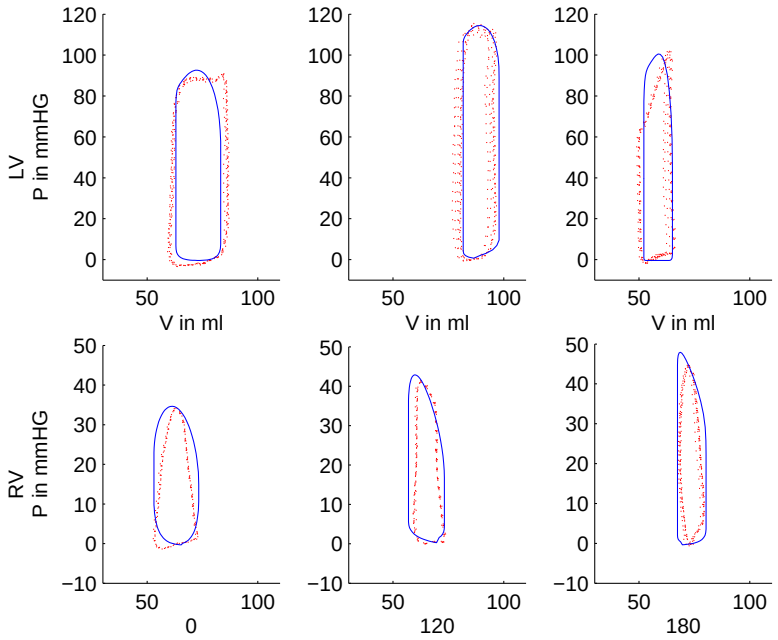

Figure 7.8: Pig 2: P-V Loops for left and right ventricle at 30, 120 and 180 mins

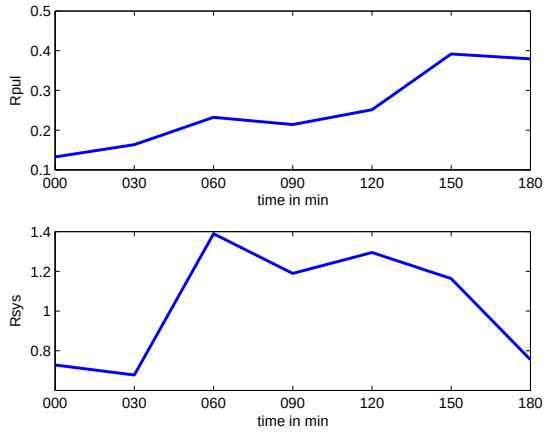

Figure 7.9: Pig 2: Pulmonary and vascular systemic resistance during pulmonary embolism experiment

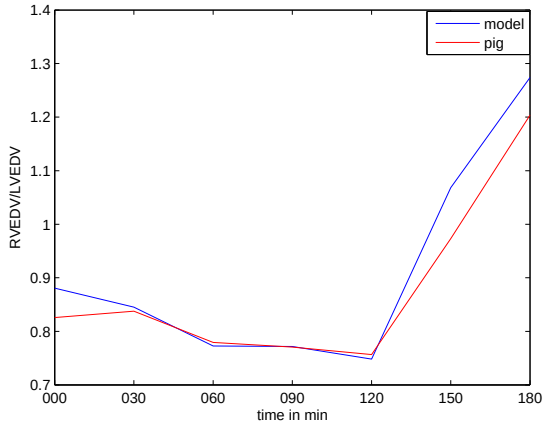

Figure 7.10: Pig 2: RVEDV/LVEDV, simulated vs porcine data

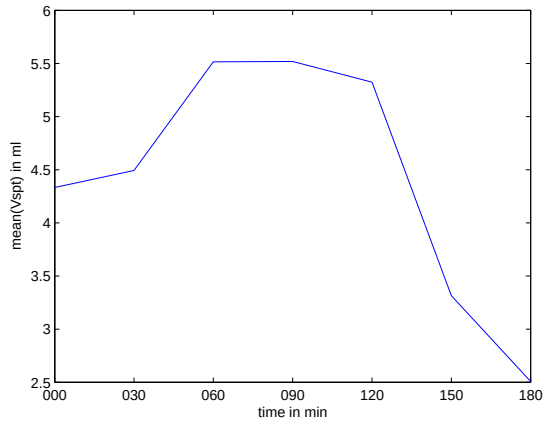

Figure 7.11: Pig 2: Mean septum volume V_{spt} during pulmonary embolism experiment

7.3.3 Summary of Results in All 6 Pigs

Table 7.1 gives the mean and standard deviation of the absolute errors for the maximum and minimum pressures and volumes. The values are shown for the pressure in aorta (P_{ao}), pulmonary artery (P_{pa}) and left and right ventricle (P_{lv},P_{rv}). Table 7.2 gives the mean error and standard deviation for the volumes in both ventricles (V_{lv},V_{rv}). Table 7.3 shows the maximum percentage increase for pulmonary vascular resistance (R_{pul}) and maximum percentage changes in

systemic vascular resistance (R_{sys}) and the contractilities (E_{eslvf}, E_{esrvf}) in the left and right ventricle during the pulmonary embolism experiment. The number of heart beat periods that are captured as well as the different points in time are shown. The primary goal is to capture rising pulmonary vascular resistance, R_{pul}, in this clinical case. Figure 7.12 shows R_{pul} over time for all 6 pigs.

	Pressures (mmHg)				
Pig	P_{ao}	P_{pa}	P_{lv}	P_{rv}	Total Error
Pig 1	3.501±3.247	2.313±1.939	2.313±2.392	1.377±1.651	2.367±2.487
Pig 2	2.693±1.545	2.666±1.445	1.894±0.880	1.308±1.172	2.210±1.404
Pig 3	2.831±2.572	2.885±1.562	1.163±1.000	1.306±1.784	2.035±1.972
Pig 4	2.567±2.130	2.305±1.796	2.414±2.607	0.571±0.708	1.956±2.097
Pig 5	5.042±3.161	2.394±1.827	1.604±1.179	1.264±1.337	2.576±2.505
Pig 6	2.753±2.048	2.542±2.177	2.102±2.457	1.701±2.587	2.275±2.341[1]
All Pigs	3.207±2.638	2.472±1.788	2.022±2.007	1.186±1.525	2.223±2.173

Table 7.1: Mean model response errors and standard deviation for maximum and minimum Pressures combined.

	Volumes (ml)		
Pig	V_{lv}	V_{rv}	Total Error
Pig 1	1.666±1.682	1.273±1.187	1.477±1.473
Pig 2	2.073±1.369	1.296±1.168	1.693±1.328
Pig 3	1.150±1.042	4.182±2.055	2.642±2.218
Pig 4	3.316±2.315	2.294±2.156	2.802±2.288
Pig 5	3.468±0.870	3.007±1.609	3.242±1.300
Pig 6	3.505±3.148	2.900±2.192	2.275±2.241
All Pigs	2.537±2.063	2.202±1.944	2.372±2.011

Table 7.2: Mean model response errors and standard deviation for maximum and minimum Volumes combined

[1]Note the standard deviation as caused by outliers.

Pig	# fitted periods	Time in min	%increase R_{pul}	%increase R_{sys}	%increase E_{eslvf}	%increase E_{esrvf}	%decrease V_{spt}
Pig 1	44	0-240	261.44	40.66	29.10	154.60	9.13
Pig 2	43	0-180	89.98	49.34	74.78	20.56	40.15
Pig 3[2]	18	0-120	24.23	27.16	0.81	9.74	8.37
Pig 4	45	0-265	166.85	39.21	19.06	56.44	19.84
Pig 5	29	0-180	103.63	21.16	71.51	80.07	27.64
Pig 6	20	0-210	99.52	53.90	11.00	14.64	14.00

Table 7.3: CVS porcine specific parameters

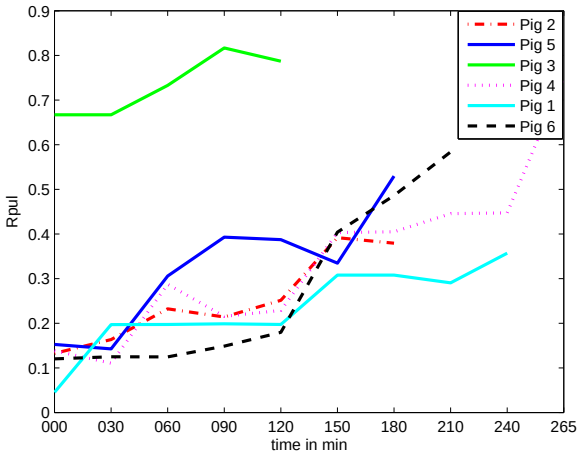

Figure 7.12: Pulmonary vascular resistance (R_{pul}) for all 6 pigs during the experiment

[2]This pig only had limited data and insufficient time for the parameters to change significantly.

7.4 Discussion

The results presented show that the minimal CVS model is capable of capturing the essential dynamics of porcine CVS response to induced pulmonary embolism. More specifically, the clinical and physiological changes expected in pulmonary embolism include:

- Pulmonary vascular resistance (R_{pul}) increases (Goldhaber, 1998)
- Systemic vascular resistance (R_{sys}) increases as a reflex response (Klabunde, 2004)
- Contractilities in the left and right ventricles (E_{eslvf}, E_{esrvf}) increase as a reflex response, but are expected to drop at the end of the experiment, where the pig is in a near death state and is no longer able to regulate its circulation (Burkhoff & Tyberg, 1993; Klabunde, 2004)
- Right ventricle expansion index ($RVEDV/LVEDV$) increases during the experiment as the overfilled right ventricle compresses the underfilled left ventricle (Gan *et al.*, 2006; Lualdi & Goldhaber, 1995)
- Septum volume (V_{spt}) decreases as the septum is shifted towards the left ventricle (Desaive *et al.*, 2005; Gan *et al.*, 2006)
- Total blood volume in the circulation decreases in this case as the pigs were bled during the experiment (Desaive *et al.*, 2005)
- Other model parameters would be expected to remain largely constant evidencing the ability to distinguish this clinical case without non-physiological parameter values elsewhere in the model.

The parameter identification method correctly identifies the physiologically expected changes in porcine hemodynamics during the pulmonary embolism experiment. Figures 7.9 and 7.12 show the increase in pulmonary and systemic vascular resistance (R_{pul},R_{sys}), as expected. The pulmonary vascular resistance (R_{pul}) increases significantly from the initial healthy state to the disease state in all pigs with a range of percentage increases of 89.98% to 261.44%. Thus, it matches common physiological signs seen in pulmonary embolism as pulmonary arterial obstruction and the release of vasoactive substances increase pulmonary

vascular resistance (Goldhaber, 1998). Figure 7.12 shows the time evolution of R_{pul} for all six pigs during the experiment.

Figures 7.7 and 7.9 show the ability of the model to pick up reflex response, where the pig increases systemic resistance to help restore blood pressure. However, near the end, when the pig is near death, systemic resistance (R_{sys}) drops off. This last result is potentially a sign that the pig can no longer regulate hemodynamics effectively.

The left and right ventricle contractilities (E_{eslvf}, E_{esrvf}) also increased during the pulmonary embolization experiment as shown by Table 7.3. These contractilities are known to be part of reflex response (Burkhoff & Tyberg, 1993) and could be used as an index of ventricular inotropic state. An increased heart rate for example also stimulates inotropy which is known as the Bowditch effect (Klabunde, 2004). Thus, the observed increase in left and right ventricle contractility together with the observed increase in heart rate also agree well with known physiological principles.

The right ventricle expansion towards the left ventricle is captured and shown in Figure 7.13. The model simulates blood backing up in the right ventricle due to increased afterload causing an expansion of the right ventricle. This effect is captured by the index RVEDV/LVEDV, matching known physiological response (Lualdi & Goldhaber, 1995).

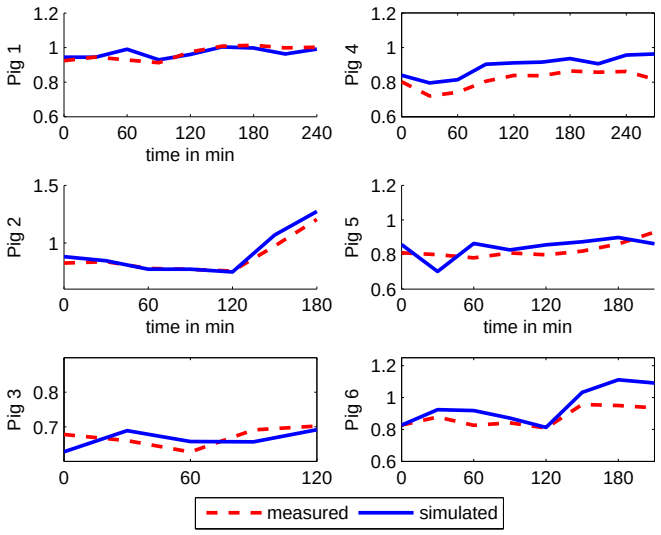

Figure 7.13: RVEDV/LVEDV index for all 6 pigs during the experiment

Table 7.3 displays the percentage decrease in the septum volume from the beginning to the end of the experiment. This decrease agrees with the fact that the right ventricle compresses the left ventricle as the level of embolization grows (Gan *et al.*, 2006). Similarly, Figure 7.11 shows the time evolution of the mean septum volume, (V_{spt}), during the experiment for pig 2.

The blood loss in these clinical experiments was accounted for by approximately linearly reducing the volume available in the circulation during the simulations. The blood loss for the six pigs ranges from 84ml to 515ml, 9% to 44% of the total blood volume respectively. These values seem reasonable when compared to the values in (Preisman *et al.*, 2002) but cannot be fully validated as this data was not explicitly collected in the tests (Desaive *et al.*, 2005).

Finally, Table 7.3 summarizes the percentage increases in the parameters associated with pulmonary embolism. It is worth noting that the remaining model parameters stayed relatively constant throughout the experiment. Specific changes in these parameters over all time frames and pigs was $< 15\%$.

7.5 Conclusions

This research demonstrates the potential of using a minimal CVS model (Hann *et al.*, 2005; Smith *et al.*, 2004) and integral-based parameter identification method (Hann *et al.*, 2006) for real time patient specific modelling and diagnosis. A wide range of clinically measured porcine hemodynamics in pulmonary embolism were successfully captured over time. The integral method identified all model parameters with less than 5% error in clinical pressure and volume outputs. More importantly, critical measures and expected physiological responses to pulmonary embolism were all successfully captured in the presence of noise and using real clinical data.

The accurate diagnosis and treatment of pulmonary embolism requires an interdisciplinary approach and remains a difficult and expensive task due to non-specific and challenging clinical signs, which sometimes do not coincide with clinical suspicion (Goldhaber, 1998; Nijkeuter & Huisman, 2005). A real-time patient specific CVS model as demonstrated here could thus potentially assist clinical staff in diagnosing pulmonary embolism using data and catheters typically available in the ICU.

Chapter 8

Application to Porcine Experiments of PEEP Titrations

This chapter presents the results of a further porcine validation study during PEEP titrations at different volemic levels. The first part[1] describes the identification process of different PEEP levels, whereas the second part[2] concentrates on the prediction of future patient responses towards changes in PEEP. Both parts of this chapter have also been presented to the 37^{th} annual SCCM congress.[3]

8.1 Clinical Importance of PEEP

Positive end-expiratory pressure (PEEP) is an operator-controlled variable that can be set during mechanical ventilation. The application of PEEP can be beneficial or detrimental for the patient dependent on how much the applied value differs from the optimal value with the greatest benefit. More specifically, in patients with lung injury, high PEEP levels may be necessary to maintain or restore oxygenation and for each individual patient the right balance between too much and too little PEEP has to be found. Too little PEEP may result in airway or alveolar collapse, whereas too much PEEP can cause alveolar overdistention and hemodynamic problems as caused by changes in intrathoracic pressure and consequently reductions in SV and CO, as already discussed in 4.1.2.1.

Thus, an important goal during mechanical ventilation is finding the optimal PEEP for each individual patient. This PEEP value will provide the best oxy-

[1]The first section is based on (Starfinger *et al.*, 2008d).
[2]The second section is based on (Starfinger *et al.*, 2008e).
[3]Abstract published in (Starfinger *et al.*, 2007a).

genation with the least detrimental impact on cardiopulmonary function. Figure 8.1 summarizes the effects too little or too much PEEP has.

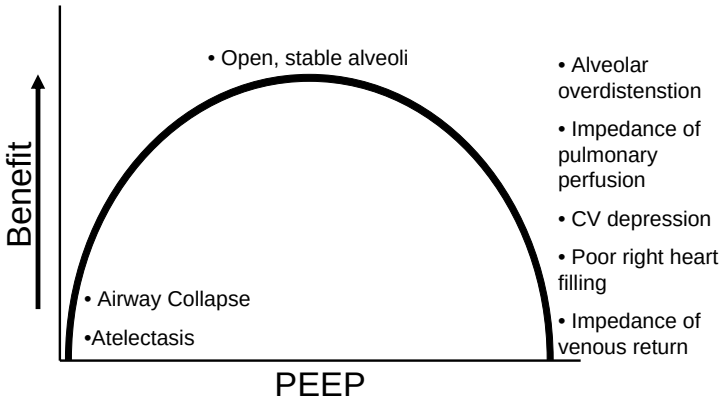

Figure 8.1: Determining optimal PEEP, source: (Courtney & Asselin, 2006).

The goal of this part of the research is to validate the CVS model using a porcine experiment of PEEP titrations at different volemic levels. The CVS model and methods are used to identify the patient-specific parameters during the experiment. These model parameters are then furthermore used to predict the patient's response towards a change in PEEP and/or volume status. The long-term goal is to use the CVS model and methods as a device assisting clinical staff in choosing the appropriate therapy for each individual patient, as for example determining the optimal PEEP.

8.2 Part I: Identifying Different PEEP Levels

8.2.1 Introduction

The CVS model can be formulated in terms of equations and its parameters identify the model making it patient-specific. Therefore, when the patient-specific parameters can be identified from measured clinical data so that the model matches the clinical measurements, then a model of the patient with their fundamental dynamic (Pressure-Volume, PV) behavior can be created. These parameters can

then be used to assist clinical staff with diagnosis, as for example the contractility index of the left ventricle can be elevated or depressed, thus giving an idea about the performance of the ventricle. A similar example would be the parameter representing the pulmonary vascular resistance, and thus giving information about the pressures in the pulmonary arteries - for example if an embolus is developing.

Therefore, by observing the trends, how the parameters change over time (new identifications can be performed for any few heartbeats of data) valuable information about the patient's hemodynamic condition can be tracked, diagnosed and overall monitored for more effective treatment. This use of the model has already been validated on clinical data from animal trials (pigs) in induced pulmonary embolism (Starfinger *et al.*, 2007b). This research presents a further validation of the model and methods by identifying the different hemodynamic conditions as caused by changing PEEP and volemic levels.

Spontaneous breathing and ventilation can have extensive effects on cardiovascular function. These effects are usually well tolerated in healthy subjects but may cause detrimental hemodynamic effects in critically ill patients, where pulmonary and or cardiovascular diseases and dysfunctions are present. It is thus important to understand the cardiopulmonary interactions and account for them when modelling the cardiovascular system. In this research, the CVS model is extended to capture more realistically different hemodynamic conditions as caused by the application of different PEEP values and levels of normo-, hypo- and hypervolemia. The amount of necessary data for the parameter identification process has, compared to previous work, further been reduced, to make the whole approach even more applicable for a clinical environment. Instead of using the left and right ventricle end-systolic and end-diastolic volumes, now only the global end-diastolic volume (GEDV) and an estimated total blood volume (TBV) are needed to identify the different PEEP and volemic levels correctly. The identification process has also been modified to allow for a more robust identification.

8.2.2 Methods

8.2.2.1 CVS Model

The CVS model is a simple, yet clinically validated model for the heart and circulation (Smith *et al.*, 2004, 2006) as previously presented in Section 3.2. This model comprises a series of connected pressure-volume chambers with greater detail for the active ventricular portions of the heart and their interaction. More

specifically, the left/right ventricle, aorta, pulmonary artery/vein and vena cava are captured as explicit physiological regions with independent fundamental circulatory (PV) dynamics. A more detailed description of the CVS model can be found in (Hann *et al.*, 2005; Smith, 2004; Smith *et al.*, 2004, 2006; Starfinger *et al.*, 2007b).

In this research, the original CVS model has been extended to include one compartment for the lung capillaries and a second for the body capillaries as described in Section 3.2 and Chapter 4, thus separating the venous and arterial systems and resistances. This is important when heart-lung interactions during positive pressure ventilation (PPV) and more specifically during the application of different PEEP levels have to be simulated. Increases in intrathoracic pressure (P_{th}) cause right ventricular preload to decrease by increasing the resistance to venous return (R_{vr}), and left ventricular afterload to decrease (Fessler, 1997; Miro & Pinsky, 2005). This afterload reduction is achieved by a decrease in systemic resistance (R_{sys}). One can see, that two resistances on either side, the arterial and venous side, are necessary to correctly simulate the complex behaviors during mechanical or spontaneous breathing.

8.2.2.2 Integral-Based Parameter Identification

The parameter identification method used in this research has previously been shown to rapidly and accurately identify virtually the entire parameter set in the presence of significant measurement noise (Hann *et al.*, 2006; Starfinger *et al.*, 2007b). The identification method is slightly adjusted in this research to allow a more robust parameter identification. Details of the adjustments are given in Chapter 5. For clarity, a short summary of the main identification steps is provided in the following paragraph.

As for discrete measurements the waveforms are not known, the integral method of (Hann *et al.*, 2006) cannot be directly applied. However, waveforms can be artificially generated by scaling a set of previously calculated model outputs to best fit the maximum and minimum measured data values for the pressures and volumes. The assumption is that these validated model waveforms are reasonably conformable with the actual clinical case. The scaled signals are then re-identified and a new CVS forward simulation is performed with the previously identified parameters producing a much closer match to the clinical data than the first initial parameter set. The simulated output is then compared to the

clinical data. Subsequently, the output signals are re-scaled and new parameters are identified which are then again used to run another simulation. This iterative process is stopped when the relative error between model output and clinical data reaches a set tolerance. This identification process is also illustrated in Figure 5.6.

8.2.2.3 Volume Calculations

All volume calculations performed for the CVS model compartments during the identification process are described in detail in Section 4.2. The following paragraph provides a short summary of the volume estimations as specifically performed for the PEEP titration experiment.

The parameter identification process needs the two ventricle volumes as input signals to accurately determine some of the parameters. More specifically, the end-diastolic and end-systolic volumes (EDV, ESV) are needed. However, these volume measurements are usually not available in a clinical environment and thus need to be estimated. Currently, the LVEDV and RVEDV are estimated based on an estimated total blood volume (TBV) and the measured global end-diastolic volume (GEDV). As the stroke volume (SV) is a measured variable too, ESV can be calculated by subtracting SV from EDV. The remaining model volumes are estimated based on known blood distributions. Importantly, the volume in the pulmonary capillary and vein compartments (V_{cap}, V_{pv}) are given by the pulmonary blood volume (PBV) which is obtained as $GEDV/4$. The volumes in aorta and pulmonary artery are also directly given, as the pressures P_{ao} and P_{pa} are given and the elastances E_{ao} and E_{pa} are calculated.

Note that as a result of these estimations, specific detailed questions cannot be answered, as information is lost on how one ventricle expands relative to the other (e.g. RVEDV/LVEDV expansion index). However, in this research we are not so much interested in identifying specific ventricular volumes, but we are rather interested in identifying the change in SV, which is directly given as a measured signal.

8.2.2.4 PEEP Experiment Study Protocol

Instrumentation and Monitoring The experiment was approved by the National animal ethics committee and data of seven 20-22kg pigs was analyzed for

this research. A detailed description of the anesthesia, ventilation, instrumentation and monitoring procedure has been published in (Lambert *et al.*, 2007). Here, only a limited and brief discussion of the study protocol is given where it is relevant for this analysis. Measurements were obtained from the right femoral artery, right carotid artery and the right internal jugular vein for monitoring the intravascular pressures and cardiac output. Pulmonary artery pressure was recorded using a PAC (Swan-Ganz, CCO mbo CCO/SvO_2 7.5F, Edwards Lifesciences, Irvine, CA) and esophageal pressure was measured via a latex balloon catheter (Viasys Healthcare, Hochberg, Germany). The esophageal catheters were connected to transducers (T450545A, Edwards Lifesciences, Irvine, CA) and the signals were transferred to a monitor (CM4008, Cardiomed, Ontario, Canada). Data was continuously measured and stored on a computer using Matlab (The MathWorks, MA). Analysis was performed using Matlab.

Interventions The measurements were performed at three different PEEP levels of $0, 10$ and $20 cmH_2O$ and at 5 different volemic levels: baseline (normovolemia, N), 10% volume loss (hypovolemia, H), re-transfusion of blood (normovolemia, I1), infusion of a volume equal to 10% of the estimated blood volume (10% hypervolemia, I2) and infusion of a volume equal to 20% of the estimated blood volume (20% hypervolemia, I3). Each blood infusion or removal was done over a period of 5 minutes, followed by a 10 minutes stabilization period with $5 cmH_2O$ PEEP to guarantee steady-state measurements.

8.2.3 Results

8.2.3.1 PEEP Titration Experiment at Different Volemic Levels

The integral-based parameter identification is applied to clinical porcine data for a true clinical validation. Detailed results for three of the seven pigs are presented and a summary of all seven pigs is given in Table 8.1. Figure 8.2 shows in the upper panel the simulated model output for the systolic and diastolic pressures in the aorta (SAP and DAP, solid line). The circles are the measured systolic and diastolic pressures. Note, that the x-axis shows the interventions performed during the PEEP titration protocol, where $0 - 20$ represent the beginning of a PEEP sequence of $0, 10$ and $20 cmH_2O$. The symbols N, H, I1, I2 and I3 stand for baseline normovolemia (N), hypovolemia (H), re-transfusion normovolemia (I1), 10%- and 20% hypervolemia (I2 and I3), respectively. The middle panel shows

the systolic and diastolic pulmonary artery pressures (SPAP and DPAP) and the lower panel shows the central venous pressure (CVP). The simulation data matches the measured porcine data very well with errors well below 5% for the maximum and minimum pressures.

Difference in % for measured and simulated pressures and volumes						
	SAP	DAP	SPAP	DPAP	CVP	SV
μ	3.57	5.51	3.79	4.98	3.55	5.35
σ	2.22	3.34	2.36	3.35	2.36	3.38

Table 8.1: Mean error and standard deviation in % for measured and simulated pressures and volumes over all 96 identified segments. SAP = systolic arterial pressure, DAP = diastolic arterial pressure, SPAP = systolic pulmonary artery pressure, DPAP = diastolic pulmonary artery pressure, CVP = central venous pressure, SV = stroke volume.

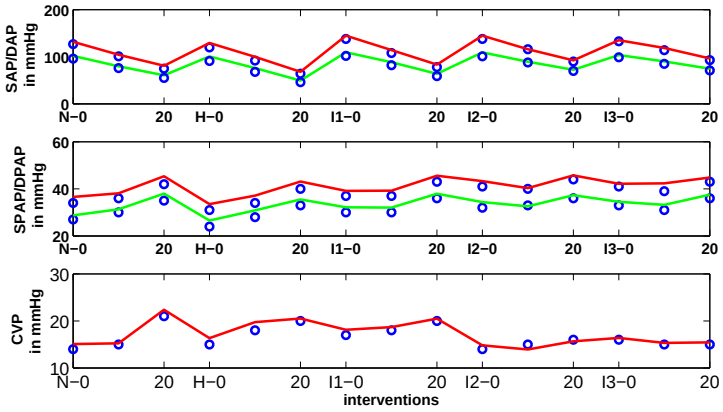

Figure 8.2: Model output (solid lines) vs clinical (circles) pressures for pig 1. The upper panel shows the systolic and diastolic arterial pressures (SAP, DAP), the middle panel shows the systolic and diastolic pulmonary artery pressures (SPAP, DPAP) and the lower panel shows the central venous pressure (CVP).

Figure 8.3 displays in the upper panel the measured GEDV (one measurment/circle per intervention) and the simulated ventricle end-diastolic volume VEDV (VEDV=LVEDV+RVEDV, upper solid line). Note that as the atria volumes are not simulated, VEDV is multiplied by a factor of 1.5 to enable a direct

comparison between the two volumes. The second line in the upper panel represents measured PBV (one measurment/circle per intervention) and the solid line represents the simulated pulmonary venous and capillary blood volume. The lower panel shows the measured (circles) and simulated SV (solid line). Again, the simulation data matches the measured porcine data very well with errors well below 10% for the maximum and minimum volumes.

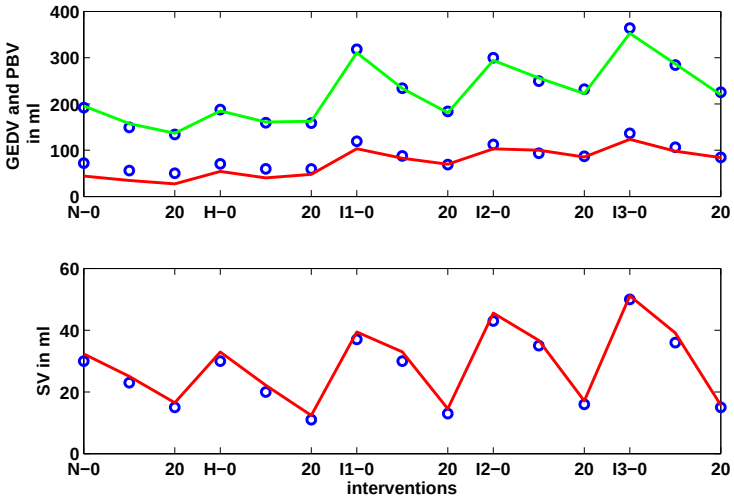

Figure 8.3: Model output (solid lines) vs clinical (circles) volumes for pig 1. The upper panel shows the GEDV and PBV and the lower panel shows the stroke volume (SV).

Figures 8.4 and 8.5 show the simulated vs clinally measured pressure and volume signals for a second pig and Figures 8.6 and 8.7 show the same results for a third pig. Similar good results were obtained for all other pigs as can be seen in Table 8.1. Figures 8.8 and 8.9 clearly show that the identified subject (pig) specific parameters venous return resistance (R_{vr}) and pulmonary vascular resistance (R_{pulin}), differ significantly between PEEP $0cmH_2O$ and PEEP $20cmH_2O$ states. For all seven pigs, R_{vr} increases when PEEP is applied, this is particularly significant during the volemic levels of hypo- and normovolemia (H, N and I1). Less significant changes are observed during hypervolemia (I2 and I3). Likewise, R_{pulin} increases with increasing levels of PEEP.

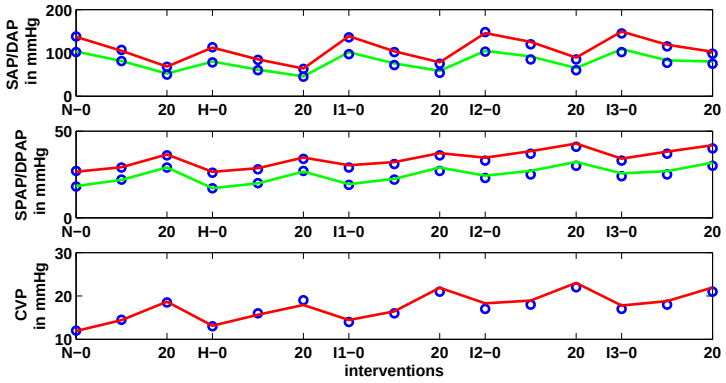

Figure 8.4: Model output (solid lines) vs clinical (circles) pressures for pig 3. The upper panel shows the systolic and diastolic arterial pressures (SAP, DAP), the middle panel shows the systolic and diastolic pulmonary artery pressures (SPAP, DPAP) and the lower panel shows the central venous pressure (CVP).

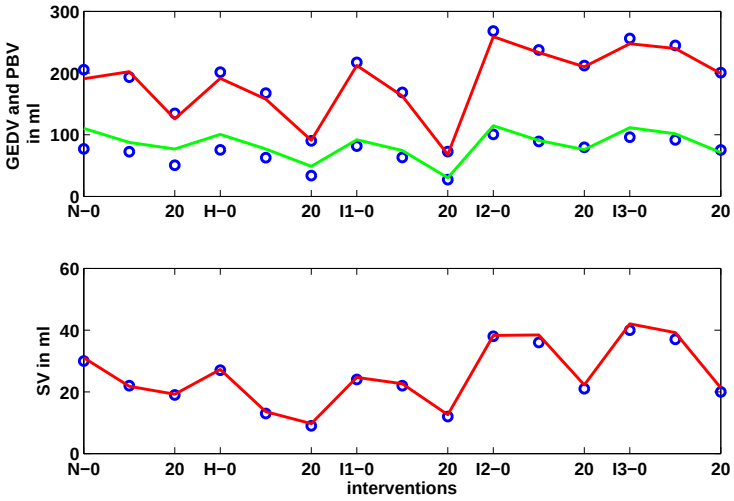

Figure 8.5: Model output (solid lines) vs clinical (circles) volumes for pig 3. The upper panel shows the GEDV and PBV and the lower panel shows the stroke volume (SV).

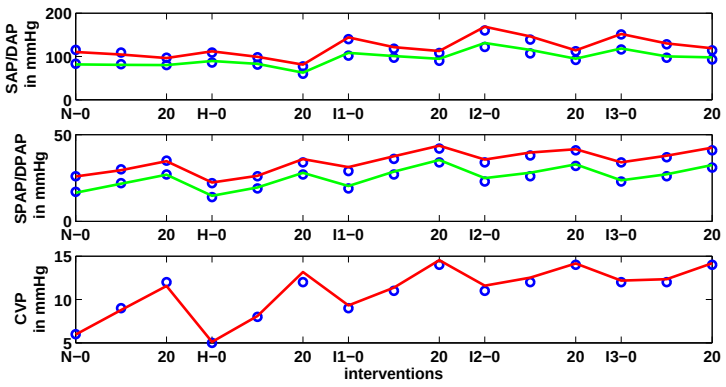

Figure 8.6: Model output (solid lines) vs clinical (circles) pressures for pig 5. The upper panel shows the systolic and diastolic arterial pressures (SAP, DAP), the middle panel shows the systolic and diastolic pulmonary artery pressures (SPAP, DPAP) and the lower panel shows the central venous pressure (CVP).

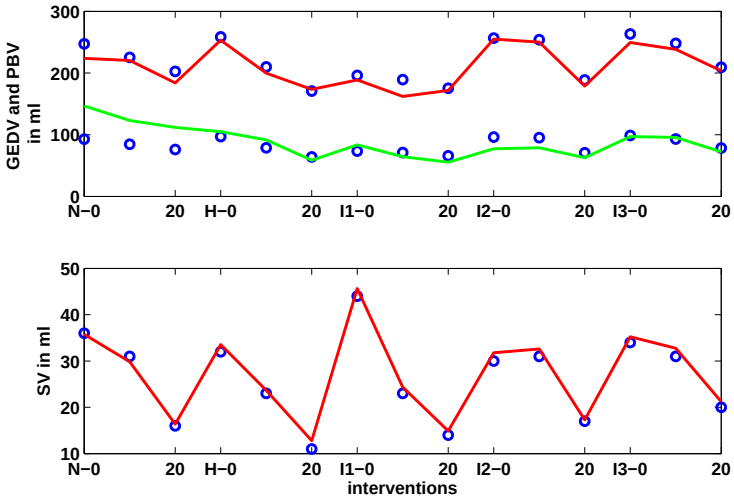

Figure 8.7: Model output (solid lines) vs clinical (circles) volumes for pig 5. The upper panel shows the GEDV and PBV and the lower panel shows the stroke volume (SV).

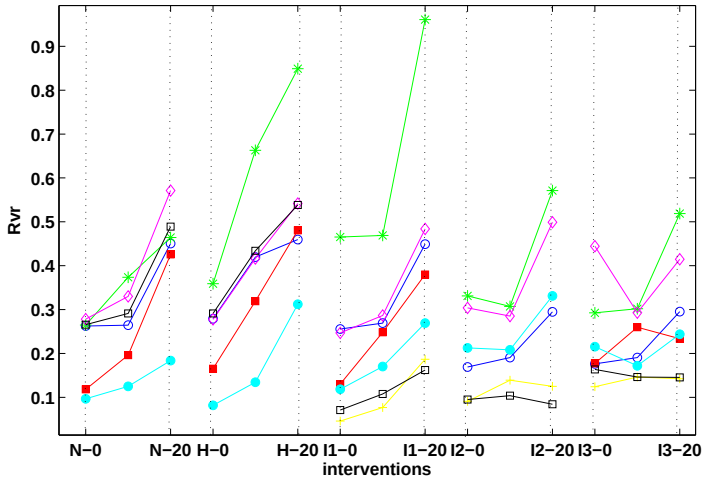

Figure 8.8: Identified R_{vr} for all 7 pigs and all PEEP/volume interventions.

Figure 8.10 shows how R_{vr} directly correlates with P_{sys}/SV and Figures 8.11 and 8.12 show the good correlations obtained for systemic vascular resistance (R_{sys}) and $(SAP - P_{sys})/SV$ and R_{pulin} and $(SPAP - P_{cap}/SV)$, respectively. Finally, Figures 8.13 and 8.14 show the correlations for the ventricle contractilities E_{eslvf}, E_{esrvf} and the ratio of systolic arterial pressure and end-systolic volume.

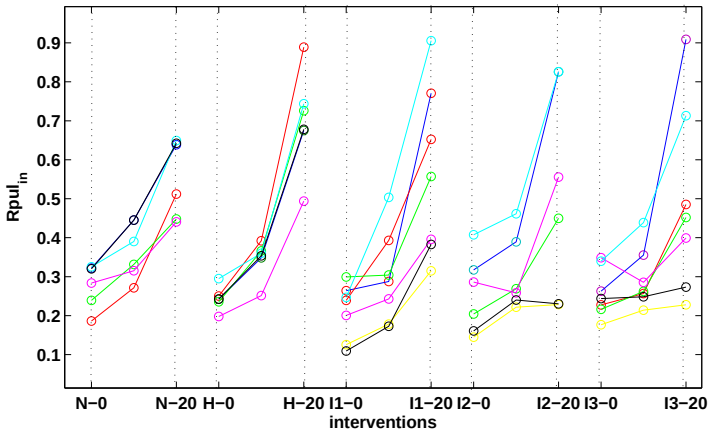

Figure 8.9: Identified R_{pulin} for all 7 pigs and all PEEP/volume interventions.

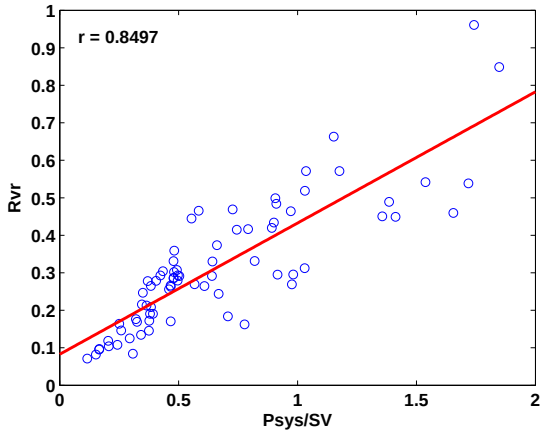

Figure 8.10: Correlation for P_{sys}/SV and R_{vr} for all 96 identified segments for all 7 pigs and all PEEP/volume interventions.

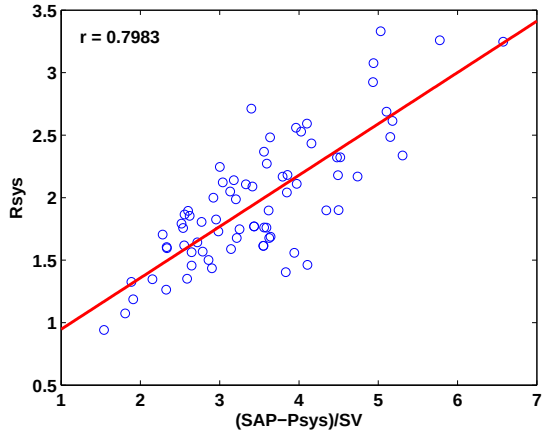

Figure 8.11: Correlation for $(SAP - P_{sys})/SV$ and R_{sys} for all 96 identified segments for all 7 pigs and all PEEP/volume interventions.

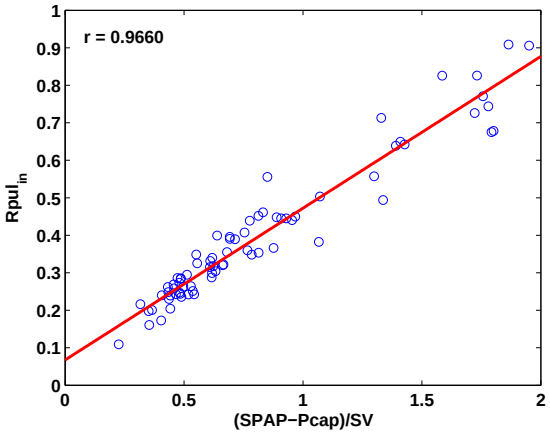

Figure 8.12: Correlation for $(SPAP - P_{cap})/SV$ and R_{pulin} for all 96 identified segments for all 7 pigs and all PEEP/volume interventions.

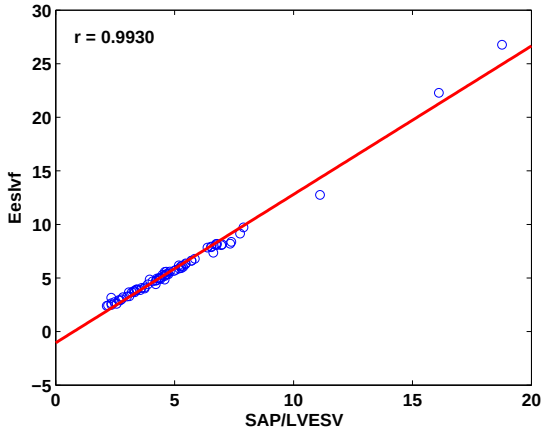

Figure 8.13: Correlation for $SAP/LVESV$ and E_{eslvf} for all 96 identified segments for all 7 pigs and all PEEP/volume interventions.

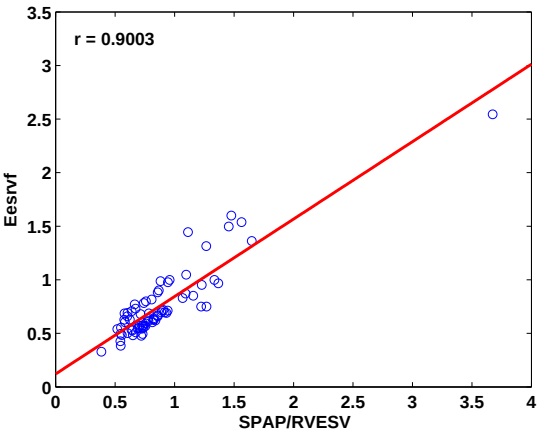

Figure 8.14: Correlation for $SPAP/RVESV$ and E_{esrvf} for all 96 identified segments for all 7 pigs and all PEEP/volume interventions.

8.2.4 Discussion

Mechanical ventilation, for example PPV with additional PEEP, can cause profound steady-state effects in critically ill patients. As respiratory-induced changes in P_{th} are transmitted directly to all vessels in the thoracic cavity, the pressure in the right atrium increases during PPV. It is known that PEEP often reduces venous return (VR) and thus cardiac output (CO) (Cassidy *et al.*, 1948; Fessler,

1997; Miro & Pinsky, 2005; Shekerdemian & Bohn, 1990). Over the years there has been some controversy how exactly PEEP alters VR. Some investigators have concluded that PEEP decreases VR by reducing the pressure gradient ($P_{sys} - P_{ra}$) (Johnston *et al.*, 1989; Wise *et al.*, 1981). Note, that P_{sys} is the mean systemic pressure, which is also known as mean circulatory filling pressure (MCFP). Note furthermore, that as the CVS model does not explicitly model the right atrium, but lumps it together with the vena cava, P_{ra} is in the model represented by P_{vc}. However, other researchers have demonstrated that P_{sys} and P_{ra} change equally during positive airway pressure and thus a change in the driving pressure gradient cannot be the reason for decreases in VR during PEEP (Fessler, 1997; Jellinek *et al.*, 2000; Peters *et al.*, 1997). Recent publications suggest that the main effect by which PEEP decreases venous return is by increasing the resistance to venous return (Fessler, 1997; Miro & Pinsky, 2005; Shekerdemian & Bohn, 1990).

Thus, during PEEP, VR is decreased not by altering the pressure gradient ($P_{sys} - P_{ra}$) but by increasing the resistance to venous return R_{vr}. Hence, different PEEP levels should result in different values for R_{vr} or more specifically, R_{vr} should increase during elevated PEEP levels, which is shown in Figure 8.8 and matches physiological expectations. Furthermore, it is also known that right ventricular afterload increases during PPV, so one would expect R_{pulin} to increase with increasing levels of PEEP. Figure 8.9 shows this result, as expected.

Additionally, reflex response mechanisms of the body decrease unstressed systemic volume (V_{dsys}) and thus rise stressed systemic volume (V_{sys}) which in turn leads to a rise in P_{sys} and helps to sustain the pressure gradient for VR (Jacobsohn *et al.*, 1997; Peters *et al.*, 2001). The CVS model successfully simulates this behavior, as can be seen in Figure 8.15. Figure 8.15 displays, how the effective systemic volume V_{syseff} (with $V_{syseff} = V_{sys} - V_{dsys}$) rises during PEEP levels from 0 to $20 cm H_2O$. Figure 8.15 shows the systemic volume V_{sys} normalized by the baseline value for PEEP $0 cm H_2O$. The increase in V_{sys} is more accentuated during hypo- and normovolemia, as expected as the central venous pressure and intrathoracic pressure are both higher during these states compared to 10%- and 20% hypervolemia. Note, that PBV decreases with rising PEEP levels, as the volume is shifted form the pulmonary circulation centrally to help raise V_{sys} (Peters *et al.*, 2001) as seen in Figures 8.3 - 8.7.

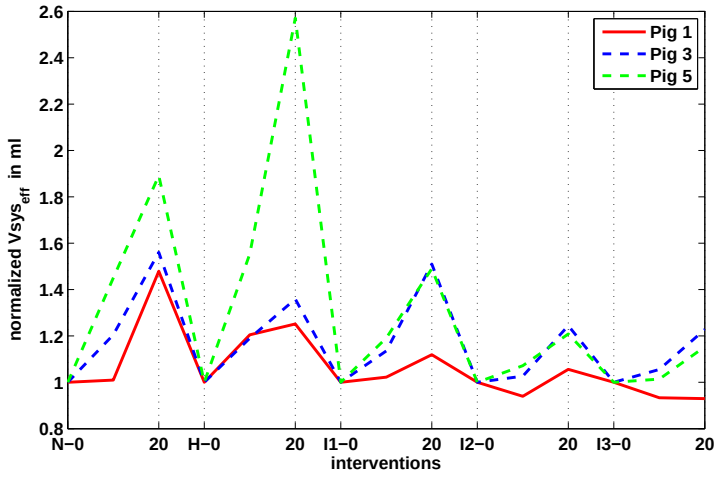

Figure 8.15: Effective normalized systemic volume for all 15 identified segments for pigs 1,3 and 5 over all PEEP/volume interventions.

In Figures 8.2 - 8.6 it can be seen how well the increase in CVP is matched by simulated data from the CVS model for the different PEEP levels. Furthermore, Figure 8.10 shows that R_{vr} correlates directly with the ratio of P_{sys} and stroke volume, this is as expected, as the pressure gradient $(P_{sys} - P_{vc})$ divided by SV gives the mean resistance to venous return. Note, that as the pressure gradient remains relatively equal and both pressures change similarly, it does not matter if $(P_{sys} - P_{vc})/SV$ or P_{sys}/SV is calculated.

Similar good correlations for R_{sys} and R_{pulin} are obtained and shown in Figures 8.11 and 8.12. Note, that these correlations further validate the CVS model and identification method as the identified parameters behave as physiologically expected. Likewise, good correlations for the two ventricle contractilities (E_{eslvf}, E_{esrvf}) are given in Figures 8.13 and 8.14 and are as expected. As in our model, V_d (ESPVR and x-axis intercept) is set to zero for simplicity reasons, one can see that ESPVR is approximately given by the ratio of systolic arterial pressure to end-systolic volume.

Finally, Table 8.1 summarizes all results for all seven pigs and a total of 96 separate identifications. Note, that 9 measurements had to be omitted from final analysis as they contained corrupted data, such as produced by disconnected catheters. These results show that the minimal CVS model is able to capture

the essential dynamics of the porcine CVS response to increasing levels of PEEP over a variety of volemic conditions and over a selection of subjects.

8.2.5 Conclusions

The integral-based optimization successively identified pig-specific parameters for the minimal cardiac model. This further validation shows the ability of the model to adequately and realistically capture (with unique values) the impact of pressure-volume changes with PEEP and fluid therapy. This research thus increases our confidence in the clinical applicability and validity of this overall diagnostic monitoring approach.

8.3 Part II: Predicting Future Response Towards Different PEEP Levels

8.3.1 Introduction

Circulatory dysfunctions and disease account for a significant number of ICU admissions. For example, a recent study found that 58% of ICU admissions for patients aged 65-74 years in Olmsted County, Minnesota were due to cardiovascular dysfunction, with a further 17% due to respiratory disease (Seferian & Afessa, 2006). The treatment and management of this large group of patients is significantly affected by the difficulty in monitoring and managing circulatory status and efficiency.

However, cardiac disease states are highly patient-specific, such that every patient has a unique expression of the disease or dysfunction. They are thus difficult to accurately diagnose given the sometimes limited measurements available and the body's natural reflex responses to restore circulatory equilibrium, both of which can mask the underlying symptoms. Clinical staff must therefore consider many combinations of different disease scenarios based on frequently conflicting patient data, including clinical history and non-invasive and/or invasive studies (Grenvik *et al.*, 1989). Hence, successful diagnosis and treatment often rely on the experience and intuition of clinical staff, increasing the likelihood for clinical error, which is common with rates up to 50% (Abramson *et al.*, 1980; Donchin *et al.*, 1995; Morris, 2001; Suresh *et al.*, 2004).

Tools for diagnosis and guiding therapy can help reduce variation and provide a more consistent care. Computerized protocols have thus become more widespread as they can be applied to complex clinical problems to create patient-specific therapy instructions (Kortgen *et al.*, 2006; Leibovici *et al.*, 2007; Rees *et al.*, 2002). A cardiovascular (CVS) model could be integrated into the clinical decision making process by offering clinicians the possibility of not only assisting in diagnosing, but also providing a model-based means to test different therapeutic procedures and their likely effect on the patient. Hence, treatment could be optimized for each patient and unnecessary interventions avoided.

A previously published integral-based parameter identification method (Hann *et al.*, 2006) has been shown to successively identify pig-specific parameters for a minimal cardiac model (Starfinger *et al.*, 2007b). These models and methods were further validated using a porcine experiment of PEEP titrations at different

volemic levels (Starfinger *et al.*, 2008d), where the model's ability to capture the impact of pressure-volume changes with PEEP and fluid therapy was shown.

This research is a further clinical validation of the overall diagnostic monitoring approach and extends the previously described methods. It illustrates one method for using this CVS model and integral-based parameter identification for therapy guidance and decision support by forward simulating the expected patient response to different interventions. Thus, this research provides a predictive validation of the model's capability and efficiency in a decision support role, rather than a physiological data matching validation. More specifically, general rules are developed relating PEEP to specific model parameters such that the model can then be used to predict the general patient response to increases in PEEP from 0 to $10cmH_2O$ and from 10 to $20cmH_2O$ during different volemic states.

8.3.2 Methods

8.3.2.1 Prediction Process and PEEP-Specific Model Parameters

As shown previously, the CVS model parameters can be obtained accurately and repeatedly for the porcine experiment of PEEP titrations (Starfinger *et al.*, 2008d). Furthermore, very good correlations were found between specific model parameters and specific output signals (Starfinger *et al.*, 2008d). These initial good results allow the assumption that an overall rule can be created that links changes in PEEP to corresponding changes in specific CVS model parameters. A general rule that is true for all studied pigs would allow the implementation of PEEP-specific parameters that change according to the currently applied PEEP. Such PEEP-varying parameters would enable more realistic and physiologically correct simulation of the cardiovascular system with the potential for using such forward simulations for diagnosis and therapy decision support.

The rules for PEEP-specific parameters are obtained by examining the percentage changes in the CVS model parameters for pig 1 during the different PEEP settings and volemic levels. As it is assumed, that the CVS model parameters are identified reliably, it can be expected that the rules obtained from only one pig also hold true for predicting the response of the remaining pigs. These parameter changes can however also be explained by reflecting on the known physiological effects of mechanical ventilation and especially PEEP on the circulation. Specifically, during the application of positive pressure ventilation (PPV) with PEEP,

intrathoracic pressure increases and venous return is decreased. This decrease occurs not by altering the pressure gradient ($P_{sys} - P_{ra}$), but by increasing the resistance to venous return R_{vr} (Fessler, 1997; Miro & Pinsky, 2005; Shekerdemian & Bohn, 1990). Hence, different PEEP levels should result in different values for R_{vr}. More specifically, R_{vr} should increase during elevated PEEP levels. Furthermore, it is also known that right ventricular afterload increases during PPV (Fessler, 1997; Miro & Pinsky, 2005), so one would expect R_{pulin} to also increase with increasing levels of PEEP.

8.3.3 Results

8.3.3.1 PEEP-Specific Changes in Resistances and Volumes

Table 8.2 shows how the CVS model identified parameters are affected by changes in PEEP from 0 to 10cmH_2O and from 10 to 20cmH_2O. The percentage changes represent values obtained from pig 1 as studied as detailed in (Starfinger *et al.*, 2008d). The CVS model volumes are calculated for PEEP 0cmH_2O as described previously (Starfinger *et al.*, 2008d). Table 8.3 shows how the volumes are then adjusted for predicting the volume changes for PEEP of 10 and 20cmH_2O, respectively. These values were obtained by observing the model identified volume changes, but could also be explained by expected physiological PEEP-induced changes (Jacobsohn *et al.*, 1997; Peters *et al.*, 2001; Rothe, 1979) and direct examination of the data.

PEEP-specific parameter changes		
Parameter	$0cmH_2O \Rightarrow 10cmH_2O$	$10cmH_2O \Rightarrow 20cmH_2O$
E_{ao}	plus 10%	plus 20%
E_{pa}	plus 10%	plus 60%
E_{vc}	plus 10%	plus 10%
E_{pu}	plus 5%	plus 5%
R_{sys}	minus 10%	minus 10%
R_{vr}	plus 30%	plus 50%
R_{pulin}	plus 40%	plus 60%
R_{pulout}	plus 15%	plus 30%
E_{cap}	plus 40%	plus 50%
P_{opcd}	plus 10%	plus 10%

Table 8.2: Parameter changes for forward simulating changes in PEEP from 0 to $10cmH_2O$ and from 10 to $20cmH_2O$.

PEEP-specific volume changes		
Volume	$0cmH_2O \Rightarrow 10cmH_2O$	$10cmH_2O \Rightarrow 20cmH_2O$
V_{lv}	minus 25%	minus 25%
V_{rv}	minus 20%	minus 20%
V_{pv}	minus 30%	minus 30%
V_{vc}	minus 30%	minus 50%
V_{pa}	minus 10%	minus 35%
V_{ao}	minus 25%	minus 50%
V_{sys}	plus 2%	plus 2%
V_{cap}	minus 2%	minus 2%

Table 8.3: Volume changes for forward simulating changes in PEEP from 0 to $10cmH_2O$ and from 10 to $20cmH_2O$.

8.3.3.2 Prediction of Arterial Pressures and Stroke Volume

Predictions are made using data identified at PEEP of $0cmH_2O$ for each of the remaining 6 pigs. Note that data of pig 1 used for identification, is not used in the prediction process. The estimated PEEP-specific parameter and volume changes in Tables 8.2 and 8.3 are used to predict changes in a given pigs model parameters and initial volume conditions. The modified PEEP-specific parameters are then

used to simulate the therapy intervention with results compared to the clinical data.

Figure 8.16 shows the prediction results obtained for Pig 2. In the upper panel, the predicted stroke volume (SV) is displayed with a cross, whereas the measured clinical values are shown as a dotted line. Predictions were made for PEEP values of 10 and $20 cmH_2O$ for the different volemic levels of normovolemia (N and I1), hypovolemia (H) and the two infusion-induced hypervolemic states (I2 and I3). Note that the values for PEEP of $0 cmH_2O$ are not shown as no predictions were performed for these PEEP values. The middle panel shows the predicted (cross) versus clinical (dotted line) systolic arterial pressure values (SAP) and the lower panel shows the results for predicting systolic pulmonary artery pressure (SPAP). Figures 8.17 to 8.21 show the same results as obtained for Pigs 3-7 respectively. Table 8.4 summarizes the prediction results for all 6 pigs and gives the median and maximum absolute percentage errors and the interquartile range (IQR) for predicting stroke volume (SV), systolic arterial pressure (SAP) and systolic pulmonary artery pressure (SPAP).

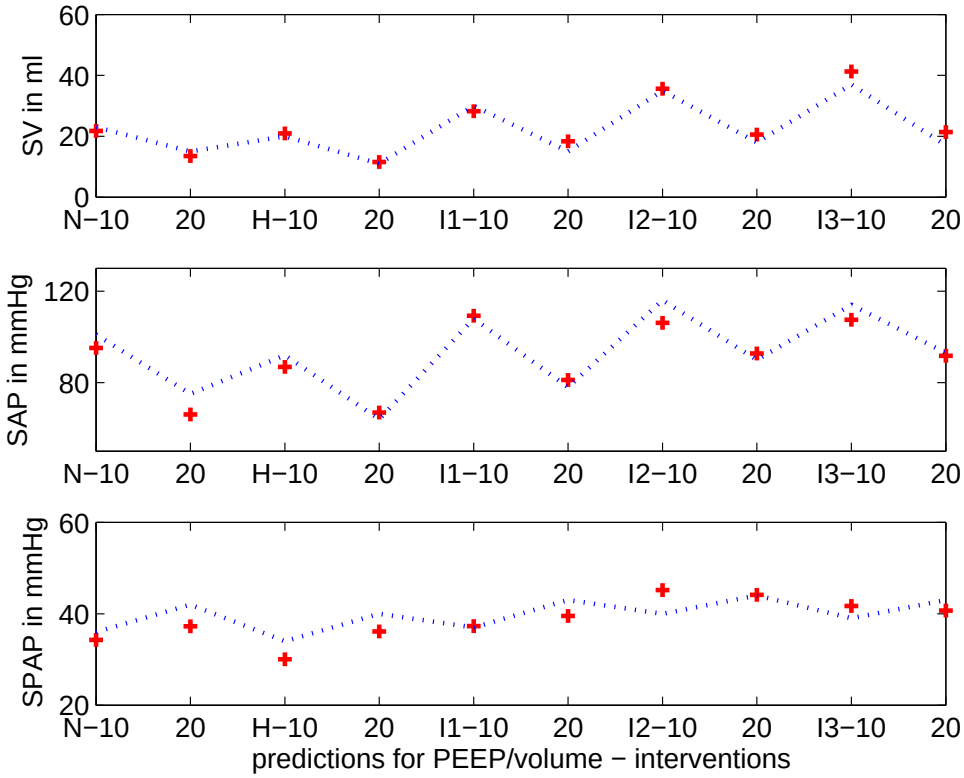

Figure 8.16: Model prediction (cross) vs clinical (dotted line) pressures and volumes for pig 2 for PEEP 10 and 20cmH_2O. The upper panel shows the stroke volume (SV), the middle panel shows the systolic arterial pressure (SAP) and the lower panel shows the systolic pulmonary artery pressure (SPAP).

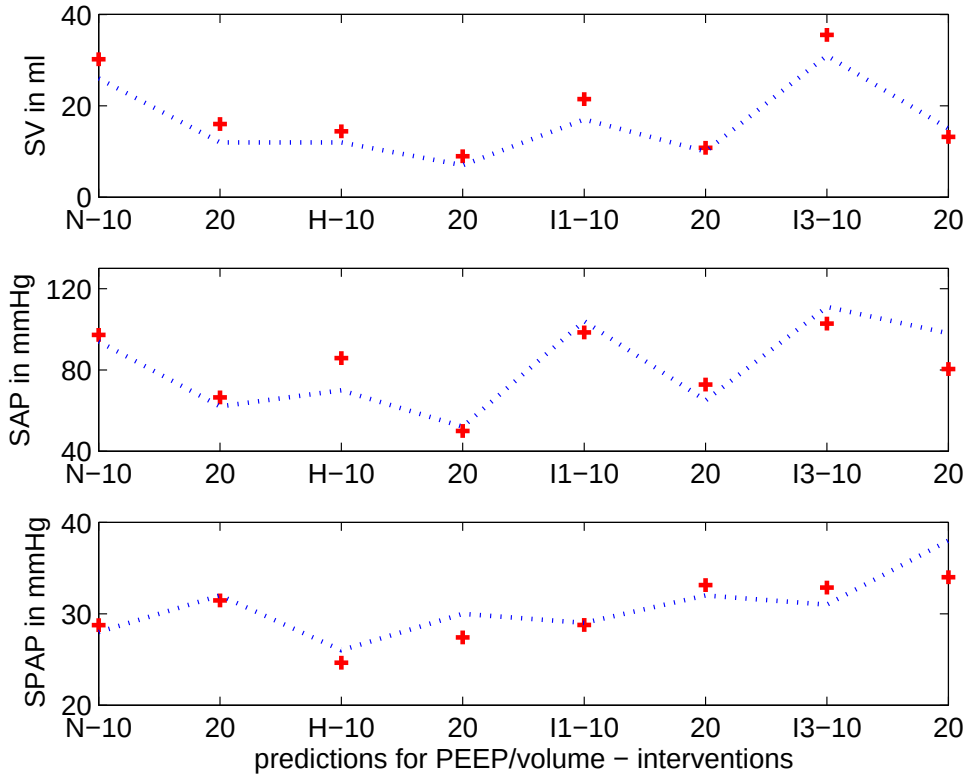

Figure 8.17: Model prediction (cross) vs clinical (dotted line) pressures and volumes for pig 3 for PEEP 10 and 20cmH_2O. The upper panel shows the stroke volume (SV), the middle panel shows the systolic arterial pressure (SAP) and the lower panel shows the systolic pulmonary artery pressure (SPAP).

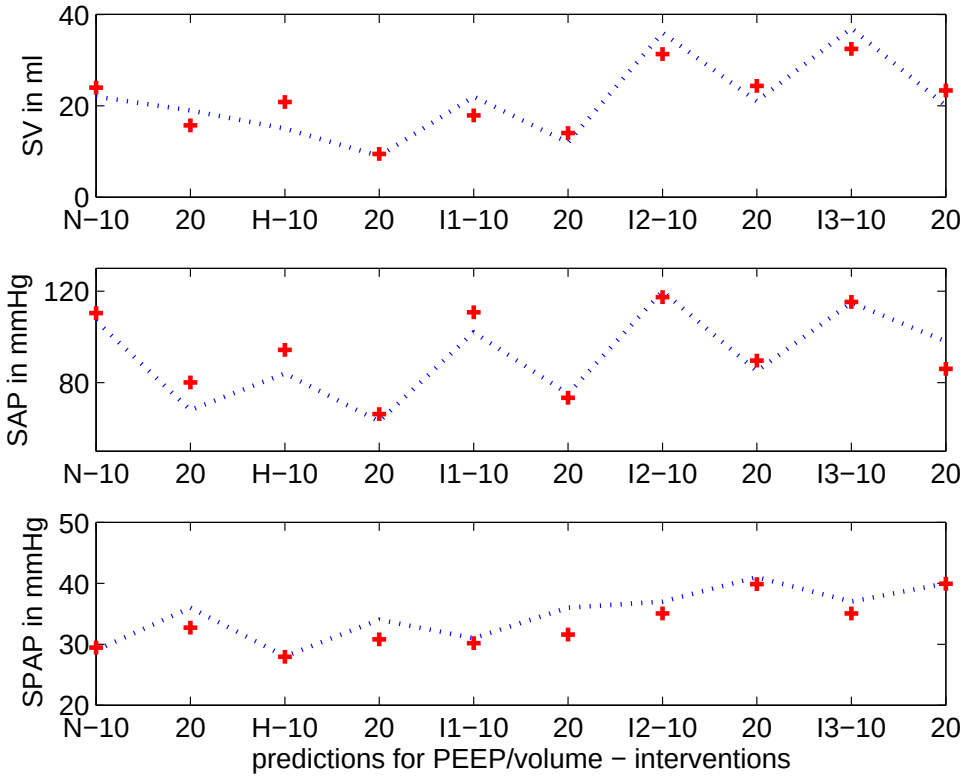

Figure 8.18: Model prediction (cross) vs clinical (dotted line) pressures and volumes for pig 4 for PEEP 10 and 20cmH_2O. The upper panel shows the stroke volume (SV), the middle panel shows the systolic arterial pressure (SAP) and the lower panel shows the systolic pulmonary artery pressure (SPAP).

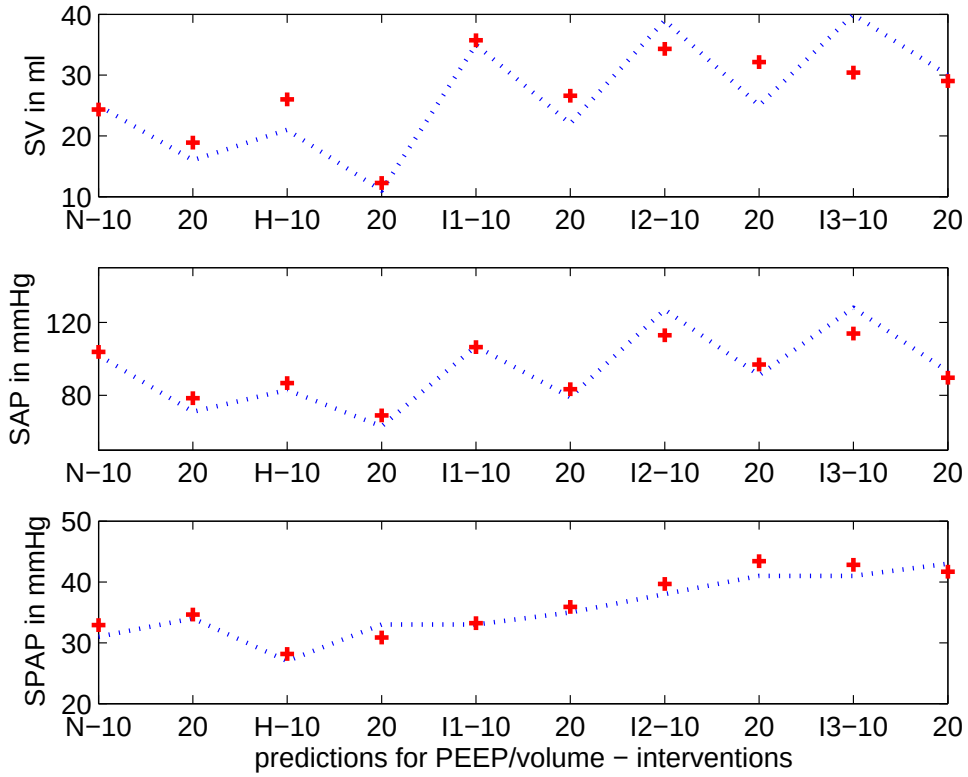

Figure 8.19: Model prediction (cross) vs clinical (dotted line) pressures and volumes for pig 5 for PEEP 10 and 20cmH_2O. The upper panel shows the stroke volume (SV), the middle panel shows the systolic arterial pressure (SAP) and the lower panel shows the systolic pulmonary artery pressure (SPAP).

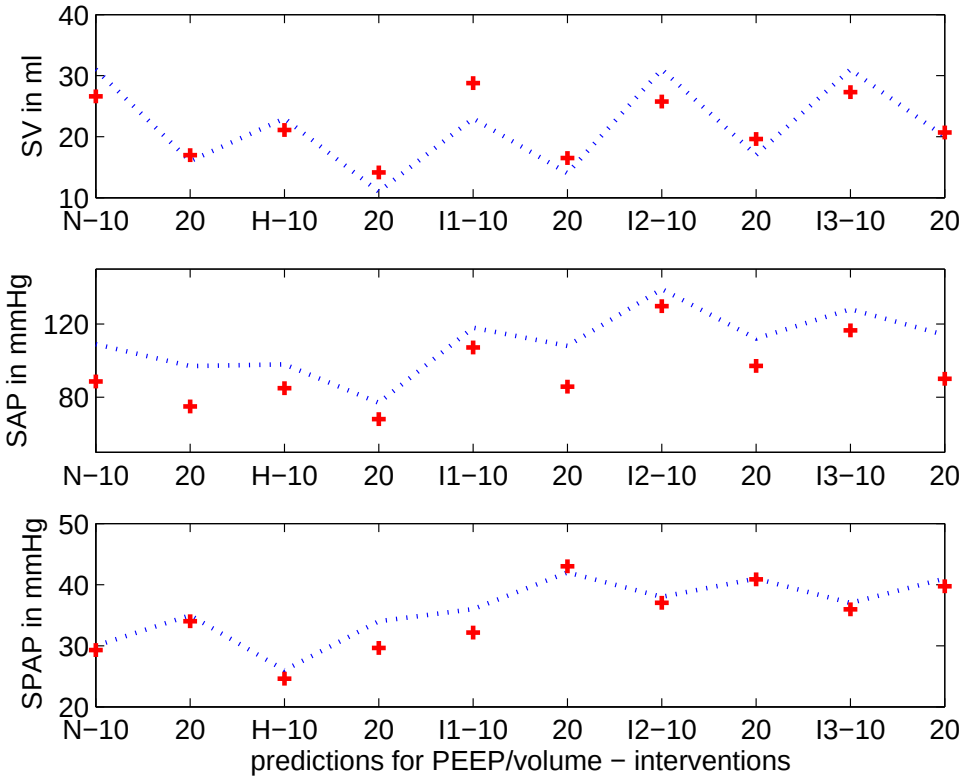

Figure 8.20: Model prediction (cross) vs clinical (dotted line) pressures and volumes for pig 6 for PEEP 10 and 20cmH_2O. The upper panel shows the stroke volume (SV), the middle panel shows the systolic arterial pressure (SAP) and the lower panel shows the systolic pulmonary artery pressure (SPAP).

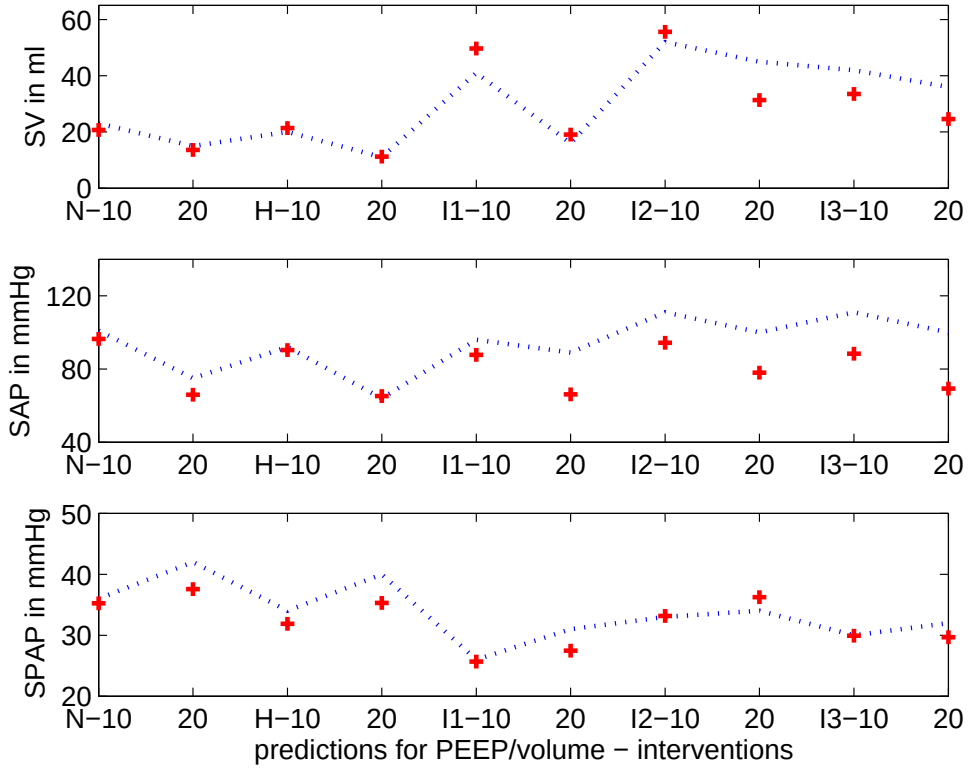

Figure 8.21: Model prediction (cross) vs clinical (dotted line) pressures and volumes for pig 7 for PEEP 10 and 20cmH_2O. The upper panel shows the stroke volume (SV), the middle panel shows the systolic arterial pressure (SAP) and the lower panel shows the systolic pulmonary artery pressure (SPAP).

Prediction of PEEP-induced hemodynamic changes					
All pigs, PEEP 10	SAP	DAP	SPAP	DPAP	SV
median	6.65	9.80	4.24	5.94	12.24
max	22.62	31.89	12.92	18.71	38.95
iqr	7.64	11.14	3.78	5.52	13.05
All pigs, PEEP 20	SAP	DAP	SPAP	DPAP	SV
median	10.47	12.99	6.51	7.14	16.86
max	30.69	33.82	12.82	18.24	33.61
iqr	13.26	14.03	6.98	5.25	13.08
All pigs, all predictions	SAP	DAP	SPAP	DPAP	SV
median	7.93	11.52	4.62	7.02	14.49
max	30.69	33.82	12.92	18.71	38.95
iqr	8.10	13.86	5.54	8.40	12.58

Table 8.4: Absolute median and maximum percentage error and interquartile range for predicted values of SAP/DAP = systolic/diastolic arterial pressure, SPAP/DPAP = systolic/diastolic pulmonary artery pressure and SV = stroke volume.

8.3.4 Discussion

It is well known that PEEP often reduces venous return (VR) and thus cardiac output (CO). Recent publications suggest that the main effect by which PEEP decreases venous return is by increasing the resistance to venous return (R_{vr}) (Fessler, 1997; Miro & Pinsky, 2005; Shekerdemian & Bohn, 1990). Hence, different PEEP levels should result in different values for R_{vr} or more specifically, R_{vr} should increase during elevated PEEP. Table 8.2 shows how R_{vr} is increased with increasing PEEP values, matching physiological expectations. Furthermore, it is also known that right ventricular afterload increases during PPV (Fessler, 1997; Miro & Pinsky, 2005), so one would expect R_{pulin} to also increase with increasing levels of PEEP. Analogously, the parameter changes for LV afterload (R_{sys}) and LV preload (R_{pulout}) can be derived.

All other parameter changes can be explained similarly. Thus, for example, increasing arterial elastance values (E_{ao} and E_{pa}) are observed during the PEEP titration experiment and are expected because the pulse pressure/stroke volume ratio (PP/SV) determines the arterial elastances and during PEEP, stroke volume decreases more than pulse pressure does. Venous elastances (E_{vc} and E_{pu}) are

assumed to increase as well because positive end-expiratory pressure elevates the transpulmonary pressure which compresses the large intrathoracic veins and right atrium. Note however that the systemic elastance (E_{sys}) remains constant as it has been shown that increases in PEEP decrease unstressed volume and thereby increase stressed volume with no change in compliance (Nanas & Madger, 1992).

It can also be expected, that the pericardium becomes stiffer (diastolic elastance P_{0pcd} increases) with increasing levels of PEEP, as the heart becomes more and more compressed by the expanding lung and pressurized thoracic cavity. Similarly, E_{cap}, the lung capillaries elastance is expected to increase with falling pulmonary blood volume (PBV) values and thus decreases in compliance. Note, that R_{sys} remains constant during hypovolemia, assuming a compensation caused by an increased sympathetic activity in response to the blood loss. Table 8.2 shows these parameter variations matching clinical observations in their general trends.

Changes in the volumes can be similarly explained. As GEDV decreases with increasing PEEP levels, it can be followed that LVEDV and RVEDV have to decrease, as well. V_{pv} and V_{cap} are expected to decrease as given by the drop in pulmonary blood volume. Note, that V_{sys} remains constant as blood is shifted centrally to help maintain CVP. However, V_{sys} is simulated to slightly decrease during hypovolemia, as hypovolemia inhibits fluid reabsorption due to high capillary pressures (Peters *et al.*, 2001). Table 8.3 shows the general trend of these volume variations.

Figures 8.16 to 8.21 and Table 8.4 show how the CVS model and these PEEP-specific variable changes were able to predict the main trends in the clinically relevant systolic and diastolic arterial pressures (SAP, DAP), systolic and diastolic pulmonary artery pressures (SPAP, DPAP) and stroke volume (SV). Note, that starting from only one pig it has been shown that a general population rule, valid over all studied pigs, can be formulated and used to predict hemodynamic changes, thus showing that all pigs react along similar trends. This assumption makes sense as the pigs were healthy and no other diseases or hemodynamic instabilities were induced. Overall, the prediction error results are within clinical variation and close to measurement error in some cases. These results thus show the general applicability of this CVS model and methods to predictively capture the main hemodynamic trends due to this often applied intervention over a number of different pigs.

8.3.4.1 Study Limitations

It has to be mentioned that for this research all model volumes had to be estimated, based only on an estimated TBV and measured GEDV. This approximation naturally introduces a potentially significant degree of uncertainty and possible source of model error. As can be seen in Figures 8.16 to 8.21, the prediction results during normo- and hypovolemia are relatively good with median absolute percentage errors less than 6% for the arterial pressures and less than 10% for the stroke volume. However, the prediction results are not that good for the hypervolemia states, suggesting a model error. In particular, the approximated volumes and any error they contain may well be exacerbated in this case. Further research will thus need to be conducted to better model or estimate the different volume compartments, especially during hypervolemic states.

8.3.5 Conclusions

The integral-based optimization led to the successful definition of PEEP-specific population parameters for a minimal cardiac model. These PEEP-specific population values were used to validate the predictive ability of the model for use in guiding this often used therapy. This further validation shows the ability of the model to adequately and realistically simulate the impact of pressure-volume changes with PEEP and fluid therapy. Moreover, such rules can be similarly derived and used to predict the response towards a variety of interventions, while errors or deviations from can point out developing disease states or hemodynamic instabilities.

Chapter 9

Application to Porcine Experiments of Septic Shock

This chapter presents the results of a porcine validation study during induced endotoxic shock. The first section analyzes right ventricular (RV)-vascular coupling during hemofiltration and compares the model-based identified RV-vascular coupling to previously reported results in (Lambermont *et al.*, 2006).[1]

The second part of this chapter analyzes and identifies the different effects on the hemodynamic status of the pigs during induced endotoxic shock with and without hemofiltration (HF). Results of the identified RV-vascular coupling are also compared to the results available in (Lambermont *et al.*, 2006).[2]

9.1 Pathophysiology of Septic Shock

Sepsis is a very complex and serious systemic response to infection that also has a significant impact on cardiovascular and circulatory performance. Sepsis results in as many deaths in the USA as out-of-hospital cardiac arrests, and four times the number for breast cancer (Angus & Crowther, 2003). More specifically, mortality rates have ranged from 25% to 80% over the last few decades (Angus *et al.*, 2001). In the USA, the annualized increase in the incidence of sepsis is estimated to be about 9% and its associated mortality rate 18% (Martin *et al.*, 2003). Septic shock, the most severe form of sepsis, accounts for about 9% of admissions to ICUs and its short-term mortality ranges between 40% and 60%

[1] The first section is based on (Desaive *et al.*, 2008; Starfinger *et al.*, 2008b).
[2] The second section is based on (Starfinger *et al.*, 2008c).

(Annane *et al.*, 2003). Figure 9.1 shows the trend and improvement of mortality rates over the last decades (Dellinger, 2003; Friedman *et al.*, 1998).

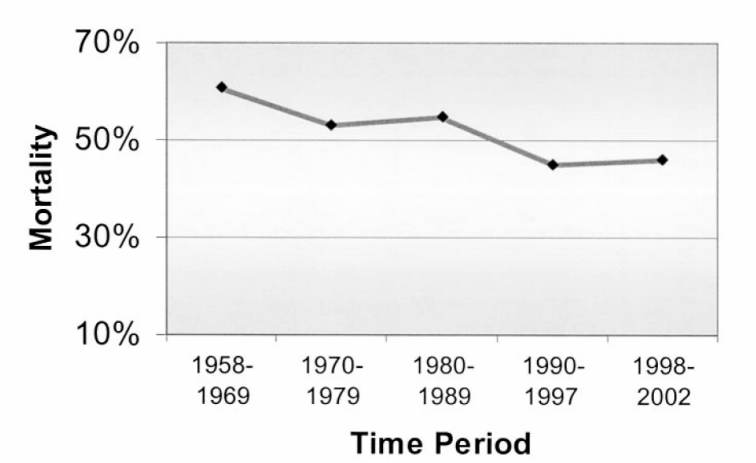

Figure 9.1: Septic shock mortality rates. Source: (Dellinger, 2003; Friedman *et al.*, 1998)

Septic shock or severe sepsis and multiple organ failure are thus one of the leading causes for morbidity and mortality in the critical care setting. The current definition of septic shock as defined by the ACCP/SCCM Consensus Conference Meeting in 1992 is: " ... sepsis-induced hypotension (systolic blood pressure $<$ 90mmHg or a reduction of $\leq$ 40mmHg from baseline) despite adequate fluid resuscitation along with the presence of perfusion abnormalities that may include, but are not limited to, lactic acidosis, oliguria, or an acute alteration in mental status. Patients who are receiving inotropic or vasopressor agents may have a normalized blood pressure at the time that perfusion abnormalities are identified ... " (ACCP/SCCM, 1992; Dellinger, 2003).

Figure 9.2 shows the normal circulation whereas Figure 9.3 shows the circulatory system during septic shock, but before fluid resuscitation. Figure 9.4 shows the circulatory status after fluid resuscitation. In septic shock, as seen in Figure 9.3, venous return to the right heart is decreased as caused by the combinatory effects of capillary leaks, less stressed systemic volume and loss of circulatory tone leading to systemic arterial resistance. Moreover, venous capacitance and pulmonary resistance are usually increased, which together with a reduced ventricle

contractility lead to impaired stroke volume and cardiac output. A decreased systemic arterial resistance therefore leads to a low blood pressure and consequently hypotension. Fluid resuscitation can compensate for the capillary leak and result in increased venous return. Most patients in septic shock after fluid resuscitation thus have a high cardiac output, but a low systemic vascular resistance state (Dellinger, 2003), indicating the key clinically important diagnostic characteristics and treatments.

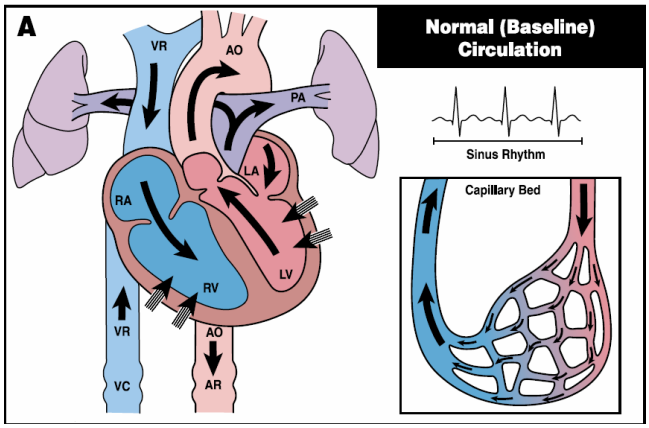

Figure 9.2: Normal, baseline circulatory status. Source: (Dellinger, 2003)

9. APPLICATION TO PORCINE EXPERIMENTS OF SEPTIC SHOCK

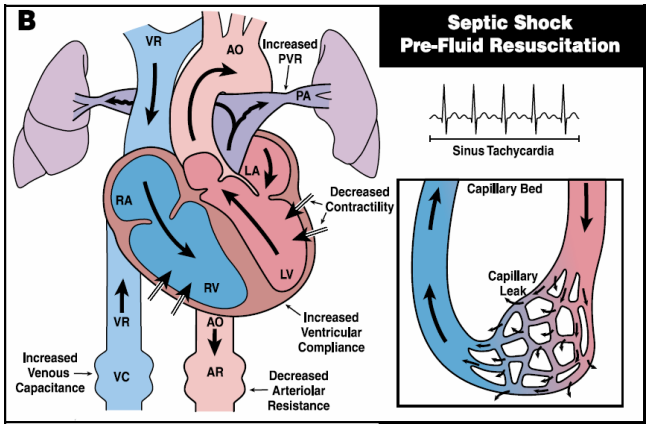

Figure 9.3: Circulatory status in septic shock before fluid resuscitation. Source: (Dellinger, 2003)

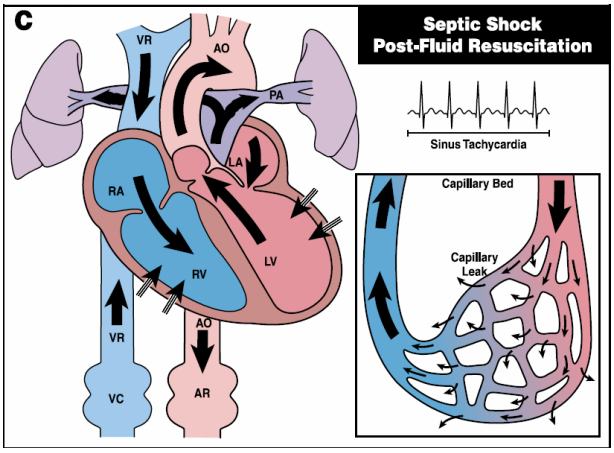

Figure 9.4: Circulatory status in septic shock after fluid resuscitation. Source: (Dellinger, 2003)

The hemodynamic profile of septic shock can therefore be summarized with the causative physiological effects as follows (Dellinger, 2003):

- Hypovolemia (loss of cardiac filling and volume)
  - Capillary leak
  - Venous dilation
- Cardiogenic effects:
  - Decrease in contractility of the ventricles
- Obstructive effects:
  - Increase in pulmonary vascular resistance
- Distributive (hypoperfusion despite normal or increased CO) effects:
  - Decreased splanchnic blood flow
  - Shunting
- Cytotoxic effects:
  - Inability of tissues to utilize O_2 (despite adequate supply)

9.2 Part I: Model-Based Analysis of RV-Vascular Coupling During Endotoxic Shock

9.2.1 Introduction

Since continuous hemofiltration (HF) was first described as a new form of renal replacement therapy (Kramer *et al.*, 1977), a lot of experimental research has shown that hemofiltration can also improve hemodynamics and survival in septic shock. This research identifies parameters using the previously described CVS model and parameter identification process (Hann *et al.*, 2006; Starfinger *et al.*, 2007b, 2008d), using data from a porcine experiment of induced endotoxic shock, combined with continuous veno-venous hemofiltration (CVVH) (Lambermont *et al.*, 2006). Measurements used to identify the model parameters are the: minimum and maximum volumes in the ventricles (V_{lv}, V_{rv}), pressures in

aorta, pulmonary artery (P_{ao}, P_{pa}) and heart rate (HR). All of these are reasonably measured or estimated in a critical care setting. Every 30 minutes into the experiment new parameters are identified that uniquely represent the pig's hemodynamic condition at that time. It is shown that the model is able to accurately capture all the pressures and volumes when compared to measured clinical data.

RV-vascular coupling has been widely studied during septic shock as right heart failure is one of the numerous and more severe complications seen in septic shock. Impaired RV function results from an inappropriate matching between the ventricular inotropic or activation state and pulmonary vascular impedance, with secondary altered ventricular-vascular coupling (D'Orio *et al.*, 1998). RV-vascular coupling can be used to analyze how effectively right myocardial performance is transmitted to the pulmonary circulation. The wave pattern of flows and pressures in the main pulmonary artery represent a result of a collision between a forward wave from the RV with a backward wave from the more peripheral parts of the pulmonary arterial tree. Such a wave reflection has a negative effect as a phase shift between pressure and flow waves is produced, which in turn reduces the hydraulic power output of the RV delivered into the main pulmonary artery (D'Orio *et al.*, 1998). As a result, there is not enough RV output compared to the resistance of the pulmonary circulation, leading to an impeded power transfer to the pulmonary circulation and therefore consequently to inadequate left ventricle (LV) inflow and reduced cardiac output (CO). The CVS model parameters produce similar results in identifying RV-vascular coupling, as published earlier (Lambermont *et al.*, 2006), and thus show the potential to use this type of model-based physiological monitoring to diagnose developing disease states.

9.2.2 Methods

9.2.2.1 CVS Model

The CVS model is a lumped parameter model which was previously developed by (Smith, 2004) and is based on earlier work of (Chung *et al.*, 1997; Olansen *et al.*, 2000). The new and extended model is presented in Section 3.2.

9.2.2.2 Integral-Based Parameter Identification

The parameter identification methods are presented in Chapter 5 and Section 8.2.2.2. The parameters given in Table 9.1 are identified based on the previously

published integral-based identification process (Hann *et al.*, 2006; Starfinger *et al.*, 2007b).

Parameters used in CVS model
Taken from literature or measured
$P_{th}, period, \lambda_{lvf}, \lambda_{rvf}, \lambda_{spt}, \lambda_{pcd}, E_{esspt}, Vd_{spt}, Vo_{spt}, P0_{spt}, Vo_{lvf}, Vo_{rvf}, Vd_{lvf}, Vd_{rvf}, Vd_{vc}, Vd_{ao}, Vd_{pa}, Vd_{pv}$
Optimized
$L_{av}, L_{mt}, L_{tc}, L_{pv}, E_{eslvf}, P_{0lvf}, E_{esrvf}, P_{0rvf}, R_{av}, R_{mt}, R_{tc}, R_{pv}, P_{ao0}, P_{pu0}, P_{pa0}, P_{vc0}, P_{0pcd}, E_{sys}, E_{cap}, E_{ao}, E_{pa}, E_{vc}, E_{pu}, R_{sys}, R_{pulin}, R_{pulout}, R_{vr}$

Table 9.1: Parameters used in CVS model.

9.2.2.3 Experimental Protocol

All experimental procedures for this experiment were reviewed and approved by the Ethics Committee of the Medical Faculty of the University of Liège. They were performed in accordance with the *Guide for the Care and Use of Laboratory Animals*, as adopted and promulgated by the U.S. National Institutes of Health (NIH Publication No. 85-23, revised 1996). The experiments were performed on 7 healthy pigs weighing 25-30 kg. Data from 6 pigs was analyzed and identified for this research. The animals were premedicated and anesthetized, as described previously (Lambermont *et al.*, 2003). Measurements were obtained for systemic arterial pressure (P_{ao}), pulmonary arterial pressure (P_{pa}) and the left and right ventricle pressures and volumes (P_{lv}, V_{lv}, P_{rv}, V_{rv}) as described in (Lambermont *et al.*, 2003). In particular, the volume measurements that provide data for Equations 5.1-5.4 are made by a 7F, 12-electrode (8mm interelectrode distance) conductance micromanometer-tipped catheter (CD Leycom, Zoetermeer, The Netherlands).

After a 30 min stabilization period, the animals received a 0.5 mg/kg endotoxin infusion (lipopolysaccharide from Escheria coli serotype 0127:B8; Sigma Chemical, St. Louis, MO, USA) over a 30 min period (T000 - T030). From 60 minutes (T060) into the experiment onwards, the animals underwent a zero-balance continuous veno-venous hemofiltration (CVVH) at a rate of 45 ml/kg/h. A 0.7 m^2 large-pore (78 $\mathring{A}$) membrane with a cutoff of 80 kDa (Sureflux FH 70,

Nipro, Osaka, Japan) and a Baxter BM 25- BM 14 hemofiltration device (Baxter Health Care, Munich, Germany) were used. Ultrafiltrate was replaced in the postdilution mode by a bicarbonate-buffered hemofiltration fluid (Na^+: 150mM; K^+: 3mM; bicarbonate: 30mM) at a temperature of 37℃.

9.2.3 Results

9.2.3.1 Identification of Endotoxic Shock

Figure 9.5 shows the clinically measured end-diastolic (EDV) and end-systolic (ESV) left ventricle volumes for all identified segments over all pigs (solid lines). The crosses and boxes represent the CVS model simulation output when re-run using the identified model parameters. As can be seen, the model output values match the true clinical values very well with mean absolute percentage errors less than 3%, which is well within measurement or estimate errors (Baan *et al.*, 1984; Burkhoff *et al.*, 1985). Figure 9.6 shows the same results for the right ventricle volumes, respectively.

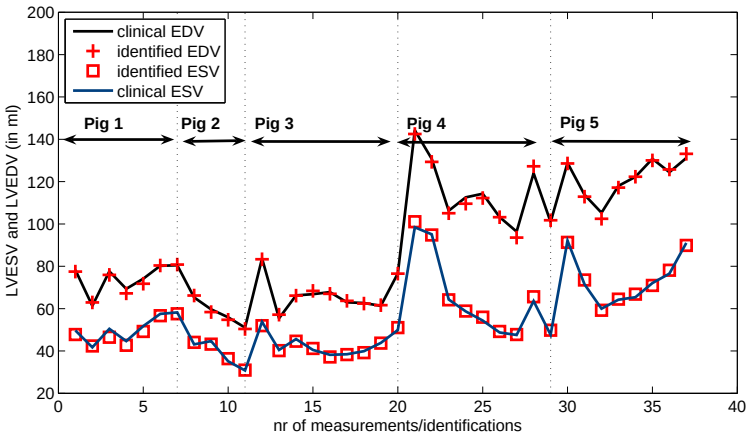

Figure 9.5: Model output (cross) vs clinical (circle, solid line) left ventricle volumes for all identified segments over all pigs. The upper line shows the clinical vs. identified end-diastolic volume (LVEDV) and the lower line shows clinical vs. identified end-systolic volume (LVESV).

Figure 9.7 shows the matched systemic arterial systolic and arterial diastolic pressure values (SAP, DAP). Solid lines represent the clinical measurements and the crosses and boxes the CVS model outputs. Again, very good matches are obtained with mean absolute percentage errors less than 7%.

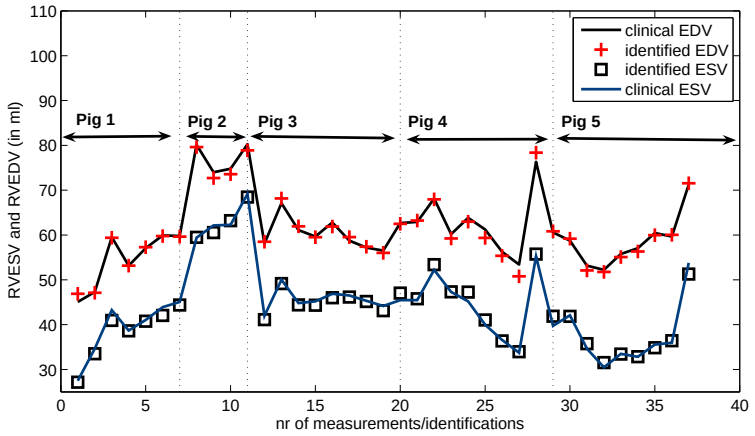

Figure 9.6: Model output (cross) vs clinical (circle, solid line) right ventricle volumes for all identified segments over all pigs. The upper line shows the clinical vs. identified end-diastolic volume (RVEDV) and the lower line shows clinical vs. identified end-systolic volume (RVESV).

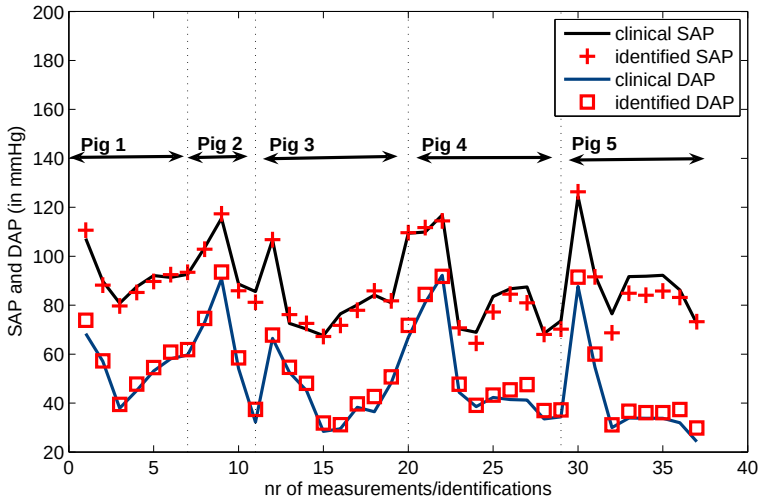

Figure 9.7: Model output (cross) vs clinical (circle, solid line) arterial pressure for all identified segments over all pigs. The upper line shows the clinical vs. identified systolic arterial pressure (SAP) and the lower line shows clinical vs. identified diastolic arterial pressure (DAP).

Figure 9.8 shows the same results for the systolic and diastolic pulmonary artery pressures (SPAP, DPAP), respectively. Note, that the match between the two sig-

nals shows larger errors for measurements 34-38, because the clinically measured P_{pa} signal went below zero, a non-physiological value that is almost certainly a measurement error rather than a true measurement. These measurements were thus ignored during the identification process, but represent the kinds of errors that can occasionally occur.

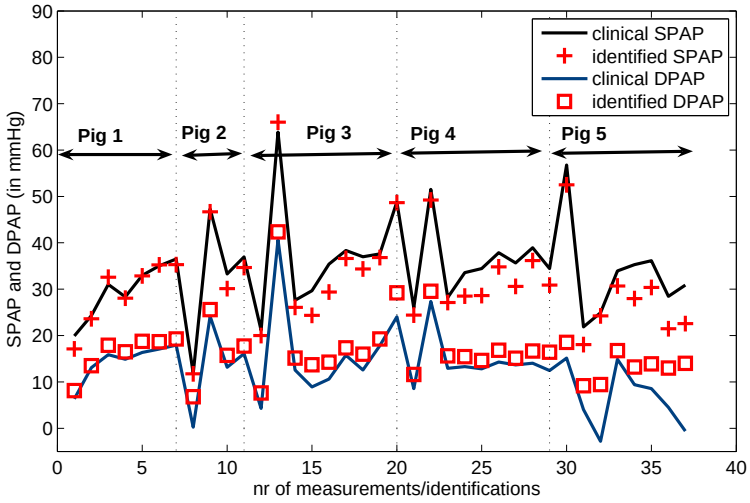

Figure 9.8: Model output (cross) vs clinical (circle, solid line) pulmonary artery pressure for all identified segments over all pigs. The upper line shows the clinical vs. identified systolic pulmonary artery pressure (SPAP) and the lower line shows clinical vs. identified diastolic pulmonary artery pressure (DPAP).

Figure 9.9 illustrates the very good matches achieved for one typical pig in greater detail. The first two subfigures show the left and right ventricle signals at the beginning of the experiment (T000). The upper panel of the left subfigure (LV) shows the clinical (V_{lvp}) vs. simulated left ventricle volume (V_{lvs}) and in the lower panel the clinical (P_{lvp}) vs. simulated left ventricle pressure (P_{lvs}) and arterial pressure (P_{aop}, P_{aos}), respectively.

It has to be noted, that during the identification process only the systolic (maximum) and diastolic (minimum) values of the measured ventricle volume (EDV, ESV) and arterial pressure (SAP, DAP) are used. The left ventricle pressure (P_{lv}) is not used as this measurement is rarely obtained in a clinical setting. However, it can clearly be seen that relatively good matches are nevertheless obtained for the ventricle pressures, further validating the model and identification process.

If desired, the ventricle pressures could easily be matched more accurately by adjusting the simple activation functions used in the CVS model (Smith *et al.*, 2004). However, this level of accuracy and added modification was not intended in this study and is not necessary given the good match between re-simulated model and clinical data.

The right subfigure (RV) illustrates the same results for the right ventricle volume (V_{rv}, upper panel) and the right ventricle pressure and pulmonary artery pressure (P_{rv}, P_{pa}, lower panel). The following 4 subfigures show the same signals at 120 minutes into the experiment and at 240 minutes. In each case, the matches between pig-specific, identified model and clinical data are qualitatively very good.

Importantly, this study did not intend to accurately match the pressure and volume waveform shapes, but only the minimum (diastolic) and maximum (systolic) values. This goal was adopted because the main focus is to identify the overall macro-hemodynamic condition, and less interest is thus placed on exactly matching specific waveforms. For example, exactly matching the dicrotic notch in the arterial pressure signals was not a goal. These smaller, less clinically relevant dynamics are often a function of small unmodelled non-linearities or small non-linearities in patient-specific cardiac activation function. In addition, a patient-specific activation function would eliminate most of these clinically insignificant differences.

Table 9.2 shows the mean absolute percentage errors for the identified minimum and maximum pressure and volume signals (SAP, SPAP, LVESV, LVEDV, RVEDV, RVESV) for the identified re-simulated model over all pigs. Generally, the errors are well below 10%, which is within measurement noise. However, as mentioned before, there are a few larger errors for the pulmonary artery pressure P_{pa}, as seen in Figure 9.7, that are caused by a suspiciously low non-physiological pressure signal that was ignored.

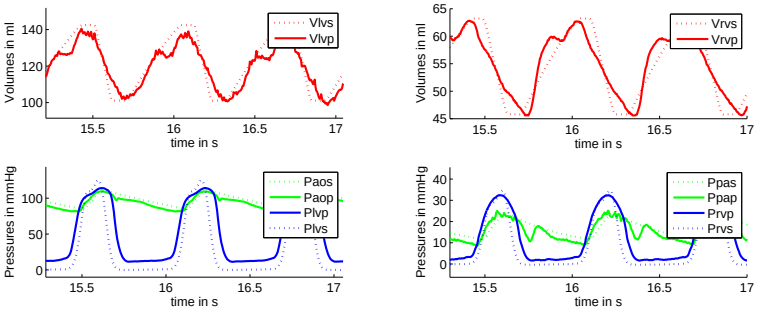

(a) time: 0 min, LV

(b) time: 0 min, RV

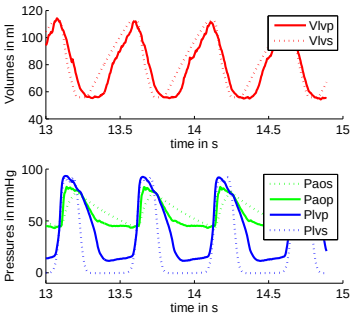

(c) time: 120 min, LV

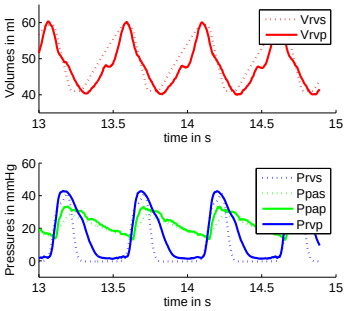

(d) time: 120 min, RV

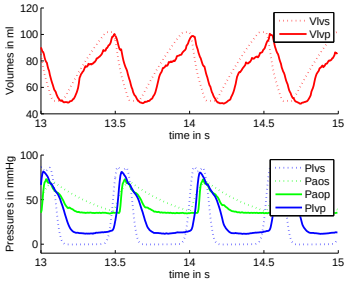

(e) time: 240 min, LV

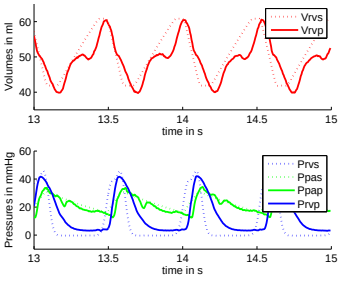

(f) time: 240 min, RV

Figure 9.9: Model output (dotted) vs clinical (solid line) volume and pressure signals for left and right ventricle (LV, RV). The upper panel shows the clinical (p) vs. simulated ventricle volume (s). The lower panel shows the clinical (p) vs. simulated (s) ventricle and arterial pressure. The results are shown for 0 (begin), 120 (middle) and 240 (end) minutes into the experiment.

Difference in % for measured and simulated pressures and volumes						
	SAP	SPAP	LVEDV	LVESV	RVEDV	RVESV
μ	3.19	7.01	1.36	2.12	1.18	1.90
σ	2.70	5.27	1.00	1.62	1.07	1.53
IQR	3.93	4.54	1.64	2.10	1.19	1.97

Table 9.2: Mean absolute percentage error (μ), standard deviation (σ) and interquartile range (IQR) in % for measured and simulated pressures and volumes over all 38 identified segments. SAP = systolic arterial pressure, SPAP = systolic pulmonary artery pressure, LVEDV = left ventricle end-diastolic volume, LVESV = left ventricle end-systolic volume, RVEDV = right ventricle end-diastolic volume, RVESV = right ventricle end-systolic volume .

9.2.3.2 Analysis of Right Ventricular-Vascular Coupling

RV-vascular coupling is a significant clinical indicator of serious circulatory and cardiac dysfunction in sepsis (D'Orio *et al.*, 1998; Lambermont *et al.*, 2003). Figure 9.10 shows the mean cardiac output (CO) for all analyzed pigs during the endotoxic shock experiment, separated for the left and right ventricle outputs. It can be seen that the identified model-based CO (crosses) matches the measured clinical data (solid/dashed line) very well. Note that the right ventricle CO remains relatively constant during the whole experiment. The lower panel of Figure 9.11 shows the mean right ventricle end-systolic elastance (E_{esrvf}) over all pigs during the experiment. This elastance is identified during the identification process. Note that the absolute values do not match the clinically estimated values in the upper panel (Lambermont *et al.*, 2006) as the value of the model-based E_{esrvf} depends on the unstressed ventricle volume (V_d). For reasons of simplicity, this value is assumed to be zero (V_d=0 ml) during the identification process. However, E_{esrvf} can easily be adjusted for a different and probably more realistic V_d. More importantly for clinical diagnosis, the identified E_{esrvf} trend matches very well with recently reported values obtained for the same experimental data (Lambermont *et al.*, 2006) as shown in the upper panel of Figure 9.11.

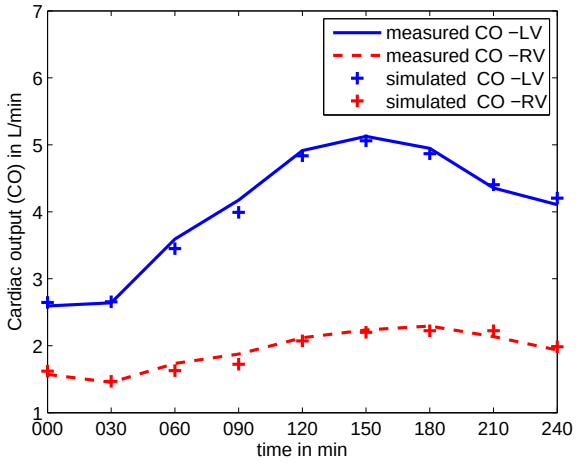

Figure 9.10: Mean measured cardiac output (CO) for all 5 analyzed pigs during the endotoxic shock experiment.

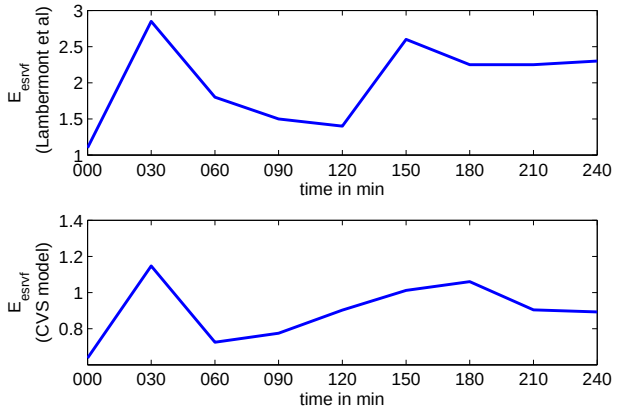

Figure 9.11: Mean identified right ventricle elastance (E_{esrvf}) for all 5 analyzed pigs during the endotoxic shock experiment.

Figure 9.12 shows in the upper panel the mean pulmonary artery elastance as obtained and published previously (Lambermont *et al.*, 2006). In the lower panel the identified mean pulmonary arterial elastance (E_{pa}) is shown during the experiment. Qualitatively the same trends are observed, validating the model. Note, the absolute values are not expected to match because E_{pa} in the CVS model is calculated based on the pulmonary artery pulse pressure and stroke volume as compared to the calculated E_{pa} values from (Lambermont *et al.*, 2006), using a four element Windkessel model as described in more detail in (Fourie

et al., 1992).

Figure 9.13 shows a similar result obtained for the mean pulmonary inflow resistance (R_{pulin}), which is likewise representing right-ventricular afterload in the CVS model. Both figures match closely with recently reported trends obtained for the same experimental data (Lambermont *et al.*, 2006). Note again that the absolute values do not match perfectly, as in the CVS model the arterial elastances are estimated and not optimized during the identification process. However, the trends are what is clinically important for diagnosis and determining the efficiency of any therapy given.

Figure 9.14 shows in the upper panel the RV-coupling reported previously (Lambermont *et al.*, 2006) and in the middle panel the coupling (E_{esrvf}/R_{pulin}) obtained from the identified CVS model parameters during the endotoxic shock experiment. The lower panel shows the difference between the two. The ratio E_{esrvf}/R_{pulin} describes the coupling efficiency of the right ventricle to the pulmonary vascular tree. If this ratio decreases and RV-vascular uncoupling occurs, less power is transferred to the pulmonary circulation and as a result, right cardiovascular performance is impaired. Again, the trends match very well. Note that the coupling in the CVS model is best represented by the ratio E_{esrvf}/R_{pulin} as both parameters, E_{esrvf} and R_{pulin} are identified directly from the clinical data during the identification process.

Figure 9.15 shows the mean identified systemic vascular resistance (R_{sys}) over all pigs during the endotoxic shock experiment. This value is clinically important due to impact of sepsis on blood pressure, where increasing sepsis and septic shock decrease blood pressure via loss of control over systemic vascular tome and reduced resistance. This loss of resistance is clearly evident in Figure 9.15 as the endotoxin experiment proceeds.

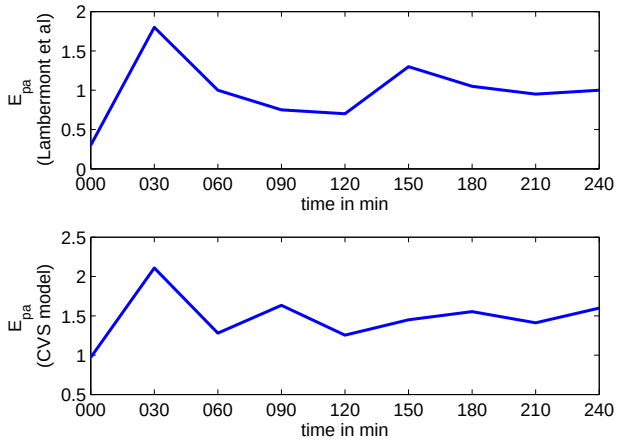

Figure 9.12: Mean identified pulmonary arterial elastance (E_{pa}), representing right ventricular afterload, for all 5 analyzed pigs during the endotoxic shock experiment.

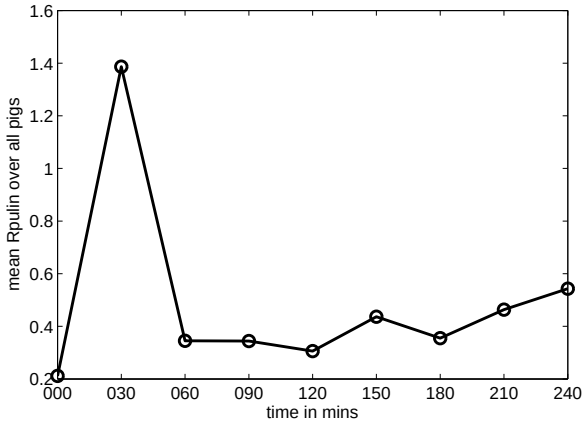

Figure 9.13: Mean identified pulmonary input resistance (R_{pulin}), representing right ventricular afterload, for all 5 analyzed pigs during the endotoxic shock experiment.

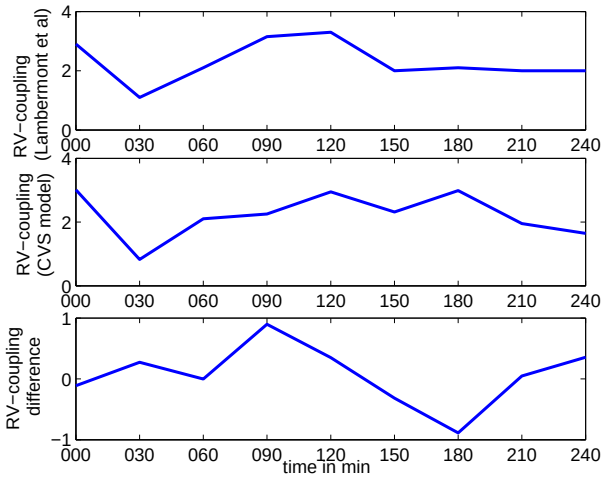

Figure 9.14: Mean identified right ventricular-vascular coupling (E_{esrvf}/R_{pulin}) for all 5 analyzed pigs during the endotoxic shock experiment.

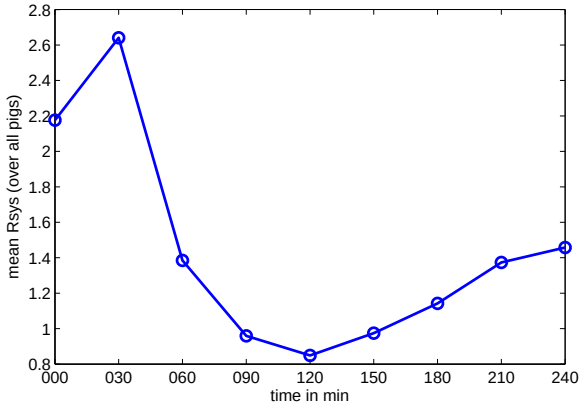

Figure 9.15: Mean identified systemic vascular resistance (R_{sys}) for all 5 analyzed pigs during the endotoxic shock experiment.

9.2.4 Discussion

The major findings of this research are twofold. Firstly, the clinical experimental results obtained previously (Lambermont *et al.*, 2006) are matched using the extended CVS model and parameter identification process. Figure 9.14 displays in the middle panel the identified RV-vascular coupling which is represented by the ratio of RV end-systolic elastance (E_{esrvf}) and pulmonary vascular resistance

(R_{pulin}). It can clearly be seen how hemofiltration (which starts at 60 min into the experiment) is able to prevent RV-vascular uncoupling that is commonly observed during the late phases of endotoxic shock (Lambermont *et al.*, 2003). The data shows that in the early phases of endotoxic shock, RV-vascular coupling is preserved by an increase in RV contractility (E_{esrvf}) as seen in Figure 9.11. During the later stages and with CVVH, RV-vascular coupling is preserved where a decrease in pulmonary vascular resistance (R_{pulin}), as seen in Figure 9.13, is suggested to be the main reason for this effect (Lambermont *et al.*, 2006). These results allow for a better understanding of the mechanisms of RV dysfunction during septic shock and thus have the potential to lead to more effective diagnosis and choice of therapies for myocardial depression in septic shock.

Secondly, the CVS model and identification process are also further validated by correctly identifying similar trends to those observed during clinical endotoxic shock experiments. Additionally, systemic vascular resistance (R_{sys}) is identified during the experiment and the mean resistance for all pigs is shown in Figure 9.15. These results match physiological expectations as low peripheral vascular resistance is a common sign in sepsis and decreases left ventricular afterload, as also seen in Figure 9.7 in reduced arterial pressures.

Table 9.2 summarizes all results for all five pigs and a total of 38 identification periods. Note, that all measurements for one pig and 8 measurements of the remaining five pigs had to be omitted from this final analysis as they contained corrupted data, such as those produced by disconnected catheters. These results show that the extended CVS model is able to capture the essential dynamics of the porcine CVS response to endotoxic shock and CVVH over a selection of subjects.

9.2.5 Conclusions

The integral-based optimization successfully identified pig-specific parameters for the extended CVS model. This further validation shows the ability of the model to adequately and realistically capture the impact of pressure-volume changes during endotoxic shock and with CVVH. Comparable results to previously reported studies are obtained when analyzing the RV-vascular coupling, further validating the methods and approach presented here. In particular, the model is able to aggregate diverse measured data into a clear, clinically and physiologically relevant diagnostic picture as the condition develops. As discussed, the results

thus offer patient-specific monitoring of otherwise unmeasurable, but clinically very significant, physiological parameters that can lead to improved therapy of care. This research thus increases confidence in the clinical applicability and validity of this overall diagnostic monitoring approach preparatory to initial studies with human subjects.

9.3 Part II: Model-Based Analysis and Comparison of Endotoxic Shock With and Without Hemofiltration

9.3.1 Introduction

The CVS model and identification process have previously been validated in the identification and model-based analysis of induced endotoxic shock with continuous veno-venous hemofiltration (CVVH) therapy (Starfinger *et al.*, 2008b). Similar RV-coupling results were obtained for a patient-specific identified CVS model compared to previously measured clinically data (Lambermont *et al.*, 2006), further validating the developed model and the identification procedure. In this research, a porcine model of induced endotoxic shock without hemofiltration is analyzed and the CVS model parameters are identified using only right heart measurements.

The novelty of this identification is that for the first time the identification process is applied to strictly right heart signals and no left ventricle signals were measured. This reduced data set is of particular clinical importance as often only data from one of the ventricles is available. The CVS model and identification process are therefore applied here to only the measured right ventricle signals. However, similar contractility, afterload and RV-coupling trends are obtained when compared to previously reported results (Lambermont *et al.*, 2006).

This research is therefore intended to show the robustness of the methods developed and the potential to use this type of model-based physiological monitoring to diagnose developing disease states. It also shows the extended clinical potential for those cases where significantly less measured data is available. Hence, this research showcases model-based monitoring and diagnosis of untreated sepsis using further reduced clinical data.

9.3.2 Methods

9.3.2.1 Experimental Protocol

All experimental procedures and protocols used in this investigation were reviewed and approved by the Ethics Committee of the Medical Faculty of the University of Liège. The investigation conforms with the Guide for the Care and

Use of Laboratory Animals published by the US National Institutes of Health (NIH Publication No. 85-23, revised 1996).

Experiments were performed on 12 healthy pure pietran pigs of either sex weighing from 20 to 30 kg. The animals were premedicated with intramuscular administration of ketamine (20 mg/kg) and diazepam (1 mg/kg). Anesthesia was then induced and maintained by a continuous infusion of sufentanil (0.5 mg/kg/h) and pentobarbital (5 mg/kg/h). Spontaneous movements were prevented by pancuronium bromide (0.2 mg/kg). After endotracheal intubation through a cervical tracheostomy, the pigs were connected to a volume cycled ventilator (Evita 2, Dräger, Lübeck, Germany) set to deliver a tidal volume of 10 ml/kg with a FiO of 0.4 and at a respiratory rate of 20 breaths /min. End-tidal CO (PETCO) measurements (Capnomac, Datex, Helsinki, Finland) were used to monitor the adequacy of ventilation. Respiratory settings were adjusted to maintain PETCO between 30 and 35 mmHg.

In both groups, the animals received a 0.5-mg/kg endotoxin infusion (lipopolysaccharide from Escherichia coli serotype 0127:B8; Sigma Chemical, St. Louis, MO, U.S.A.) over 30 mins (from T0 to T30). They were then randomized into two groups. In the Endo group (n = 6), they received no further intervention while in the EndoHF group (n = 7), they underwent, from T60 onward, a zero-balance CVVH at a rate of 45 mL/kg/h (7). A 0.7-m 2 large-pore (78 Å) membrane with a cutoff of 80 kDa (Sureflux FH 70, Nipro, Osaka, Japan) and a Baxter BM 25- BM 14 hemofiltration device (Baxter Health Care, Munich, Germany) were used. Ultrafiltrate was replaced in the postdilution mode by a bicarbonate buffered hemofiltration fluid (Na^+: 150 mM; K^+: 3 mM; bicarbonate: 30 mM) at a temperature of 37°C. Anticoagulation of the extracorporeal circuit was achieved using a loading dose of 5000 IU of heparin followed by an anticoagulation regimen based on the activated clotting time (100200 s).

Measurements were obtained for systemic arterial pressure (P_{ao}), pulmonary arterial pressure (P_{pa}) and right ventricle pressure and volume (P_{rv}, V_{rv}) as described previously in (Lambermont *et al.*, 2003).

9.3.2.2 CVS Model

The CVS model is a lumped parameter model which was previously developed by (Smith, 2004) and is based on earlier work of (Chung *et al.*, 1997; Olansen *et al.*, 2000). The new and extended model is presented in Section 3.2.

9.3.2.3 Integral-Based Parameter Identification

The parameter identification methods are presented in Chapter 5 and Section 8.2.2.2.

9.3.2.4 Estimations for Left Ventricle Signals

As the left ventricle signals are not measured in this reduced data study, they must be estimated for the identification process. The left ventricular volume (V_{lv}) is assumed to be the same as the measured right ventricular volume (V_{rv}), for reasons of simplicity. Thus, the left ventricle stroke volume (LVSV) is also assumed to be the same as the measured right ventricle stroke volume (RVESV). The left ventricular pressure (P_{lv}) is not required during the identification process and is thus not specifically estimated. These approximations are not necessarily accurate in a dynamic, septic patient, but provide an initial starting point.

9.3.2.5 Volume Calculations

The central venous pressure (CVP) or systemic pressure P_{sys} plays a central role in the CVS model and identification process. The CVP provides insight into the venous system function and, more specifically, gives information about the effective systemic volume $V_{sys,eff}$. However, CVP is not measured in this experiment and there is also no directly measured information available about the volume status of the pigs. Therefore, certain assumptions about the volumes and pressures in the CVS model have to be made. These assumptions help guarantee that the best and optimal parameters, relative to these assumed volumes, are identified. In all cases, the identified model parameters are then used to re-simulate the model and produce output signals that not only match the measured signals, but also all other estimated volumes and pressures. The overall approach thus provides consistent means of identification and validation, given clinical data.

It is known that during septic shock the effective systemic volume decreases as a result of capillary leak (absolute hypovolemia) or venodilation (relative hypovolemia) (Bridges & Dukes, 2005; Dellinger, 2003). Therefore, the evolution of septic shock was simulated in this research by a stepwise reduction of 5% of the effective systemic volume $V_{sys,eff}$ every 30 minutes. This stepwise reduction is a rather conservative estimate of the reduction in volume (Task Force of the American College of Critical Care Medicine, Society of Critical Care Medicine,

19). If necessary, the CVS model can easily be run with more severe reductions simulating more severe forms of septic shock.

Note, that all initial CVS model volumes are estimated based on the known distribution of blood, as previously described in (Starfinger *et al.*, 2008d,e) and in Section 4.2.

9.3.2.6 Summary of Methods

In this research, the main goal is to identify the CVS model parameters based only on measured input data from the right side of the heart, using only estimated left ventricle signals. The measured signals for this research that are used for identification are the pressures in the aorta and pulmonary artery (P_{ao}, P_{pa}), and the volume in the right ventricle (V_{rv}). The results obtained show that the CVS model and identification methods are able to correctly identify parameters from this significantly reduced set of data. The identified parameters are then used to re-run a pig-specific CVS model simulation producing output signals that match the measured clinical data. Output values that match the clinical data also serve to validate the left ventricle and other assumptions made in the iterative identification process.

Parameter values are presented as mean normalized values over all analyzed pigs. Previously reported values for the same experimental data of induced septic shock with (EndoHF group, (Lambermont *et al.*, 2006)) and without (Endo group, (Lambermont *et al.*, 2003)) hemofiltration are normalized for comparison. Data values are normalized with regard to the baseline (time=0 min) value to guarantee the correct representation of the parameter trends, rather than showing the absolute values where extreme low or high values for one pig can easily influence the mean value over all pigs. All the data is thus self-normalized before comparison across pigs or treatment method.

9.3.3 Results

9.3.3.1 Identification Results

Figure 9.16 shows the clinically measured right ventricular stroke volumes (RVSV) for all identified segments over all pigs (solid line). The crosses represent the CVS model simulation output when re-run using the patient-specific identified model parameters. As can be seen, the model output values match the true clinical

values very well, with median absolute percentage errors less than 5%, which is well within measurement or estimate errors (Baan *et al.*, 1984; Burkhoff *et al.*, 1985).

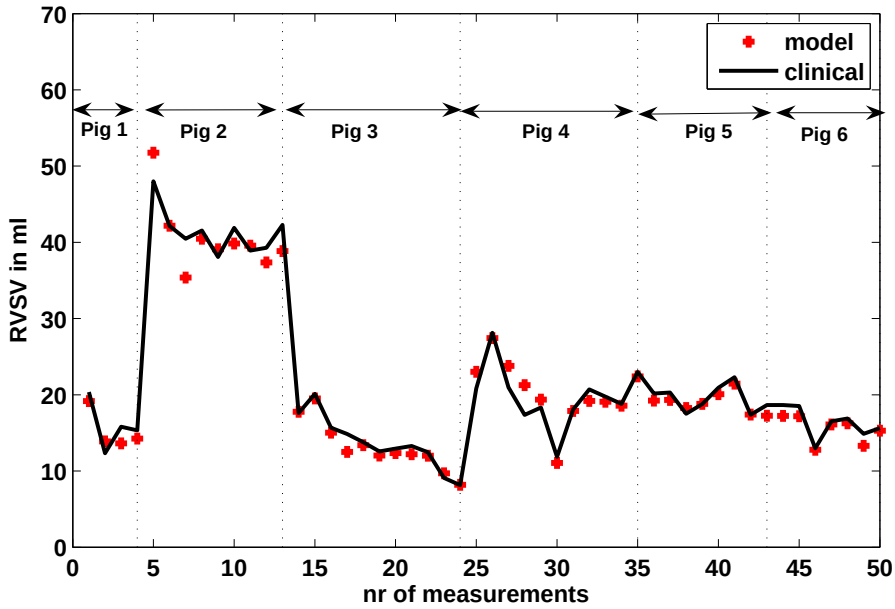

Figure 9.16: Clinical (solid line) vs simulated identified patient-specific model (cross) right ventricular stroke volume (RVSV) over all analyzed pigs.

Figure 9.17 shows the systemic arterial systolic and diastolic pressure values (SAP, DAP). The solid lines represent the clinical measurement and the $+, \square$ markers represent the identified patient-specific CVS model output for SAP and DAP respectively. Again, very good matches are obtained with median absolute percentage errors less than 3%.

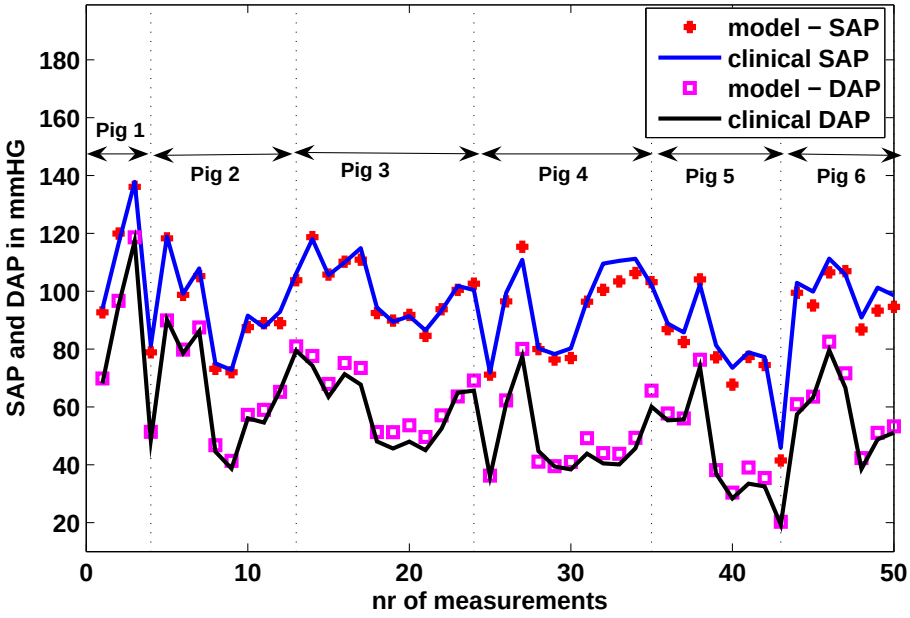

Figure 9.17: Clinical (solid lines) vs simulated systolic (cross) and diastolic (box) arterial pressures (SAP, DAP) over all analyzed pigs.

Figure 9.18 shows the pulmonary arterial systolic and diastolic pressure values (SPAP, DPAP). The solid lines represent the clinical measurement and the $+, \square$ markers represent the identified, patient-specific CVS model output for SPAP and DPAP respectively. Similarly, very good matches are obtained, with median absolute percentage errors less than 7%.

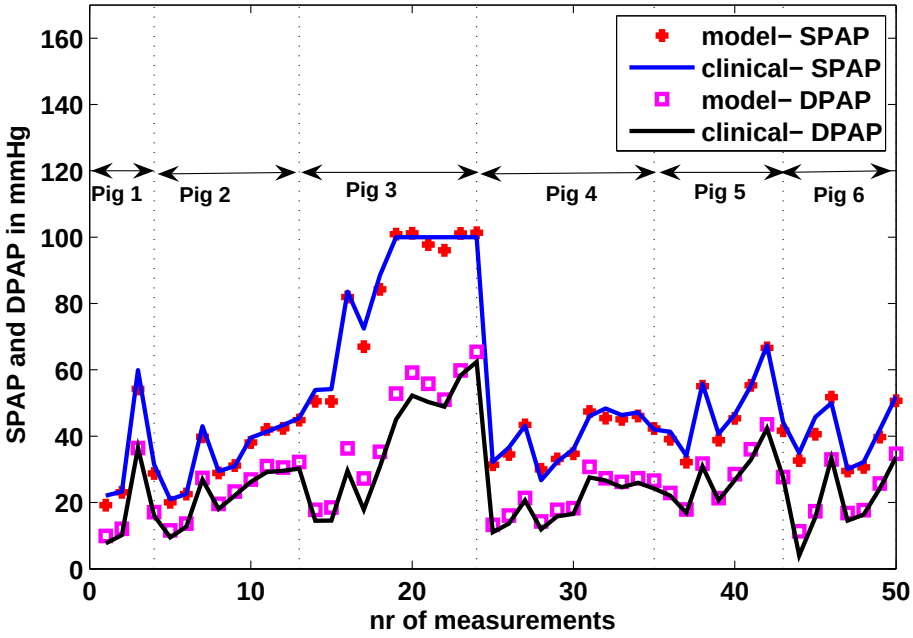

Figure 9.18: Clinical (solid lines) vs simulated systolic (cross) and diastolic (box) pulmonary artery pressures (SAP, DAP) over all analyzed pigs.

Figure 9.19 illustrates the very good matches achieved for one specific pig in greater detail. The first subfigure shows the right ventricle signals at the beginning of the experiment (T0). The upper panel shows the clinical vs. simulated right ventricular pressure and the pressure in pulmonary artery. In the lower panel, the clinical vs. simulated right ventricular volume is shown. It should be noted, that during the identification process only the systolic (maximum) and diastolic (minimum) values of the measured ventricle volume (EDV, ESV) and arterial pressure (SPAP, DPAP) are used. The right ventricular pressure is not used as this measurement is rarely obtained in a clinical setting. However, it can clearly be seen that relatively good matches are nevertheless obtained for the ventricle pressures, even where that measurement was not used in the identification process, further validating the model and identification process.

If desired, the ventricle pressures could easily be matched more accurately by adjusting the activation functions in the CVS model (Smith, 2004; Smith *et al.*, 2004). However, this level of accuracy and added modification was not intended in this study. The following subfigures illustrate the same results as in the first part of Figure 9.19, but at 90 and 120 minutes into the experiment.

It was never intended for this study to perfectly match the pressure and volume waveform shapes, but only the minimum (diastolic) and maximum (systolic) clinically measurable values. This goal was adopted because the main focus is to identify the overall macro-hemodynamic condition, and less interest is placed on exactly matching the specific waveforms. For example, exactly matching the dicrotic notch in the arterial pressure signals was not a goal. These smaller, less clinically relevant dynamics are often a function of small unmodelled non-linearities or small non-linearities in patient-specific cardiac activation function. In addition, a patient-specific activation function would eliminate most of these clinically insignificant differences.

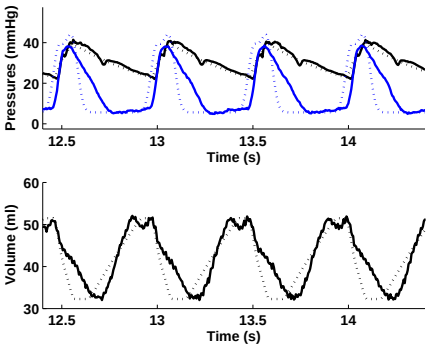

(a) Time: 0 min

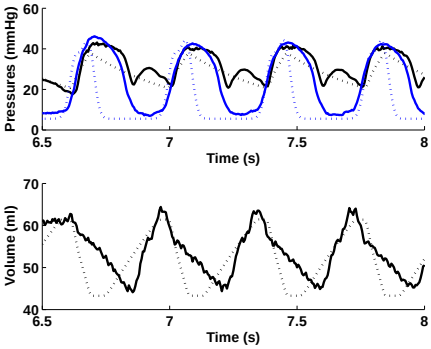

(b) Time: 90 min

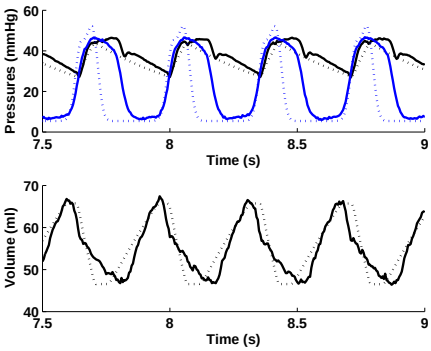

(c) Time: 120 min

Figure 9.19: Model output (dotted) vs clinical (solid line) volume and pressure signals for right ventricle (RV). The upper panel shows the clinical vs. simulated ventricle and arterial pressure. The lower panel shows the clinical vs. simulated ventricle volume. The results are shown for 0, 90 and 120 minutes into the experiment.

Table 9.3 shows the median absolute percentage errors for the identified minimum and maximum pressure and volume signals (SAP, DAP, SPAP, DPAP, RVESV, RVEDV, RVSV) for the identified re-simulated model over all pigs. Generally, the errors are well below 10%, which is within typical measurement noise levels.

Difference in % for measured and simulated pressures and volumes							
	SAP	DAP	SPAP	DPAP	RVEDV	RVESV	RVSV
median	2.87	4.33	3.02	6.40	1.37	1.55	4.71
IQR	2.89	5.82	3.99	7.98	1.43	2.09	5.11

Table 9.3: Median absolute percentage error and interquartile range (IQR) in % for measured and simulated pressures and volumes over all 38 identified segments. SAP/DAP = systolic/diastolic arterial pressure, SPAP/DPAP = systolic/diastolic pulmonary artery pressure, RVEDV = right ventricle end-diastolic volume, RVESV = right ventricle end-systolic volume, RVSV = right ventricle stroke volume.

Figure 9.20 shows the mean normalized systemic stressed volume ($V_{sys_{eff}}$), and the identified mean normalized systemic vascular (R_{sys}) and pulmonary resistance (R_{pulin}), as well as the resistance to venous return (R_{vr}) over all pigs during the endotoxic shock experiment for the Endo group. Thus this data does not include the effect of hemofiltration.

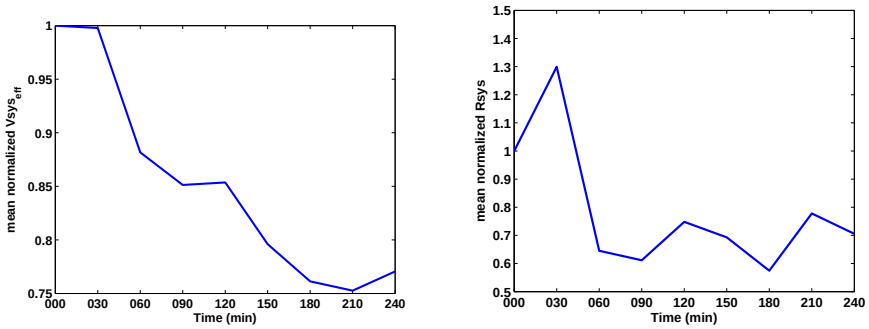

(a) $V_{sys,eff}$

(b) R_{sys}

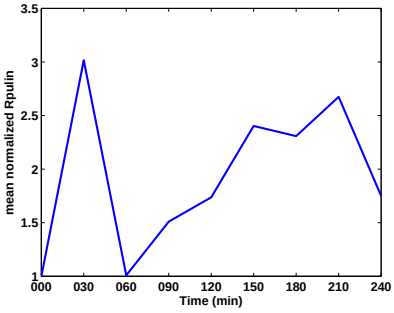

(c) R_{pulin}

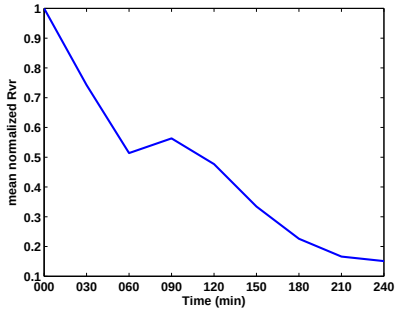

(d) R_{vr}

Figure 9.20: Mean normalized values for estimated systemic volume $V_{sys,eff}$ and the identified model parameters systemic vascular resistance R_{sys}, pulmonary vascular resistance R_{pulin} and resistance to venous return R_{vr} over all analyzed pigs during the septic shock experiment in the Endo group.

9.3.3.2 Analysis of RV-Coupling

The upper panel in Figure 9.21 shows the clinically measured right ventricular end-systolic elastance (E_{esrvf}) during the endotoxic shock experiment, as previously reported (Lambermont *et al.*, 2003, 2006). The solid line represents the obtained mean normalized E_{esrvf} value in the endotoxic group (Endo), whereas the dashed line represents the mean normalized E_{esrvf} value in the hemofiltration group (EndoHF), respectively. The lower panel of Figure 9.21 shows the similar results obtained from the CVS model and identification process. The solid line again represents the mean normalized E_{esrvf} value for the Endo group and the dashed line the mean normalized E_{esrvf} in the EndoHF group. Note that the

analysis of the EndoHF group was not part of this research and has been published previously (Desaive *et al.*, 2008; Starfinger *et al.*, 2008b). This elastance, as with all the other model parameters, is identified during the identification process.

Note that the absolute values obtained for E_{esrvf} depend on the unstressed ventricle volume (V_d). For reasons of simplicity, this value is assumed to be zero (V_d=0 ml) during the identification process. However, E_{esrvf} can easily be adjusted for a different, and probably more realistic, V_d, as these adjustments have no effect on the other identified model parameters. The identified E_{esrvf} trends match very well with recently reported values obtained for the same experimental data (Lambermont *et al.*, 2006), as shown in comparing the upper and lower panels of Figure 9.21.

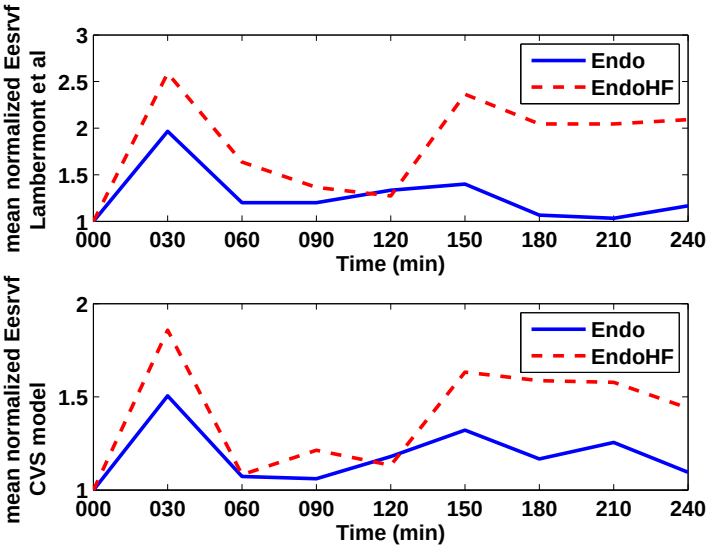

Figure 9.21: Mean normalized right ventricular end-systolic elastance E_{esrvf} over all analyzed pigs during the septic shock experiment with (EndoHF) and without (Endo) hemofiltration. Upper panel: results as obtained by (Lambermont *et al.*, 2006), lower panel: results obtained with CVS model and identification process.

9. APPLICATION TO PORCINE EXPERIMENTS OF SEPTIC SHOCK

The upper panel of Figure 9.22 shows the clinically estimated pulmonary arterial elastance (E_a) during the endotoxic shock experiment, as previously reported by (Lambermont *et al.*, 2003, 2006). The solid line represents the mean normalized E_a value obtained in the endotoxic group (Endo), whereas the dashed line represents the mean normalized E_a value clinically obtained in the hemofiltration group (EndoHF), respectively. The lower panel shows the similar results obtained for the CVS model and identification process. However, instead of showing the pre-calculated, fixed and thus not identified (optimized) E_{pa} value, the pulmonary vascular resistance R_{pulin} is shown. The value of R_{pulin}, like the value of E_a, represents right ventricular afterload, but in this case, it is identified. The solid line represents the mean normalized R_{pulin} value for the Endo group and the dashed line the mean normalized value in the EndoHF group. The analysis of the EndoHF group was not part of this research and has been published previously in (Desaive *et al.*, 2008; Starfinger *et al.*, 2008b). Comparing the upper and lower panels the trends are (qualitatively) similar.

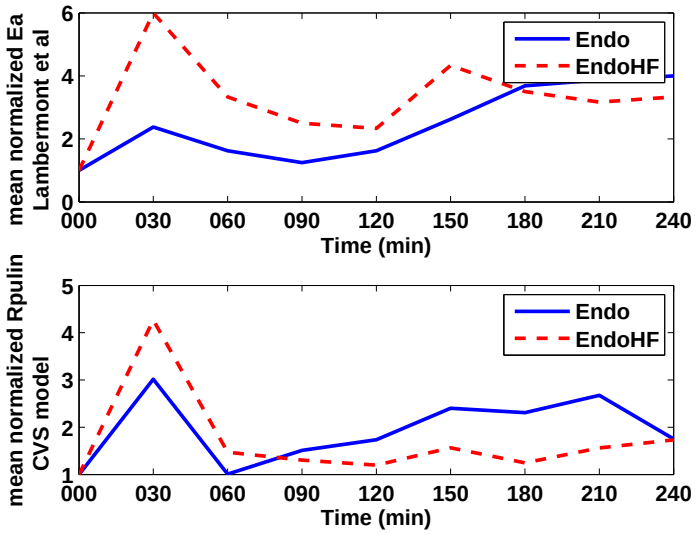

Figure 9.22: Upper panel: Mean normalized pulmonary arterial elastance E_a over all analyzed pigs during the septic shock experiment with (EndoHF) and without (Endo) hemofiltration as obtained by (Lambermont *et al.*, 2006). Lower panel: Mean normalized pulmonary vascular resistance R_{pulin} over all analyzed pigs during the septic shock experiment with (EndoHF) and without (Endo) hemofiltration as obtained with CVS model and identification process.

Figure 9.23 shows in the upper panel the RV- vascular coupling as clinically obtained by the ratio of E_{esrvf} to E_a, and how the RV-coupling evolves over time as previously reported by (Lambermont *et al.*, 2003, 2006). The solid line represents the obtained mean normalized RV-coupling value in the endotoxic group (Endo), whereas the dashed line represents the mean normalized RV-coupling value in the hemofiltration group (EndoHF), respectively. The lower panel shows the same results obtained from the CVS model and identification process. However, in this model-based case, the ratio of E_{esrvf} to R_{pulin} is shown, as it uses values identified with this limited data set.

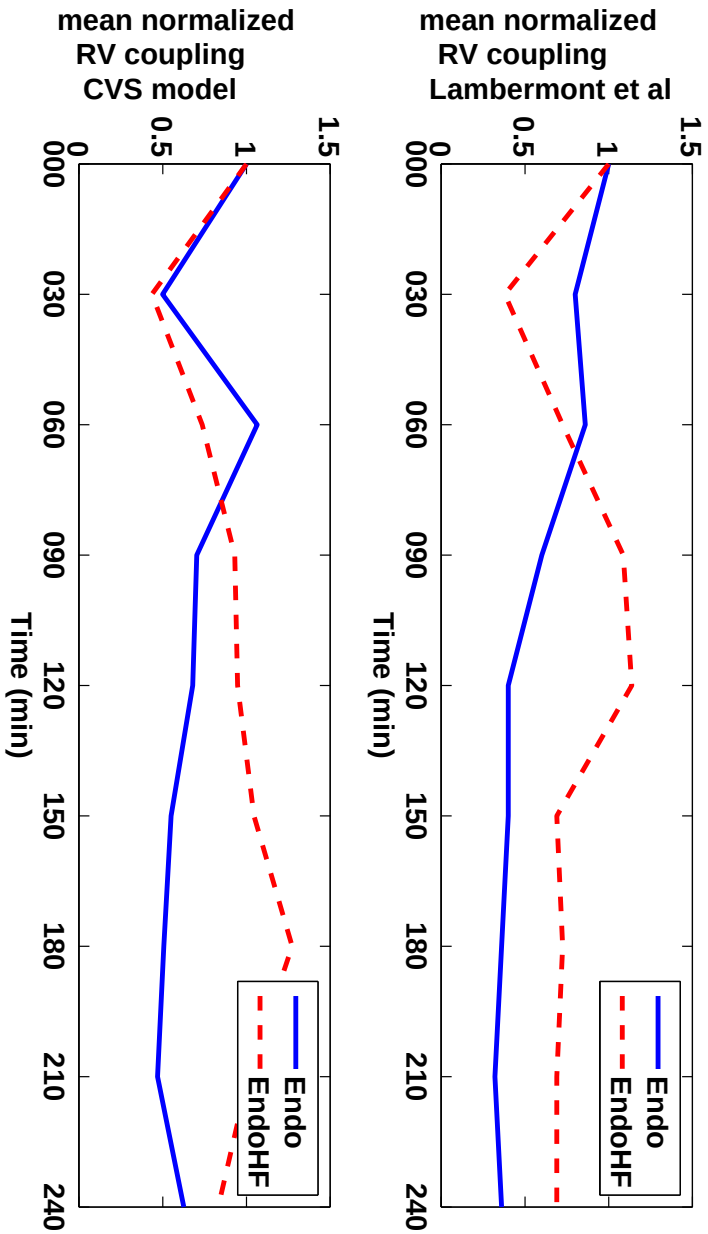

Figure 9.23: Mean normalized RV-coupling over all analyzed pigs during the septic shock experiment with (EndoHF) and without (Endo) hemofiltration. Upper panel: results as obtained by (Lambermont *et al.*, 2006), lower panel: results obtained with CVS model and identification process.

9.3.4 Discussion

One of the major goals of this research is to show the applicability of the CVS model and identification process for a severely reduced data set. In this research, only the right heart signals (V_{rv}, P_{pa}) and the arterial pressure (P_{ao}) are available for identifying the induced endotoxic shock. Despite this restricted data set and the additional assumptions made regarding the other model volumes and pressures, the CVS model parameters are consistently identified. This accurate level of identification is validated by re-simulation and comparison to clinical data including measured data not used in the identification process. Importantly, it holds true not only for the right part of the model, but for the entire parameter set.

When re-simulating the model with the identified parameters, the output signals produced match the observed clinical data very well, as shown in Figures 9.16, 9.17 and 9.18. Median absolute percentage errors are less than 5% for the volumes and less than 7% for the pressures, as shown in Table 9.3. These errors are well within typical clinical measurement errors (Baan *et al.*, 1984; Burkhoff *et al.*, 1985).

A second important finding of this research is that, despite the reduced data set and necessary assumptions made, the CVS model is able to accurately identify and re-simulate endotoxic shock. Clinically, and importantly, the identified parameter trends match physiological expectations. For example, Figure 9.20 shows the model simulated normalized systemic volume and how it decreases during the time course of the experiment, accounting for the loss of circulatory control and hypovolemia seen in septic shock (Bridges & Dukes, 2005; Dellinger, 2003). The data and results obtained from the pig-specific identified models thus match clinical measurements and expectations.

Figure 9.20 also shows the mean normalized identified trends for the CVS model parameters R_{sys}, R_{pulin} and R_{vr} over all analyzed pigs during the experiment. The value of R_{sys} is perhaps (unexpectedly) identified to initially increase at the beginning of the experiment. However, after 30mins and with the ongoing endotoxin infusion, R_{sys} is decreasing, with a further two relatively small increases at the end of the experiment. Overall, this trend indicates an initial physiological compensation followed by a failure of circulatory control that is typical of septic shock (Dellinger, 2003). From a model-based diagnostics perspective, this result accurately tracks disease onset, initial (successful) compensation and (eventual)

physiologic failure, all of which are clinically significant in determining appropriate therapies and dosing.

The mean normalized R_{pulin} values over all pigs increase during the experiment, as expected (Bridges & Dukes, 2005; Dellinger, 2003). There is a sharp drop at 60 mins into the experiment. However, this decrease is consistent with previously published results (Lambermont *et al.*, 2003), where a similar drop can be observed at 60 mins. Clinically, the model is thus capturing the known effects of sepsis in this portion of the circulation, as well. It is important to note that differences in systemic (R_{sys}) and pulmonary (R_{pulin}) behaviours and resistances can help dictate the clinical therapeutic balance between vasopressor and fluid resuscitation therapy if they are known. Hence, this model and identification method can provide this level of clinical advice and guidance.

The mean normalized resistance to venous return, R_{vr}, decreases consistently during the experiment. This result is expected, as the venous return is already impeded by a low blood volume caused by fluid losses into the tissue, as well as by the effects of veno- and vasodilation. In septic shock, proinflammatory cytokines cause an increase in endothelial-derived nitric oxide, which in turn is a major mediator for vasodilation and hypotension (Bridges & Dukes, 2005). Therefore, the body tries to restore venous return and the model identifies this behaviour as a lowered resistance to venous return that is needed to compensate for the lower venous volume, pressure and flow back to the heart. Again, this capability to very specifically capture the circulatory dysfunction due to sepsis has clinical significance and importance in balancing therapy selection and dosing.

A third finding of this research is the identification and analysis of right ventricular (RV)-vascular coupling in the endotoxic (Endo) group compared to the hemofiltration (EndoHF) group. Previously, these results were reported in (Lambermont *et al.*, 2006) and the results shown in this research confirm these results as similar coupling values and trends are obtained for the Endo and EndoHF groups, as shown in Figure 9.23. More specifically, in the upper panel the previously reported coupling values are shown as normalized mean values over all pigs and the lower panel shows the coupling as obtained using the CVS model and methods presented in this research. The data shows that in the early phases of endotoxic shock, RV-vascular coupling is preserved by an increase in RV contractility (E_{esrvf}), as seen in Figure 9.21. However, during the later stages and with

CVVH, RV-vascular coupling is preserved where a decrease in pulmonary vascular resistance (R_{pulin}), as seen in Figure 9.22, is suggested to be the main reason for this effect (Lambermont *et al.*, 2006). These results allow for a better understanding of the mechanisms of RV dysfunction during septic shock. Clinically, the crossover point in Figure 9.23 between Endo and EndoHF groups clearly delineates the time and efficiency of HF therapy selection, which is unique in model-based monitoring.

Overall, using a significantly reduced data set for identification is shown to have a very good potential for these methods to be used clinically. Such reduced sets of measurements are commonly seen clinically and obviate the need for special or costly sensors or equipment beyond what is currently used. Hence, the last result is one of validating the overall concept's potential practicality for clinical implementation.

Table 9.3 summarizes the results for all six pigs and a total of 50 identification periods. These results show that the extended CVS model is able to capture the essential dynamics of the porcine CVS response to endotoxic shock over a selection of subjects.

9.3.5 Conclusions

The integral-based optimization successively identified pig-specific parameters for the extended CVS model. This further validation shows the ability of the model to adequately and realistically capture the impact of pressure-volume changes during endotoxic shock and to do so in the presence of a significantly reduced data set for identification. Comparable results to previously reported studies are obtained when analyzing the clinically important RV-vascular coupling, further validating the methods and approach presented here. In particular, the model is able to aggregate diverse measured data into a clear, clinically and physiologically relevant diagnostic picture as the condition develops. This research thus increases confidence in the clinical applicability and validity of this overall diagnostic monitoring approach preparatory to initial studies with human subjects.

Chapter 10

Adrenaline Simulation Study

This chapter[1] describes the results obtained for simulating the effects of Adrenaline in the CVS model. These results are compared to data from literature and the predictive capability of the CVS model and methods developed are tested and the model and methods are thereby further validated.

10.1 Introduction

Drugs for supporting the cardiovascular system are selected to either improve heart rate (chronotropic effects), myocardial contractility (inotropic effects), arterial blood pressure (vasoconstrictive effects), a reduction in afterload (vasodilator effects), or a multiple combination of these effects. Many of these drugs also increase electrical conduction (dromotropy) within the heart and augment relaxation (lusitropy). However, most of these drugs are non selective and may also increase or decrease heart rate and afterload. These added changes carry the potential risk of causing cardiac arrhythmias and increasing myocardial ischemia by creating a mismatch between myocardial oxygen demand and supply (American Heart Association, 2005). Additionally, some agents have also metabolic effects that increase blood glucose, lactate and metabolic rate, and these effects should also be taken into account when prescribing such drugs.

10.1.1 Drugs in Heart Failure and Cardiogenic Shock

The main problem in heart failure and hypotension (as caused by an acute heart failure) is a loss of cardiac contractile function with a subsequently reduced or-

[1] This chapter is based on (Starfinger *et al.*, 2008a).

gan perfusion and hypotension. Drugs used in this case aim to improve cardiac output, as it will lead to improved organ perfusion and normalization of arterial blood pressure. Cardiac function and output can be improved by reducing afterload and/or increasing preload by increasing fluid volume (for example in hypovolemic and circulatory shock), and enhancing contractility of the heart.

10.1.2 Drugs in Circulatory Shock

This form of hypotensive shock is usually caused by an inadequate blood volume as might be caused by hemorrhage. It can also be due to a loss of vascular tone caused by infection and inflammation, as in septic shock for example. The main goal in this case is to improve arterial blood pressure and vasoconstrictor drugs are thus typically administered, often in the combination with fluid administration.

10.1.3 Drug Dosing and Infusion Rates

Specific drug infusion rates are typically not recommended in critically ill patients, mostly due to inter-patient variations in pharmacokinetics (drug dose - concentration relation) and pharmacodynamics (drug concentration - effect relation) (Kellum & Pinsky, 2002; Zaritsky, 1994). Such drugs are thus dosed based on an initial dose within a known therapeutic range. This dose is then varied (titrated) at the bedside to achieve the desired effect, while limiting side effects.

There are a number of broad guidelines available for the appropriate use of these drug therapies in critical care. However, sometimes it is not possible to implement these algorithms because of patient-specific conditions, resident learning curves and individual physician medication preferences (Bobek *et al.*, 2001). Hence, dosing regimes depend mainly on the intuition and experience of the clinical staff and it cannot necessarily be guaranteed that the optimal dose for each individual patient is chosen or maintained as patient condition evolves.

Therefore, a clinically validated computerized cardiovascular system (CVS) model that provides accurate and patient-specific simulations of the cardiovascular and circulatory system in response to various doses would be desirable. Such a model can then be identified for each specific patient, creating a unique representation of the patient's condition within the model, as represented by patient-specific parameters. A patient-specific model could be used to forward simulate the likely response towards a change in dose. Noting response to initial

doses, a drug sensitivity could be determined to optimize further dosing. Overall, model-based estimation of drug effect and its patient sensitivity to enable dose optimization would create unique clinical opportunity and advantages.

10.1.4 Adrenaline (Epinephrine)

Adrenaline (European Pharmacopoeia and BAN) or Epinephrine (INN) functions as a hormone in the bloodstream and as a neurotransmitter when released across a neuronal synapse. Adrenaline is released by the adrenal medulla upon activation of preganglionic sympathetic nerves innervating this tissue. This activation occurs during times of stress, such as during exercise, heart failure, hemorrhage, excitement or pain. Circulating adrenaline causes (Klabunde, 2004):

- Increased heart rate and inotropy (β_1-adrenoceptor mediated)
- Vasoconstriction in most systemic arteries and veins (postjunctional α_1- and α_2-adrenoceptors mediated)
- Vasodilation in muscle and liver vasculatures at low concentrations (β_2-adrenoceptor mediated)
- Vasoconstriction at high concentrations (α_1-adrenoceptor mediated)

10.1.4.1 Adrenaline Usage in Critically Ill Patients

An observational study, which enrolled 84 patients in an ICU between February and March 2005, showed that between 35% and 45% of patients were treated with inotropes (Biswal *et al.*, 2006). Adrenaline is used in patients who are in cardiac arrest or who require inotropic or vasopressor support. Adrenaline may additionally be used in cases of anaphylaxis associated with hemodynamic instability or respiratory distress (American Heart Association, 2005; Ellis & Day, 2003). Furthermore, it improves myocardial and cerebral hemodynamics during cardiopulmonary resuscitation (CPR).

10.1.5 Goals for this Research

The goals for this research are twofold. The first aim is to validate the CVS model for the first time in drug therapy scenarios and by doing so to provide a basis for future clinical trials. Ultimately, the goal is to use the CVS model and methods developed to predict the patient's response towards different drugs and doses over time to individualize and customize this aspect of patient care.

Pharmaceuticals represent 4% to 7% of the yearly operating expense of most hospitals (Pierpaoli, 1993) and in ICUs this value ranges from 32.6% to 41.5% of a hospital's total drug costs (Weber *et al.*, 2003). Hence, there is a growing financial demand for optimizing the amount of drugs prescribed and avoiding unnecessary prescriptions. Use of this CVS model, or similar, could help reduce these costs by allowing the appropriate patient-specific dose to be found more efficiently.

It should be pointed out that this CVS model so far has only been clinically validated using data from porcine experiments (Desaive *et al.*, 2007; Starfinger *et al.*, 2007b, 2008b,d,e) within a very controlled environment. In these cases, desired effects are induced purposefully and usually not treated. However, data obtained from clinical trials on critically ill patients, adds the challenge of a multivariate environment, where a variety of therapeutic treatments are performed and drugs are administered combined with different ventilatory support options and fluid administrations. Therefore, it is important to know the effect each individual treatment option is likely to have and how the parameters in the CVS model may need to be adjusted to correctly represent these changes.

This study uses human clinical data from 3 adrenaline dose response studies found in literature (Heringlake *et al.*, 2007; Levy *et al.*, 1997; White & Leenen, 1997). These studies present hemodynamic data, such as arterial pressures and the cardiac index, at the level of detail needed for the model identification process. Thus, this research is a first validation of the CVS model and methods in a more realistic clinical environment.

The goal is to be able to identify the underlying patient-specific parameters that allow the representation of the patient's hemodynamic status and adrenaline dose response within this CVS model. More specifically, the CVS model is identified for each data set and therefore represents the unique hemodynamic condition, expressed in the different parameter values and trends over time. These patient-specific parameter values and trends are then used to predict the patient's

response towards a change in dose of adrenaline and over time. These predictions are then compared to the clinical data given in the studies (Heringlake *et al.*, 2007; Levy *et al.*, 1997; White & Leenen, 1997). Results are presented in the form of absolute percentage errors between predicted and clinically observed data.

10.2 Methods

10.2.1 CVS Model

The CVS model is a lumped parameter model which was previously developed by (Smith, 2004) and is based on earlier work of (Chung *et al.*, 1997; Olansen *et al.*, 2000). The new and extended model is presented in Section 3.2.

10.2.2 Integral-Based Parameter Identification

The parameter identification method used in this research has previously been shown to rapidly and accurately identify almost the entire parameter set in the presence of significant measurement noise (Hann *et al.*, 2006; Starfinger *et al.*, 2007b). As the identification process has been extensively described (Desaive *et al.*, 2007; Starfinger *et al.*, 2008d,e), and in Chapter 5 and Section 8.2.2.2, only a brief summary of the individual steps is provided here.

10.2.3 Summary of the Identification Process

Figure 5.6 gives an overview of the identification process based on previous work (Hann *et al.*, 2006; Starfinger *et al.*, 2007b, 2008d,e). The following steps are performed:

1. Obtain clinical measurements and signals
2. Use volume calculations to estimate the initial volume conditions for the CVS model (Starfinger *et al.*, 2008d)
3. Use initial set of parameters to obtain first simulation output (Starfinger *et al.*, 2007b, 2008d,e)
4. Scale simulation output signals (P_{pa}, P_{ao}, V_{lv}, V_{rv}) to match the clinical data (Starfinger *et al.*, 2007b, 2008d,e)

5. Identify the patient-specific parameters for the scaled signals using the integral-based methods based on (Hann *et al.*, 2006)

6. Re-scale the simulation output signals to better match the clinical data

7. Repeat steps 4 to 6

8. Stop the iterative process when a set error tolerance is reached

10.2.4 Experimental Protocols

Three clinical studies reported in the literature were used in this research (Heringlake *et al.*, 2007; Levy *et al.*, 1997; White & Leenen, 1997). Results from each are employed here to identify and validate the CVS model. As cited, the clinical data is thus not the work of the authors and only published results are used here.

10.2.4.1 Study 1: *Effects of Age on Cardiovascular Responses to Adrenaline in Man*

In this study (White & Leenen, 1997), Adrenaline was administered to 14 young normotensive subjects (age 21-40 years, mean 30± 2 years; 8 male, 6 female) and 18 older normotensive subjects (age 50-73 years, mean 60± 2 years; 6 male, 12 female). All subjects had weight within 20% of the ideal body weight. They all had normal history, physical examination and biochemistry. The subjects were instructed to refrain from caffeine and alcohol 24 hours prior to each study morning and they did not take any other medication for the duration of the study. The study was approved by the Human Ethics Committee of the University of Ottawa and written informed consent was obtained.

Arterial blood pressure (ABP) was measured using a blood pressure cuff applied to the arm that was not used for the infusion. Blood pressure was recorded using a Roche Arteriosonde (Roche Medical Electronics Inc., Cranbury, NJ, USA). ECG electrodes were applied to measure heart rate (HR) by a Tektronic 414 monitor (Tektronic Inc., Beaverton, OR, USA). On the study morning, following a rest period of at least 60 minutes, adrenaline was started at 20 ng/kg/min and increased to 40, 80, 120 and 160 ng/kg/min or until the heart rate had increased by 20-25 beats/min or the diastolic blood pressure decreased by 15 mmHg. Each dose was infused for 8 mins. Heart rate and blood pressure

were measured every 2 mins for 10 minute periods prior to the start of an infusion and twice during the last 2-3 mins at each rate of infusion. Mean values and standard deviation were used for statistical analysis.

Table 10.1 summarizes the data obtained from this study for the different adrenaline doses and populations (young/older and male/female). The following measurements are used for the parameter identification process:

- heart rate (HR)
- systolic and diastolic arterial pressures (SAP, DAP)
- left ventricular end-systolic and end-diastolic volume indexes (LVESVI, LVEDVI)
- left ventricular stroke volume (LVSV, as calculated from LVEDVI and LVESVI)

Overall, this study provides 24 unique data sets that may be used.

Study 1: Adrenaline doses, populations and hemodynamic measurements						
Adrenaline dose ($ng/kg/min$)	number of participants	SAP ($mmHg$)	DAP ($mmHg$)	MAP ($mmHg$)	LVEDVI (ml/m^2)	LVESVI (ml/m^2)
Young (Y)						
Baseline	14	111	75	87	81	21
20	14	112	69	83.3	82	18
40	14	114	66	82	83	15
80	14	124	62	82.6	84	12
120	13	132	61	84.6	85	11
160	13	139	61	87	88	11
Older (O)						
Baseline	18	115	76	89	65	14
20	18	115	72	86.3	64	12
40	18	119	69	85.6	65	8
80	18	126	67	86.6	67	8
120	16	132	68	89.3	69	8
160	10	136	68	90.6	67	6
Young Male (YM)						
Baseline	8	114	79	90.6	86	23
40	8	117	68	84.3	86	18
Max (150)	8	143	62	89	90	12
Young Female (YF)						
Baseline	6	107	69	81.6	75	18
40	6	110	62	78	80	13
Max (160)	6	132	58	82.6	82	10
Older Male (OM)						
Baseline	6	117	74	88.3	64	16
40	6	121	67	85	66	11
Max (133)	6	140	65	90	68	8
Older Female (OF)						
Baseline	12	114	77	89.3	66	13
40	12	117	70	85.6	66	10
Max (140)	12	132	69	90	68	8

Table 10.1: Adrenaline doses, hemodynamic measurements and participants separated into *Young* and *Older* and *Young Male*, *Young Female* and *Older Male* and *Older Female*, respectively.

10.2.4.2 Study 2: *The Metabolic and Renal Effects of Adrenaline and Milrinone in Patients with Myocardial Dysfunction After Coronary Artery Bypass Grafting*

In this study (Heringlake *et al.*, 2007), during a 18-month period, 251 patients were screened for low cardiac output (CO) upon ICU admission after coronary artery bypass grafting (CABG) surgery. Approval of the local Ethics Committee and preoperative written consent was obtained. Patients having a cardiac index (CI) of less than 2.2 $l/min/m^2$ upon ICU admission (despite adequate arterial and filling pressures) were randomly assigned to 14-hour treatment with adrenaline (n=7) or milrinone (n=11) to achieve a CI of greater then 3 $l/min/m^2$.

Drugs were given by continuous infusion without a bolus. Treatment in the ICU and the care provided to the patients was at the discretion of the clinical staff in charge. With the exception of the hemodynamic goals given above and the prohibition of using diuretics or hydroxyethylstarch preparations during the treatment duration, no specific therapeutic instructions were given.

All patients had a radial arterial line, a central venous catheter and a pulmonary artery catheter for continuous measurement of mixed venous oxygen saturation (SvO_2) and CI (Vigilance, Edwards Lifesciences LLC, Irvine, CA, USA). Hemodynamics were recorded every two hours for a 14 hour treatment period after ICU admission. The hemodynamic variables recorded include: mean arterial pressure (MAP), central venous pressure (CVP), mean pulmonary artery pressure (MPAP), HR and CI. The following measurements are used for the parameter identification process:

- heart rate (HR)
- mean arterial and mean pulmonary artery pressures (MAP, MPAP)
- cardiac index (CI)
- central venous pressure (CVP)

Overall, this data from (Heringlake *et al.*, 2007) provided 8 data sets for use.

Study 2: Course of time and hemodynamic measurements								
Hour into study	t0	t2	t4	t6	t8	t10	t12	t14
MAP ($mmHg$)	79	70	73	76	80	80	82	82
MPAP ($mmHg$)	24	26	24	24	23	23	23	20
CI ($l/min/m^2$)	1.9	3.3	3.2	3.3	3.2	3.1	3.3	3.5
CVP ($mmHg$)	14	14	13	13	12	12	12	10
HR (min^{-1})	97	97	97	95	95	96	96	99

Table 10.2: Time course and hemodynamic measurements for study 2.

10.2.4.3 Study 3: *Comparison of Norepinephrine and Dobutamine to Epinephrine for Hemodynamics, Lactate Metabolism, and Gastric Tonometric Variables in Septic Shock: a Prospective, Randomized Study*

This study (Levy *et al.*, 1997) included 30 patients with hyperdynamic septic shock and was approved by the local Ethics Committee and written informed consent was obtained from the patient's closes relative. To be included in the study after volume resuscitation and treatment with dopamine up to a dose of 20μg/kg/min, the patients had to have the following baseline condition:

- MAP $\leq 60mmHg$
- signs of altered perfusion (oliguria, $< 30ml/hr$) or increased lactate level ($> 2.5mmol/l$)
- CI $> 3.5l/min/m^2$

Heart rate was monitored continuously and the routine clinical monitoring included a thermodilution pulmonary artery catheter, with continuous monitoring of mixed venous oxygen saturation (SvO_2) and a radial and femoral artery catheters. Measurements of MAP, CVP, MPAP were taken and CO was measured by the thermodilution method. Each patient received either epinephrine or norepinephrine + dobutamine. Epinephrine infusions were started at 0.3 μg/kg/min. The infusion rate was titrated on MAP at 5-min intervals to obtain a MAP $>$ 80mmHg, with a stable or increased CI.

Table 10.3 summarizes the adrenaline titration given. The following measurements are used for the parameter identification process:

- heart rate (HR)
- mean arterial and mean pulmonary artery pressures (MAP, MPAP)
- cardiac index (CI)
- central venous pressure (CVP)

Overall, 5 data sets were available for use in this study.

Study 3: Adrenaline titration, course of time and hemodynamic measurements					
	Baseline	h1	h6	h12	h24
Drug titration ($\mu g/kg/min$)	0	0.45 ± 0.09	0.52 ± 0.07	0.48 ± 0.08	0.36 ± 0.08
MAP ($mmHg$)	60	89	93	96	89
HR ($/min$)	121	114	109	115	108
MPAP ($mmHg$)	25	31	29	28	26
CI ($l/min/m^2$)	4	5.1	4.5	4.1	4.1

Table 10.3: Time course and drug titration for study 3.

10.2.5 Estimations and Prediction Process

Depending on the data available for each study, different assumptions about the rest of the data had to be made. These assumptions and estimations are briefly summarized below.

Generally, the prediction process uses some measure of past information on how the patient responded towards a change in adrenaline dose to predict how the patient is likely to respond towards a future change in dose. Depending on the data available, the prediction process is adjusted for each of the 3 studies as described below.

10.2.5.1 Adrenaline-Specific Parameters

As discussed before, the effects of adrenaline can be summarized as an increase in HR and contractility, vasoconstriction in most systemic arteries and veins and an increase in the central blood volume. These effects in turn lead to an increase in SV and systemic arterial pressure (SAP). Diastolic arterial pressure (DAP) is decreasing, and thus a relatively constant mean arterial pressure (MAP) results, but with a largely increased pulse pressure (PP). Consequently, from these physiologically expected effects the model parameters that should be most influenced by adrenaline, are:

- left and right ventricular end-systolic elastances (E_{eslvf}, E_{esrvf}); also representing the contractility
- arterial and pulmonary elastances E_{ao} and E_{pa}; as affected by the change in pulse pressure
- systemic arterial resistance R_{sys}; as affected by vasoconstriction
- systemic elastance E_{sys} (1/compliance); as affected by the increase in V_{sys}

As the most pronounced changes are expected in E_{eslvf}, E_{esrvf}, E_{ao} and E_{pa}, these parameters are termed the adrenaline-specific parameters. Changes in these parameters are therefore used for predicting the future response towards a change in dose of adrenaline or over time. However, for studies 2 and 3 (Heringlake *et al.*, 2007; Levy *et al.*, 1997), changes in R_{sys} and E_{sys} were also included in the prediction rules. This difference can be explained by the overall much longer time periods for these 2 studies, where the hemodynamic status of the patients is more likely to have changed caused by, for example, vasoconstriction and/or a change in blood volume.

10.2.5.2 Study 1

This study provided the best data for the identification process, with very detailed data reported over a variety of subjects and conditions. As this study was a planned interventional clinical trial study, it took place in a very controlled environment and adrenaline was administered into each participant following a strict protocol. It is thus safe to assume it was administered in exactly the same way, with the same dose, and over the same time, for each participant. Hence,

this research mostly concentrates on this study for validating the CVS model for both simulating the different effects of adrenaline and testing its predictive ability for changes in dose.

All 16 individual data sets obtained from the study (6 data sets, one per dose, for the Y and O groups plus one additional set for the YM, YF and OM, OF groups at baseline, also see Table 10.1) were identified using the methods described in (Starfinger *et al.*, 2007b, 2008d,e). The changes in the adrenaline-specific parameters (E_{eslvf}, E_{esrvf}, E_{ao} and E_{pa}) in the Y group were observed and a linear fit was obtained for the 5 dose changes from baseline to 160 ng/kg/min. This trend is used for prediction.

Note, that the groups YM, YF and OM, OF are subgroups of the two general groups Y (Young) and O (Older). However, there are still 24 individual data sets with different hemodynamic values, as shown in Table 10.1. The identification was performed for all 6 data sets in the Y and O groups and 4 additional data sets in the remaining 4 subgroups - resulting in a total of 16 identifications.

Predictions are performed for the O group and the YM, YF, OM and OF data sets. The first prediction uses the baseline parameters for each of these groups (O, OM, OF, YM, YF), as it is necessary to have a baseline solution vector for the model parameters to begin with. The adrenaline-specific parameters (E_{eslvf}, E_{esrvf}, E_{ao} and E_{pa}) are then re-calculated based on the linear prediction rule, obtained from the linear fit in the Y group. Having re-calculated these parameters, the forward simulation is run and the predicted output signals for SAP, DAP, MAP, LVEDVI, LVESVI and SV are compared to the clinical data from (White & Leenen, 1997). Median absolute percentage errors and the inter-quartile range (IQR) are calculated. It has to be mentioned, that the data sets (from the Y group) used for obtaining the prediction rules are completely different to the data sets used for prediction, as can also be seen in Table 10.1.

A second prediction is performed, which in comparison to prediction 1, uses the previous parameter vector identified from the previous dose, rather than those from the baseline parameter vector. The adrenaline-specific parameters (E_{eslvf}, E_{esrvf}, E_{ao} and E_{pa}) are re-calculated based on the linear prediction rule as before. Similarly, the forward simulation is run again and the predicted output signals for SAP, DAP, MAP, LVEDVI, LVESVI and SV are compared to the clinical data. Median absolute percentage errors and the inter-quartile range (IQR) are calculated.

In this study, the pulmonary artery pressure is not given and has to be estimated. The pulmonary artery pressure is estimated as a constant pressure over all dosages and participant groups with a systolic value of 25 mmHg and a diastolic value of 12 mmHg. Note, that this estimation is physiologically incorrect, as the pulmonary artery pressure is expected to change with different doses of adrenaline. However, this error can be much better managed if it is similar for all identified segments. Naturally, information about the pulmonary circulation is lost and the value of E_{pa} will also not necessarily represent a true value in this case.

10.2.5.3 Studies 2 and 3

These 2 studies are used as further validations. In particular, the potential to correctly identify patient-specific parameters in the absence of diastolic and systolic pressure measurements, given only the mean arterial pressures MAP and MPAP, is studied. In addition, these 2 studies do not provide end-systolic or end-diastolic volumes, relying instead on the cardiac index.

Thus, these 2 studies measure a very minimal amount of data. Hence, several assumptions have to be made:

- SV is calculated based on HR and CI with an assumed $BSA = 2m^2$ in all cases
- ESV is assumed as $SV + 10ml$
- EDV is calculated as $ESV + SV$
- left and right ventricular volumes are assumed to be the same
- systolic and diastolic pressures are estimated based on Figure 10.1 as obtained from (Klabunde, 2004)

In these 2 studies, there is only a limited amount of data available. In comparison to study 1, this data is very inhomogeneous and was not obtained in a controlled study. Instead, it was taken observationally over time periods of 14 and 24 hours, respectively. Therefore, these data sets were not intended to truly predict the patient's response towards a change in dose in adrenaline, or over the course of time.

The goal in these data sets is to show the accuracy of the identification process by testing if an overall rule can be found that shows a consistent way of identifying the main adrenaline-specific parameters. If such a simple, linear rule can be found, using all or most of the data points available, then this rule would show that the parameters evolved in a consistent manner. This rule could then be used to predict the patient's response for a specific point in time. If successful, it would help validate the approach of using drug-specific rules and parameter changes to enhance identification and prediction.

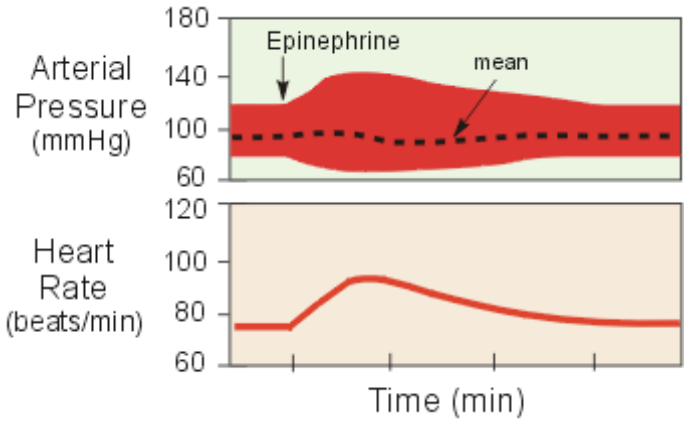

Figure 10.1: Change in diastolic and systolic blood pressure in comparison to a relatively constant mean arterial pressure with administration of epinephrine (adrenaline) over time, as obtained from (Klabunde, 2004).

For study 2, prediction rules are obtained from the absolute percentage changes in the parameters from one point in time to the next, except for the change from baseline to t2. This percentage difference is not included because this change is expected to be much higher, as the effect of adrenaline is expected to be more pronounced compared to the other time points were the adrenaline dose is kept at a more constant level. A total of 6 predictions are performed for study 2 from t4 to t14, using the previous solution as baseline solution in each case. For example, for predicting the response at t4, the parameters from t2 are used plus the re-calculated adrenaline-specific parameters using the overall population rule, as described before. In contrast to study 1, where the adrenaline-specific parameters are E_{eslvf}, E_{esrvf}, E_{ao} and E_{pa}, for this data set it was necessary to also re-calculate the systemic and pulmonary arterial resistances R_{sys} and R_{pul} and the systemic elastance E_{sys}. These 3 additional parameters changed significantly during the time course of the study and were thus included in the overall population rule.

Similarly to study 2, the prediction rules for study 3 are obtained from the absolute percentage changes in the parameters from one point in time to the next. However, here only the change from h1 to h6 is used. The baseline change was excluded for the same reason as in study 2. For similar reasons the change to h24 was excluded, as this change covers a long time period (12 hours). In addition, while the doses for h1, h6 and h12 are similar, there is a much lower dose at h24. Hence, only 1 prediction is performed for study 3 and this is the prediction for h12, using the data obtained from h1 and h6.

This prediction from study 3 serves as another validation of the CVS model and identification process. The goal is to show that all parameters are identified in such a consistent way that h1-h6 adrenaline-parameter specific rules can be found to predict h12. The adrenaline-specific parameters E_{eslvf}, E_{esrvf}, E_{ao} and E_{pa} used with study 1 are augmented for study 3 to include R_{sys}, which changed considerably during the long time course of this study. Figure 10.2 shows the prediction rules obtained for studies 2 (solid line) and 3 (dashed line) for E_{eslvf} and E_{esrvf} over a time period of 1 to 24 hours, where the similarity over disparate studies indicates a consistent underlying behaviour.

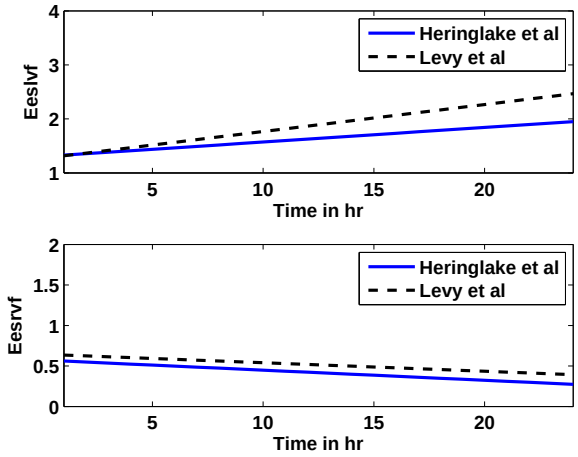

Figure 10.2: Linear prediction rules for E_{eslvf} (upper panel) and E_{esrvf} (lower panel) for studies 2 (solid line, (Heringlake *et al.*, 2007)) and 3 (dashed line, (Levy *et al.*, 1997)).

10.3 Results

10.3.1 Study 1

10.3.1.1 Identification Results

Figure 10.3 shows in the upper panel (solid line) the mean systolic arterial pressure (SAP) over all 16 segments as given in (White & Leenen, 1997). These 16 segments are the 6 measurements for the young and older groups at baseline, 20, 40, 80, 120 and 160 ng/kg/min adrenaline (segments 1-6 young, 7-12 older), plus 4 measurements, which are obtained by separating the young and older groups for male and female, respectively. The circles are the simulated CVS model outputs obtained when the CVS model is re-run with the identified patient-specific parameters.

The middle panel shows as a solid line the mean arterial pressure (MAP) as available in (White & Leenen, 1997) for all 16 segments. The circles depict the CVS model output data when re-run using patient-specific parameters. The lower panel shows the same results for the diastolic arterial pressure (DAP).

Figure 10.4 shows in the upper panel the left ventricular end-diastolic index (LVEDVI) as given in (White & Leenen, 1997), whereas the lower panel shows the left ventricular end-systolic index (LVESVI). A total of 16 identifications were

performed, with 6 identifications each in the young and older group plus another four identifications separated for male and female, as described previously. The circles represent the CVS model output signals.

Table 10.4 gives an overview of how well the CVS model output data matches the data given in (White & Leenen, 1997). The absolute median percentage error is given as well as the inter-quartile range (IQR). These two values are calculated over all 16 identified segments.

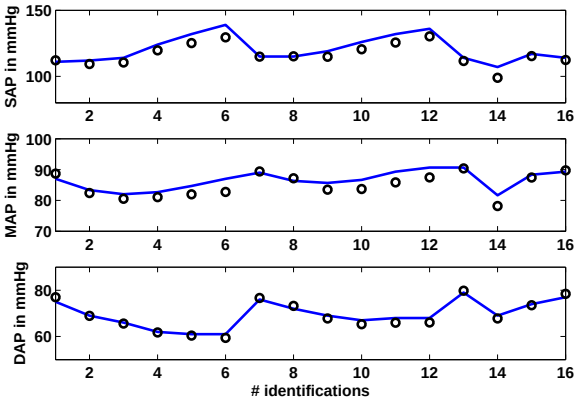

Figure 10.3: Study 1: Clinical mean systolic (SAP), diastolic (DAP) and mean (MAP) arterial pressure as obtained from (White & Leenen, 1997) vs simulated pressures. Solid lines represent the clinical data and circles represent the CVS model simulation output using identified patient-specific parameters.

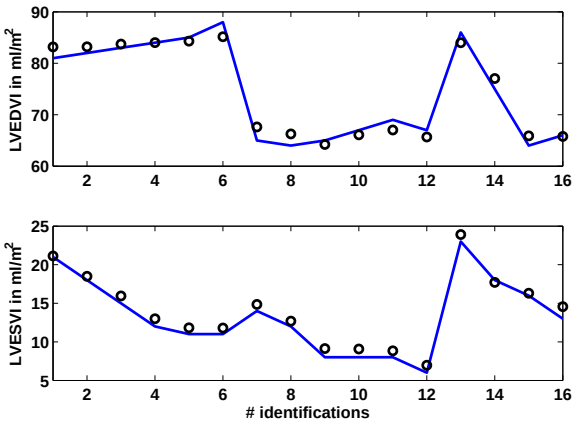

Figure 10.4: Study 1: Clinical mean left ventricular end-diastolic (LVEDVI) and end-systolic (LVESVI) volume index as obtained from (White & Leenen, 1997) vs simulated volume indexes. Solid lines represent the clinical data and circles represent the CVS model simulation output using identified patient-specific parameters.

Absolute percentage error for measured and simulated pressures and volumes						
	SAP (%)	DAP (%)	MAP (%)	LVEDVI (%)	LVESVI (%)	SV (%)
median	3.27	1.70	1.94	2.15	6.79	3.37
IQR	3.06	1.77	2.44	1.76	7.22	1.05

Table 10.4: Study 1, identification: Median error and IQR in % for measured and simulated pressures and volumes over all 16 identified segments. SAP = systolic arterial pressure, DAP = diastolic arterial pressure, MAP = mean arterial pressure, LVEDVI = left ventricular end-diastolic volume index, LVESVI = left ventricular end-systolic volume index.

10.3.1.2 Prediction Results

Table 10.5 gives the median absolute percentage errors and IQR for prediction 1 in study 1. This prediction uses a population-specific rule obtained only from the young population to describe the changes in the main adrenaline-specific model parameters caused by an increase in the adrenaline dose from baseline and 20 ng/min/kg to 160 ng/min/kg. Note that the baseline solution vector was used

as initial solution for each time step and only the adrenaline-specific parameters were updated according to the population-specific rule.

Table 10.6 gives the median absolute percentage errors and IQR for prediction 2 in study 1. This second prediction uses the same population-specific rules as were used in prediction 1. However, in contrast to prediction 1, the previous solution is used as initial solution, rather than the baseline solution. Thus, for example, for predicting and calculating the parameters for a dose of 120 ng/min/kg, the identified parameters for a dose of 80 ng/min/kg are used.

Absolute percentage error for measured and predicted pressures and volumes						
	SAP (%)	DAP (%)	MAP (%)	LVEDVI (%)	LVESVI (%)	SV (%)
median	11.03	11.47	10.21	3.49	0.48	7.66
IQR	5.76	13.81	9.58	4.88	11.35	4.45

Table 10.5: Study 1, prediction 1: Median error and IQR in % for measured and predicted pressures and volumes over all 13 predicted episodes when the baseline parameter vector is used as initial solution. SAP = systolic arterial pressure, DAP = diastolic arterial pressure, MAP = mean arterial pressure, LVEDVI = left ventricular end-diastolic volume index, LVESVI = left ventricular end-systolic volume index.

Absolute percentage error for measured and predicted pressures and volumes						
	SAP (%)	DAP (%)	MAP (%)	LVEDVI (%)	LVESVI (%)	SV (%)
median	2.60	6.72	4.66	2.99	8.78	6.62
IQR	3.33	5.59	4.29	2.93	12.00	4.76

Table 10.6: Study 1, prediction 2: Median error and IQR in % for measured and predicted pressures and volumes over all 13 predicted episodes when the previous parameter vector is used as initial solution. SAP = systolic arterial pressure, DAP = diastolic arterial pressure, MAP = mean arterial pressure, LVEDVI = left ventricular end-diastolic volume index, LVESVI = left ventricular end-systolic volume index.

10.3.2 Study 2

10.3.2.1 Identification Results

Figure 10.5 shows in the upper panel (solid line) the mean arterial pressure (MAP) over 14 hours as given in (Heringlake *et al.*, 2007). The circles represent the simulated CVS model outputs obtained when the CVS model is re-run with the identified patient-specific parameters. The middle panel shows as a solid line the mean pulmonary artery pressure (MPAP) as obtained from (Heringlake *et al.*, 2007) over the 14 hour study period. The circles depict the CVS model output data when re-run using the identified parameters. The lower panel shows the same results for the cardiac index (CI).

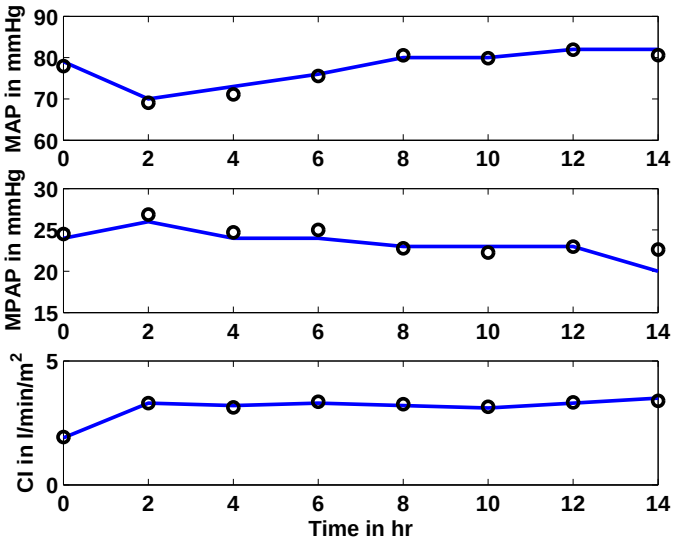

Figure 10.5: Study 2: Clinical mean arterial (MAP), mean pulmonary artery (MPAP) pressure and cardiac index (CI) as obtained from (Heringlake *et al.*, 2007) vs simulated pressures and CI. Solid lines represent the clinical data and circles represent the CVS model simulation output using identified patient-specific parameters.

Table 10.7 gives an overview of how well the CVS model output data matches the data given in (Heringlake *et al.*, 2007). The median absolute percentage error is given, as well as the inter-quartile range (IQR). These two values are calculated over all 8 identified segments for the total study period of 14 hours.

Absolute percentage error for measured and simulated arterial pressures and CI			
	MAP (%)	MPAP (%)	CI (%)
median	0.99	3.05	1.57
IQR	0.94	1.67	0.45

Table 10.7: Study 2, identification: Median error and IQR in % for measured and simulated pressures and volumes over all 8 identified segments. MAP = mean arterial pressure, MPAP = mean pulmonary artery pressure, CI = cardiac index.

10.3.2.2 Prediction Results

Table 10.8 gives the median absolute percentage errors and IQR for predicting the hemodynamic responses in MAP, MPAP and CI based on the time in the study. Note, that the rules for the adrenaline-specific parameters were obtained from the middle time segments at 2 to 12 hours. The hemodynamic responses are predicted for 6 different time segments at 4, 6, 8, 10, 12 and 14 hours. The previous parameter solution vector was used as initial solution for each predicted segment.

Absolute percentage error for measured and predicted arterial pressures and CI			
	MAP (%)	MPAP (%)	CI (%)
median	4.26	5.51	4.50
IQR	3.73	4.46	2.95

Table 10.8: Study 2, prediction: Median error and IQR in % for measured and predicted pressures and volumes over all 6 predicted segments when the previous solution vector is used as initial parameter vector. MAP = mean arterial pressure, MPAP = mean pulmonary artery pressure, CI = cardiac index.

10.3.3 Study 3

10.3.3.1 Identification Results

Figure 10.6 shows in the upper panel (solid line) the mean arterial pressure (MAP) over 24 hours as given in (Levy *et al.*, 1997). The circles represent the simulated CVS model outputs obtained when the CVS model is re-run with the identified patient-specific parameters. The middle panel shows as a solid line the mean pulmonary artery pressure (MPAP) as obtained from (Levy *et al.*, 1997) over the 24 hour study period. The circles represent the CVS model output data when re-run using the identified parameters. The lower panel shows the same results for the cardiac index (CI).

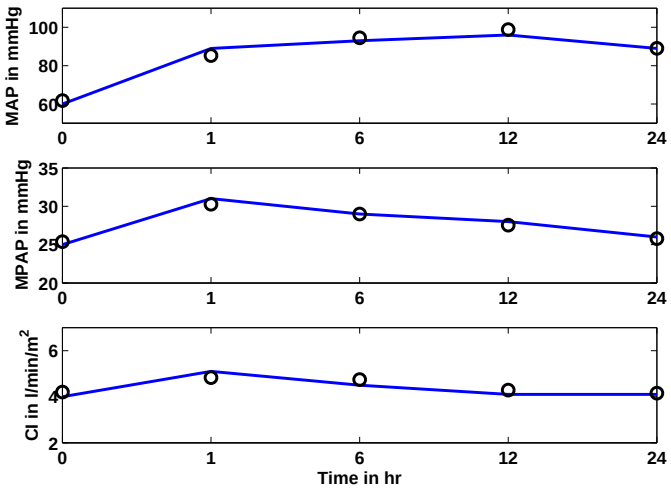

Figure 10.6: Study 3: Clinical mean arterial (MAP), mean pulmonary artery (MPAP) pressure and cardiac index (CI) as obtained from (Levy *et al.*, 1997) vs simulated pressures and CI. Solid lines represent the clinical data and circles represent the CVS model simulation output using identified patient-specific parameters.

Table 10.9 gives an overview of how well the CVS model output data matches the data in (Levy *et al.*, 1997). The median absolute percentage error is shown, as well as the inter-quartile range (IQR). These two values are calculated over all 5 identified segments for the total study period of 24 hours.

Absolute percentage error for measured and simulated arterial pressures and CI			
	MAP (%)	MPAP (%)	CI (%)
median	2.93	1.54	5.00
IQR	1.31	8.83	0.73

Table 10.9: Study 3, identification: Median error and IQR in % for measured and simulated pressures and volumes over all 5 identified segments. MAP = mean arterial pressure, MPAP = mean pulmonary artery pressure, CI = cardiac index.

10.3.3.2 Prediction Results

Table 10.10 gives the median absolute percentage errors for predicting the hemodynamic responses in MAP, MPAP and CI based on the time in the study. The rules for the adrenaline-specific parameters were obtained from the time segments h1 and h6 to predict the response at h12. The parameter solution vector at h6 was used as initial solution for the prediction of h12.

Absolute percentage error for measured and predicted arterial pressures and CI		
MAP ($mmHg$)	MPAP ($mmHg$)	CI ($l/min/m^2$)
6.87	1.06	10.34

Table 10.10: Study 3, prediction: Absolute difference in % for measured and predicted pressures and CI for predicted segment h12 when the parameter trends for h1 to h6 are used. MAP = mean arterial pressure, MPAP = mean pulmonary artery pressure, CI = cardiac index.

10.4 Discussion

For all 3 studies, the model simulation output signals match the clinical data very well, as can be seen in Figures 10.3 and 10.4 for study 1, and Figures 10.5 and 10.6 for studies 2 and 3, respectively. The absolute percentage errors (median and IQR) between simulated and clinical data for arterial pressures (SAP, DAP and/or MAP), ventricle volume indexes (LVEDVI and LVESVI), stroke volume (SV) and/or cardiac index (CI) for all 3 studies are given in Tables 10.4-10.9. It can clearly be seen, that all median identification percentage errors are less than 9%. This value is within or near expected measurement errors.

These results show the good overall accuracy of the identification method and parameters found. It also validates the models ability to capture these dynamics in physiologically expected ways, as well as the assumptions and estimations made. In particular, such generally good identifications are not likely possible without a fundamentally valid model and approach.

Table 10.5 shows the median absolute percentage errors and IQR for prediction 1 for study 1. This first prediction used the population-specific rule obtained only from the Y population to describe the changes in the adrenaline-specific model parameters that are caused by an increase in the adrenaline dose from 20 ng/min/kg to 160 ng/min/kg. Predictions were performed for the O, YM, YF, OM and OF groups with absolute percentage errors less than 14% in the pressures and less than 8% for the stroke volume. This low level of prediction error is a very good result, as bigger differences might be expected in the adrenaline dose response between the young (Y) and older (O) group, and also between male (M) and female (F) groups. Nevertheless, reasonably good predictions were obtained, showing the general applicability of the CVS model and methods.

More specifically, MAP in the older (O) group was consistently under-predicted (median absolute percentage error 10%). However this bias is in accordance with the results from (White & Leenen, 1997), where MAP decreases more in the Y group then it does for the O group. Thus, this trend, when calculating the prediction rules from the Y group, is transferred to the predictions in the O group. However, these prediction errors are still within clinically reasonable or acceptable ranges. This result also shows that some cohorts may well require cohort-specific rules, even if the general trends are similar.

Table 10.6 shows the median absolute percentage errors and IQR for prediction 2 for study 1. This second prediction uses the same population-specific rules

as used in prediction 1. However, in contrast to prediction 1, the previous solution is used as initial solution and not the baseline solution. Thus, better information is included in the prediction process, especially for predictions at the end of the study (for higher doses) where it would be expected that the remaining model parameters have also changed slightly over the longer time scale of the study. Hence, better prediction results are obtained with median errors less than 7% for arterial pressures and stroke volume.

These 2 predictions in study 1 show how the CVS model could potentially be used in a real clinical application. Firstly, a baseline solution for the specific patient needs to be obtained. Prediction rules, likely pre-existing, for the adrenaline-specific parameters are then used to predict the response to, for example, an increase in the current adrenaline dose. This first prediction might well yield a reasonable result, and different doses can be tested and predicted with the most appropriate chosen for the patient. However, as time progresses and the dose changes, much better predictions will be obtained when the previous solution vector, for example at 60 ng/kg/min or time=2hr, is used as the initial parameter set for the prediction at 80 ng/kg/min or time=3hr. Hence, once started the process enables the ability to track patient evolution in response, which is a potential clinical datum on its own right.

Tables 10.8 and 10.10 show the absolute percentage errors for the predictions performed for studies 2 and 3. The median prediction errors are less than 6% and less than 11% for studies 2 and 3, respectively. These are good results when the very limited data available in these 2 studies is considered. In particular, all the minimum and maximum arterial pressures and volumes had to be estimated creating a substantial level of potential error for a limited result. Nevertheless, reasonably good prediction results are obtained, illustrating the robustness of the estimations and identification process.

Comparisons of the adrenaline-specific prediction rules between the 3 studies are not fully possible. Study 1 is based on a dose change for a short time, where each infusion lasts 8 minutes, in healthy subjects. In contrast, studies 2 and 3 are observational studies in an ICU environment over a much longer time period of 14 and 24 hours with different doses in between. Hence, the different time scales prevent direct comparison.

However, the linear prediction rules for studies 2 and 3 are, despite the many assumptions that have to be made, relatively similar, as seen in Figure 10.2. The

upper panel shows the prediction rule for E_{eslvf} for study 2 (solid line) and 3 (dashed line), the lower panel shows the prediction rule for E_{esrvf}. In particular, it should be noted how the right ventricular contractility E_{esrvf} decreases, instead of the expected increase. This result could be due to inaccurate estimations in the right ventricle volume based on the assumptions made and/or due to the underlying cardiac and circulatory dysfunctions present in the critically ill patients for studies 2 (myocardial dysfunction after CABG) and 3 (septic shock). This type of inconclusive result is the expected limitation of using severely restricted data and making compensatory assumptions that may not hold for broader cohorts.

Obviously, more studies are needed to confirm these initial results. The overall goal remains to develop an overall adrenaline-specific parameter rule that can easily be adjusted to the individual patient regarding age, sex, current drug dose and underlying disease state. Such a rule could then directly be used in a clinical application and only one baseline solution would be necessary, rather than a whole set of identifications as in this current study. However, despite limitations, this study has been able to demonstrate the potential. Particularly, when there is clinically dense data.

10.5 Conclusion

The integral-based optimization method successively identified patient-specific parameters for the minimal cardiac model for 3 studies of adrenaline therapies. This validation study shows the ability of the model to adequately and realistically capture (with unique values) the impact of pressure-volume changes with adrenaline in healthy subjects as well as in critically ill patients.

Furthermore, the integral-based optimization led to the successful definition of adrenaline-specific parameters for the CVS model. These adrenaline-specific parameter values were used to validate the predictive ability of the model. This further validation shows the ability of the model to adequately and realistically simulate the impact of pressure-volume changes with adrenaline in healthy subjects and critically ill patients. Moreover, such rules can be similarly derived and used to predict the response towards a variety of interventions, while errors or deviations from them can point out developing disease states or hemodynamic instabilities. This research thus increases the confidence in the clinical applicability and validity of this model and its use in clinical diagnostic monitoring and drug dose guidance.

Chapter 11

Conclusions and Future Work

The first section of this chapter summarizes the main conclusions that can be drawn from the research presented in this thesis. The second section describes the future work that could be integrated into the CVS model or the parameter identification process to make this approach to model-based diagnosis and therapy guidance more applicable in a clinical environment.

11.1 Conclusions

The motivation behind the research presented in this thesis is the creation of (minimal) models and methods to enable CVS diagnostic and decision support systems in critical care.

The main accomplishments of this research include extending the CVS model of Smith *et al.* (2004) to allow for a more accurate and physiological representation of the cardiovascular system. This extension includes accounting for the effects of spontaneous and mechanical ventilation. Secondly, the theoretical parameter identification framework based on the integral methods of Hann *et al.* (2006) has been transferred into a real-time clinically applicable identification process. Third, parameter relationships have been analyzed and rules formulated that allow the prediction of patient response to interventions such as administering a fluid bolus, changing PEEP and increasing the dose of adrenaline. Finally, the models and methods developed are validated on: porcine experiments of pulmonary embolism (PE), porcine experiments of PEEP titrations at varying volemic levels, two different sets of induced septic shock and human adrenaline data found in the literature.

Extending the CVS model added complexity and adjustments had to be made to the identification process. It is important to remember that there has to be a balance between model complexity and clinical applicability. Figure 11.1 shows the model complexity versus clinical applicability with the optimal model for a given intended purpose.

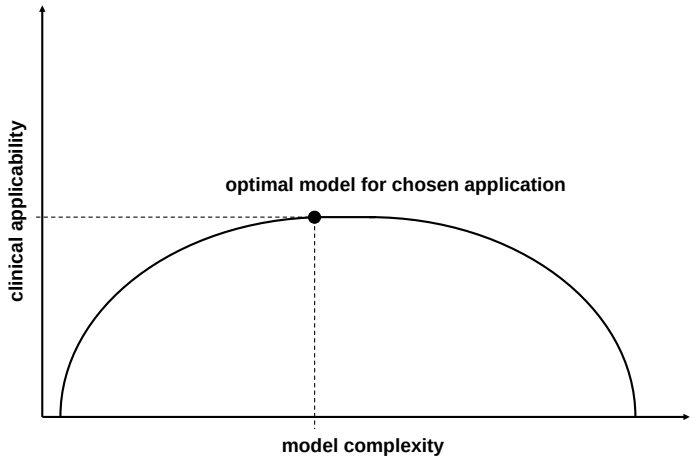

Figure 11.1: Clinical applicability of a model as given by the model complexity.

As can be seen in Figure 11.1, when the model is too simple and thus does not adequately represent the system to be modelled, the clinical applicability is small. An example is the simplified original CVS model (Smith, 2004; Smith *et al.*, 2004). In that model there is no separation between the systemic arterial and venous sides, making the correct simulation of mechanical ventilation and cardiopulmonary interactions difficult.

When the model complexity is increased, the clinical applicability increases, but only to a certain point. The model at this point could be termed the optimal model for the intended purpose or application. For example, the optimal CVS model for a general ICU may not need a highly detailed simulation of the ventricular interaction and heart valve mechanics. In contrast, a CVS model, intended for the use in a cardiology unit, for example before and after heart surgery, might not be useful without these characteristics.

If even more complexity is added, the clinical applicability tends to decrease again. Adding more complexity is usually only warranted for improving simula-

tion results, as it allows a more detailed simulation. For example, the current CVS model could easily be extended by adding the 2 atria and thus providing a more accurate representation of the physiology and anatomy. However, these extensions might significantly hinder the correct identification of the system, and more parameters would have to be fixed at population values and unknown volumes and/or pressures would have to be estimated. These requirements would increase not only the computational time, but also the likelihood of incorrectly identified parameters and poor clinical results.

Therefore, the model approach chosen in this thesis is guided by the principle of parsimony, i.e. the goal is to apply the simplest model to be effective and the CVS model structure is only extended where results and physiology dictate to do so. This approach is fundamentally different to the approach of creating a larger, more physiological model and reducing the model structure until the model becomes identifiable and applicable for use in a real-time clinical environment.

In this thesis, Chapters 7 to 10 clearly demonstrate how the extended CVS model and patient-specific parameter identification process created can successfully be applied to capture critical measures and expected physiological responses in the presence of noise using real clinical data. This diagnostic identification process is successfully adjusted to the number of measured input signals available, which is critical for accounting for different clinical environments. For the identification of porcine PE (Chapter 7), the full set of hemodynamic signals were measured continuously and, importantly, both ventricle volumes (V_{lv}, V_{rv}) as well as the pulmonary artery pressure (P_{pa}) were measured. However, even in the absence of direct volume measurements, as was the case for the PEEP experiment (Chapter 8), good clinically valid identification results and predictions were obtained.

The identification process was further extended to account for only discrete measurements, such as the minimum and maximum ventricle volumes and arterial pressures. These methods were then further developed and extended by volume estimations for V_{lv} and V_{rv} and the other CVS model volume compartments, based on a known blood distribution and the measured values GEDV and PBV. As a result, several difficult to measure or unknown values are better or more robustly accounted for in the diagnostic parameter identification process. This approach significantly increases potential clinical utility with no loss of efficacy.

The extended CVS model and methods are now much more applicable to an ICU environment where it is very unlikely that ventricle volumes are recorded. The methods developed and, more specifically, the way the volume compartments are estimated have also been proven to be robust as in the case of the porcine septic shock experiment of Chapter 9. This septic shock experiment is made up of 2 different experiments where different hemodynamic signals were recorded. In the first experiment of induced septic shock with hemofiltration (HF), all main hemodynamic signals (P_{ao}, P_{pa}, V_{lv} and V_{rv}) were recorded. However, in the second experiment without HF, only the right heart signals were recorded and the left ventricle volume had to be estimated. The CVS model was nevertheless able to capture the main hemodynamic changes required for effective diagnostics during septic shock, showing the engineering and clinical robustness of the developed methods.

Overall, the model has been able to aggregate diverse measured data into a clear, clinically and physiologically relevant diagnostic picture as the condition develops. Furthermore, methods were developed that allow the prediction of the patient's response towards interventions. This research thus increases confidence in the clinical applicability and validity of this overall diagnostic monitoring and therapy guidance approach.

11.2 Future Work

This section investigates and summarizes potential further changes and extensions to the CVS model structure that would enable it to more accurately simulate some aspects of CVS or CPS function. Additional ideas are described related to improving the computational time of the identification process and thus making the methods developed more applicable for the effective real-time assessment of cardiac and circulatory function.

11.2.1 O_2 and CO_2 Gas Exchange

Despite the many options available, most ICUs still only monitor and display heart rate and blood pressure, however, they do usually measure oxygen saturation by pulse oximetry (SpO_2). Furthermore, especially for the hemodynamic monitoring of septic shock patients, where microcirculation is impaired, it is vital to keep the oxygen supply and demand in balance. Hence, over the past several

years, tissue and organ perfusion became more and more important concepts and are now monitored as part of the standard care in most ICUs. A variety of new hemodynamic monitoring techniques have also been developed, such as sublingual PCO_2 monitoring, near infrared spectroscopy for tissue oxygenation and tissue hemoglobin monitoring, as well as fluorescence spectroscopy for monitoring the mitochondrial energy state.

In addition, for mechanically ventilated patients, information about the in- and expired O_2 and CO_2 concentration is now available. Blood gas analysis (BGA) also provides information about the amounts of O_2 and CO_2 in the blood. BGA thus evaluates, how effectively the lungs are delivering O_2 to the blood and are eliminating CO_2 from it. BGA studies are usually done in patients with respiratory diseases to assess their lung status and in patients who receive O_2 therapy. In addition, the pH value gives insight into the patient's acid-base balance and thus provides information about the kidney function.

Consequently, it would be desirable to make use of these additional signals and thus the additional amount of information they provide. For example, oxygenation parameters such as the arterial and mixed venous O_2 saturation (SaO_2, $S\overline{v}O_2$), the O_2 delivery and consumption index (DO_2I, VO_2I) could be incorporated into the model. The arterial-venous O_2 content difference ($C(a-v)O_2$) on the other hand, can be used to evaluate the amount of shunting in the lung, i.e. the amount of air that bypasses the normal gas exchange route. More specifically, the fraction of pulmonary blood flow that passes from the right to the left heart without undergoing complete oxygenation by the lung. Details of models and methods that incorporate O_2 and CO_2 components can be found in a variety of reports (Batzel *et al.*, 2005; Harada *et al.*, 2005; Hardman *et al.*, 1998; Kappel *et al.*, 2007; Lu *et al.*, 2003).

11.2.2 Blood Volume Calculations

A very basic exponential relationship has been presented in Section 4.2.3.2 and Equation 4.21 for characterizing the total effective blood TBV_{eff} as based on blood losses or infusions, taking into account the reflex mechanisms of constriction and/or dilation. However, as already mentioned, better models are needed here. For example, there are diseases and circulatory dysfunctions where no blood is lost to the outside and thus $BV = 0$. However, blood can be lost into the tissues or shifted to other organs, etc.

This scenario is currently not well studied and improvements should be made in the modelling of these blood shifts. Equation 4.21 should take these effects into account by allowing for a different representation of BV. For example, BV should not only represent the change in TBV as caused by external fluid losses or infusions, but also serve as an internal BV, thus taking into account any blood shifts that occur inside the body.

A first and very simple idea would be to relate this internal BV to the measured SV. This makes physical sense, as a reduced effective circulating blood volume (V_{syseff}) will cause a drop in VR and thus a consequent reduction in SV. Hence, Equation 4.21 could be extended:

$$BV_{internal} \quad [in\%] = \nu \cdot SV_{reduction} \quad [in\%] \tag{11.1}$$

with for example $\nu = 0.25$, stating that a 40% reduction in SV is modelled by a 10% reduction in effective circulating volume.

11.2.3 Additional Diseases and Treatments

It is beneficial to know how to simulate the most common diseases and dysfunctions typically found in an ICU environment, using the CVS model. Because only then correct diagnosis and the following patient-specific forward simulations and decision support predictions can be performed. A first step is made in Chapter 10, where the effects of the Catecholamine Adrenaline are investigated. Other drug simulation studies should be included. For example, the commonly used Norepinephrine and Dobutamine would be obvious first steps and data may already exist in the literature.

11.2.4 Modelling the Septum and Activation Function

This part of the research is completely based on simulations, as validation studies for this particular behaviour are very hard to obtain. It would be desirable to concentrate more specifically on the septum volume calculation and cardiac activation (driver) function. For example, for patients who suffer from arrhythmias and/or abnormal electrical impulse conduction, such improvements, if clinically validated, would help offer better insight into local heart function.

A first step is made in Section 3.2.1, where a left bundle branch block (LBB) is simulated. However, the current driver function is based on a very simple system

of Gaussian terms. The CVS model is able to handle 3 different driver functions to account for time differences in the activation of the left and right ventricle and the septum, as also presented in Section 3.2.1. However, these 3 different representations are based on the same shape given by Equation 3.46 and Table 3.3. As the driver function shape is kept constant throughout the identification process and largely also over different subjects (for comparability of the identified parameters), some errors are introduced. For example, the ventricle pressure waveform may not be matched by the CVS model output due to differences in the simulated electrical activation of the ventricle.

These differences in the ventricle pressures in turn have effects. For example, they will impact the filling periods of the ventricles, as filling (diastole) is defined by the pressure gradient of the ventricle pressure and the corresponding pressures P_{pu} and P_{vc}, respectively. These differences in the filling periods will then, in turn, cause a difference in the ventricle volumes.

Hence, it would be desirable to improve the driver function definition and make it more physiologically accurate. This change would also have potential benefits on more accurately capturing ventricle pressures. However, this change should be done with caution, as changing the driver function throughout the identification process will have significant effects on all other CVS parameters. Therefore, any changes should be made after evaluating the effects on all other CVS model parameters.

To improve the matching of the filling and ejection times (diastolic and systolic times), it is planned to integrate electrocardiogram (ECG) data as an additional input signal into the identification process. The ECG will not only give insights into any conduction disorders, but also provide some indication for filling and ejection times. More specifically, the systolic times are roughly given by the beginning of the QRS-complex (the R-peak) and the end of the T-wave. These ejection and filling times can then be used to match the ventricle volumes more correctly to the true signals, thus improving the quality of the model fit.

11.2.5 Extended Scaling Function

During the iterative identification process, CVS model output signals are scaled to match the true, recorded signals. These scaled signals are then used to identify the model parameters. The CVS model parameters are used to re-run a new simulation and produce new output signals, which in turn are scaled to match

the true signals. This iterative process is stopped, when a set tolerance between simulated model output and true signal is reached.

At the moment, the scaling function only takes the minimum and maximum volume and pressure values (EDV, ESV and SAP, DAP) into account, ignoring the signal waveform and time axis. For future work, the scaling function could be extended to also allow a time scaling, taking into account the filling and ejection times, thus better matching the signal waveform. Information about ejection (systolic) and filling (diastolic) times can either be obtained from the measured signal waveform itself or from the ECG. Commonly, direct waveform measurements of the volumes are not available in a clinical setting, however the ECG is routinely recorded and hence, information about the different filling and ejection times is available.

Improving the scaling function and thus the better and more physiologically accurate matching of the simulated and true signals might significantly improve the parameter identification. More specifically, it is aimed to use the new extended scaling function in simpler CVS models, for example separated for left/right heart and systemic/pulmonary circulation, to create model output signals and waveforms that can then be used in the identification process. These output signals, which will be used as initial input signals for the identification process, will then potentially reduce the time it takes for convergence in the iterative identification process.

Appendix A

CVS Model Equations

Equations which are used in the CVS model:

Ventricle volumes and flows:

$$V_{lv} = V_{lvf} + V_{spt} \tag{A.1}$$

$$V_{rv} = V_{rvf} - V_{spt} \tag{A.2}$$

$$V_{pcd} = V_{lv} + V_{rv} \tag{A.3}$$

$$P_{pcd} = P_{0pcd} \cdot (e^{\lambda_{pcd}(V_{pcd} - V_{0pcd})} - 1) \tag{A.4}$$

$$P_{peri} = P_{pcd} + P_{th} \tag{A.5}$$

$$\dot{Q_{av}} = \frac{(P_{lv} - P_{ao} - Q_{av} \cdot R_{av})}{L_{av}} \tag{A.6}$$

$$\dot{Q_{mt}} = \frac{(P_{pu} - P_{lv} - Q_{mt} \cdot R_{mt})}{L_{mt}} \tag{A.7}$$

$$\dot{Q_{pv}} = \frac{(P_{rv} - P_{pa} - Q_{pv} \cdot R_{pv})}{L_{pv}} \tag{A.8}$$

$$\dot{Q_{tc}} = \frac{(P_{vc} - P_{rv} - Q_{tc} \cdot R_{tc})}{L_{tc}} \tag{A.9}$$

Pressures:

$$P_{pu} = E_{pu} \cdot (V_{pu} - V_{dpu}) + P_{th} \tag{A.10}$$
$$P_{pa} = E_{pa} \cdot (V_{pa} - V_{dpa}) + P_{th} \tag{A.11}$$
$$P_{vc} = E_{vc} \cdot (V_{vc} - V_{dvc}) + P_{th} \tag{A.12}$$
$$P_{ao} = E_{ao} \cdot (V_{ao} - V_{dao}) \tag{A.13}$$
$$P_{sys} = E_{sys} \cdot (V_{sys} - V_{dsys}) \tag{A.14}$$
$$P_{cap} = E_{cap} \cdot (V_{cap} - V_{dcap}) \tag{A.15}$$

Volumes:

$$\dot{V}_{pv} = Q_{pulout} - Q_{mt} \tag{A.16}$$
$$\dot{V}_{pa} = Q_{pv} - Q_{pulin} \tag{A.17}$$
$$\dot{V}_{vc} = Q_{vr} - Q_{tc} \tag{A.18}$$
$$\dot{V}_{ao} = Q_{av} - Q_{sys} \tag{A.19}$$
$$\dot{V}_{sys} = Q_{sys} - Q_{vr} \tag{A.20}$$
$$\dot{V}_{cap} = Q_{pulin} - Q_{pulout} \tag{A.21}$$

Flows:

$$Q_{sys} = \frac{(P_{ao} - P_{sys})}{R_{sys}} \tag{A.22}$$
$$Q_{vr} = \frac{(P_{sys} - P_{vc})}{R_{vr}} \tag{A.23}$$
$$Q_{pulin} = \frac{(P_{pa} - P_{cap})}{R_{pulin}} \tag{A.24}$$
$$Q_{pulout} = \frac{(P_{cap} - P_{pu})}{R_{pulout}} \tag{A.25}$$

Activation (driver) function:

$$e(t) = \sum_{i=1}^{3} A_i \cdot e^{-B_i(t-C_i)^2} \tag{A.26}$$

Driver Function $e(t)$			
Parameter [Unit]	i = 1	i = 2	i = 3
$A_i[unitless]$	0.9556	0.6249	0.018
$B_i[s^{-2}]$	255.4	225.3	4225.0
$C_i[s]$	0.3060	0.2026	0.2491

Table A.1: Driver Function e(t) parameters.

Ventricular interaction and septum volume:

$$P_{lv} = P_{lvf} + P_{peri} \tag{A.27}$$

$$P_{rv} = P_{rvf} + P_{peri} \tag{A.28}$$

$$\begin{aligned} P_{lvf} &= driL \cdot E_{eslvf} \cdot (V_{lvf} - V_{dlvf}) \\ &\quad + (1 - driL) \cdot P_{0lvf} \cdot (e^{\lambda_{lvf}(V_{lvf} - V_{0lvf})} - 1) \end{aligned} \tag{A.29}$$

$$\begin{aligned} P_{rvf} &= driR \cdot E_{esrvf} \cdot (V_{rvf} - V_{drvf}) \\ &\quad + (1 - driR) \cdot P_{0rvf} \cdot (e^{\lambda_{rvf}(V_{rvf} - V_{0rvf})} - 1) \end{aligned} \tag{A.30}$$

$$P_{lv} = P_{lvf} + P_{peri} \tag{A.31}$$

$$P_{rv} = P_{rvf} + P_{peri} \tag{A.32}$$

$$P_{spt} = driS \cdot E_{esspt}(V_{spt} - V_{dspt}) + (1 - driS) \cdot P_{0spt}(e^{\lambda_{spt}(V_{spt} - V_{ospt})} - 1) \tag{A.33}$$

$$V_{spt} = a/b \tag{A.34}$$

with a and b defined:

$$\begin{aligned} a = \Bigg(& driS \cdot E_{esspt} \cdot V_{dspt} \\ & + driL \cdot E_{eslvf} \cdot (V_{lv} - V_{dlvf}) \\ & - driR \cdot E_{esrvf} \cdot (V_{rv} - V_{drfv}) \\ & - (1 - driS) \cdot P_{0spt} \cdot (b_{spt} e^{-\lambda_{spt} V_{ospt}} - 1) \\ & + (1 - driL) \cdot P_{0lvf} \cdot (b_{lvf} e^{\lambda_{lvf}(V_{lv} - V_{olvf})} - 1) \\ & - (1 - driR) \cdot P_{0rvf} \cdot (b_{rvf} e^{\lambda_{rvf}(V_{rv} - V_{orvf})} - 1) \Bigg) \end{aligned} \tag{A.35}$$

$$\begin{aligned} b = \Bigg(& driS \cdot E_{esspt} \\ & - driL \cdot E_{eslvf} - driR \cdot E_{esrvf} \\ & + (1 - driS) \cdot P_{0spt} \cdot a_{spt} e^{-\lambda_{spt} V_{ospt}} \\ & - (1 - driL) \cdot P_{0lvf} \cdot a_{lvf} e^{\lambda_{lvf}(V_{lv} - V_{olvf})} \\ & + (1 - driR) \cdot P_{0rvf} \cdot a_{rvf} e^{\lambda_{rvf}(V_{rv} - V_{orvf})} \Bigg) \end{aligned} \tag{A.36}$$

where a_{spt}, a_{lvf}, a_{rvf}, b_{spt}, b_{lvf} and b_{rvf} are defined:

$$x_1 = V_{spt,old} + \triangle V_{spt} \tag{A.37}$$

$$x_2 = V_{spt,old} - \triangle V_{spt} \tag{A.38}$$

$$a_{spt} = \frac{e^{\lambda_{spt} x_2} - e^{\lambda_{spt} x_1}}{x_2 - x_1} \tag{A.39}$$

$$a_{lvf} = \frac{e^{\lambda_{lvf} x_2} - e^{\lambda_{lvf} x_1}}{x_2 - x_1} \tag{A.40}$$

$$a_{rvf} = \frac{e^{\lambda_{rvf} x_2} - e^{\lambda_{rvf} x_1}}{x_2 - x_1} \tag{A.41}$$

$$b_{spt} = e^{\lambda_{spt} x_1} - (e^{\lambda_{spt} x_2} - \frac{e^{\lambda_{spt} x_1}}{x_2 - x_1} x_1) \tag{A.42}$$

$$b_{lvf} = e^{\lambda_{lvf} x_1} - (e^{\lambda_{lvf} x_2} - \frac{e^{\lambda_{lvf} x_1}}{x_2 - x_1} x_1) \tag{A.43}$$

$$b_{rvf} = e^{\lambda_{rvf} x_1} - (e^{\lambda_{rvf} x_2} - \frac{e^{\lambda_{rvf} x_1}}{x_2 - x_1} x_1) \tag{A.44}$$

where $V_{spt,old}$ is the V_{spt} in the previous time step and $\triangle V_{spt} = 0.1ml$.

Appendix B

CPS Model Equations

Equations which are used in the CPS (cardiopulmonary and circulatory) model:

Volume calculations:

$$V_{dsys} = V_{unstressed} + V_{extravascular} \tag{B.1}$$

$$LVEDV = GEDV \cdot 0.6 \cdot 0.4 \tag{B.2}$$

$$RVEDV = GEDV \cdot 0.6 \cdot 0.6 \tag{B.3}$$

$$PBV = \frac{GEDV}{4} \tag{B.4}$$

$$ITBV = GEDV + PBV \tag{B.5}$$

$$ITBV = 1.25 \cdot GEDV \tag{B.6}$$

$$V_{capeff} = PBV \cdot 0.4 \tag{B.7}$$

$$V_{pv} = PBV \cdot 0.6 \tag{B.8}$$

$$V_{vc} = \kappa \cdot SV \tag{B.9}$$

$$V_{syseff} = TBV_{eff} - V_{ao} - LVEDV - RVEDV \tag{B.10}$$
$$- V_{pa} - V_{capeff} - V_{pv} - V_{vc}$$

$$V_{dsys} = TBV_{ineff} \cdot 0.8 \tag{B.11}$$

$$V_{dcap} = TBV_{ineff} \cdot 0.2 \tag{B.12}$$

$$TBV_{eff,norm} = (25 + \triangle)[ml/kg] \tag{B.13}$$

$$TBV_{ineff,norm} = (60 - \triangle)[ml/kg] \tag{B.14}$$

$$TBV_{eff} = TBV_{eff,norm} \cdot KG + BV \tag{B.15}$$

$$TBV_{ineff} = TBV_{ineff,norm} \cdot KG \tag{B.16}$$

References

(2008). The Ohio Heart and Vascular Center Inc., Cincinnati OH, USA. (downloaded from http://www.ohioheartandvascular.com; March 10, 2008). xiv, 27

Abramson, N.S., Wald, K.S., Grenvik, A.N., Robinson, D. & Snyder, J.V. (1980). Adverse occurrences in intensive care units. *JAMA*, **244**, 1582–1584. 2, 148

ACCP/SCCM (1992). American college of chest physicians/society of critical care medicine consensus conference: definitions for sepsis and organ failure and guidelines for the use of innovative therapies in sepsis. *Crit Care Med*, **20**, 864–874. 164

American Heart Association (2005). Guidelines for cardiopulmonary resuscitation and emergency cardiovascular care, part 7.4: Monitoring and medications. *Circulation*, **112**, IV–78 – IV–83. 201, 203

Angus, D.C. & Crowther, M.A. (2003). Unraveling severe sepsis: why did optimist fail and what's next? *JAMA*, **290**, 256–258. 163

Angus, D.C., Linde-Zwirble, W.T., Lidicker, J., Clermont, G., Carcillo, J. & Pinsky, M.R. (2001). Epidemiology of severe sepsis in the united states: analysis of incidence, outcome, and associated costs of care. *Crit Care Med*, **29**, 1303–1310. 163

Annane, D., Aegerter, P., Jars-Guincestre, M.C. & Guidet, B. (2003). Current epidemiology of septic shock: the CUB-Réa Network. *Am J Respir Crit Care Med*, **168**, 165–172. 164

Baan, J., van der Velde, E., de Bruin, H., Smeenk, G., Koops, J., van Dijk, A., Temmerman, D., Senden, J. & Buis, B. (1984). Continuous

measurement of left ventricular volume in animals and humans by conductance catheter. *Circulation*, **70**, 812–823. 116, 170, 186, 197

Backer, D.D., Heenen, S., Piagnerelli, M., Koch, M. & Vincent, J.L. (2005). Pulse pressure variations to predict fluid responsiveness: influence of tidal volume. *Intensive Care Med*, **31**, 517–523. 6

Batzel, J.J., Kappel, F. & Timischl-Teschl, S. (2005). A cardiovascular-respiratory control system model including state delay with application to congestive heart failure in humans. *J Math Biol*, **50**, 293–335. 233

Beers, M.H. (2006). *The Merck Manual of Diagnosis and Therapy*. Merck, 18th edn. xiv, 30, 31

Biswal, S., Mishra, P., Malhotra, S., Puri, G.D. & Pandhi, P. (2006). Drug utilization pattern in the intensive care unit of a tertiary care hospital. *J Clin Pharmacol*, **46**, 945–951. 203

Bobek, M., Hoffman-Hogg, L., Blair, N., Slomka, J., Mion, L. & Arroliga, A. (2001). Utilization patterns, relative costs, and length of stay following adaptation of MICU sedation guidelines. *Formulary*, **36**, 664–673. 202

Bridges, E.J. & Dukes, S. (2005). Cardiovascular aspects of septic shock: pathophysiology, monitoring, and treatment. *Crit Care Nurse*, **25**, 18–20. 184, 197, 198

Brimioulle, S., Wauthy, P., Ewalenko, P., Rondelet, B., Vermeulen, F., Kerbaul, F. & Naeije, R. (2003). Single-beat estimation of right ventricular end-systolic pressure-volume relationship. *Am J Physiol Heart Circ Physiol*, **284**, H1625–H1630. xvii, 103, 104, 105

Burkhoff, D. (2002). Mechanical properties of the heart and its interaction with the vascular system. Course Material, Cardiac Physiology, Columbia University, New York, USA. 18, 21, 22

Burkhoff, D. & Tyberg, J.V. (1993). Why does pulmonary venous pressure rise after onset of lv dysfunction: a theoretical analysis. *Am J Physiol*, **265**, H1819–H1828. 127, 128

Burkhoff, D., van der Velde, E., Kass, D., Baan, J., Maughan, W.L. & Sagawa, K. (1985). Accuracy of volume measurement by conductance catheter in isolated, ejecting canine hearts. *Circulation*, **72**, 440–447. 170, 186, 197

Cassidy, S., Robertson, C., Pierce, A. & Johnson, R. (1948). Cardiovascular effects of positive end-expiratory pressure in dogs. *Journal of Applied Physiology*, **44**, 734–750. 54, 144

Chemla, D., Hbert, J.L., Coirault, C., Zamani, K., Suard, I., Colin, P. & Lecarpentier, Y. (1998). Total arterial compliance estimated by stroke volume-to-aortic pulse pressure ratio in humans. *Am J Physiol*, **274**, H500–H505. 81

Chung, D.C., Niranjan, S.C., Clark JR, J.W., Bidani, A., Johnston, W.E., Zwischenberger, J.B. & Traber, D.L. (1997). A dynamic model of ventricular interaction and pericardial influence. *Am. J. Physiol.*, **272**, H2942–2962. xiv, 25, 33, 34, 39, 41, 43, 45, 47, 122, 168, 183, 205

Connors, A.F., Speroff, T., Dawson, N.V., Thomas, C., Harrell, F.E., Wagner, D., Desbiens, N., Goldman, L., Wu, A.W., Califf, R.M., Fulkerson, W.J., Vidaillet, H., Broste, S., Bellamy, P., Lynn, J. & Knaus, W.A. (1996). The effectiveness of right heart catheterization in the initial care of critically ill patients. support investigators. *JAMA*, **276**, 889–897. 3

Courtney, S.E. & Asselin, J.M. (2006). High-frequency jet and oscillatory ventilation for neonates: which strategy and when? *Respir Care Clin N Am*, **12**, 453–467. xvii, 132

Dellinger, R.P. (2003). Cardiovascular management of septic shock. *Crit Care Med*, **31**, 946–955. xix, xx, 164, 165, 166, 167, 184, 197, 198

Desaive, T., Dutron, S., Lambermont, B., Kolh, P., Hann, C.E., Chase, J.G., Dauby, P. & Ghuysen, A. (2005). Closed-loop model of the cardiovascular system including ventricular interaction and valve dynamics: application to pulmonary embolism. *12th Intl Conference on Biomedical Engineering (ICBME)*. 116, 127, 129

Desaive, T., Ghuysen, A., Lambermont, B., Kolh, P., Dauby, P.C., Starfinger, C., Hann, C.E., Chase, J.G. & Shaw, G.M. (2007). Study of ventricular interaction during pulmonary embolism using clinical identification in a minimum cardiovascular system model. *Conf Proc IEEE Eng Med Biol Soc*, **1**, 2976–2979. 99, 204, 205

Desaive, T., Lambermont, B., Ghuysen, A., Kolh, P., Dauby, P.C., Starfinger, C., Hann, C.E., Chase, J.G. & Shaw, G.M. (2008). Cardiovascular modelling and identification in septic shock - experimental validation. *Proceedings of the 17th IFAC World Congress July 6-11, 2008, Seoul, Korea*. 99, 163, 193, 194

Donchin, Y., Gopher, D., Olin, M., Badihi, Y., Biesky, M., Sprung, C.L., Pizov, R. & Cotev, S. (1995). A look into the nature and causes of human errors in the intensive care unit. *Crit Care Med*, **23**, 294–300. 2, 148

D'Orio, V., Lambermont, B., Detry, O., Kolh, P., Potty, P., Gerard, P. & Marcelle, R. (1998). Pulmonary impedance and right ventricular-vascular coupling in endotoxin shock. *Cardiovasc Res*, **38**, 375–382. 168, 175

Ellis, A.K. & Day, J.H. (2003). Diagnosis and management of anaphylaxis. *CMAJ*, **169**, 307–311. 203

Elzinga, G., van Grondelle, R., Westerhof, N. & van den Bos, G.C. (1974). Ventricular interference. *Am J Physiol*, **226**, 941–947. 26

Fessler, H.E. (1997). Heart-lung interactions: applications in the critically ill. *Eur Respir J*, **10**, 226–237. 29, 30, 51, 54, 55, 56, 58, 134, 144, 145, 150, 159

Fourie, P.R., Coetzee, A.R. & Bolliger, C.T. (1992). Pulmonary artery compliance: its role in right ventricular-arterial coupling. *Cardiovasc Res*, **26**, 839–844. 176

Frank, O. (1895). Zur Dynamik des Herzmuskels. *Zeitschrift fuer Biologie*, **32**, 370–447. 15

Frank, O. (1899). Die Grundform des arteriellen Pulses. *Zeitschrift fuer Biologie*, **37**, 483–586. 34

Friedman, G., Silva, E. & Vincent, J.L. (1998). Has the mortality of septic shock changed with time. *Crit Care Med*, **26**, 2078–2086. xix, 164

Gan, C.T.J., Lankhaar, J.W., Marcus, J.T., Westerhof, N., Marques, K.M., Bronzwaer, J.G.F., Boonstra, A., Postmus, P.E. & Vonk-Noordegraaf, A. (2006). Impaired left ventricular filling due to right-to-left ventricular interaction in patients with pulmonary arterial hypertension. *Am J Physiol Heart Circ Physiol*, **290**, H1528–H1533. 47, 127, 129

Ghuysen, A., Lambermont, B., Kolh, P., Tchana-Sato, V., Magis, D., Gerard, P., Mommens, V., Janssen, N., Desaive, T. & D'Orio, V. (2008). Alteration of right ventricular-pulmonary vascular coupling in a porcine model of progressive pressure overloading. *Shock*, **29**, 197–204. 116

Goldhaber, S.Z. (1998). Pulmonary embolism - review article. *Medical Progress*, **339**, 93–104. 114, 127, 128, 129

Goldhaber, S.Z., Visani, L. & Rosa, M.D. (1999). Acute pulmonary embolism: clinical outcomes in the international cooperative pulmonary embolism registry (icoper). *Lancet*, **353**, 1386–1389. 115

Grenvik, A., Ayres, S.M., Holbrook, P.R. & Shoemaker, W.C., eds. (1989). *Textbook of Critical Care*. W.B. Saunders Company, 2nd edn. 2, 148

Guyton, A. & Hall, J. (2000). *Textbook of medical physiology*. W.B. Saunders Company, Philadelphia, 10th edn. 63, 67

Hann, C.E., Chase, J.G. & Shaw, G.M. (2005). Efficient implementation of non-linear valve law and ventricular interaction dynamics in the minimal cardiac model. *Comput Methods Programs Biomed*, **80**, 65–74. 5, 129, 134

Hann, C.E., Chase, J.G. & Shaw, G.M. (2006). Integral-based identification of patient specific parameters for a minimal cardiac model. *Comput Methods Programs Biomed*, **81**, 181–192. 5, 47, 75, 86, 90, 95, 99, 129, 134, 148, 167, 169, 205, 206, 229

Harada, T., Kubo, H., Mori, T. & Sato, T. (2005). Pulmonary and cardiovascular integrated model controlled with oxygen consumption. *Conf Proc IEEE Eng Med Biol Soc*, **1**, 304–307. 233

Hardman, J.G., Bedforth, N.M., Ahmed, A.B., Mahajan, R.P. & Aitkenhead, A.R. (1998). A physiology simulator: validation of its respiratory components and its ability to predict the patient's response to changes in mechanical ventilation. *Br J Anaesth*, **81**, 327–332. 233

Heldt, T., Long, B., Verghese, G.C., Szolovits, P. & Mark, R.G. (2006). Integrating data, models, and reasoning in critical care. *Conf Proc IEEE Eng Med Biol Soc*, **1**, 350–353. 75

Heringlake, M., Wernerus, M., Grünefeld, J., Klaus, S., Heinze, H., Bechtel, M., Bahlmann, L., Poeling, J. & Schoen, J. (2007). The metabolic and renal effects of adrenaline and milrinone in patients with myocardial dysfunction after coronary artery bypass grafting. *Crit Care*, **11**, R51. xxii, 204, 205, 206, 209, 212, 217, 221

Hess, O.M., Turina, J. & Krayenbuehl, H.P. (1979). Validity of echocardiographic assessment of septal motion. *Basic Res Cardiol*, **74**, 240–249. 24

Hunter, P. & Smaill, B. (1991). *Structure and function of the diastolic heart: material properties of passive myocardium*. Springer-Verlag, Harrisonburg. 33

Jacobsohn, E., Chorn, R. & O'Connor, M. (1997). The role of the vasculature in regulating venous return and cardiac output: historical and graphical approach. *Can J Anaesth*, **44**, 849–867. 56, 145, 150

Jellinek, H., Krenn, H., Oczenski, W., Veit, F., Schwarz, S. & Fitzgerald, R.D. (2000). Influence of positive airway pressure on the pressure gradient for venous return in humans. *J Appl Physiol*, **88**, 926–932. 54, 145

Johnston, W., Vinten-Johansen, J., Santamore, W., Case, L. & Little, W. (1989). Mechanism of reduced cardiac output during positive end-expiratory pressure in the dog. *Am Rev Respir Dis*, **140**, 1257–1264. 54, 145

Kappel, F., Fink, M. & Batzel, J.J. (2007). Aspects of control of the cardiovascular-respiratory system during orthostatic stress induced by lower body negative pressure. *Math Biosci*, **206**, 273–308. 34, 233

Karlsson, S., Varpula, M., Ruokonen, E., Pettil, V., Parviainen, I., Ala-Kokko, T.I., Kolho, E. & Rintala, E.M. (2007). Incidence, treatment, and outcome of severe sepsis in ICU-treated adults in Finland: the Finnsepsis study. *Intensive Care Med*, **33**, 435–443. 2

Kellum, J.A. & Pinsky, M.R. (2002). Use of vasopressor agents in critically ill patients. *Curr Opin Crit Care*, **8**, 236–241. 202

Klabunde, R.E. (2004). *Cardiovascular Physiology Concepts*. Lippincott Williams and Wilkins. xiii, xxii, 14, 15, 19, 61, 63, 64, 66, 116, 127, 128, 203, 214, 215

Korakianitis, T. & Shi, Y. (2006). Numerical simulation of cardiovascular dynamics with healthy and diseased heart valves. *J Biomech*, **39**, 1964–1982. 34

Kortgen, A., Niederprüm, P. & Bauer, M. (2006). Implementation of an evidence-based "standard operating procedure" and outcome in septic shock. *Crit Care Med*, **34**, 943–949. 148

Kramer, P., Wigger, W., Rieger, J., Matthaei, D. & Scheler, F. (1977). Arteriovenous haemofiltration: a new and simple method for treatment of over-hydrated patients resistant to diuretics. *Klin Wochenschr*, **55**, 1121–1122. 167

Kroeker, C.A.G., Shrive, N.G., Belenkie, I. & Tyberg, J.V. (2003). Pericardium modulates left and right ventricular stroke volumes to compensate for sudden changes in atrial volume. *Am J Physiol Heart Circ Physiol*, **284**, H2247–H2254. 26

Lambermont, B., Ghuysen, A., Kolh, P., Tchana-Sato, V., Segers, P., Grard, P., Morimont, P., Magis, D., Dogn, J.M., Masereel, B. & D'Orio, V. (2003). Effects of endotoxic shock on right ventricular systolic function and mechanical efficiency. *Cardiovasc Res*, **59**, 412–418. 169, 175, 180, 183, 185, 192, 194, 195, 198

Lambermont, B., Delanaye, P., Dogn, J.M., Ghuysen, A., Janssen, N., Dubois, B., Desaive, T., Kolh, P., D'Orio, V. & Krzesinski, J.M. (2006). Large-pore membrane hemofiltration increases cytokine clearance and improves right ventricular-vascular coupling during endotoxic shock in pigs.

Artif Organs, **30**, 560–564. xxi, xxii, 163, 167, 168, 175, 176, 177, 179, 180, 182, 185, 192, 193, 194, 195, 196, 198, 199

Lambert, P., Sloth, E., Smith, B., Hansen, L.K., Koefoed-Nielsen, J., Tonnesen, E. & Larsson, A. (2007). Does a positive end-expiratory pressure-induced reduction in stroke volume indicate preload responsiveness? an experimental study. *Acta Anaesthesiol Scand*, **51**, 415–425. 69, 136

Lanzarone, E., Liani, P., Baselli, G. & Costantino, M.L. (2007). Model of arterial tree and peripheral control for the study of physiological and assisted circulation. *Med Eng Phys*, **29**, 542–555. 34

Laurenceau, J. & Dumesnil, J. (1976). Right and left ventricular dimensions as determinants of ventricular septal motion. *Chest*, **69**, 388–393. xiii, xiv, 24, 25, 26

Lazzari, C.D., Ferrari, G., Mimmo, R., Tosti, G. & Ambrosi, D. (1994). A desk-top computer model of the circulatory system for heart assistance simulation: effect of an LVAD on energetic relationships inside the left ventricle. *Med Eng Phys*, **16**, 97–103. 34

Legrice, I., Hunter, P. & Smaill, B. (1997). Laminar structure of the heart: mathematical model. *Am.J.Physiol.*, **272**, H2466H2476. 33

Leibovici, L., Paul, M., Nielsen, A.D., Tacconelli, E. & Andreassen, S. (2007). The TREAT project: decision support and prediction using causal probabilistic networks. *Int J Antimicrob Agents*, **30 Suppl 1**, S93–102. 148

Levy, B., Bollaert, P.E., Charpentier, C., Nace, L., Audibert, G., Bauer, P., Nabet, P. & Larcan, A. (1997). Comparison of norepinephrine and dobutamine to epinephrine for hemodynamics, lactate metabolism, and gastric tonometric variables in septic shock: a prospective, randomized study. *Intensive Care Med*, **23**, 282–287. xxii, xxiii, 204, 205, 206, 210, 212, 217, 223

Liang, F. & Liu, H. (2005). A closed-loop lumped parameter computational model for human cardiovascular system. *JSME*, **48**, 484–493. 34

Little, W. & Freeman, G. (2006). Pericardial disease. *Circulation*, **113**, 1622–1632. 26

Long, W.J., Naimi, S. & Criscitiello, M.G. (1994). Evaluation of a new method for cardiovascular reasoning. *J Am Med Inform Assoc*, **1**, 127–141. 76

Lu, K., Clark, J.W., Ghorbel, F.H., Ware, D.L. & Bidani, A. (2001). A human cardiopulmonary system model applied to the analysis of the valsalva maneuver. *Am J Physiol Heart Circ Physiol*, **281**, H2661–H2679. 39

Lu, K., Clark Jr, J., Ghorbel, F., Ware, D., Zwischenberger, J. & Bidani, A. (2003). Whole-body gas exchange in human predicted by a cardiopulmonary model. *Cardiovascular Engineering*, **3**, 1–19. 233

Lualdi, J. & Goldhaber, S. (1995). Right ventricular dysfunction after acute pulmonary embolism: pathophysiologic factors, detection, and therapeutic implications. *Am Heart J.*, **130(6)**, 1276–1282. 127, 128

Luecke, T., Roth, H., Herrmann, P., Joachim, A., Weisser, G., Pelosi, P. & Quintel, M. (2004). Assessment of cardiac preload and left ventricular function under increasing levels of positive end-expiratory pressure. *Intensive Care Med*, **30**, 119–126. 61

Mangano, D.T. (1994). Perioperative cardiac morbidity–epidemiology, costs, problems, and solutions. *West J Med*, **161**, 87–89. 1

Martin, G.S., Mannino, D.M., Eaton, S. & Moss, M. (2003). The epidemiology of sepsis in the United States from 1979 through 2000. *N Engl J Med*, **348**, 1546–1554. 163

Martis, M. (2006). Validation of simulation based models: A theoretical outlook. *The Electronic Journal of Business Research Methods*, **4**, 39–46. 99

McKinley, M. & O'Loughlin, V. (2007). *Human Anatomy*. McGraw-Hill Science/Engineering/Math. xiii, xiv, 10, 13, 28

McQueen, D.M., Peskin, C.S. & Yellin, E.L. (1982). Fluid dynamics of the mitral valve: physiological aspects of a mathematical model. *Am J Physiol*, **242**, H1095–H1110. 33

Mehler, R.E. & Sompayrac, L. (2001). *How the Circulatory System Works*. Blackwell Science Inc. 11, 69, 70, 72, 73

Metnitz, P.G.H., Reiter, A., Jordan, B. & Lang, T. (2004). More interventions do not necessarily improve outcome in critically ill patients. *Intensive Care Med*, **30**, 1586–1593. 5

Michard, F. & Teboul, J.L. (2002). Predicting fluid responsiveness in ICU patients: a critical analysis of the evidence. *Chest*, **121**, 2000–2008. 6

Miro, A. & Pinsky, M. (2005). *Pediatric Critical Care*, chap. 24, 249–256. Mosby, 3rd edn. 30, 51, 52, 54, 55, 56, 58, 134, 145, 150, 159

Morris, A.H. (2001). Rational use of computerized protocols in the intensive care unit. *Critical Care*, **5**, 249–254. 2, 148

Morton, D., Abbot, D., Barclay, R., Close, B., Ewbank, R., Gask, D., Heath, M., Mattic, S., Poole, T., Seamer, J., Southee, J., Thompson, A., Trussell, B., West, C. & Jennings, M. (1993). Removal of blood from laboratory mammals and birds - first report of the BVA/FRAME/RSPCA/UFAW joint working group on refinement. *Laboratory Animals*, **27**, 1–22. 116

Mukkamala, R. & Cohen, R.J. (2001). A forward model-based validation of cardiovascular system identification. *Am J Physiol Heart Circ Physiol*, **281**, H2714–H2730. 34

Nanas, S. & Madger, S. (1992). Adaptations of the peripheral circulation to PEEP. *Am Rev Respir Dis*, **146**, 658–693. 56, 60, 160

Neumann, P. (1999). Extravascular lung water and intrathoracic blood volume: double versus single indicator dilution technique. *Intensive Care Med*, **25**, 216–219. 61

Nijkeuter, M. & Huisman, M.V. (2005). Diagnostic methods in pulmonary embolism - review article. *European Journal of Internal Medicine*, **16**, 247–256. 115, 129

Nirmalan, M., Niranjan, M., Willard, T., Edwards, J.D., Little, R.A. & Dark, P.M. (2004). Estimation of errors in determining intrathoracic blood volume using thermal dilution in pigs with acute lung injury and haemorrhage. *Br J Anaesth*, **93**, 546–551. 61

Noordergraaf, A. (1978). *Circulatory System Dynamics*. New York: Academic Press. 33

Olansen, J., Clark, J., Khoury, D., Ghorbel, F. & Bidani, A. (2000). A closed-loop model of the canine cardiovascular system that includes ventricular interaction. *Computers and Biomedical Research*, **33**, 260–295. 25, 34, 35, 39, 45, 49, 168, 183, 205

Ottesen, J.T., Olufsen, M.S. & Larsen, J.K. (2004). *Applied mathematical models in human physiology*. Philadelphia : Society for Industrial and Applied Mathematics. 33, 34, 35, 39

Pedley, T.J. (1980). *The Fluid Mechanics of Large Blood Vessels (Cambridge Monographs on Mechanics)*. Cambridge University Press. 33, 34

Peskin, C. & McQueen, D. (1992). Cardiac fluid dynamics. *Rev.Biomed.Eng.*, **20 (5 6)**, 451 459. 33, 34

Peters, J., Lister, G., Nadel, E. & Mack, G. (1997). Venous and arterial reflex responses to positive-pressure breathing and lower body negative pressure. *J Applied Physiology*, **82**, 1889–1896. 145

Peters, J., Mack, G. & Lister, G. (2001). The importance of the peripheral circulation in critical illness. *Intensive Care Medicine*, **27**, 1446–1458. xiv, 54, 56, 57, 67, 145, 150, 160

Pierpaoli, P.G. (1993). The rising cost of pharmaceuticals: a director of pharmacy's perspective. *Am J Hosp Pharm*, **50**, S6–S8. 204

Pinsky, M.R. (2004). Using ventilation-induced aortic pressure and flow variation to diagnose preload responsiveness. *Intensive Care Med*, **30**, 1008–1010. 6

Pinsky, M.R. (2005). Cardiovascular issues in respiratory care. *Chest*, **128**, 592S–597S. 51, 56, 58

Pinsky, M.R. (2007). Hemodynamic evaluation and monitoring in the ICU. *Chest*, **132**, 2020–2029. 3, 5, 6

Preisman, S., DiSegni, E., Vered, Z. & Perel, A. (2002). Left ventricular preload and function during graded haemorrhage and retranfusion in pigs: analysis of arterial pressure waveform and correlation with echocardiography. *Br J Anaesth*, **88**, 716–718. 61, 116, 129

Pulsion Medical Systems (2005). Munich, Germany: PiCCO plus user presentation. 62

Ramsey, J.G. (1999). Cardiac management in the ICU. *Chest*, **115**, 138–144. 1

Rees, S.E., Kjaergaard, S., Perthorgaard, P., Malczynski, J., Toft, E. & Andreassen, S. (2002). The automatic lung parameter estimator (ALPE) system: non-invasive estimation of pulmonary gas exchange parameters in 10-15 minutes. *J Clin Monit Comput*, **17**, 43–52. 148

Reuter, D.A., Kirchner, A., Felbinger, T.W., Weis, F.C., Kilger, E., Lamm, P. & Goetz, A.E. (2003). Usefulness of left ventricular stroke volume variation to assess fluid responsiveness in patients with reduced cardiac function. *Crit Care Med*, **31**, 1399–1404. 6

Rivers, E., Nguyen, B., Havstad, S., Ressler, J., Muzzin, A., Knoblich, B., Peterson, E. & Tomlanovich, M. (2001). Early goal-directed therapy in the treatment of severe sepsis and septic shock. *N Engl J Med*, **345**, 1368–1377. 4

Rothe, C.F. (1979). Reflex control of the veins in cardiovascular function. *Physiologist*, **22**, 28–35. 61, 64, 150

Samar, Z., Heldt, T., Verghese, G. & Mark, R. (2005). Model-based cardiovascular parameter estimation in the intensive care unit. *Comput Cardiol*, **32**, 635–638. 75

Sandham, J.D., Hull, R.D., Brant, R.F., Knox, L., Pineo, G.F., Doig, C.J., Laporta, D.P., Viner, S., Passerini, L., Devitt, H., Kirby, A. & Jacka, M. (2003). A randomized, controlled trial of the use of pulmonary-artery catheters in high-risk surgical patients. *N Engl J Med*, **348**, 5–14. 3

Sargent, R. (1998). Verification and validation of simulation models. In *Proceedings of the 1998 Winter Simulation Conference*. 99

Schlesinger, S. (1980). Terminology for model credibility. *Simulation*, **34**, 101–105. xvii, 98

Schulz, S., Bauernschmitt, R., Maar, F., Schwarzhaupt, A., Vahl, C.F. & Kiencke, U. (1998). Modeling of the baroreceptor reflex in a pulsatile model. *Biomed Tech (Berl)*, **43 Suppl**, 310–311. 34

Seferian, E.G. & Afessa, B. (2006). Demographic and clinical variation of adult intensive care unit utilization from a geographically defined population. *Crit Care Med*, **34**, 2113–2119. 2, 148

Senzaki, H., Chen, C.H. & Kass, D. (1996). Single-beat estimation of end-systolic pressure-volume relation in humans. *Circulation*, **94**, 2497–2506. 44

Shekerdemian, L. & Bohn, D. (1990). Cardiovascular effects of mechanical ventilation. *Arch. Dis. Child*, **80**, 475–480. 30, 54, 55, 145, 150, 159

Smith, B.W. (2004). *Minimal haemodynamic modelling of the heart & circulation for clinical application*. Ph.D. thesis, University of Canterbury. 4, 35, 39, 99, 100, 110, 122, 134, 168, 183, 189, 205, 230

Smith, B.W., Chase, J.G., Nokes, R.I., Shaw, G.M. & David, T. (2003). Velocity profile method for time varying resistance in minimal cardiovascular system models. *Phys Med Biol*, **48**, 3375–3387. 33

Smith, B.W., Chase, J.G., Nokes, R.I., Shaw, G.M. & Wake, G. (2004). Minimal haemodynamic system model including ventricular interaction and valve dynamics. *Medical Engineering & Physics*, **26**, 131–139. 4, 33, 39, 99, 100, 129, 133, 134, 173, 189, 229, 230

Smith, B.W., Chase, J.G., Shaw, G.M. & Nokes, R.I. (2006). Simulating transient ventricular interaction using a minimal cardiovascular system model. *Physiol Meas*, **27**, 165–179. 99, 110, 133, 134

Smith, B.W., Andreassen, S., Shaw, G.M., Jensen, P.L., Rees, S.E. & Chase, J.G. (2007). Simulation of cardiovascular system diseases by including the autonomic nervous system into a minimal model. *Comput Methods Programs Biomed*, **86**, 153–160. 99

Smith, P.K., Tyson, G.S., Hammon, J.W., Olsen, C.O., Hopkins, R.A., Maier, G.W., Sabiston, D.C. & Rankin, J.S. (1982). Cardiovascular effects of ventilation with positive expiratory airway pressure. *Ann Surg*, **195**, 121–130. 51

Starfinger, C., Chase, J.G., Hann, C.E. & Shaw, G.M. (2007a). Model-based hemodynamic analysis and prediction of PEEP interventions. *Crit Care Med*, **35, 12 (Suppl)**, A86. 131

Starfinger, C., Hann, C.E., Chase, J.G., Desaive, T., Ghuysen, A. & Shaw, G.M. (2007b). Model-based cardiac diagnosis of pulmonary embolism. *Comput Methods Programs Biomed*, **87**, 46–60. 75, 90, 99, 113, 133, 134, 148, 167, 169, 204, 205, 213

Starfinger, C., Chase, J.G., Hann, C.E. & Shaw, G.M. (2008a). Simulating the patient-specific adrenaline dose response using a cardiovascular system model. *Cardiovascular Engineering*, in review. 201

Starfinger, C., Chase, J.G., Hann, C.E., Shaw, G.M., Lambermont, B., Ghuysen, A., Kolh, P., Dauby, P.C. & Desaive, T. (2008b). Model-based identification and diagnosis of a porcine model of induced endotoxic shock with hemofiltration. *Math Biosci*. 163, 182, 193, 194, 204

Starfinger, C., Chase, J.G., Hann, C.E., Shaw, G.M., Lambermont, B., Ghuysen, A., Kolh, P., Dauby, P. & Desaive, T. (2008c). Model-based diagnosis of endotoxic septic shock using a minimum data set. *Math Biosci*, in review. 163

Starfinger, C., Chase, J.G., Hann, C.E., Shaw, G.M., Lambert, P., Smith, B.W., Sloth, E., Larsson, A., Andreassen, S. & Rees, S. (2008d). Model-based identification of PEEP titrations during different volemic levels. *Comput Methods Programs Biomed*, **91**, 135–144. 99, 131, 149, 150, 167, 185, 204, 205, 213

Starfinger, C., Chase, J.G., Hann, C.E., Shaw, G.M., Lambert, P., Smith, B.W., Sloth, E., Larsson, A., Andreassen, S. & Rees, S. (2008e). Prediction of hemodynamic changes towards PEEP titrations at different volemic levels using a minimal cardiovascular model. *Comput Methods Programs Biomed*, **91**, 128–134. 99, 131, 185, 204, 205, 213

Stergiopulos, N., Segers, P. & Westerhof, N. (1999). Use of pulse pressure method for estimating total arterial compliance in vivo. *Am.J.Physiol.*, **276 (2 Pt 2)**, H424 H428. 34

Sun, Y., Ko, Y., Lucariello, R. & Chiaramida, S. (2000). System identification for a complex nonlinear model of the cardiovascular system. *Bioengineering Conference, 2000. Proceedings of the IEEE 26th Annual Northeast*, 135–136. 76

Suresh, G., Horbar, J.D., Plsek, P., Gray, J., Edwards, W.H., Shiono, P.H., Ursprung, R., Nickerson, J., Lucey, J.F. & Goldmann, D. (2004). Voluntary anonymous reporting of medical errors for neonatal intensive care. *Pediatrics*, **113**, 1609–1618. 2, 148

Task Force of the American College of Critical Care Medicine, Society of Critical Care Medicine (1999). Practice parameters for hemodynamic support of sepsis in adult patients in sepsis. *Crit Care Med*, **27**, 639–660. 184

Ursino, M. (1999). A mathematical model of the carotid baroregulation in pulsating conditions. *IEEE Trans.Biomed.Eng.*, **4**, 382 392. 34

Vieillard-Baron, A., Prin, S., Chergui, K., Dubourg, O. & Jardin, F. (2002). Echo-doppler demonstration of acute cor pulmonale at the bedside in the medical intensive care unit. *Am J Respir Crit Care Med*, **166**, 1310–1319. 24

Weber, R.J., Kane, S.L., Oriolo, V.A., Saul, M., J.Skledar, S. & Dasta, J.F. (2003). Impact of intensive care unit (ICU) drug use on hospital costs: a descriptive analysis, with recommendations for optimizing icu pharmacotherapy. *Crit Care Med*, **31**, S17–S24. 204

White, M. & Leenen, F.H. (1997). Effects of age on cardiovascular responses to adrenaline in man. *Br J Clin Pharmacol*, **43**, 407–414. xxii, 204, 205, 206, 213, 217, 218, 219, 225

Wise, R., Robotham, J., Bromberger-Barnea, B. & Permutt, S. (1981). Effect of PEEP on left ventricular function in right-heart bypassed dogs. *Journal of Applied Physiology*, **51**, 541–546. 54, 145

REFERENCES

Yu, D.T., Platt, R., Lanken, P.N., Black, E., Sands, K.E., Schwartz, J.S., Hibberd, P.L., Graman, P.S., Kahn, K.L., Snydman, D.R., Parsonnet, J., Moore, R. & Bates, D.W. (2003). Relationship of pulmonary artery catheter use to mortality and resource utilization in patients with severe sepsis. *Crit Care Med*, **31**, 2734–2741. 3

Zaritsky, A. (1994). *The Pharmacologic Approach to the Critically Ill Patient*, chap. Catecholamines, inotropic medications, and vasopressor agents, 387–404. Baltimore, Md: Williams & Wilkins. 202

Zhu, Y., Dai, J. & Li, J.K.J. (1995). Total systemic arterial compliance: evaluation of time and frequency domain methods. *Bioengineering Conference, Proceedings of the 1995 IEEE 21 Annual Northeast*. 81